STRUCTURAL AND METAMORPHIC CONTROL ON THE BORDEN GOLD DEPOSIT, CHAPLEAU, ONTARIO

DANIEL LAFONTAINE

A thesis submitted to the Department of Geology in partial fulfillment of the requirements for a Master of Science degree

Department of Geology
Lakehead University
May 2016

ABSTRACT

The Borden gold property is a multi-million-ounce deposit that is located 10 km east of Chapleau and 160 km southwest of Timmins. It occurs within the Wawa Subprovince of the Archean Superior Province. What is atypical about the Borden gold deposit is its location near the southern margin of the Kapuskasing Structural Zone (KSZ), a structurally controlled region of granulite and upper amphibolite facies metamorphic rock. The deposit occurs within the Borden Lake Belt, an east-striking lithological assemblage, consisting of metasedimentary, felsic and mafic gneisses. Gold mineralization is hosted by garnet-biotite gneiss (±sillimanite), amphibolite (±garnet) and deformed quartz veins. Lithons of granulite facies rock are surrounded by foliated amphibolite facies gneisses and schists. Structure and microstructure indicate polymetamorphism with retrograde amphibolite facies metamorphism after granulite facies metamorphism. Garnet-biotite geothermometry based on the composition of unzoned almandine garnet, matrix biotite in the rock and biotite inclusions in garnet yields temperatures ranging from 411°C to 933°C ±50°C for metamorphism of the garnet-biotite schist at the Discovery Outcrop. Although garnet compositions are fairly consistent, biotite compositions vary from inclusions in garnet cores to inclusions in garnet rims and to matrix biotite, yielding temperatures that increase from the garnet core towards the rim, recording prograde metamorphism from the upper amphibolite to granulite facies during garnet growth. To compliment metamorphic parameters and establish metamorphic geochronology, Lu-Hf geochronology of garnet was conducted.

Results suggest that peak granulite facies metamorphism associated with garnet growth took place at ca. 2629 Ma, consistent with earlier estimates of the age of granulite facies metamorphism.

Competency contrasts between the granulite and retrograde amphibolite facies lithologies created heterogeneous strain, ideal for gold mineralization, during ductile deformation at amphibolite facies metamorphic temperatures. On the macroscopic scale, the relict granulite facies lithons behaved more competently than the reaction-softened retrograde amphibolite. On the microscopic scale competent relict orthopyroxene, garnet and pyrite provided an adjacent low-strain site for gold mineralization. Gold is typically observed in competent lithologies with weakly developed foliation and also in competent units that are bordered by strongly foliated units. Retrograde metamorphism is critical to the structural control of mineralization at this deposit. Results indicate an important relationship between gold mineralization, retrograde metamorphism and deformation. Understanding this relationship will benefit further exploration and development of the Borden gold deposit.

ACKNOWLEDGEMENTS

I am most grateful to Breanne Beh. We have spent consecutive summers together completing research- and economic-mapping projects, which have been unforgettable. We met David Palmer and Sharon Allen during the 2012 PDAC and were given the opportunity to work on the Borden gold deposit as field geologists that summer. I invited Mary Louise Hill for a site visit the first summer and the following year Probe Mines Limited expressed interest in post-graduate thesis research on the property, leading to the most important and exciting learning experience of my geology career.

Probe Mines Limited, specifically David Palmer, shared the opportunity to be a part of this team to study the Borden deposit and provided funding for research, which has been greatly appreciated. Since the transfer of ownership in early 2015, Goldcorp has been a great partner, honouring the research agreement established by Probe.

Dr. Mary Louise Hill has been an outstanding mentor throughout the duration of my research. Her expertise and knowledge have invaluably broadened my understanding of metamorphic and structural geology, which I will be able to use throughout the rest of my career as a geologist. Breanne Beh has been the most supportive and reliable companion during all of my fieldwork and writing. As an employee of Probe Mines Limited and Goldcorp, she has assisted me compiling data for analysis, set up academic site visits and helped me organize my first sample suite.

Without Anne Hammond and Kristi Tavener, I would not have been able to analyze thin sections, and I commend their hard work in the LU rock preparation lab.

I would also like to thank Victoria Stinson for her advice and coordination as we both conducted academic research on the project. I cannot overlook the assistance and troubleshooting help I received from Dr. Guosheng Wu while using the SEM at Lakehead University. Dr. Audrey Bouvier at Western University has also been a great contributor, working with me on Lu/Hf dating of garnet from the Borden property. Finally, I would like to thank my parents, Rebecca and James, for their constant encouragement and support during my entire academic career.

TABLE OF CONTENTS

LIST OF FIGURES

LIST OF TABLES

1. INTRODUCTION

1.1 Objective

The purpose of this study was to investigate the structural and metamorphic control on gold mineralization at the Borden gold deposit in Chapleau, Ontario. The relationship between amphibolite to granulite facies metamorphism and high-temperature ductile deformation within the Kapuskasing Structural Zone and the Wawa Subprovince was analyzed in relation to gold mineralization. The Borden deposit demonstrates the potential for economic gold mineralization associated with heterogeneous strain environments at great crustal depths, an environment that conventional wisdom has tended to discount.

1.2 The Borden Gold Deposit

The Borden gold deposit is located in the Cochrane township of Ontario, 10 km east of Chapleau and 160 km southwest of Timmins (Fig. 1.1). It is situated less than 1 km south of Highway 101 and is bordered to the south, east and west by Borden Lake. The Borden land package extends 2 km north of Highway 101 and approximately 80 km east to Foleyet, for a total area greater than 1000 km^2. Within this region, there are three First Nation communities of the Wabun Tribal Council: Chapleau Cree, Chapleau Ojibwe and Brunswick House First Nation.

Figure 1.1. Location of the Borden gold deposit near Chapleau, ON (Modified after Probe Mines Limited, 2013).

1.3 Exploration History

The Kapuskasing Structural Zone has been historically underexplored due to the high-grade of metamorphism, even though the location of the Borden gold deposit is favourable due to major east-west trending structures, subparallel to surrounding gold camps in Timmins and Wawa (Fig. 1.2). In the early 1990s low-grade gold findings were first sampled from the location known as the "Discovery Outcrop" by two prospectors, Jack Robert and Mike Tremblay. Encouraged by their findings, they tried to monetize the low-grade gold prospect. Lack of interest, likely due to low gold prices, meant that the property was left unnoticed for many years. Robert and Tremblay returned to the area in 2008 when they did some follow-up prospecting and acquired more encouraging results from the Discovery Outcrop. Dr. David Palmer, President

and CEO of Probe Mines Limited (currently Probe Metals Inc.), was sold on the idea of a project located within working distance to the town of Chapleau and took a chance by acquiring ownership of the property's mineral rights. The first drilling program began in 2010 at the Discovery Outcrop with a campaign of 10 holes, approximately 1 km south of Highway 101. Probe Mines Limited encountered widespread gold mineralization, which has ultimately developed into the current Borden gold deposit.

Since the initial drill campaign, there have been more than 1000 holes drilled between 50 and 1000 metres in length (Goldcorp, 2016). Probe Mines Limited fire assay and diamond drill hole lithological analysis has identified gold in a variety of lithologies. The ore body is greater than 3.5 km long with a width ranging from 150 to 500 m; it trends to the southeast with a shallow plunge to the southeast (Fig. 1.3).

Recent economic assessments have identified an open pit-constrained resource of 2.32 million ounces of gold averaging 1.03 g/t Au in the indicated resource category and 0.01 million ounces of gold averaging 0.80 g/t Au in the inferred resource category at 0.5 g/t Au cut-off and a high-grade underground constrained resource of 1.60 million ounces of gold averaging 5.39 g/t Au in the indicated resource category and 0.43 million ounces of gold averaging 4.37 g/t Au in the inferred resource category at 2.5 g/t of gold cut-off (Probe Mines Limited, 2014). Metallurgical reports are ongoing and indicate that the gold is non-refractory and has an average recovery rate greater than 90% (Probe Mines Ltd., 2015).

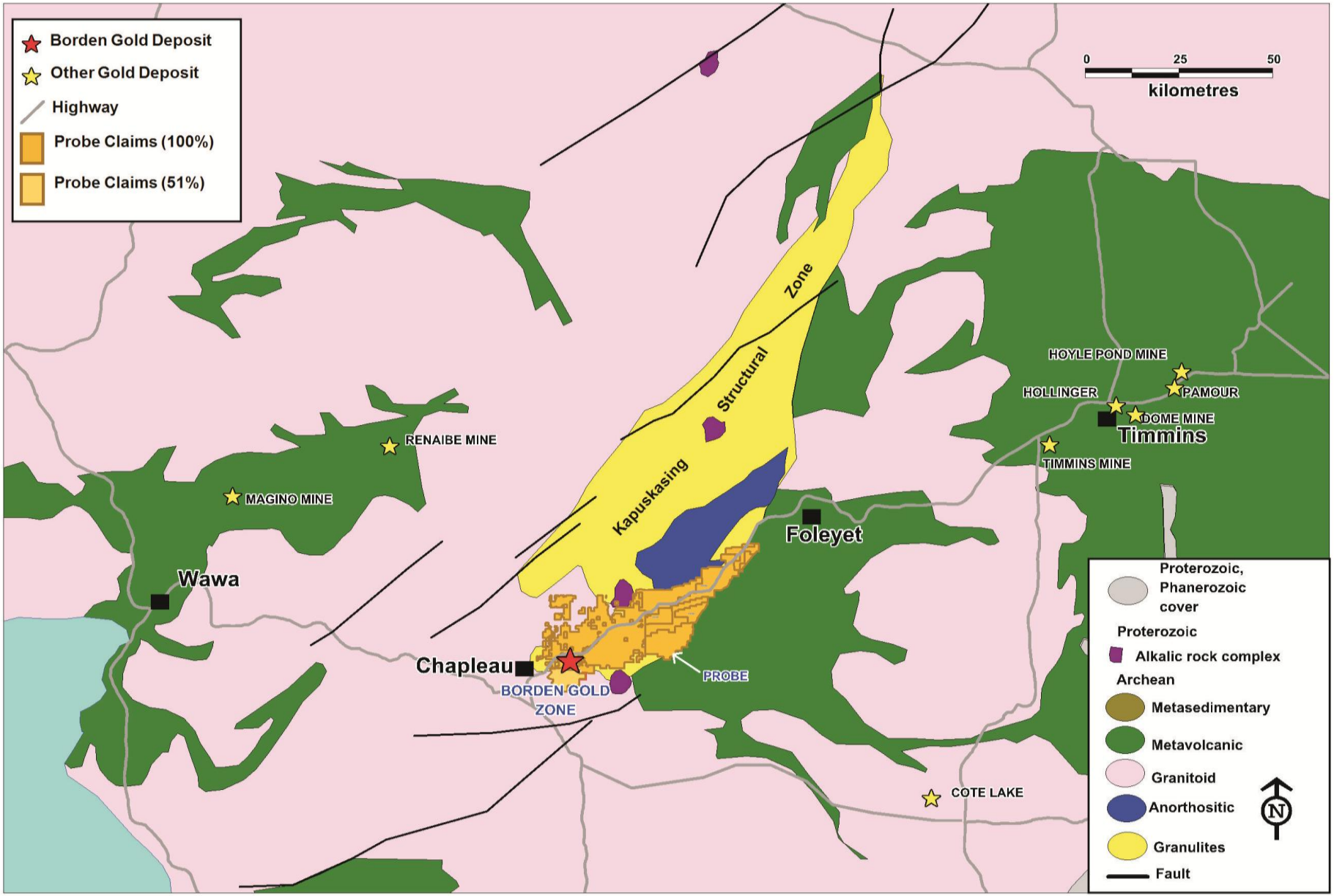

Figure 1.2. Map of the Borden gold project land package, regional geology and surrounding gold camps (Probe Mines Limited, 2015).

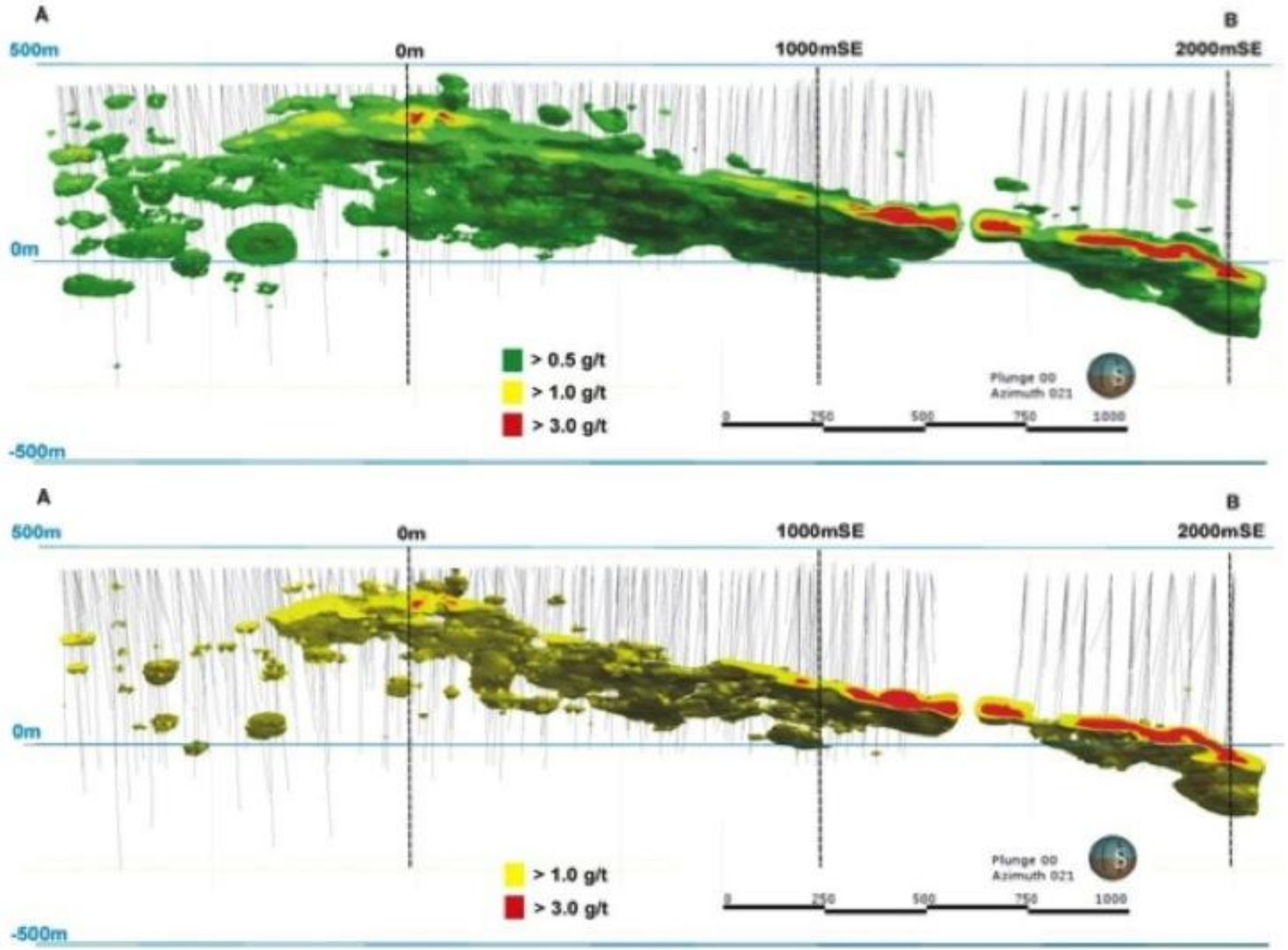

Figure 1.3. Long-hole section of the Borden Gold ore body, facing north (Probe Mines Ltd., 2013).

Probe Mines Limited was a well-funded junior exploration company, and the deposit has been regarded as one of the most important greenfield gold discoveries in Ontario since Hemlo in the early 1980s. In 2013, Probe Mines Limited won the Ontario Prospectors Award from the Ontario Prospectors Association for their discovery and fast-paced exploration program. In 2015, Dr. David Palmer was awarded the Prospectors and Developers Association of Canada Bill Dennis Award for a Canadian mineral discovery. The Borden project was also globally recognized by New Gen Gold in 2015. This opportunity highlighted the discovery, development and research in a detailed paper and presentation at the 2015 conference in Perth, Australia. This project has become an overnight success story in the gold exploration industry.

Probe took the project to the advanced exploration stages, completing condemnation drilling, metallurgical testing and environmental baseline studies. Further exploration included drilling on the "East Limb" of the land package. In March 2015, Goldcorp Inc. acquired the Borden gold property and the adjacent East Limb land package for $532 million (CAD). Goldcorp has since been completing definition drilling on the project in the hopes of submitting a resource estimate and a plan for underground extraction. The project hopes to attain a bulk sample and sink a portal for underground extraction of the high-grade zone in the near future.

The Borden gold project represents a gold discovery in an underexplored part of the Kapuskasing Structural Zone. The deposit still remains open in both directions along strike and has strong potential for further expansion.

2. REGIONAL GEOLOGY

2.1 The Kapuskasing Structural Zone (KSZ)

The Superior Province is one of the oldest cratons in the world. It is hypothesized to have been assembled by the end of the Archean through the accretion of terranes now represented by narrow subprovinces (Corfu and Davis, 1992; Moser et al., 2008). The Abitibi and Wawa Subprovinces are interpreted to be the last terranes accreted between 2750-2670 Ma (Corfu and Davis, 1992) during northward subduction during the Kenoran Orogeny (Moser et al., 2008).

The KSZ is a 500 km long Belt of high-grade metamorphic rock that strikes north-northeast to south-southwest and crosscuts the east-west trend of the adjacent Abitibi and Wawa Subprovinces (Fig. 2.4). It represents a deep crustal assemblage that has been exhumed along a major crustal structure. The grade of metamorphism ranges from upper-amphibolite to granulite facies, and the presence of a large anorthosite complex, the Shawmere anorthosite, is consistent with exhumation from the deep crust. The KSZ is sharply bounded on the east by the Ivanhoe Lake Deformation zone (ILDZ), across which the metamorphic grade decreases sharply from granulite facies, in the KSZ, to greenschist facies in the Abitibi Belt. To the southwest, the metamorphic grade decreases gradually through amphibolite facies to greenschist facies in the Wawa Sub-province. Aeromagnetic anomalies suggest sinistral displacement of approximately 100 km along the Ivanhoe Lake Structure. The contrast in metamorphic grade suggests a component of vertical displacement with the KSZ being exhumed and uplifted with respect to the Abitibi Subprovince to the east.

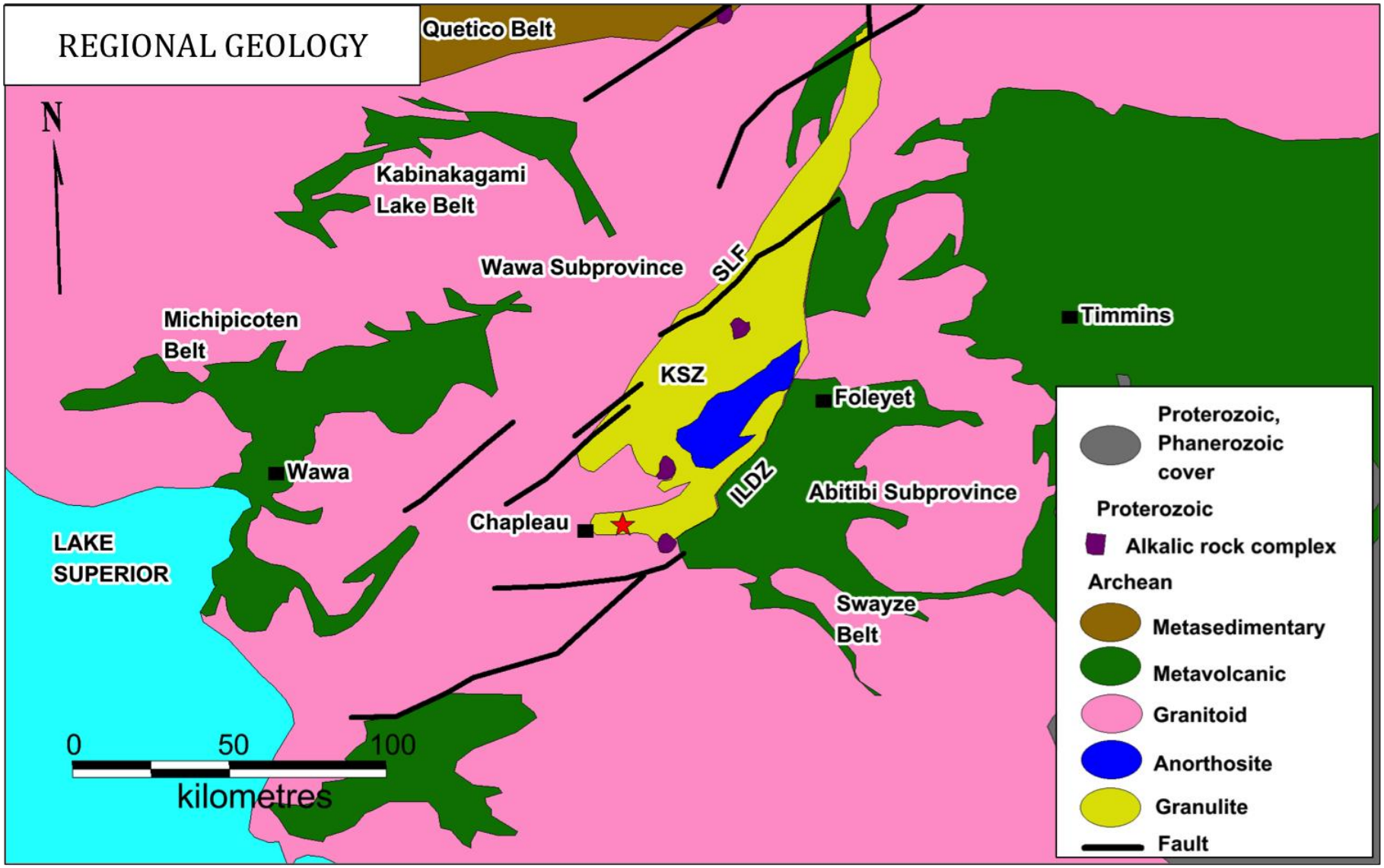

Figure 2.4. Regional map of the Kapuskasing Structural Zone, Wawa and Abitibi Subprovinces. The Borden gold deposit is denoted by the red star (Modified after Heather et al., 1995; Probe Mines Ltd., 2015).

The Kapuskasing Structural Zone was first discovered in the 1950s due to the associated high positive gravity and aeromagnetic anomalies (Innes, 1960). Early interpretation by Watson (1980) regarded the KSZ regional positive Bouguer anomaly as a result of upfaulted strips of granulite and associated rocks and the probable redistribution of densities in the lower crust. The KSZ can be seen on aeromagnetic and gravity maps as a linear zone, and as noted by Watson (1980), outcrops of gneisses, metavolcanic and metasedimentary rocks do not match up across the KSZ border.

Northeastern-southwestern lineaments of the Thompson Belt, the Wollaston Lake Belt and the Kapuskasing Structural Zone were regarded as members of a genetically related set of shear zones formed during the late Archean in the interior of a large continental mass (Watson 1973; Sutton and Watson 1974; Piper 1976). Deep crustal metamorphism was predicted to be coeval with orogen-parallel ductile flow in the middle and lower crust between 2660 Ma and 2630 Ma (Moser et al., 2008). Percival and Krogh (1983) dated the metamorphism in the KSZ as Archean, inferred from U-Pb dates on zircon from leucosones in paragneisses (2627±5 Ma) and on metamorphic zircon in mafic gneisses (2650±2 Ma). Paleopressures in the KSZ gradually increase to the east across the granulite facies domain, ranging from 0.56 GPa proximal to the Borden Lake Belt to 1.1 GPa in the northeast part of the KSZ with peak temperatures of >850°C (Moser et al., 2008).

Lithologies that display a strong foliation are characteristic of ductile shear zones formed at depth. Layering in granulites and unit discontinuity across the Ivanhoe structure suggests that displacement was achieved partly by movement on ductile

shear zones, at temperatures high enough to promote recrystallization and potentially preventing retrogression of granulites (Watson, 1980).

The Ivanhoe Lake Deformation zone sharply bordering the KSZ to the east is a prominent feature related to the oblique movement of the KSZ. The trend of the layering and prominent fabric within the KSZ is variable, from highly discordant (east-west) to subparallel to the strike of the Ivanhoe Lake Deformation zone. Within the Chapleau block, mild deflection, where layering is at a high angle to the Ivanhoe structure, suggests some component of sinistral offset, particularly where the strike of the Ivanhoe Lake Deformation zone (ILDZ) is north-northeasterly (Moser et al., 2008). The southern segment of the ILDZ contains two distinct fault orientations in a zone where the trace of the fault swings from its prominent north-northeast direction to east-northeast. The more easterly fault trend, which is parallel to a strong subhorizontal stretching lineation, offsets the north-northeast segment dextrally. A progressive ductile to brittle transition, from thin mylonitic seams through cataclasites to fault breccias is exhibited by the sequential development of structures at many localities within the Ivanhoe Lake Deformation zone and may be viewed as responses to the late stages of progressive erosion and uplift, unroofing the KSZ plate. In a few localities, mylonites postdate brittle structures (Bursnall and Moser, 1989; Percival et al., 1991). Variations in uplift rate could explain the local transition from brittle to ductile behaviour and could also explain many of the complexities present within the deformation zone. Watson (1980) suggested that the KSZ line did not originate as a rift structure but rather a deep transcurrent shear zone, analogous to that in other continents. A long history of oblique displacement on the Ivanhoe Lake Structure is

indicated by overprinting of brittle structures, including pseudotachylite, on earlier ductile shear-zone fabrics.

Rehydration of granulite facies mineralogy in boudin neck zones shows that final boudinage postdates peak metamorphism. Magmatic activity during this period includes infilling of metre-scale boudin necks with pegmatitic tonalite. In the KSZ, boudinage of gently dipping high-strain fabrics at 2630 Ma (Krogh, 1993) indicates that the last increments of extension are younger with increasing paleodepth. The Ivanhoe Lake Deformation Zone represents a complex polyphase deformation history (Bursnall et al., 1994), and isotopic studies indicate significant cooling around 2500 Ma (Krogh and Moser, 1994; Percival and Peterman, 1994).

In migmatitic mafic gneisses, paragneisses, diorites and tonalitic rocks, a lower-grade garnet-clinopyroxene-plagioclase (Grt-Cpx-Pl) zone and higher-grade orthopyroxene zone are distinguished (Percival, 1983). Based on mineral-melt equilibria, minimum conditions for the clinopyroxene zone are 750°C, 0.6 GPa and for the orthopyroxene zone, 770°C and 0.6 GPa (Percival, 1983). Within the KSZ various garnet-biotite and garnet-pyroxene geothermometers and geobarometers yield apparent temperatures ranging from <600°C in the west to locally >800°C (Percival, 1983). Percival (1983) previously calculated garnet-biotite geothermometry for areas in the KSZ and temperature ranges are between 580°C to 825°C and more specifically 630°C ±50°C proximal to the Borden gold zone.

2.2 Shawmere Anorthosite

The Shawmere anorthosite is proximal to the Borden property within the Kapuskasing Structural Zone. It is composed of anorthite phenocrysts 1 to 10 cm in diameter with pyroxene around the anorthite (Fig. 2.5). The anorthite phenocrysts have porphyroclast shapes with pyroxene as porphyroclast tails. Other areas within the KSZ, the Shawmere anorthosite appears massive with very coarse anorthite phenocrysts and no preferred orientation of the pyroxene grains.

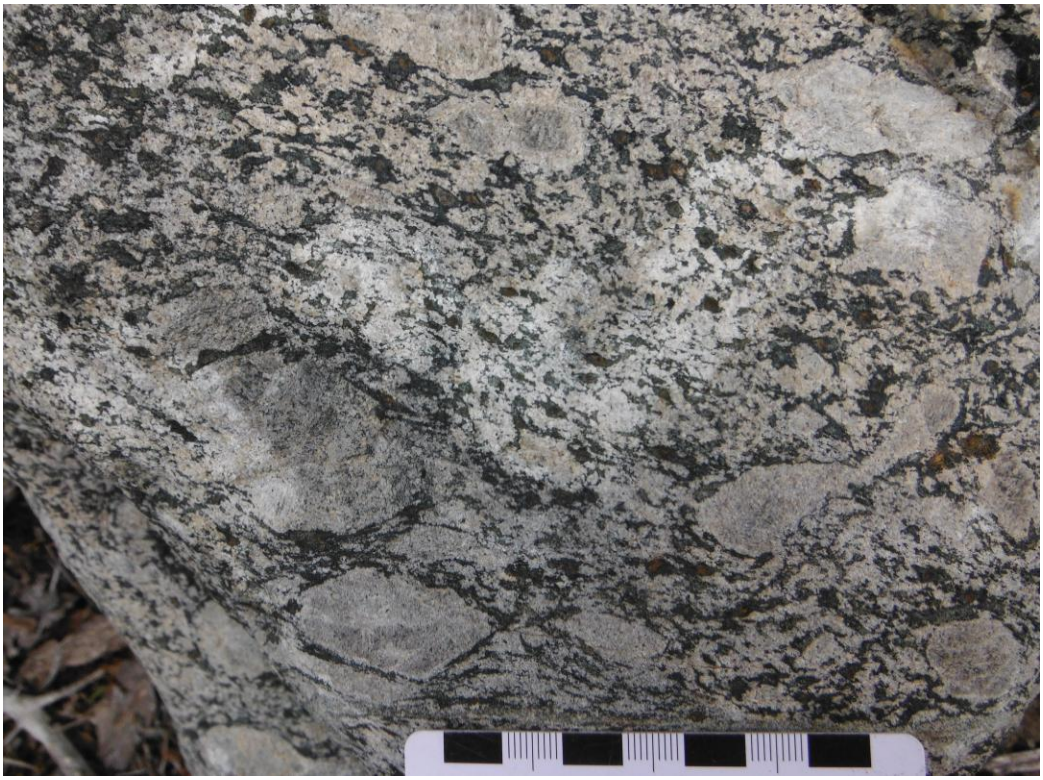

Figure 2.5. Shawmere anorthosite with coarse anorthite phenocrysts (white) and pyroxene (green).

Hornblende from the Shawmere anorthosite complex yields a K–Ar age of 2519 Ma (Watkinson et al., 1972). The east-northeast strike of layering of the complex is parallel to that of the associated granulites and is truncated by the Ivanhoe Lake Deformation Zone related to the Kapuskasing Structural Zone (Watson, 1980).

2.3 The Borden Lake Belt

The Borden property is located within the Borden Lake Belt (BLB) near the southern margin of the KSZ. The BLB is a 5 km by 25 km east-striking lithological assemblage, consisting of metasedimentary, felsic and mafic gneisses (Fig. 2.6). The Borden zone is defined by lithological, structural, density and seismic velocity changes reflecting the transition from granulite to amphibolite facies (Percival 1986; Moser 1994). Moser (1994) observed that the oblique transect of the dominant east-west lithological trend allows for lithological and structural correlation between deep-crustal (KSZ) and the mid-crustal levels of the Borden Lake Belt (Bursnall et al., 1994; Moser, 1994). The Kapuskasing Structural Zone is composed of gneisses in the upper amphibolite to granulite facies with the metamorphic grade decreasing abruptly to greenschist facies in the Abitibi Subprovince to the southeast, across the Ivanhoe Lake Deformation zone. A gradual transition from granulite to amphibolite facies metamorphism occurs through the Wawa Gneiss Domain across the Saganash Lake Fault to the northwest (Bursnall et al., 1994). The Borden Lake Belt consists of paragneiss (metapelites and metaconglomerate), orthogneiss (metavolcanic rock), felsic and mafic gneisses, all of which display high-grade metamorphism from upper-amphibolite to granulite facies.

Percival and Krogh (1983) dated a granodiorite that crosscuts the mafic gneiss at the southern margin of the KSZ at 2677 +5/-3 Ma, which is implied to establish a minimum age for mafic volcanism. Published zircon estimations derived from metaconglomerate matrix yield a maximum age for metaconglomerate deposition at the Borden Belt of: 2671 ±12 Ma (Moser et al., 2008) and 2667±2 Ma (Krogh, 1993).

Garnet formation is assumed to have been at 2660 Ma, based on the age of the oldest metamorphic zircon in retrograde mafic granulite (Moser, 1994). Detrital zircon dating by Moser et al. (2008) utilizes unrecrystallized zircon cores constraining a lower age bracket of 2659 ± 8 Ma for burial of Borden Lake metasediments in the lower crust. This age is derived from zircon rims with concentric changes in U-Pb ages, oxygen isotope values and trace elements (Moser et al., 2008). Moser and others (2008) conclude that protracted radial growth of zircon, rather than short-lived in situ recrystallization, aids in the prediction that growth would have occurred around detrital cores for as much as 80 m.y., during which apparent Ti in zircon temperatures vary between 706°C and 660°C. Metamorphic growth events appear to have been most frequent at ca. 2620 Ma, when temperatures were above 650°C, and the events coincided with boudinage in the lower crust and crustal-scale fluid flow along brittle structural breaks at higher levels (Krogh, 1993). Evidence for late Archean (ca. 2630 Ma) fault activity exists along the Ivanhoe Lake fault zone (Krogh and Moser 1994).

Mapping by Moser (1994) describes the western portion of the Borden Lake Belt as a tight synform that preserves sedimentary and volcanic structures (Fig. 2.6). In contrast to the amphibolite facies units in the western BLB, the eastern metavolcanic rocks are interlayered with felsic orthogneiss and have granulite facies mineralogy. Moser (1994) also notes areas with relict granulite-facies assemblages in retrogressed metavolcanic rocks to the west and north. Amphibolite and garnet-amphibolite gneiss extending from the Belt margin inward are described as metavolcanic rocks with preserved deformed pillow structures with garnetiferous selvedges (Moser et al., 2008).

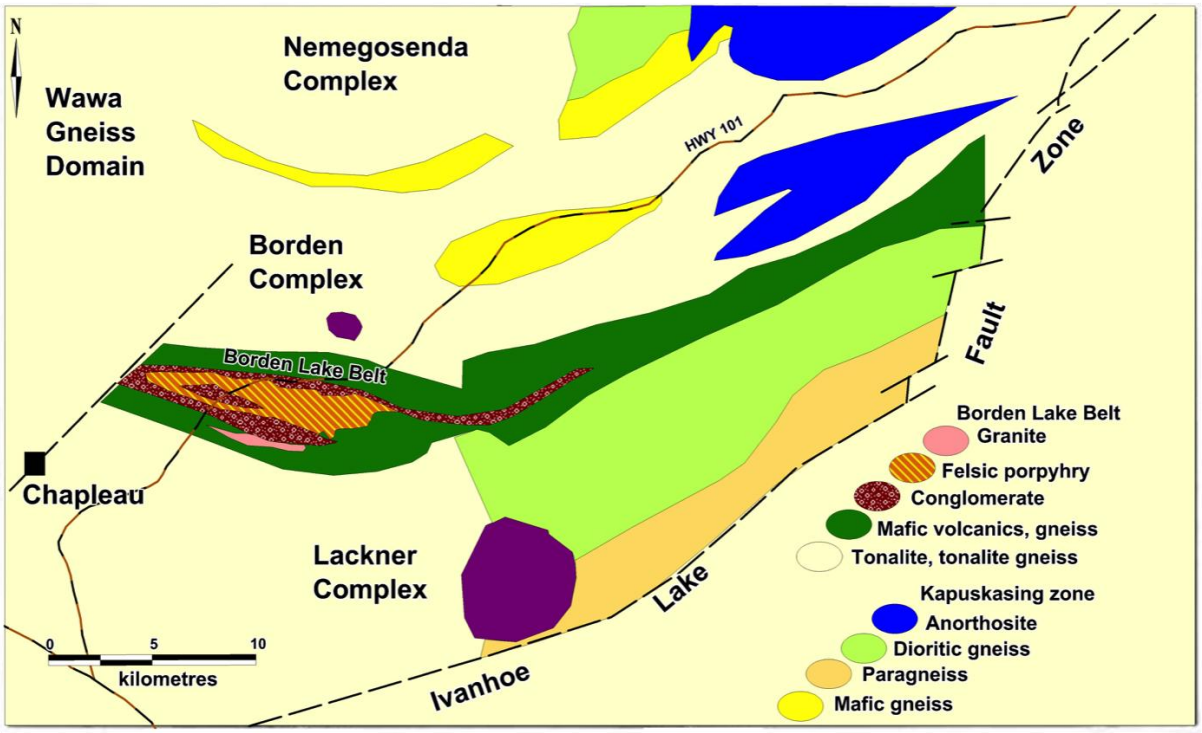

Figure 2.6. Map of the Borden Lake Belt geology (Moser, 1994).

Granitoid pegmatites are abundant in the Chapleau Wawa Gneiss Domain. Moser (1993) defines four generations of pegmatite with the oldest being highly deformed, sub-parallel to country-rock gneissosity. Later generations of tonalitic pegmatite are structurally controlled by boudinage and extensional shear planes and have been dated at 2640±2 Ma (Moser, 1993; Krogh 1993, Moser et al., 2008). The granulite facies gneisses are cut locally by metre-scale tonalitic melt pods and granitic pegmatite dikes dated at 2640±2Ma and 2584±2Ma, respectively (Krogh, 1993).

The Wawa Gneissic Domain preserves the structural transition between upper and lower crustal levels of the Abitibi-Wawa Orogeny. In Moser's (1994) tectonic model, during early history of the Abitibi-Wawa Orogen (2700-2680 Ma) the tectonic and deformation sequence began with northward subduction. Subsequent folding and thrusting of Timiskaming-age sediments, between 2680 and 2670 Ma and continued

north-south shortening resulted in burial to mid-crustal depths of the Borden Lake Belt between 2670 to 2660 Ma (Moser, 1994). A final episode of compression, loosely bracketed between 2637 and 2580 Ma, was directed parallel to the length of the orogen, causing folding in the Kapuskasing exhumation, reactivation of major faults in the Abitibi and Michipicoten Greenstone Belts, and, possibly, reverse faulting in the vicinity of the Ivanhoe Lake Deformation zone (Moser, 1994).

3. METHODS

Data for this study was gathered by a combination of field mapping, core logging, reflected and transmitted light petrography, microstructural analysis, quantative EDS using a SEM, garnet-biotite geothermometry and Lu/Hf dating of garnet. Mapping and petrography provided a useful means to explore the relationship between macroscopic and microscopic lithological and rheological contrasts at the Borden gold deposit. Garnet-biotite geothermometry and garnet dating helped to constrain the metamorphic and structural evolution relative to the timing of gold mineralization.

3.1 Fieldwork

The Borden gold property (Fig. 3.7) is located 1 km south of Highway 101 and can be accessed from a marked dirt road, navigable by a 4x4 truck. Thesis field research was conducted during the months of May to September 2014. Bedrock mapping was conducted on the Borden property by traversing line-cuts perpendicular to the length of the ore zone. Geographic locations (UTM) and detailed lithological descriptions were recorded for exposed country rock. Foliation, lineation, modal mineral composition, contacts, kinematic indicators, minor folding or boudinage, quartz veining and overall crosscutting relationships were documented. Structural measurements, such as strike and dip of foliation as well as lineation measurements, can be found in Appendix A.

Pre-existing drill roads on the property were navigated by ATV and selected outcrops on the Borden property were stripped in order to complete detailed trench mapping. Logging roads and road-cuts along Highway 101 also exposed large areas of

country rock. The Discovery Outcrop had been stripped previously and a channel sample was taken there for this thesis. Both natural and excavated exposures were examined in detail to create a property scale map. Samples collected from the channel cut were labeled using the "FD" sample suite and samples used for thin section and SEM analysis were labeled "BL".

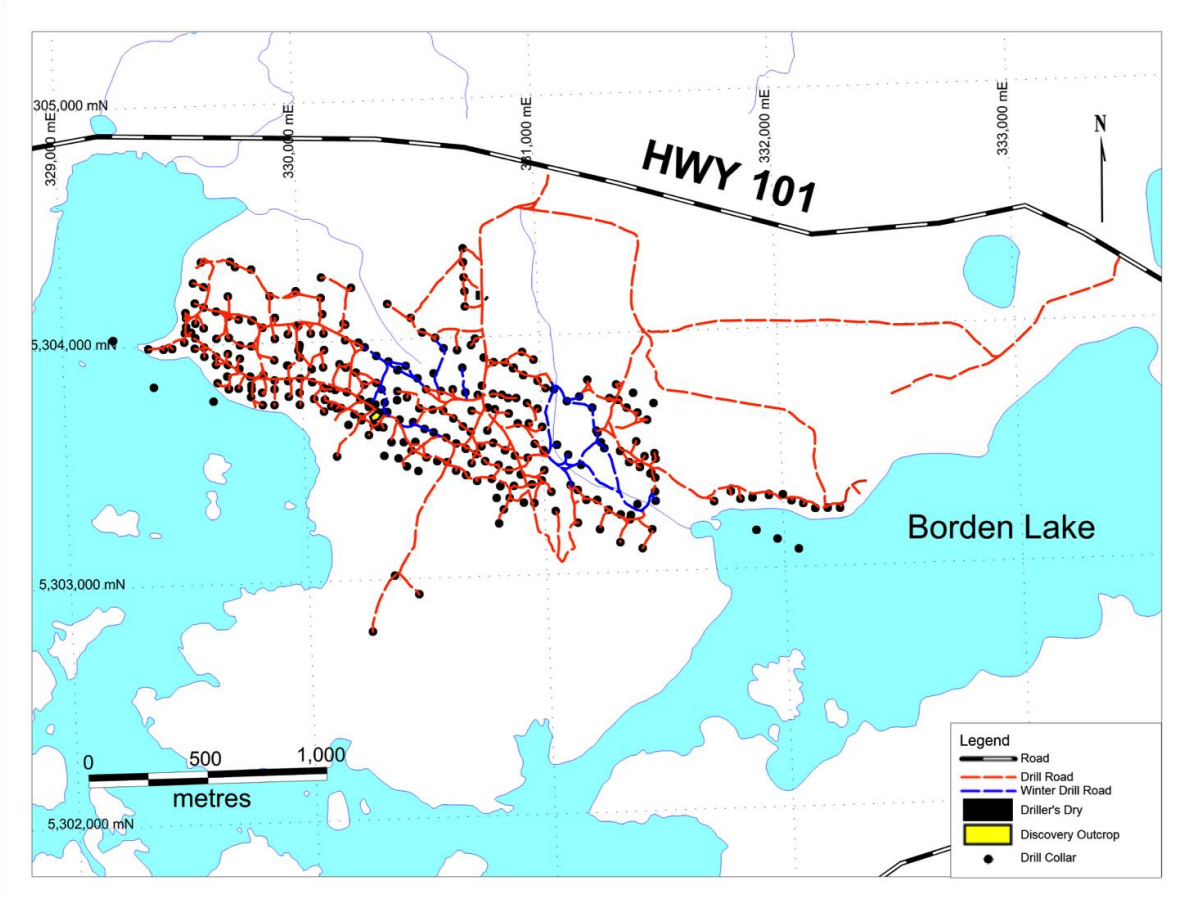

Figure 3.7. Property map of the Borden gold deposit with roads and trails used for navigation and mapping (Probe Mines Ltd., 2013).

The channel samples on the Discovery Outcrop (Fig. 3.8) were conducted to constrain the low-grade gold showings at surface and their relationship to lithology and lithological contacts. The channels were cut in August 2013 and samples were taken at contacts and within lithologies. The channels themselves measured 8 cm wide

and were cut perpendicular to the dominant strike of the foliation in the outcrop. There is a total of two channel cuts representing the northern and southern portions of the Discovery Outcrop. The north outcrop channel cut had a trend of 204°, a total length of 12.5 m and there were 22 samples taken. The southern outcrop channel cut had a trend of 216°, a total length of 15.9 m and 21 samples were taken. The samples were no greater than 1.0 m in length. At lithological contacts, the sample included 5 cm from either side of the contact. Samples were sent to ActLabs in Timmins for fire-assay and whole-rock geochemistry. Polished thin sections were made for each of the 43 samples gathered in the "FD" sample suite. A detailed trench map and channel sample map were created using MapInfo Professional.

Figure 3.8. Discovery Outcrop, facing south-southwest. Preparing for the channel cut, August 2013.

3.2 Core Logging

In the summer of 2014, diamond drill holes previously logged by Probe Mines Limited's exploration program were relogged for the purpose of lithological and structural interpretation related to gold mineralization. Holes were reassessed with focus on structural relationships related to the high-grade metamorphism. All holes, which had been previously logged by Probe geologists and fire-assay results conducted by ActLabs in Timmins, ON were made available for this study. A total of twenty-three drill holes from six section lines perpendicular to the strike of the deposit were reassessed (Fig. 3.9 and Table 3.1) in order to create 2D sections.

Drill holes were relogged using the International Union of Geological Sciences (IUGS) metamorphic nomenclature classification (Fettes and Desmons, 2007), which differs slightly from the naming scheme used by Probe Mines Limited and Goldcorp Inc. The drill holes were relogged using Microsoft Excel and full drill logs can be found in Appendix B. The new logs were uploaded into MapInfo Professional and 2-D sections were created for each section line with their corresponding drill holes. Discover 3-D was used to create a fence diagram based on the 2-D sections generated from drill hole reassessment.

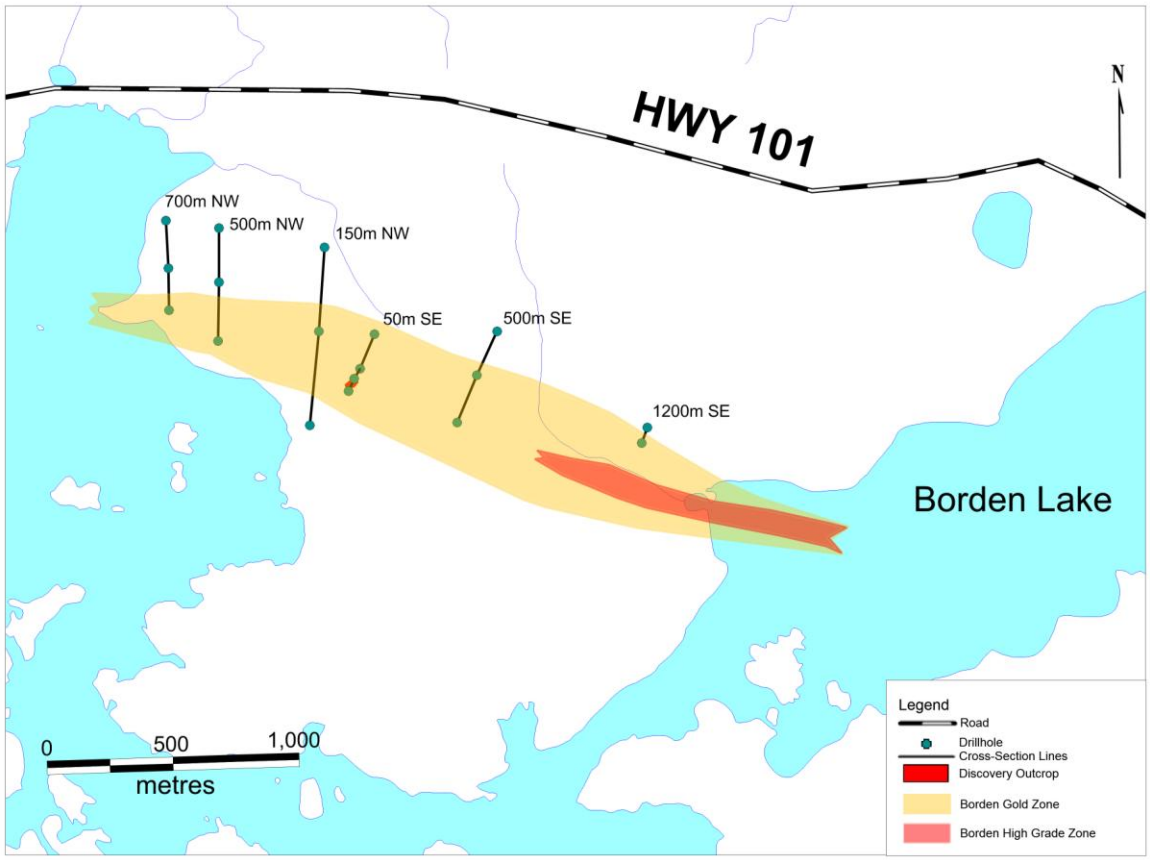

Figure 3.9. Borden gold property, highlighting section lines and drill hole locations used for cross-section interpretation (Modified after Probe Mines Limited, 2014).

Table 3.1. Diamond drill holes reassessed during field research with corresponding section line.

Section Line	Holes Reassessed	Section Line	Holes Reassessed
700mNW	BL11-24 BL11-25 BL11-115	50mSE	BL10-05 BL10-06 BL12-333 BL12-336
500mNW	BL11-19 BL11-20 BL12-255	500mSE	BL11-36 BL11-139 BL12-183 BL12-186
150mNW	BL10-08 BL12-178 BL12-199 BL12-204 BL12-329	1200mSE	BL12-256 BL12-268 BL13-375 BL13-406

3.3 Polished Thin Section Analysis

Polished thin sections were prepared by Anne Hammond and Kristi Tavener at Lakehead University's Rock Preparation Laboratory. Petrographic and microstructural analysis was conducted at Lakehead University using an Olympus BX51 transmitted and reflected light microscope with an attached Nikon 8 MP microscopic camera for photomicrographs. A total of 123 polished thin sections were analyzed. Full petrographic analysis with modal mineral abundance based on visual inspection, mineral association and mineralization can be found in Appendix C.

3.4 Compositional Analysiss using a Scanning Electron Microscope

The scanning electron microscope (SEM) at Lakehead University Instrumentation Laboratory (LUIL) is a Hitachi Su-70 Schottky Field Emission SEM. This has a resolution of 1.0 nm at 15 kv and 1.5 nm at 1 kV, 110 mm stage, Oxford Aztec 80 mm/124 ev EDX and specimen exchange airlock and column Faraday cup with HTC current monitor liquid nitrogen-based anti-contamination device. For the purpose of this thesis, 15 kV was the optimal output power, with an analytical working distance of 15 mm and using a solid-state five segment backscatter electron (BSE) detector below the lens. Quantitative mineral compositions obtained using the Oxford Aztec X-ray energy dispersive software package were Mn-Hort (Si, Fe, Mn), Wolastonite (Ca), Jadite (Al, Na), Apatite (P) and $SiTiO_3$ (Ti, Sr). Selected thin sections were carbon coated and analyzed using LUIL's SEM for garnet and biotite elemental composition in order to complete garnet-biotite geothermometry.

3.5 Garnet-Biotite Geothermometry

Garnet-biotite geothermometry has been utilized for many decades in metamorphic geology. Beginning with initial analytical tests by Ferry and Spear (1978), on synthetic garnet and biotite, many variations have since been calibrated to account for differing garnet and biotite compositions. The Ferry and Spear (1978) calibration for garnet-biotite geothermometry was applied to the Borden gold deposit garnet-biotite schist unit. Quantitave EDS analysis was used to measure the iron-magnesium ratios between garnet and biotite. Scanning electron microscope elemental mapping of garnet was conducted to observe potential chemical zoning in garnet. Iron-magnesium ratios were calculated to compare garnet core to biotite inclusion and garnet rim to matrix biotite for metamorphic temperature analysis. The geothermometer has a maximum practical resolution of approximately ±50°C, which corresponds to the error in temperature that results when ±0.01 errors in X_{ann}, X_{phl}, X_{alm} and X_{py} are propagated through the equation: $\ln K = -2109/T + 0.782$, where $K = [(X_{pyrope}/X_{almandine})/(X_{phlogopite}/X_{annite})]$ and temperature is measured in Kelvin.

Ferry and Spear (1978) determined this to be a useful geothermometer without correction for minor components equal or less than approximately 0.2 from (Ca + Mn)/(Ca + Mn + Fe + Mg) in garnet. The garnet compositions measured from the Borden gold deposit garnet-biotite schist unit contained low amounts of Al, Mn and Ca making this a reliable geothermometer based on the synthetic garnet and biotite Fe-Mg exchange in the Ferry and Spear (1978) laboratory equilibrium calculations.

3.6 Lu/Hf Geochronology of Garnet

Garnet from the garnet-biotite schist unit on the Discovery Outcrop was used for Lu/Hf geochronology at the University of Western Ontario, completed by Dr. A. Bouvier. This process constrains the timing of garnet growth during metamorphism. Approximately 25 kg of rock from the channel sample was further ground in a jaw crusher. A fine, homogenized whole-rock powder was produced in a stainless steel mill. The remaining materials were crushed and sieved into three-grain fractions. Garnet grains were concentrated from the 125-250 micron fraction using a Frantz magnetic separator followed by heavy liquid density separation (methylene iodide, density approximately 3.2 g/cm^3) prior to further purification by hand picking in the Geometric Laboratory at Western University.

Three splits of whole-rock (WR) powder of sample FD 01340 between 0.15 to 0.65 g were dissolved following two methods. First, WR1 was dissolved using Parr bomb vessel dissolution at 155°C (methods described in Bouvier et al., 2008) to ensure that all refractory minerals, including zircons, were fully dissolved. Second, a hot plate dissolution method at atmospheric pressure and 120°C was utilized to avoid dissolving refractory minerals, which may be at isotopic disequilibrium.

Garnet was prepared according to the methods described in Zirakparvar et al. (2010). About 0.10 to 0.15 g of grains were first acid washed in 1 M hydrochloric acid (HCl) at room temperature, sonicated for 5 minutes, then rinsed in Millipore H_2O, sonicated for 5 minutes, and water was pipetted off. Concentrated 14 M nitric acid (HNO_3) and ultrapure 29 M hydrofluoric acid (HF) (1:10 of HNO_3:HF), were added to the beakers for digestion at 120°C for 24 hours. Samples were dried, before being

covered with perchloric acid evaporated at 150-180°C. For whole-rocks and garnets, the final dissolution step consists of uptaking samples in 6 M HCl and H_2O_2. A fraction of the whole-rock solution was split for ICP-MS trace element analysis to optimize spike addition. After that, solutions were dried once more and dissolved again in 6 M HCl. Mixed ^{149}Sm-^{150}Nd and ^{176}Lu-^{176}Hf spikes were finally added to the sample solutions, fluxed together, and once again dried to ensure sample-spike equilibration.

Detailed protocol for Hf-REE separation and purification is described in Bouvier et al. (2008). In summary, 8.5 mL cation Biorad AG50W-X8 200-400 mesh resin in PFA Teflon columns were used to separate HFSE from the matrix and REE fractions. Hafnium was further purified using a Eichrom Ln-spec resin chemistry protocol in teflon columns modified from Münker et al. (2001) and Lu+Yb were subsequently separated from the rest of the REE on Ln-spec resin in quartz columns (Bouvier et al, 2008).

Teflon beakers used were PFA Savillex® and PTFE vessels for the Parr® bombs. Chemicals (HF, HNO_3, HCl, $HClO_4$, and H_2O_2) used during this protocol were Aristar Ultra from BDH or Plasma Pure *Plus* Optima Grade from SCP Science. Water was purified to a resistivity of 18.2 MΩ using a Millipore Advantage system and QPOD Element dispenser. Chemistry was carried out in a Class 10 HEPA filtered total exhaust polypropylene fume hood and a perchloric acid polypropylene fume hood within a Class 1000 clean laboratory. Total analytical blanks were 20-30 pg for Hf and 5-10 pg for Lu, which are negligible.

Purified fractions of Hf and Lu with Yb (used to correct the instrumental mass bias on $^{175}Lu/^{176}Lu$) were analyzed by plasma source mass spectrometry. The average

$^{176}Hf/^{177}Hf$ ratios and two standard deviation (2SD) for the JMC 475 Hf isotopic standards measured in static mode (75 ratios) during three analytical sessions were respectively 0.282155 ± 0.000012 (2SD, 25 ppb Hf) using an Aridus nebulizer with a Neptune MC-ICP-MS at Washington State University (USA) (whole-rocks 1 and 2), and 0.282160 ± 0.000009 (2SD, 10 ppb Hf) and 0.282154 ± 0.000008 (2SD, 20 ppb Hf) using an Aridus II nebulizer with a Neptune Plus MC-ICP-MS at Laboratoire Magmas et Volcans, University of Clermont-Ferrand (France) (whole-rock 3 and garnet fractions 1 and 2). The Lu fractions of the samples were collected with part of the Yb and thus analyzed together to correct for interference and instrumental mass bias using the method described in Vervoort et al. (2004). External reproducibility on isotopic ratios used for age calculations are ±0.000010 for $^{176}Hf/^{177}Hf$ and ±0.5% for Lu/Hf based on repeated measurements of BCR-2 standards using the same isotopic dilution method.

4. LITHOLOGIES

Lithological observations were compiled from core logging and bedrock mapping on the Borden property. A property-scale map of the Borden gold deposit was produced from field observations (Fig. 4.10). Specific holes from section lines perpendicular to the length of the deposit were reassessed to produce 2-D cross-section interpretations. All 2-D sections summarize three important geologic factors used for understanding and interpretation of the macroscopic geology. These factors are lithology, structure and relative gold concentration. Gold-hosting lithologies include garnet-biotite schist (±sillimanite), amphibolite (±garnet), quartzofeldspathic gneiss, deformed quartz veins and pegmatite. Unmineralized units on the Borden property include metaconglomerate and diabase dikes. A significant contribution from core reassessment for this study was the focus on textural and structural characteristics of these lithologies. The structure column of the legend describes metamorphic textures with the lowest strain at the top of the column grading to the highest strain at the bottom of the column. Mineralogically similar units were differentiated by the strain intensity observed in metamorphic minerals. Low-strain indicated by massive and undeformed textures were differentiated from foliated and schistose textures indicating moderate to high strain. High strain units displaying gneissic banding and mylonitization were also identified. Detailed structural descriptions will be further discussed in Chapter 6. Gold values had been previously assayed and results were made available for subsequent analysis and comparison.

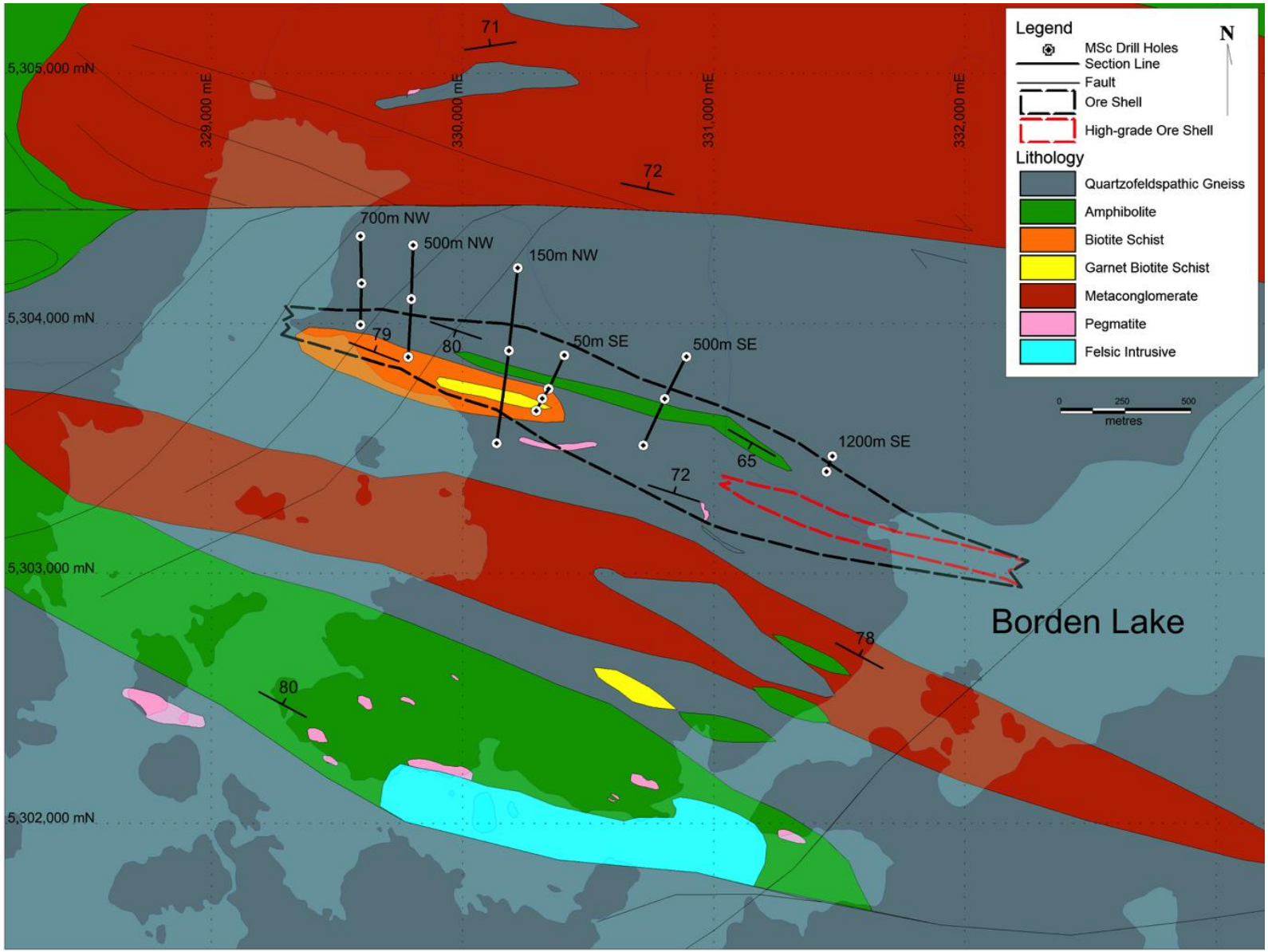

Figure 4.10. Map of the Borden Lake Belt geology overlaid on a map of land and lakes, produced from Probe Mines Limited geologic mapping between 2012-2015. The ore zone is projected to surface in black and red stippled lines. Section lines highlight reassessed drill hole locations that were utilized for thesis research core reassessment and sampling. Modified after B. Beh for Probe Mines Ltd., 2015.

4.1 Garnet-Biotite Schist (±Sillimanite)

The garnet-biotite schist is the most important indicator lithology when logging core because it is commonly associated with economic gold mineralization on the Borden property. Interestingly, it is exposed at the Discovery Outcrop where the first grab samples were obtained, sparking the development of the Borden project. At surface, it is only visible in the northwestern portion of the deposit. Due to the high modal abundance of biotite the unit is quite friable and easily eroded. Bedrock mapping has identified large and small outcrops of the garnet-biotite schist with some difficulty characterizing continuity and true thickness. Outcrop-scale occurrences are moderately to strongly foliated garnet-biotite schist with variable modal abundances of garnet, sillimanite and cordierite. Outcrops can also display biotite-rich layers, which anastomose around quartzofeldspathic lithons. Foliation is defined dominantly by biotite, minor sulphides and hornblende (Fig. 4.11).

Core logging and 2-D cross-section interpretations indicate the lateral continuity of the garnet-biotite schist, while also highlighting the variability in thickness throughout the property. Core logging has also identified multiple layers of the garnet-biotite schist separated by quartzofeldspathic gneiss and amphibolite units.

Figure 4.11. A) Fine- to medium-grained garnet-biotite schist with moderate foliation. B) Fine- to medium-grained biotite schist with a moderate to strong fabric defined by biotite and sulphide (pyrite and pyrrhotite) stringers. C) Strongly foliated garnet-biotite schist with biotite-rich melanosomes, quartzofeldspathic leucosomes and coarse garnet porphyroclasts.

Gneissosity is common within the biotite schist, characterized by quartz-rich and garnet-biotite-rich gneissic banding observed in core (Fig. 4.12). Biotite comprises between 20 to 50 modal percentage of the unit and grainsize can vary from fine- to coarse-grained. Correlations between biotite grainsize and foliation have been identified; fine- to medium-grained biotite commonly defines a strong foliation while local coarse-grained, biotite-rich sections display weak to no foliation. When the garnet-biotite schist unit displays a weak foliation, the biotite is randomly oriented and chaotic suggesting localized low strain. Garnet porphyroblasts vary in size and modal

abundance. Garnet is anhedral to subhedral, fine- to very coarse-grained and appears red in colour. Garnet observed on the outcrop and in core can occur as stringers aligned parallel to dominant foliation or as randomly disseminated grains throughout the unit. Biotite commonly forms a complete or partial corona around the garnet crystals with some occurrences of biotite forming asymmetric tails. The strain shadows adjacent to the garnet commonly have increased quartz content or sulphide mineralization. The garnet presumably grew as porphyroblasts, although within the strongly foliated garnet-biotite schist unit, the garnet is often observed to be subhedral to anhedral. The diminution of the crystal shape, abundant internal fractures and setting within a strongly foliated groundmass suggest that deformation occurred during and after garnet growth. The strong foliation of surrounding groundmass is deflected around the garnet, suggesting that the competent garnet behaved as a porphyroclast during subsequent ductile deformation.

Garnet-biotite schist in Figure 4.12A displays a weak gneissosity with biotite- and garnet-rich melanosomes and quartzofeldspathic leucosomes. Parallel alignment of biotite defines a strong foliation of the overall unit. Figure 4.12B displays coarse sillimanite grains in massive garnet-biotite schist.

Figure 4.12. A) Strongly foliated garnet-biotite schist with coarse garnet porphyroclasts. B) Massive sillimanite-garnet-biotite schist with coarse sillimanite in a finer-grained groundmass of garnet, biotite, quartz and feldspar.

Reassessment of core, conducted during summer fieldwork, provided an opportunity to rename Borden lithologies with consistent metamorphic lithological nomenclature as well as careful structural interpretation. These logs were then digitized to produce 2-D cross-sections for each section line perpendicular to the length of known mineralization. Section line 50m SE (Fig. 4.13) best exemplifies the variable thickness and repetition of the garnet-biotite schist. It also highlights the close association between gold mineralization and the garnet-biotite schist unit.

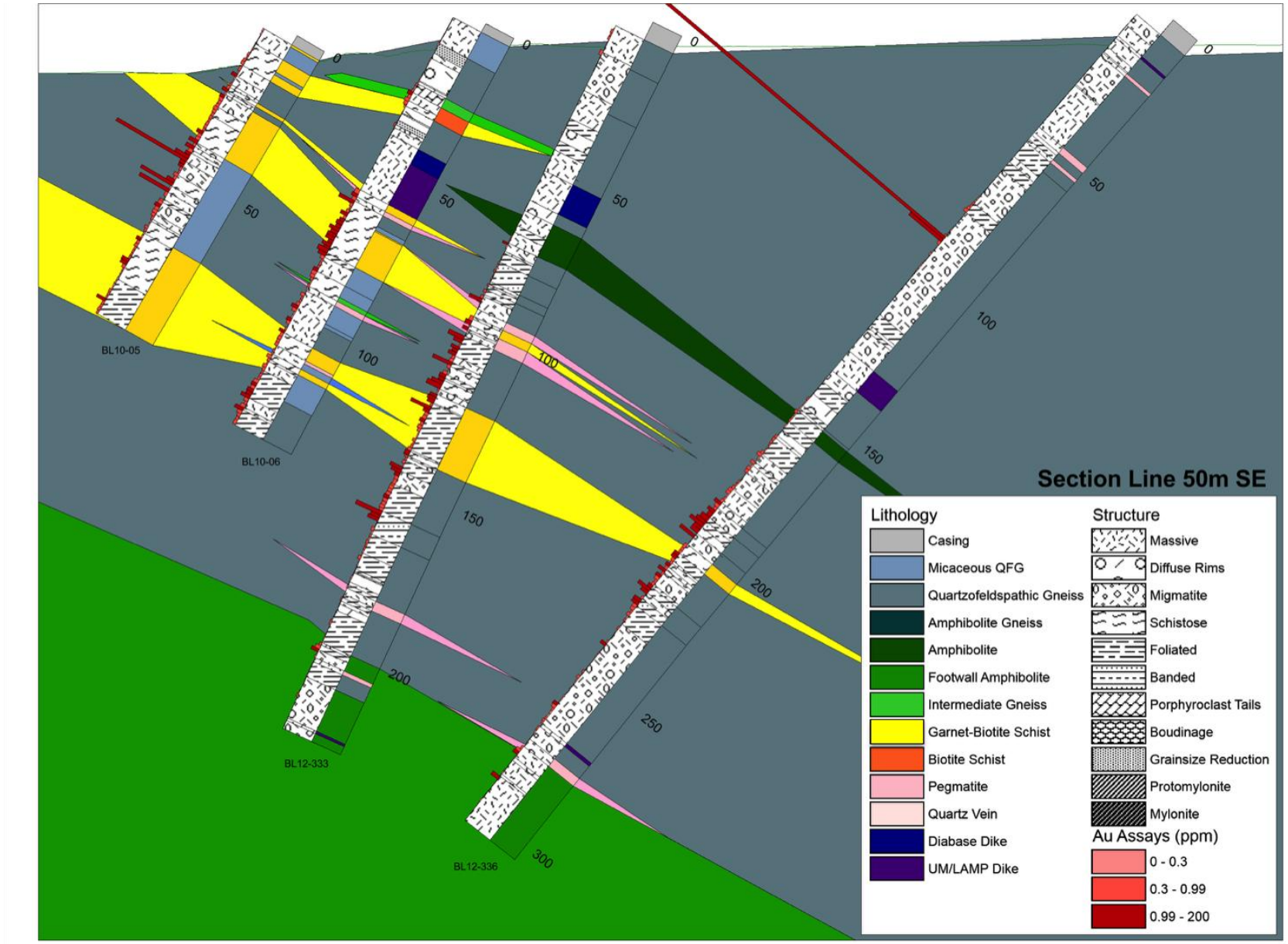

Figure 4.13. Section line 50m SE 2-D cross section. Drill hole azimuths at 205°. Lithological and structural interpretation compiled during summer field research in 2014.

From the 2-D interpretation of section line 50m SE, a notable feature of the garnet-biotite schist unit is the anastomosing continuity between large blocks of biotite-quartzofeldspathic gneiss. The foliated garnet-biotite schist appears to be ductilely deforming around the competent biotite-quartzofeldspathic gneiss unit. The pinched necks of the garnet-biotite schist appear to preferentially host pegmatitic and migmatitic quartzofeldspathic gneiss units. This lithological relationship appears to be a favorable location for gold mineralization as well as an important exploration indicator.

The garnet-biotite schist (±sillimanite) is typically composed of biotite, quartz, plagioclase, potassium feldspar, garnet, sillimanite and cordierite with accessory minerals magnetite and zircon. Other opaque minerals were identified as gold, pyrite, and pyrrhotite.

Biotite comprises a dominant modal proportion of the unit ranging between 20% to 50% and grainsize can also vary from fine- to coarse-grained. Biotite is euhedral with yellow-brown pleochroism and second order birefringence in transmitted light. When present in high modal proportion of 35% to 50%, the biotite fabric has a schistose texture and coarse grainsize. A coarse-grained and chaotic biotite texture is common where in contact with pegmatite, quartz veins or quartzofeldspathic gneiss units. Where biotite has lower modal proportion between 20% to 35%, the fabric displays a strong foliation, with fine- to medium-grainsize and within an equigranular quartzofeldspathic groundmass.

The quartz grains (10% to 30%) throughout the unit consistently have undulose extinction and subgrains. Quartz and K-feldspar grains are anhedral, fine- to medium-

grained and occur in millimetre- to centimetre-scale bands parallel to foliation or less commonly as boudinaged blebs. In thin section, K-feldspar (5% to 10%) grains were observed to be poikiloblastic with abundant inclusions and irregular growth habit between quartz and biotite. Plagioclase was observed in a majority of samples and occurred in variable percentages (5% to 15%). Plagioclase is anhedral and shows albite twinning; undulose extinction and subgrain formation are evidence of ductile deformation. Zircon was identified commonly in groundmass biotite and within biotite inclusions in garnet.

Garnet is anhedral to subhedral, colourless to pink under plane-polarized light and isotropic under crossed polarized light. The diameter varies in size from 0.1 to 1.5cm and local areas contain increased garnet as tight clusters of 3 to 25 grains. The garnet grains commonly contain inclusions of quartz with minor biotite and comprise 0% to 20% of the modal mineral abundance. Garnet can be observed to have partial or complete biotite corona (Fig. 4.14A).

Sillimanite is observed in petrographic analysis as both fibrolite and coarse sillimanite (Fig. 4.14B,C). Some coarse sillimanite grains can be observed as part of large lithons surrounded by strongly foliated biotite. The fibrolite occurs as small grains on quartz and mica. Fibrolite grows as small clusters of needles in a fan shape.

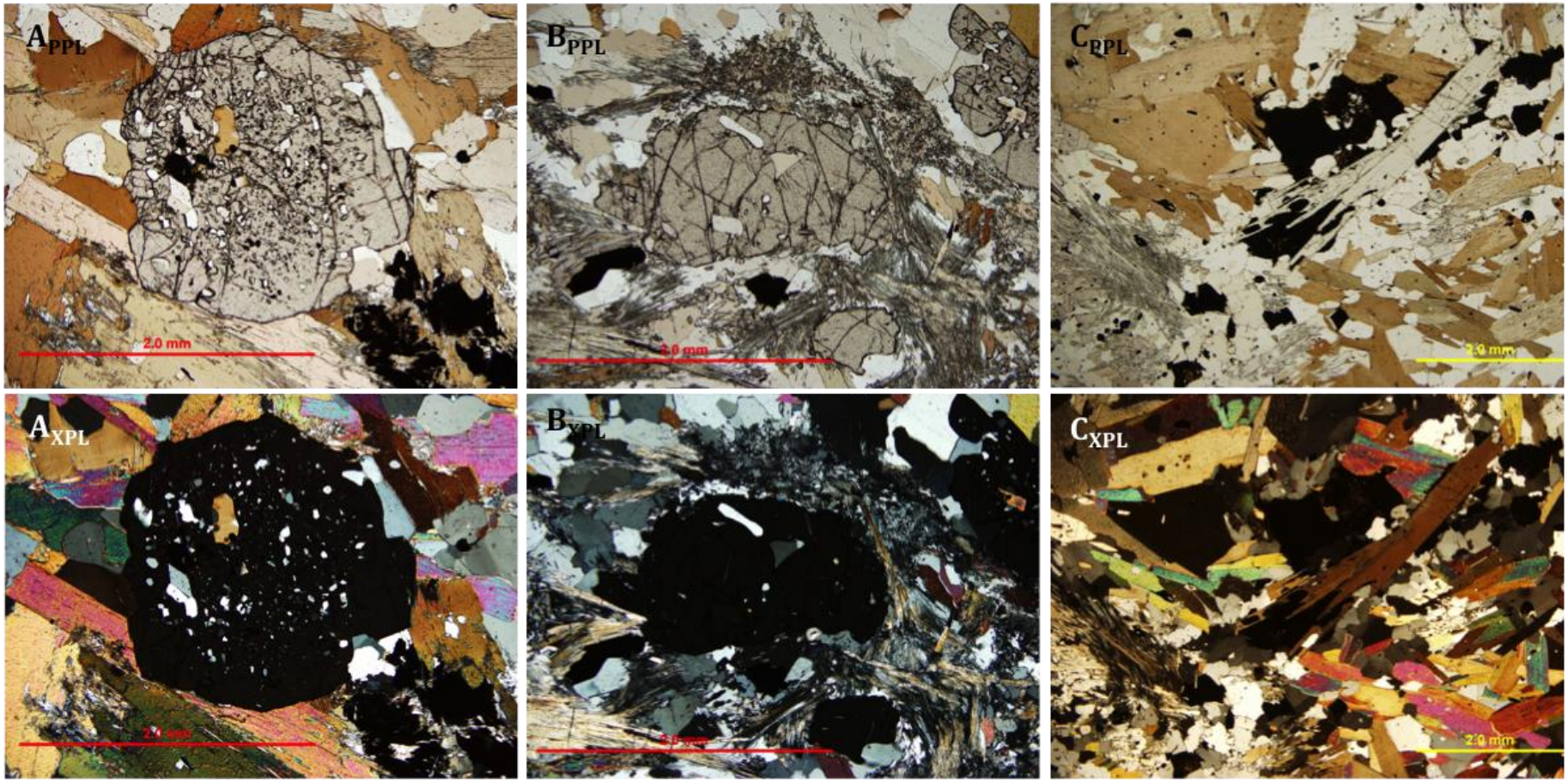

Figure 4.14. A) Garnet porphyroblast in garnet-biotite schist from sample FD 01340 (117 ppb Au). B) Central garnet porphyroblast surrounded by sillimanite, quartz and biotite from sample FD 01341 (237 ppb Au). C) Coarse sillimanite within a quartz, K-feldspar and biotite groundmass in sample FD 01342 (176 ppb Au).

4.1.1 Garnet Composition

Garnet and biotite compositions were analyzed using the SEM for the purpose of garnet-biotite geothermometry. The analysis provided further information on overall garnet composition and consistency. In thin section, the garnet is subhedral and commonly contains inclusions of quartz and biotite. The inclusions are typically abundant at the garnet core and less abundant at the outer rim of the garnet. Since, the diffusion rate of ions is a function of temperature, inclusions become increasingly rare and more coarse-grained at higher metamorphic grade (upper amphibolite and granulite facies), which could explain the abundance of inclusions at the core of the Borden garnets and relatively inclusion-free rims.

Garnet elemental mapping provides a detailed understanding of the overall garnet composition. SEM spot analysis was taken at intervals across the diameter of each garnet grain capturing the compositions of the rim and core. The overall composition and specifically Fe/Mg ratios of the garnet were consistent from the core to the rim. Unlike the garnet, biotite inclusions and biotite in the groundmass had highly variable compositions. Garnet grains viewed under the SEM are unzoned (Fig. 4.15) and have similar composition in both the garnet-biotite schist and amphibolite units. Garnet grains were individually characterized to end-member compositions from elemental data and the results identified them as dominantly almandine (60 to 70%), with moderate components of pyrope (15%), spessartine (15%) and minor components of andradite (<5%) and grossular (<3%). The specific mineral formula for Borden garnet was determined to be $Fe_2\,Mg_{0.5}\,Mn_{0.4}\,Ca_{0.1}\,Al_2\,(SiO_4)_3$.

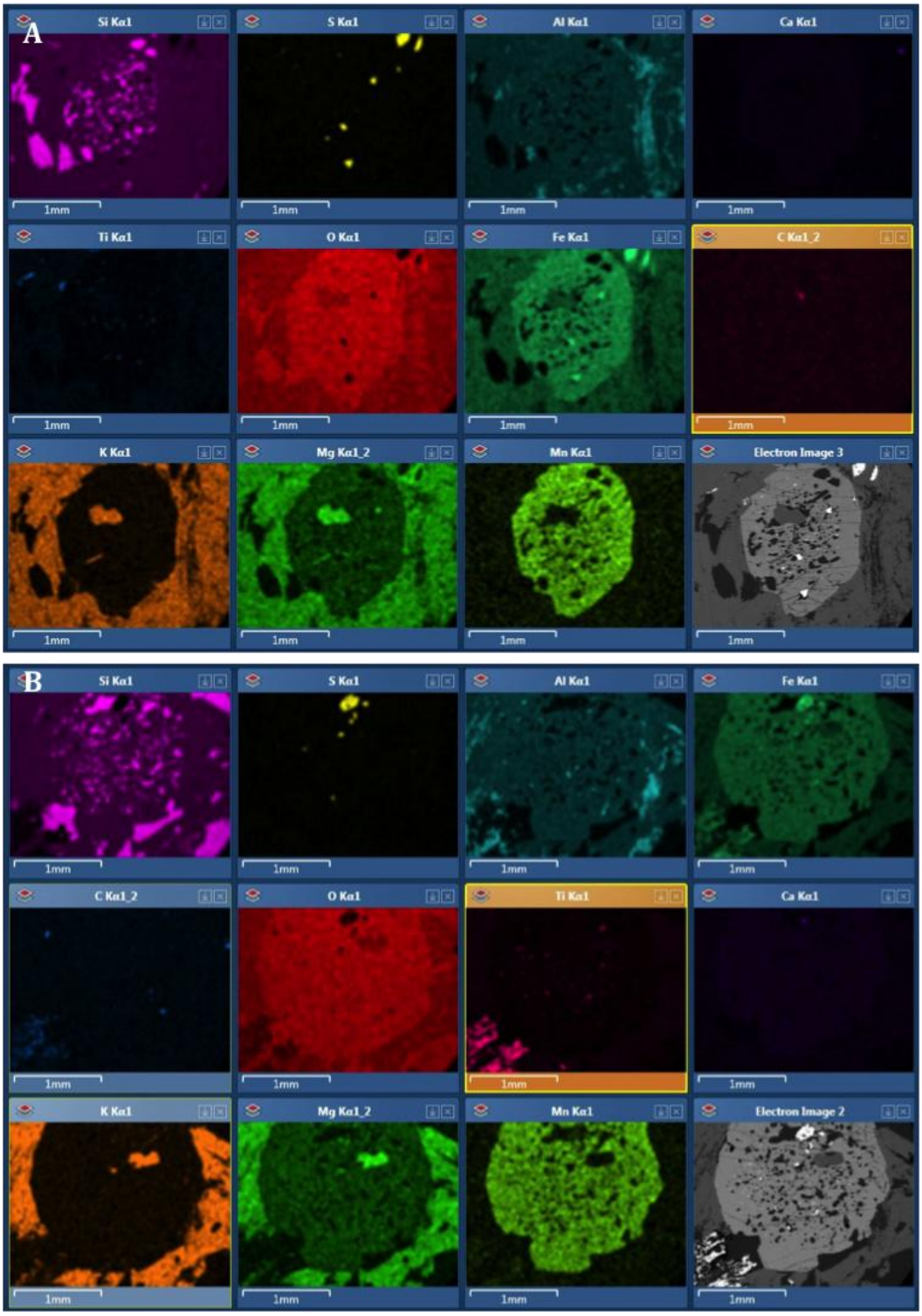

Figure 4.15. A) Elemental maps from sample FD 01340 displaying individual mineral abundances and highlighting its consistent composition from core to rim. B) Elemental maps from sample FD 01341 displaying individual mineral abundances and highlighting its consistent composition from core to rim.

4.2 Amphibolite

Amphibolite is a common unit on the property and displays a variety of textures. Core logging at the Borden gold deposit has historically categorized three separate amphibolite units: amphibolite ± garnet (Fig. 4.16A,B), amphibole felsic gneiss (Fig. 4.16C) and the footwall amphibolite (Fig. 4.16D).

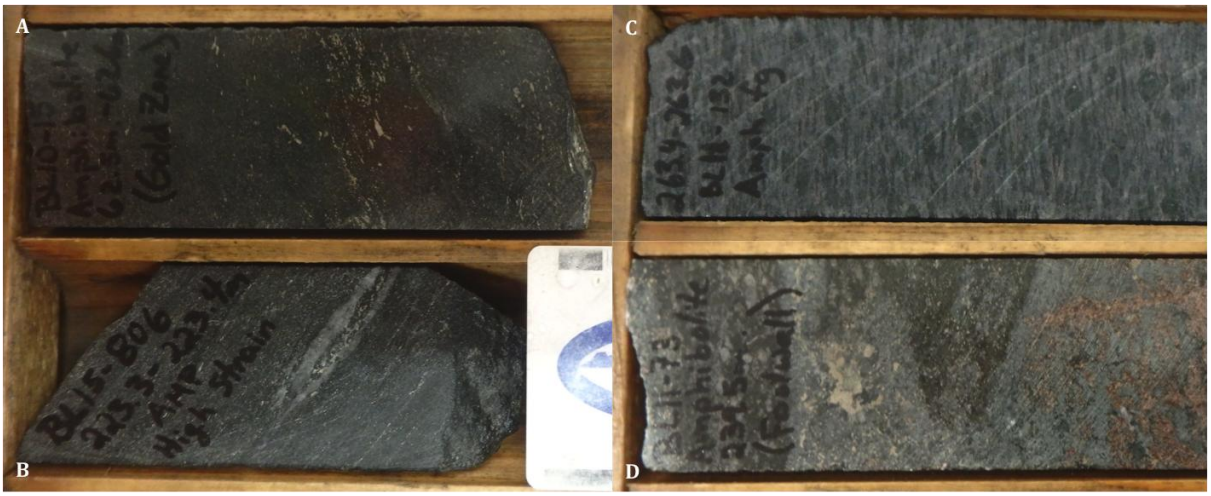

Figure 4.16. A) Massive amphibolite (±garnet) from the gold zone. B) Foliated amphibolite (±garnet) from the gold zone. C) Amphibole felsic gneiss. D) Footwall amphibolite.

Three distinct amphibolite units can be stratigraphically characterized across the entire Borden gold deposit and are expemplified in Section line 700m NW (Fig. 4.17). The "footwall" amphibolite is located below the ore zone and spans the entire deposit. This unit typically displays lower strain and a true granulite facies mineral assemblage including orthopyroxene, clinopyroxene, plagioclase and garnet. The amphibolite ± garnet is discontinuous and commonly displays high strain. The amphibole felsic gneiss (intermediate gneiss) is consistently barren and crosscuts quartzofeldspathic units. This unit is massive to strongly foliated and contains porphyroblastic pyroxene grains with a complete corona of hornblende.

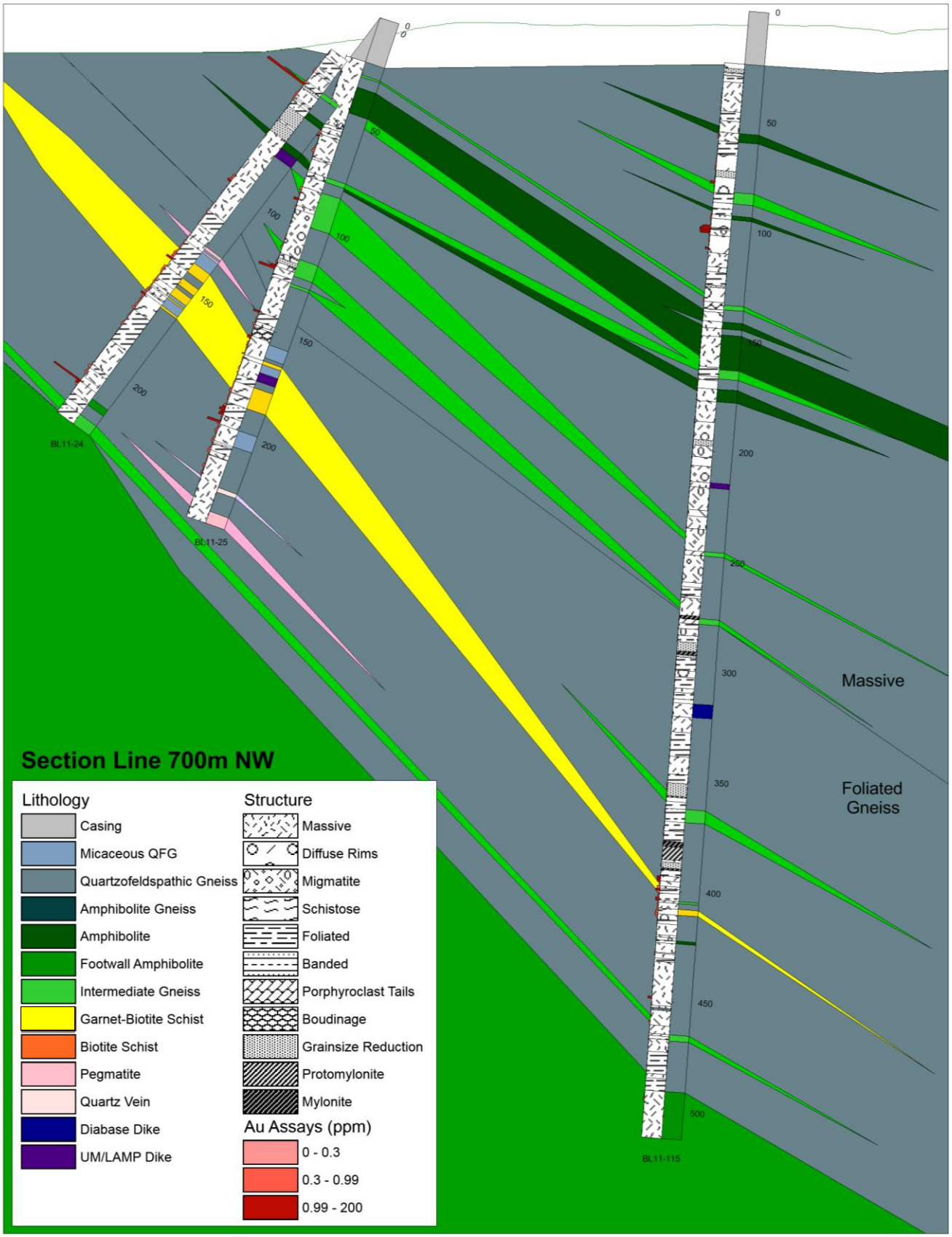

Figure 4.17. Section line 700m NW 2-D cross section. Drill hole azimuths of 180°. Lithological and structural interpretation compiled during summer field research in 2014.

The amphibolite (±garnet) appears in core as a medium-grained, dark green to black rock with variable amounts of patchy, light-coloured felsic blebs. The unit may be massive to weakly foliated indicating lower strain and a more competent rheology. Hornblende ranges from 30 to 80 modal percent with plagioclase ranging from 10% to 25%. Minor amounts of quartz, biotite and garnet can be identified with common occurrences of magnetite. Sulphides are commonly pyrrhotite and pyrite, which may be finely disseminated or in some cases present as stringers parallel to foliation. This unit is the most consistently mineralized of all the amphibolite units (Fig. 4.18).

Figure 4.18. Variation in amphibolite (±garnet) in drill core. A) A fine-grained weak to moderately foliated amphibolite with no garnet. B) Amphibolite from the gold zone, which has a moderate to strong foliation defined by hornblende, sulphides (pyrite and pyrrhotite) and minor biotite. C) Strongly foliated amphibolite with a boudinaged quartz vein.

Quartz occurs in variable modal proportion at 0% to 20%, ranging in grainsize from fine- to coarse-grained. Biotite, where present in a sample, ranges from 5 to 15 modal percent. Garnet occurs as large, anhedral to subhedral crystals and ranges from 1 to 15 modal percent.

Above the ore zone, the unmineralized amphibolite ±garnet is massive and fine- to medium-grained. Mineralogically it contains high modal percentages of hornblende from 40% to 60% and does not typically host quartz or pegmatite veining. The unit is consistently thick, between 3 to 10 metres and has sharp contacts. Transitioning into the ore zone, mineralized amphibolite units typically display moderate to strong foliation defined by hornblende and sulphide minerals (pyrite and pyrrhotite). This foliation is consistent with surrounding quartzofeldspathic gneiss (QFG) contacts and QFG foliation orientation. The amphibolite in this setting is fine-grained and in places has diffuse contacts with a gradual reduction in hornblende content and increased biotite content.

The amphibolite unit can be identified in drillcore by its distinctive melanocratic and leucocratic banding, with a consistent location above the ore zone. These alternating gneissic bands may range in thickness from centimetres to decimetres. The leucosomes are fine- to medium-grained, quartz- and feldspar-rich with minor hornblende (1% to 10%) while the melanosomes are fine- to medium-grained and hornblende-rich (60% to 80%) with feldspar (10% to 20%) and minor quartz (1% to 5%). The overall strong banding indicates moderate to high strain.

Some local areas within melanosomes contain small lithons or blebs of pyroxene, medium- to coarse-grained and massive in texture. The pyroxene grains occur in clusters and commonly have a reaction-rim corona of hornblende.

Dominantly, the amphibolite (± garnet) unit, associated with gold mineralization, is composed of euhedral hornblende within a plagioclase groundmass with minor quartz and biotite. The unit commonly exhibits a moderate to strong foliation but can also display an overall massive texture. Thin sections obtained from core samples show a general mineral assemblage of hornblende, pyroxenes and plagioclase ± quartz, biotite, microcline, carbonates and garnet, with titanite and zircon present as accessory minerals. Opaque minerals were identified as gold, pyrite and pyrrhotite with trace occurrences of magnetite. Hornblende occurs as subhedral to euhedral crystals of varying sizes with modal percentages between 30 to 80. It is commonly green, but ranges from bluish-green to yellow in thin section.

Plagioclase is present in the majority of samples and occurs in variable percentages (10% to 30%). Plagioclase is anhedral and shows albite twinning; undulose extinction and subgrain formation are evidence of ductile deformation. The Michel-Levy method was used to determine anorthite content, although some crystals were too deformed to display twinning. Suitable twinned grains yielded a range of An_{19} to An_{40} with an average of An_{30}, indicating oligoclase composition. In many samples the plagioclase is partially to almost completely altered to fine-grained sericite. Microcline is less common, although when present, it is in great abundance. It occurs as medium- to coarse-grained anhedral grains and displays characteristic tartan twinning. Quartz occurs in variable percentages (0% to 20%), ranging in grainsize

from fine- to coarse-grained. Anhedral quartz crystals commonly display undulose extinction, subgrain formation and grain boundary area reduction. Biotite is present and occurs as individual grains as well as subhedral to anhedral books. Where biotite is present in the sample it ranges in modal proportion from 5% to 15%. If there is a foliation defined by hornblende, the biotite will be aligned parallel to dominant foliation. Carbonate minerals occur in trace amounts as anhedral crystals of varying size. In some of the samples carbonate also appears commonly as discontinuous veinlets in the host rock. Garnet occurs as large, anhedral to subhedral crystals (1% to 15%) and commonly contains inclusions of quartz and in some cases biotite, with common microfractures. Titanite crystals appear as subhedral, rounded diamond-shaped crystals commonly found in pods, and also present disseminated throughout the amphibolite. Zircon occurs commonly as inclusions in biotite and hornblende crystals.

Clinopyroxene is present in the majority of samples in variable percentages (10% to 45%). It occurs as both large, subhedral crystals with inclusions and fractures and as small rounded crystals, less commonly together within the same thin section.

Orthopyroxene was also observed, but in smaller percentages and in fewer samples. Crystals of orthopyroxene are euhedral, blocky, and fractured. They occur in clusters and are possibly fragments of a larger crystal that was replaced at grain boundaries leaving relict euhedral grains defining old cleavage planes.

Relict mineral vestiges and lithons consisting of clinopyroxene, orthopyroxene, K-feldspar and garnet are typical of the granulite facies metamorphism. Hornblende grains are commonly observed to be in clean contact with the clinopyroxene and

orthopyroxene. The amphibolite commonly contains plagioclase and garnet representing the characteristic mineral assemblage for amphibolite facies metamorphism. The amphibolite facies mineral euhedral hornblende typically defines a moderate to strong foliation with a sharp discordant contact to the massive granulite facies pyroxenes. The relationship between the euhedral, strongly foliated hornblende grains surrounding orthopyroxene and clinopyroxene is a common microstructural feature in amphibolite at Borden (Fig. 4.19).

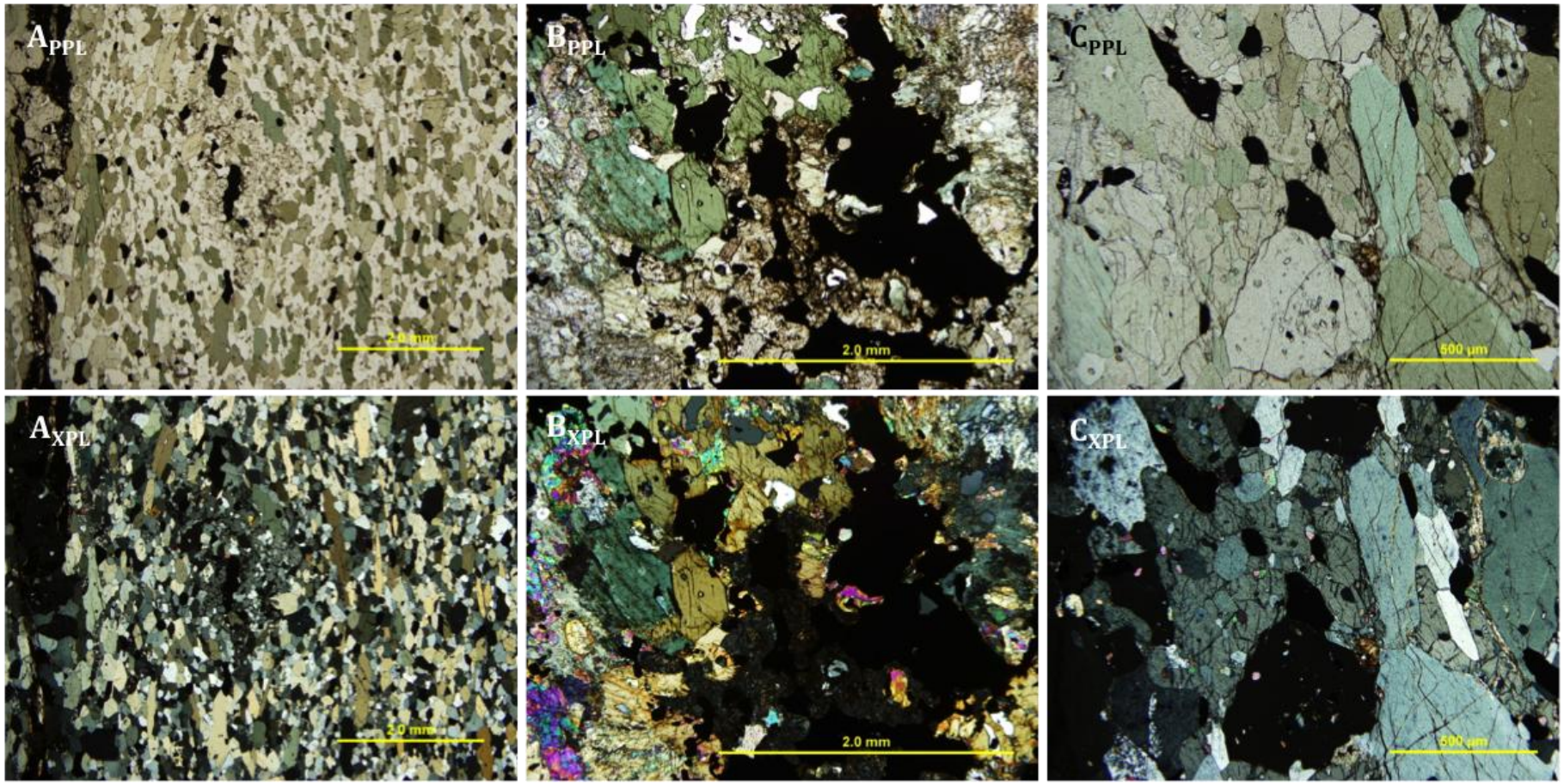

Figure 4.19. A) Amphibolite with euhedral hornblende replacing a central orthopyroxene (central grey mineral in XPL) from sample FD 01322 (511 ppb Au). B) Amphibolite with subhedral hornblende replacing clinopyroxene (purple in XPL) from sample FD 01307 (654 ppb Au). C) Garnet-amphibolite with subhedral hornblende (green) and garnet (isotropic in XPL) from sample FD 01322 (511 ppb Au).

Amphibolite samples from above the gold zone generally contain higher percentages of hornblende than the other zones (40% to 85%) with generally low percentages of quartz (<1% to 20%). Opaque minerals appear in either very low (<1%) quantities. Within the gold zone, samples show higher percentages of opaque minerals (1% to 5%). Quartz is consistently present with content ranging from 5% to 30%, while hornblende content is 15% to 40% in the majority of samples. Samples from below the gold zone consistently have higher percentages of pyroxene (10% to 45%) than those from other zones. Hornblende content is generally 20% to 30% and quartz content is low (0% to 5%). The most common gold-bearing unit is the amphibolite ± garnet, which contains minor amounts of quartz and biotite. These mineralized units are commonly adjacent to the garnet-biotite schist unit and occasionally interlayered with it. Minor alteration is common as chlorite replacement at grain boundaries of hornblende and less commonly as sericite alteration of plagioclase grains at the core and along the grain boundaries.

The amphibole felsic gneiss has a massive to moderately foliated texture, identified by pyroxene porphyroclasts and hornblende coronas that define a lineation. The modal proportions of amphibole range between 25% to 50% and biotite between 10% to 30%. The felsic groundmass is composed dominantly of fine-grained feldspar with modal proportions of 30% to 40% and fine-grained quartz between 10% to 20%.

Massive amphibole felsic gneiss commonly has high hornblende content with low biotite proportions and reduced quartzofeldspathic groundmass. As foliation increases in the unit, the biotite modal composition increases as well as the quartzofeldspathic groundmass. Biotite forms partial to complete coronas around hornblende

porphyroblasts within the unit. Typically, strongly foliated units also have complete coronas of biotite surrounding the hornblende porphyroblasts. The textural variation within this unit is a marker for strain and deformation at the Borden gold deposit (Fig. 4.20).

Figure 4.20. Core samples of amphibole felsic gneiss. The two core samples on the right display a massive texture with porphyroblastic amphibole grains within a felsic groundmass. Core samples in the center and to the left display an increasing foliation defined by amphibole and biotite porphyroclast tails.

The "footwall" amphibolite is identifiable by distinctive, pervasive, patchy white to light-green alteration (Fig. 4.21). The unit has been renamed under the IUGS metamorphic classification (Fettes and Desmons, 2007) as a granulite and consistently contains negligible amounts of gold except for a gold spike present within 1 to 2 metres of the deposit-scale contact to the overlying quartzofeldspathic gneiss or garnet-biotite

schist. Confirmation of the granulite grade metamorphism is based on the presence of orthopyroxene, clinopyroxene, plagioclase and garnet. The massive texture has a "soupy" or migmatitic appearance and in rare occurrences has a weak foliation of the mafic zones. Evidence of later overprinting by amphibolite and greenschist facies minerals was observed in thin sections and indicates a substantial degree of retrograde metamorphism. This unit typically has sulphide minerals dominated by pyrrhotite and less commonly pyrite.

Figure 4.21. Variations in "footwall" amphibolite, consistently barren and composed of clinopyroxene, orthopyroxene, garnet and plagioclase.

Below the ore zone in the northwestern portion of the deposit, the "footwall" amphibolite has a consistent thickness between 15 to 30 metres. Beneath the ore zone

in the east (east of section line 1400m SE), the footwall amphibolite begins to taper and alternates with layers of quartzofeldspathic gneiss between 1 to 5 metres thick.

4.3 Quartzofeldspathic Gneiss

The quartzofeldspathic gneiss (QFG) is the unit with the most variety in texture and composition. It is present in all areas of the Borden gold property. In previous core logging procedures, the QFG has been referred to as "felsic gneiss (S)" and "diorite". Detailed thin section analysis and metamorphic classification under the IUGS nomenclature (Eds. Fettes and Desmons, 2007) suggest the name quartzofeldspathic gneiss or biotite-QFG. Modal abundance and dominant mineral assemblage in the QFG is quartz (20% to 40%), plagioclase feldspar (25% to 55%) and biotite (3% to 20%). Accessory minerals such as garnet (0% to 5%), muscovite (0% to 5%), hornblende (0% to 15%), pyroxenes (0% to 5%), magnetite (0% to 5%), and the sulphides pyrite and pyrrhotite (<0.5%) are also common. These lithologies generally have similar compositional groundmass with varying amounts of accessory minerals and sulphides. The most significant difference is the textures that the minerals define giving them different appearances in core (Fig. 4.22). These variations in texture may reflect strain intensities and rheology of the unit.

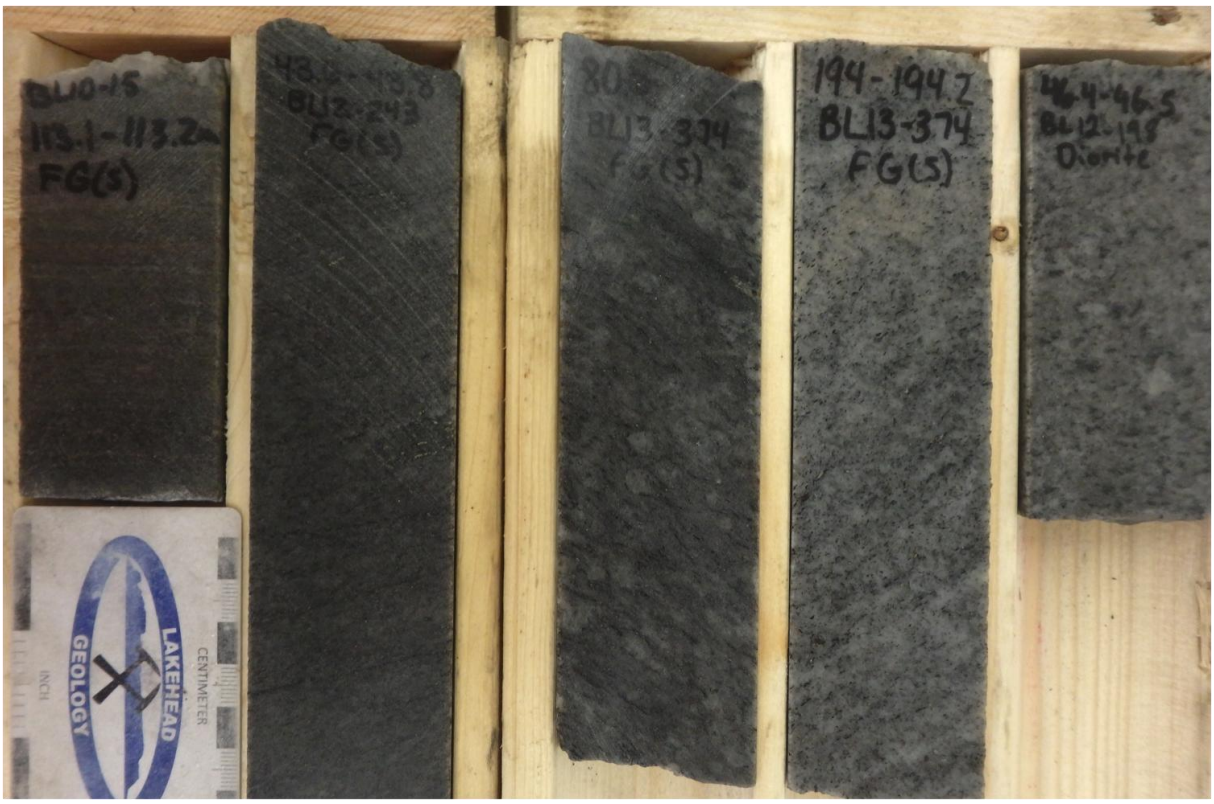

Figure 4.22. Textural variation in the quartzofeldspathic gneiss, increasing strain from massive texture (right) to strong foliation (left).

The relative modal abundance of accessory minerals is typically reflected in the overall texture of the unit. Low accessory mineral content, particularly biotite and hornblende, leave the dominant mineral abundance to be quartz and feldspar. This unit displays massive to recrystallized texture with an overall coarse to very coarse grainsize. Quartz eyes are common as well as local sections of blebby very coarse-grained quartzofeldspathic material surrounded by medium- to coarse-grained quartzofeldspathic material.

Massive, migmatitic and weakly foliated quartzofeldspathic gneiss is the dominant unit above the ore zone. Typically, pyrite is the most common sulphide, less than 0.5% and pyrrhotite is negligible to less than 0.1%. Magnetite is the most

common oxide mineral and can be identified as fine- to coarse-grained surrounded by quartz.

As biotite modal abundance increases to between 5% and 10%, the foliation becomes weak to moderate. Foliation is defined by biotite grains and minor hornblende (0% to 3%), which can be disseminated throughout the coarse-grained quartzofeldspathic groundmass and also around quartz eyes.

Units with higher biotite content, between 10% to 20%, often display moderate to strong foliation and grainsize is typically fine- to medium-grained. This texture is more common in core logging when progressing into the ore zone where increased strain is identified. At the margins of quartz veins, pegmatites and amphibolite units the biotite content is more abundant relative to the presence in the remainder of the unit. Contacts between QFG and garnet-biotite schists are often gradational contacts with a gradual increase in biotite over 0.2 to 1m margins. The garnet-biotite unit is typically differentiated by the presence of aluminous metamorphic minerals such as garnet or sillimanite. Section line 150m NW effectively displays the change in strain defined by biotite content and subsequent foliation strength (Fig. 4.23).

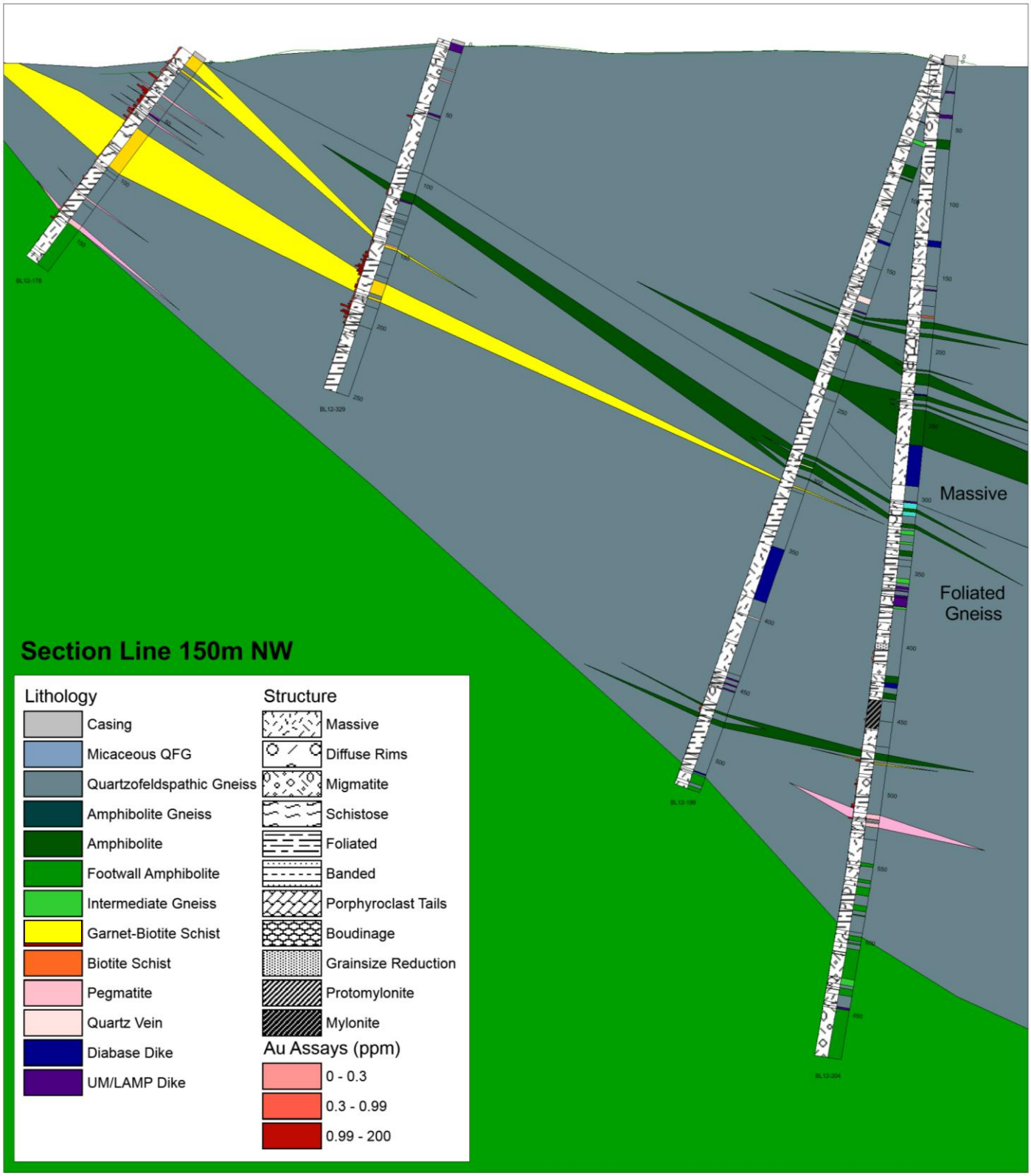

Figure 4.23. Section line 150m NW 2-D cross-section. Drill hole azimuths of 190° (BL12-199, BL12-204) and 205° (BL12-178, BL12-329). Lithological and structural interpretation compiled during summer field research in 2014.

During core logging, a consistent pattern of increased foliation downhole was noticed. Strongly foliated units would become thicker and more frequently spaced between unfoliated units within the ore zone. Above the ore zone, biotite-quartzofeldspathic gneiss displays a low-strain, massive and migmatitic texture. The biotite is less abundant and randomly oriented. Mineralized lithologies and surrounding rocks display high strain with strong foliation and mylonitic fabric. This strain progression is carefully observed in drill core reassessment and the overall increase in strain approaching the ore zone is consistent. This strain progression is confirmed in the summary and interpretation of results from core reassessment. Gold mineralization seems to be generally associated with strongly foliated, banded and schistose textures in units, as observed in the 2-D cross-section interpretations.

Microstructural analysis of the quartzofeldspathic gneiss unit further illustrates the wide variety in texture. The general mineral assemblage is relatively consistent, although grainsize and fabric intensity gives this lithology different appearance in core.

Quartz ranges in grainsize from fine- to coarse-grained. Anhedral crystals commonly display undulose extinction, subgrains and smooth grain boundaries due to grain boundary area reduction. Plagioclase is observed in a majority of samples and occurs in variable percentages (15% to 25%). Crystals of plagioclase are anhedral and show albite twinning; undulose extinction and subgrains are evidence of ductile deformation. In some samples the plagioclase is partially to almost completely altered to fine-grained sericite. Microcline is less common, occurring as medium to coarse-grained anhedral crystals, and displays characteristic tartan twinning.

Within the quartzofeldspathic gneiss, the massive, medium- to coarse-grained, "sugary" or granular texture of the quartz and feldspar is most common and typically does not contain gold mineralization. Straight grain boundaries tend to meet at triple junctions at angles of 120˚ (Fig. 4.24A). Some local patchy or blebby zones of coarse-grained quartz and feldspar with occurrences of biotite and hornblende may represent undeformed sections of quartzofeldspathic gneiss. These undeformed zones of quartzofeldspathic gneiss contain increased biotite, minor pyroxene and fibrolite, surrounded by the quartzofeldspathic groundmass (Fig. 4.24E).

In hand sample, fine- to medium-grained QFG appears dark grey and massive but at a closer look it displays a preferred orientation of the biotite crystals (Fig. 4.24B,C,D). The fine grainsize and strong foliation indicate high strain and grainsize reduction by dislocation creep processes. This evidence for ductile deformation is specifically noticeable above the ore zone. In some cases this fine-grainsize represents mylonitic quartzofeldspathic gneiss.

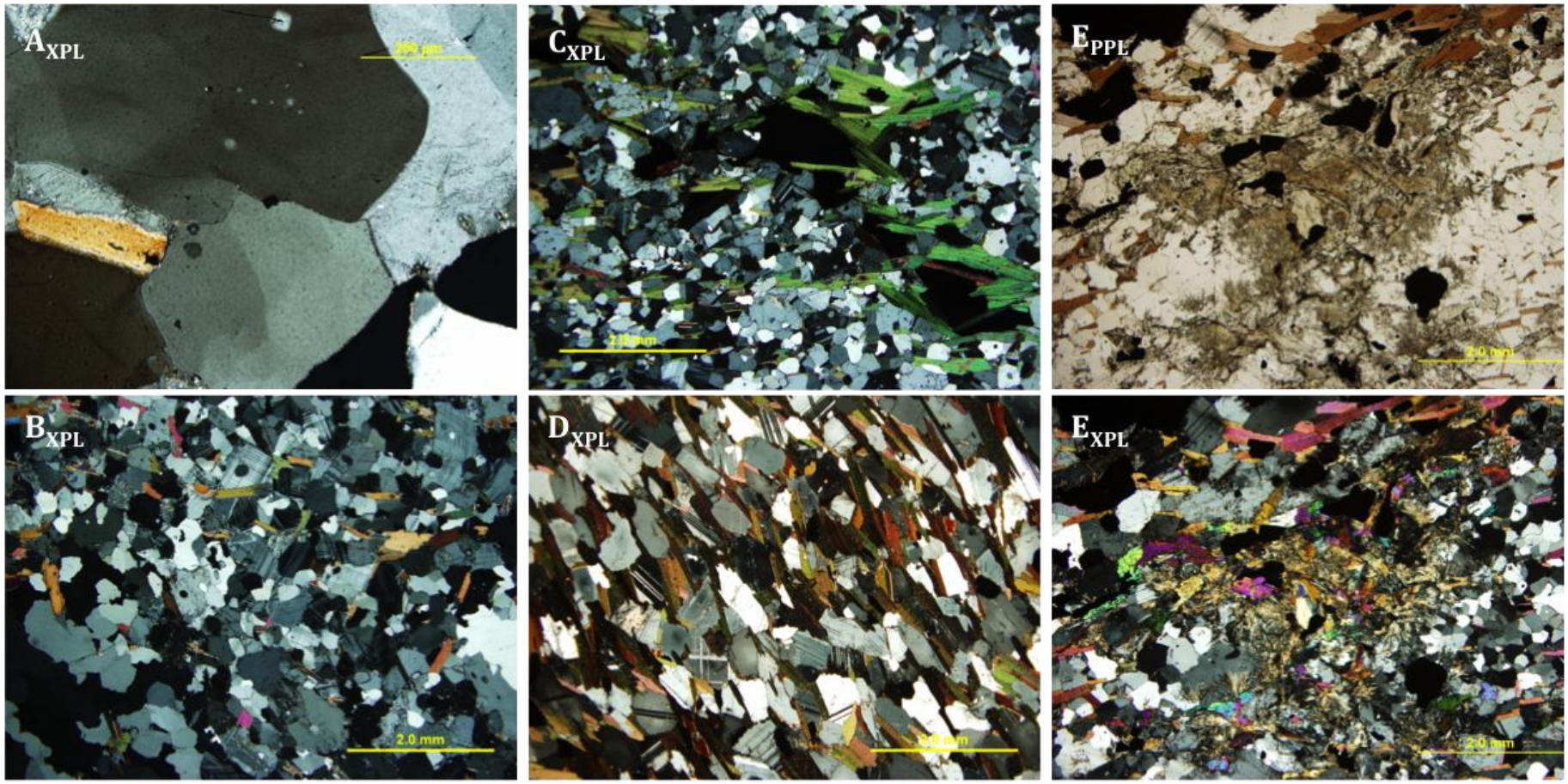

Figure 4.24. A) Quartzofeldspathic gneiss with quartz grain boudnaries at a 120° from sample BL 10-09 (111.5m) (1194 ppb Au). B) Massive quartzofeldspathic gneiss with randomly oriented biotite from sample FD 01305 (30 ppb Au). C) Moderately foliated quartzofeldspathic gneiss coarse-grained biotite surrounding sulphides from sample FD 01303A (127 ppb Au). D) Strongly foliated quartzofeldspathic gneiss with fine- to medium-grained quartz, feldspar and biotite from sample FD 01315 (923 ppb Au). E) Massive quartzofeldspathic gneiss with minor pyroxene and biotite within a quartz and feldspar groundmass from sample BL12-161 (61.5m) (386 ppb Au).

4.4 Pegmatite

The pegmatite on the Borden property is a minor unit and although it has been identified proximal to mineralization in adjacent units it rarely hosts economic concentrations of gold when undeformed. Pegmatite is typically composed of very coarse-grained quartz, feldspar, ±biotite, ±muscovite (Fig. 4.25). Rare pegmatites have euhedral magnetite grains visible to the naked eye. Sulphides, pyrite and pyrrhotite, are typically minor (<2%) in the pegmatite unit. The unit ranges from centimetre-scale veinlets to large dikes up to 3m, with sharp or irregular contacts. The larger dikes typically strike parallel to the foliation of adjacent lithologies. Field relationships indicate that some pegmatites may have resulted from partial melting during granulite facies metamorphism, with small splay veins parallel to foliation in adjacent units.

Figure 4.25. A) Coarse-grained, undeformed pegmatite. B) Strongly deformed pegmatite with increased biotite and grainsize reduction of quartz and feldspar.

Pegmatite veins are more abundant proximal to the ore zone and typically display increased deformation along their margins. Deformed pegmatite veins occur parallel to dominant foliation and have diffuse contacts to surrounding host rock. Section line 500m SE displays prominent pegmatite veins at the margins of the ore zone between garnet-biotite schist units and quartzofeldspathic gneiss (Fig. 4.26).

Undeformed pegmatite units do not contain gold mineralization. Deformed pegmatite, aligned parallel to surrounding host rock foliation does host low-grade gold mineralization on the gradational contacts to surrounding mineralized host rock. Increased mineralization has been identified at the contact between pegmatite and adjacent garnet-biotite schist or amphibolite units.

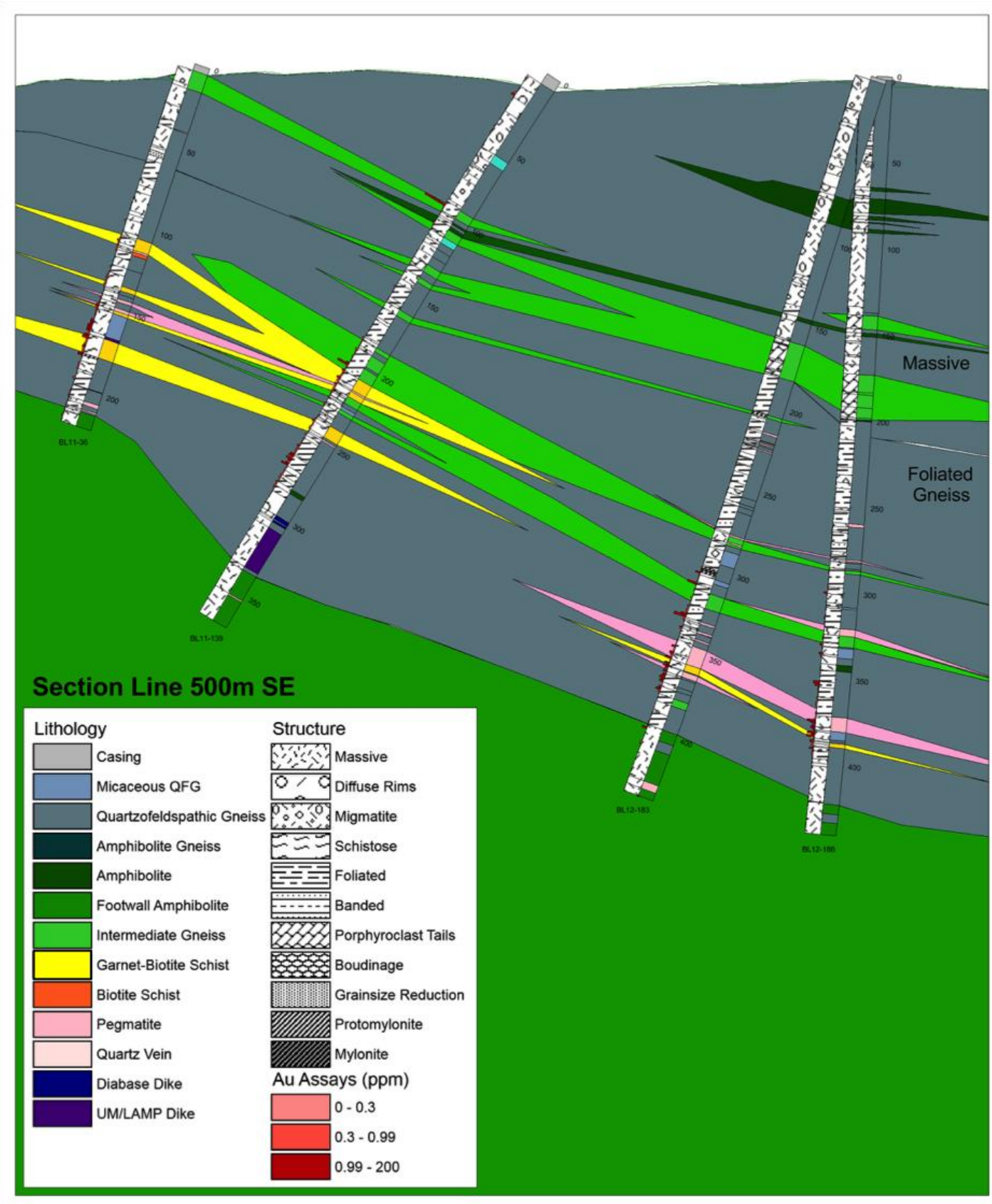

Figure 4.26. Section line 500m SE 2-D cross section. Drill hole azimuths of 205°. Lithological and structural interpretation compiled during summer field research in 2014.

4.5 Quartz Veins

Quartz veins in the Borden lithologies appear highly variable. Unstrained lithologies with no foliation contain fewer quartz veins. When present in unstrained lithologies, the quartz veins do not display strong deformation features. Undeformed quartz veins have milky white colour, coarse grainsize and sharp contacts. The unstrained lithologies and quartz veins contain barren to subeconomic gold concentrations with minor sulphide mineralization.

Mineralized lithologies display strong foliation and also contain more abundant quartz veins than unstrained units. Quartz veins in mineralized lithologies are oriented parallel to dominant foliation and some are boudinaged. These veins have a grey to blue hue with irregular contact boundaries and may have abundant coarse-grained biotite at the margin (Fig. 4.27). Microstructural analysis of the high-grade zone quartz veins reveals prominent evidence for ductile deformation including undulose extinction, subgrain formation and deformation lamellae.

In the northwestern portion of the deposit, the quartz veins do not host gold mineralization. In the southeastern mineralized zone at depth, highly deformed quartz veins display recrystallized quartz with minor inclusions of host lithology minerals and visible gold with no sulphide association. The deformed quartz veins associated with this section of the ore zone are commonly logged by drill geologists at Borden as "siliceous alteration" or "quartz flooding". Quartz veins associated with the ore zone in the southeastern section are up to 10 metres thick and not laterally continuous. Mineralized quartz veins located in the southeast of the deposit display strong evidence for ductile deformation.

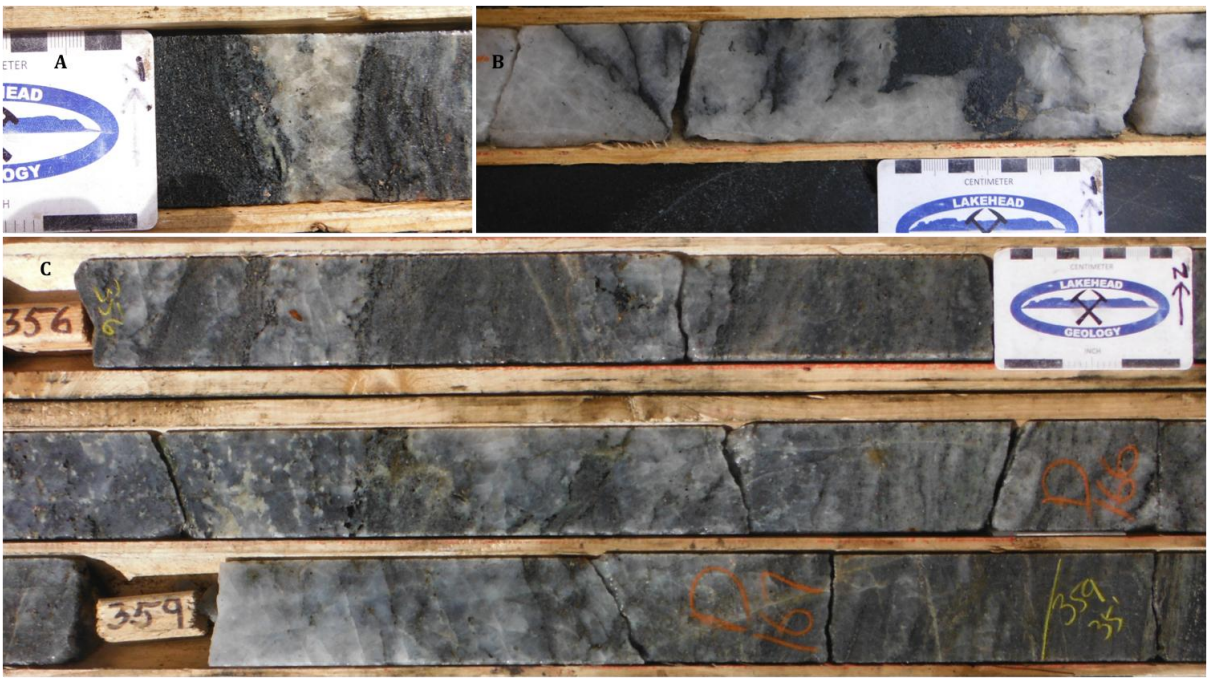

Figure 4.27. A) Deformed quartz vein with moderate pinch and swell structure. B) Weakly mineralized quartz vein with minor deformation and overall unstrained, milky appearance. C) Mineralized, strongly deformed quartz veins with cloudy, grey appearance and inclusions of biotite lithons from host rock.

Deformed quartz veins within the Borden gold zone become prominent in section line 1200m SE. Quartz veins with visible gold showings are specifically associated with the high-grade section of the deposit from section line 1200m SE (Fig. 4.28) and further east. Core logging and assay have identified increased gold concentration at depth within highly-deformed quartz veins. The discontinuous nature of the quartz veins is evident in the 2-D cross-sectional interpretation from core reassessment in section line 1200m SE (Fig. 4.28). A highly-deformed quartz vein hosting high-grade gold mineralization is continuous between section lines along the length of the deposit, although does not appear to have lateral continuity between drill holes.

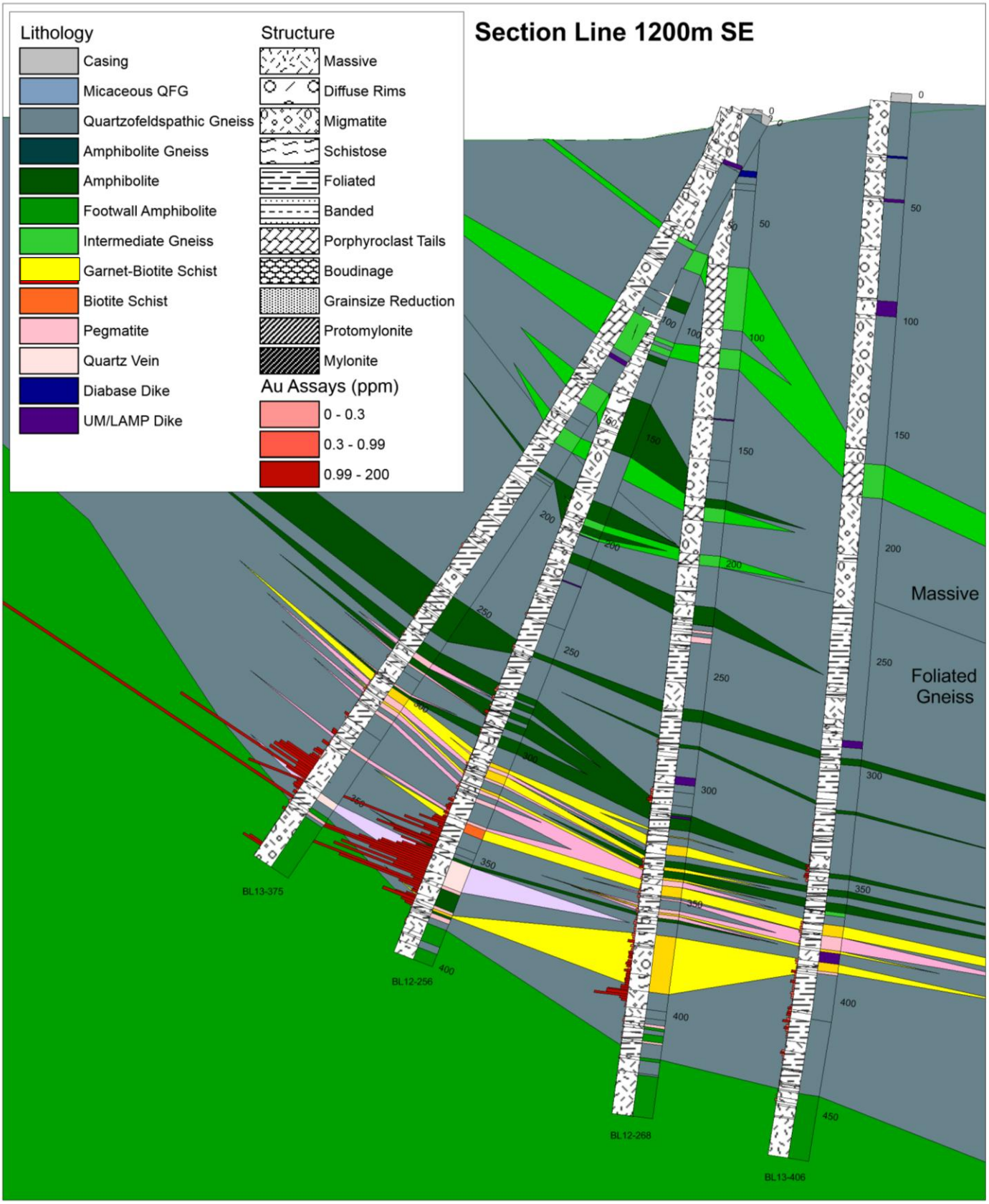

Figure 4.28. Section line 1200m SE 2-D cross section. Drill hole azimuths of 205°. Lithological and structural interpretation compiled during summer field research in 2014.

4.6 Metaconglomerate

The metaconglomerate on the Borden property is a heterolithic, clast-supported unit that displays variable strain. Clast compositions include: felsic (granodioritic), quartzite, mafic (amphibolite) and intermediate (diorite). The matrix is composed of fine-grained quartz, feldspars and mica with minor fine-grained garnet (Fig. 4.29).

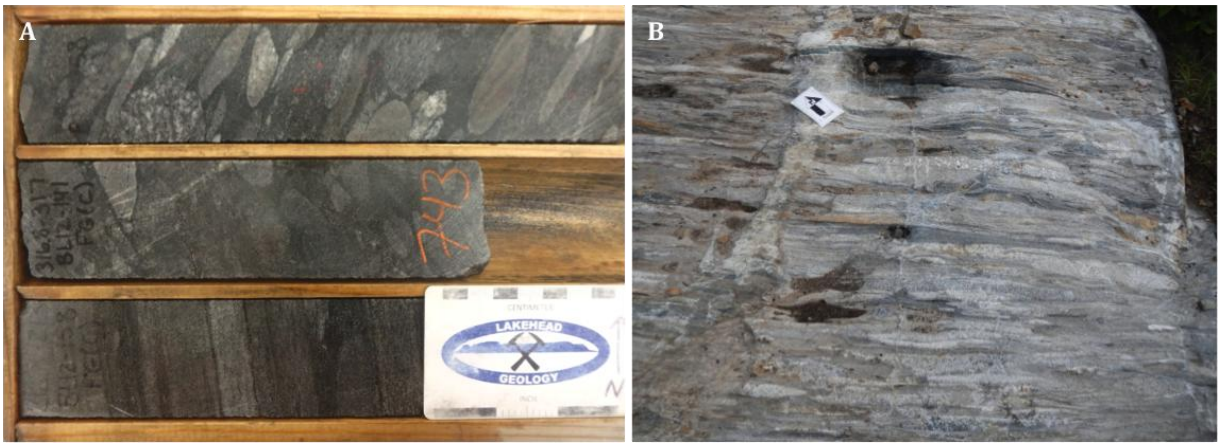

Figure 4.29. A) Variation in strain of the metaconglomerate in drill core. The upper two samples represent a low-strain regime while the lower-most core sample appears gneissic due to the high-strain of the heterogeneous clast composition. B) High-strain metaconglomerate in outcrop (scale card is 15cm).

4.7 Diabase Dike

One diabase dike set has been identified at the Borden gold property, and does not host gold mineralization. One diabase dike can be seen on the Discovery Outcrop. It is massive, fine- to medium-grained and crosscuts the dominant strike of contacts and foliation of units. It is composed of pyroxene and plagioclase with no visible sulphides and is typically weakly to moderately magnetic. Thicknesses range from 3 cm to 30 m. There is commonly a 0.5 to 2 cm chill margin in the dike. The diabase dike has been regarded to be part of the Metachewan dike swarm dated at 2450 Ma (Halls and Davis, 2004).

5. METAMORPHISM

Little historical exploration was undertaken in the Borden area, owing to the high grade of metamorphism. At Borden the most important aspect of metamorphism is the history of retrograde amphibolite facies metamorphism after granulite facies metamorphism.

5.1 Amphibolite Facies Metamorphism

Lithologies on the Borden deposit dominantly display amphibolite facies metamorphism. The diagnostic mineral assemblage in mafic rocks for the amphibolite facies is hornblende, plagioclase (oligoclase to andesine) ± garnet. The amphibolite (±garnet) unit at Borden is composed dominantly of hornblende and plagioclase with minor garnet, clinopyroxene, orthopyroxene, quartz and biotite. Based on whole-rock geochemistry, an ACF diagram was created to plot stable metamorphic mineral assemblages (Fig. 5.30). The samples represented in the ACF diagram represent mineralized amphibolite (±garnet). The samples plot in an expected range for metamorphosed mafic igneous rock and most have the typical metamorphic mineral assemblage of hornblende, plagioclase and garnet.

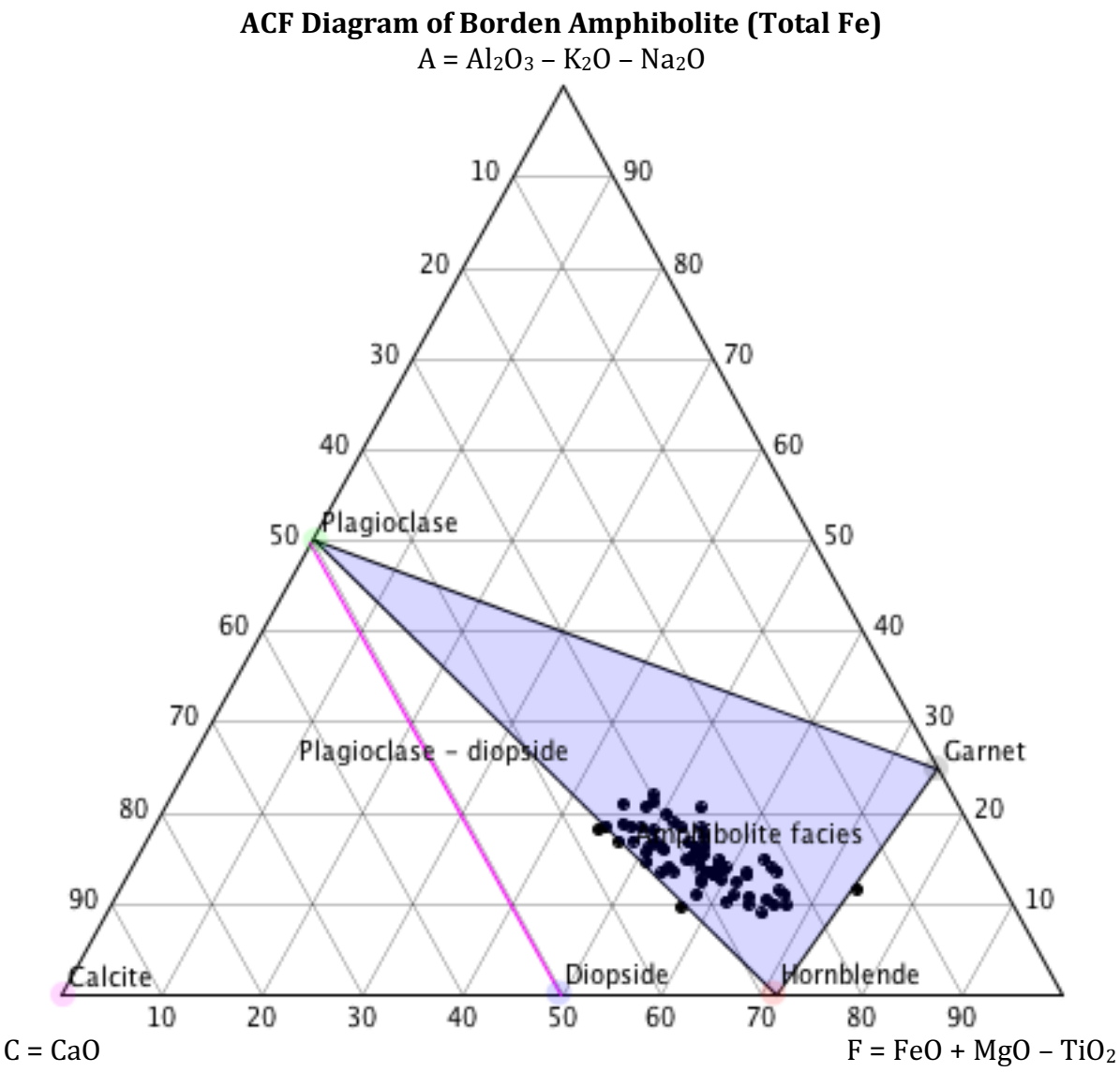

Figure 5.30. ACF compatibility diagram illustrating representative metamorphic mineral assemblages for mafic rocks in the amphibolite facies, shaded in purple. Mineralized amphibolite (±garnet) from Borden drill core geochemistry is plotted as black dots.

Similarly, the garnet-biotite (±sillimanite) schist unit dominantly displays amphibolite facies mineral assemblages. The presence of quartz, feldspar, biotite, almandine garnet, fibrolite and coarse sillimanite are consistent with upper amphibolite facies metamorphism in the Barrovian facies series.

The quartzofeldspathic gneiss is present in all areas of the Borden gold property. High-temperature ductile deformation processes like dislocation creep in feldspar and features such as undulose extinction in quartz are typical of deformation at amphibolite facies metamorphic temperatures or higher.

5.2 Granulite Facies Metamorphism

The Kapuskasing Structural Zone is recognized as a region of granulite facies metamorphic lithologies. Stable granulite facies mineral assemblages and presence of the Shawmere anorthosite are consistent with this distinction. On the Borden property, relict lithons and minerals of the granulite facies are preserved, indicating peak granulite facies metamorphism. The transition from amphibolite to granulite facies metamorphism occurs in the range of 650°C to 850°C.

The critical metamorphic mineral assemblage for granulite facies metamorphism in mafic rocks is orthopyroxene, clinopyroxene, plagioclase, quartz and commonly garnet. The amphibolite (±garnet) unit contains some typical granulite facies metamorphic minerals such as clinopyroxene and orthopyroxene. These minerals are present in low proportions and appear to be metastable relicts of a granulite facies mineral assemblage. Clinopyroxene is present in the majority of mineralized amphibolite samples in low modal abundance. It occurs as both large, subhedral crystals with inclusions and fractures and small anhedral crystals. Orthopyroxene is also observed, but in smaller percentages and in fewer samples. Crystals of orthopyroxene are subhedral, blocky and fractured. They occur in clusters and are possibly fragments of a larger crystal that was replaced at grain boundaries leaving

relict euhedral grains defined by old cleavage planes. The vestiges of granulite facies metamorphism are typically observed as relict pyroxene minerals and microlithons in amphibolite.

The "footwall" amphibolite also preserves the granulite facies mineral assemblage. Samples from the "footwall" amphibolite consistently have higher modal proportions of pyroxene (20% to 45%) than those from mineralized amphibolite. All of the "footwall" amphibolite samples contain K-feldspar and orthopyroxene, and have been classified as granulite. The consistently higher grade of peak metamorphism observed in the "footwall" rocks may have been a detrimental factor in gold mineralization, resulting in the present barren condition.

In metapelitic rocks the granulite facies is characterized by the absence of muscovite and the presence of sillimanite, cordierite, garnet, quartz, K-feldspar and orthopyroxene. The metamorphic reaction of muscovite and quartz produces potassium feldspar, sillimanite and H_2O, which occurs at about 640°C and 0.3 GPa (Powell & Holland, 1990). In the sillimanite-garnet-biotite schist unit, the presence of coarse sillimanite and poikiloblastic K-feldspar represent the granulite facies metamorphism at temperatures above the second sillimanite isograd or K-feldspar and sillimanite isograd. The absence of muscovite in the garnet-biotite schist unit indicates that muscovite, if present, was completely consumed during this prograde granulite facies metamorphic reaction.

5.3 Sequence of Polymetamorphism

What sets the mineralized units on the Borden property apart from the regional granulite facies metamorphism of the Kapuskasing Structural Zone is the small quantity of granulite facies assemblages within dominantly retrograde amphibolite facies assemblages. On the Borden property mineralized units preserve vestiges of unstable granulite facies minerals within stable amphibolite facies assemblages.

Retrograde amphibolite facies metamorphism is observed in the two prominent gold-hosting lithologies amphibolite (±garnet) and garnet-biotite schist (±sillimanite). Both lithologies display strong evidence of retrograde amphibolite facies metamorphism after granulite facies metamorphism, and this retrograde metamorphism appears to be significant to gold mineralization.

Retrograde metamorphism was initially documented within the amphibolite (±garnet) unit in core. Subsequent microstructural analysis of amphibolite (±garnet) supported the retrograde amphibolite facies metamorphic reactions. Relict mineral vestiges and lithons consisting of clinopyroxene, orthopyroxene, K-feldspar and garnet representing granulite facies mineral. Anhedral clinopyroxene and orthopyroxene with eroded crystals commonly contain abundant microfractures and irregular grain shapes. Surrounding these unstable pyroxenes are abundant euhedral hornblende, plagioclase and garnet. The contacts between amphibolite and granulite facies lithons are sharp and discordant to the foliation in amphibolite. Hornblende either fully or partially surrounds the clinopyroxene, or replaces it along cleavage planes indicating thermodynamic instability and reaction (Fig. 5.31A). In drill core, the mineralized, amphibolite (±garnet) has a strong foliation defined by hornblende, minor biotite and

sulphides. Massive, green, pyroxene-rich lithons have a reaction rim corona of black hornblende (Fig. 5.31B,C). These lithons are elongated parallel to the dominant foliation and are from 1.0 to 5.0 cm long. The black hornblende reaction rims are typically 0.1 to 0.3 cm thick and completely encase the massive pyroxene lithons.

In the amphibolite (±garnet) units, euhedral hornblende typically defines a moderate to strong foliation indicating growth during synchronous deformation and retrograde amphibolite facies metamorphism. These microstructural relationships indicate that the once stable granulite facies minerals orthopyroxene and clinopyroxene participated as reactants during retrograde amphibolite facies metamorphism producing hornblende, plagioclase and garnet. Consistently, gold mineralization is present at the contact between retrograde amphibolite and relict granulite facies lithons. The relationship between gold and its emplacement in these distinct environments speaks to the timing of mineralization and dependence on structure and metamorphism.

In many samples of sillimanite-garnet-biotite schist there is both fibrolite and coarse sillimanite (Fig. 5.32). Fibrolite is unlikely to be stable at granulite facies temperatures and would be expected to recrystallize as coarse sillimanite. Therefore, the presence of fibrolite suggests secondary growth of sillimanite at amphibolite facies temperatures during retrograde metamorphism.

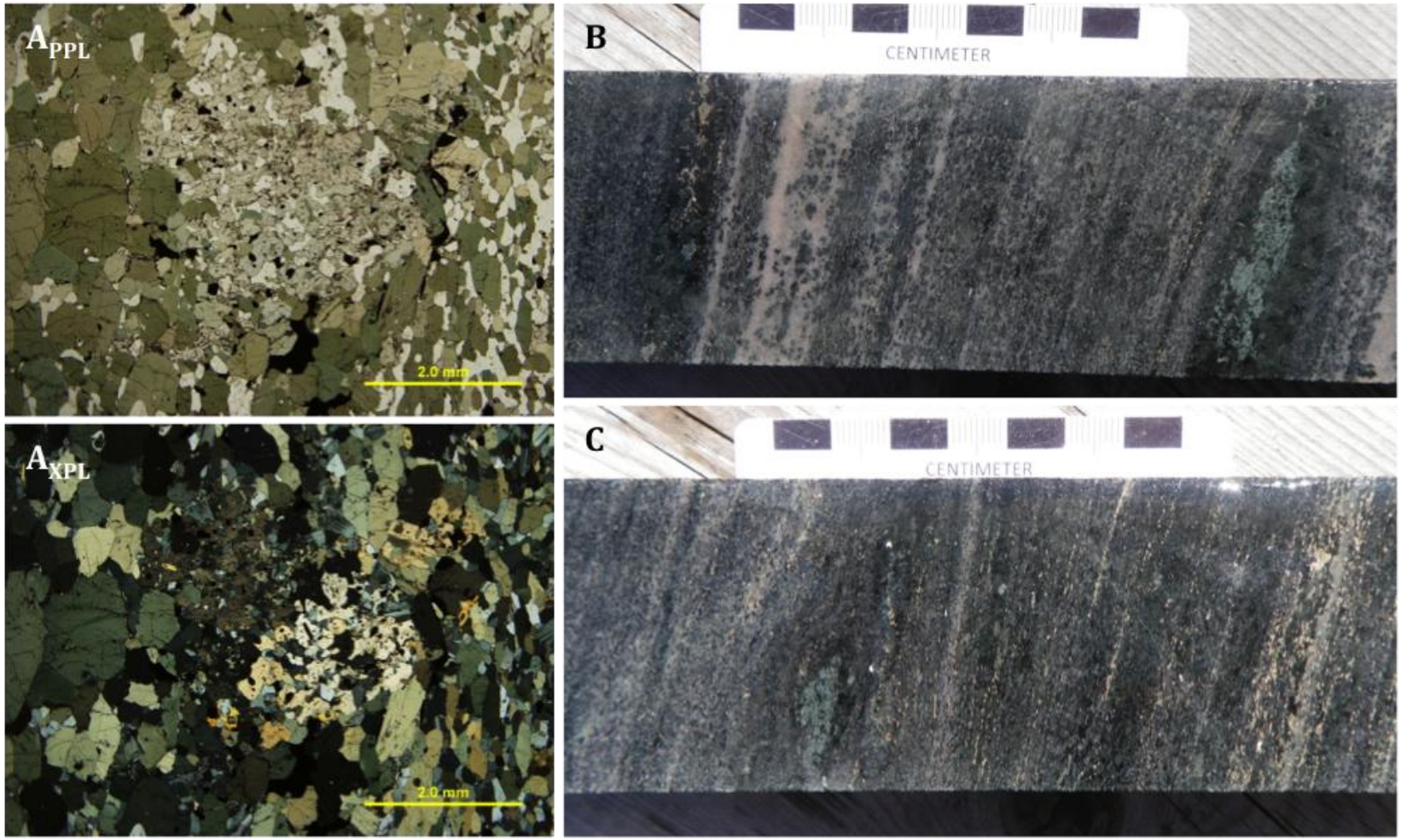

Figure 5.31. A) Amphibolite (±garnet) with euhedral, foliated hornblende minerals replacing a central orthopyroxene grain. Sample FD 01321, 923 ppb Au. B) and C) Strongly foliated amphibolite in core. Both contain a green pyroxene rich lithon surrounded by a black hornblende reaction rim, indicating retrogression from granulite to amphibolite facies metamorphism.

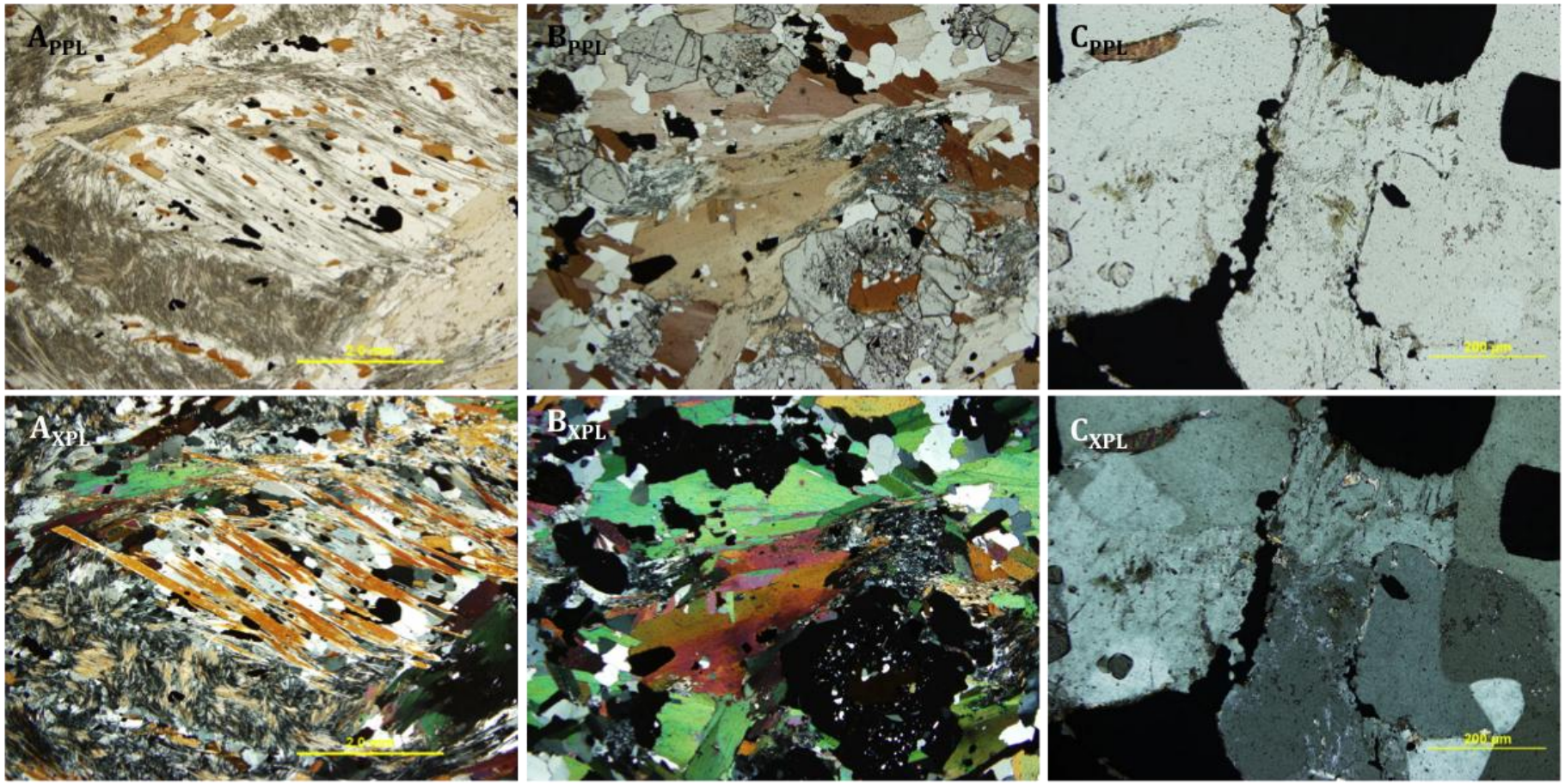

Figure 5.32. A) Sillimanite-garnet-biotite schist, with coarse, prismatic sillimanite at the centre and retrograde fibrolite in the bottom left from sample FD 01339 (1440 ppb Au). B) Deformed garnet porphyroclast present in the bottom right with a partial corona of biotite and minor fibrolite in sillimanite-garnet-biotite schist from sample FD 01342 (176 ppb Au). C) Weakly sericitized feldspar grains within a quartzofeldspathic gneiss from sample BL10-09 (111.5m) with 1194 ppb Au.

5.4 Garnet-Biotite Geothermometry

The garnet-biotite geothermometer developed by Ferry and Spear (1978) was used to determine metamorphic temperatures for garnet-biotite schist samples from the Borden gold deposit's Discovery Outcrop. The geothermometer is based on the partitioning of Fe^{2+} and Mg between garnet and biotite as expressed by the cation exchange reaction $Fe_3Al_2Si_3O_{12}$ (almandine) + $KMg_3AlSi_3O_{10}(OH)_2$ (phlogopite) = $Mg_3Al_2Si_3O_{12}$ (pyrope) +$KFe_3AlSi_3O_{10}(OH)_2$ (annite). Quantative EDS analyses were used for mineral compositions. A total of 12 garnet grains from three separate samples (FD 01340, FD 01341 and BL11-19) were utilized for garnet-biotite geothermometry calculations. The almandine garnet in the samples contains low concentrations of Al, Mn and Ca, a condition for use of the Ferry and Spear (1978) geothermometer (Table 5.2).

Individual garnet compositions were analyzed across the diameter of the crystal from rim to core to rim (Fig. 5.33). Garnet compositions are consistent throughout the crystal and subsequent element maps do not record chemical zoning in any of the garnet grains analyzed (Fig. 4.15). Biotite compositions vary from inclusions in garnet cores to inclusions in garnet rims and to groundmass biotite. Garnet rims were compared to matrix biotite directly adjacent to the garnet. Biotite inclusions in garnet were compared to garnet core spot analyses directly adjacent to the inclusion. Based on spot analyses of individual garnet and biotite grains, weight percents were converted to cations per formula unit for each oxide within garnet and biotite.

Table 5.2. Calculations for each garnet spot analysis used for garnet-biotite geothermometry. Each garnet is required to have no greater than 0.2 of (Ca + Mn)/(Ca + Mn + Fe + Mg).

FD 01340									
Grt-Bt 1		**Grt-Bt 2**		**Grt-Bt 3**		**Grt-Bt 4**		**Grt-Bt 5**	
Grt Core 1	0.18	Grt Core 1	0.19	Grt Core 1	0.19	Grt Core 1	0.18	Grt Core 1	0.09
Grt Core 2	0.18	Grt Core 2	0.19	Grt Core 2	0.18	Grt Core 2	0.17	Grt Core 2	0.19
Grt Core 3	0.17	Grt Core 3	0.18	Grt Core 3	0.17	Grt Core 3	0.18	Grt Core 3	0.19
Grt Core 4	0.17	Grt Core 4	0.19	Grt Core 4	0.17	Grt Core 4	0.17	Grt Core 4	0.18
Grt Rim 1	0.21	Grt Rim 1	0.20	Grt Core 5	0.17	Grt Core 5	0.17	Grt Core 5	0.18
Grt Rim 2	0.19	Grt Rim 2	0.20	Grt Rim 1	0.20	Grt Core 6	0.18	Grt Rim 1	0.20
Grt Rim 3	0.21	Grt Rim 3	0.20	Grt Rim 2	0.21	Grt Rim 1	0.21	Grt Rim 2	0.21
Grt Rim 4	0.20			Grt Rim 3	0.20	Grt Rim 2	0.21	Grt Rim 3	0.20
Grt Rim 5	0.19			Grt Rim 4	0.20	Grt Rim 3	0.20	Grt Rim 4	0.19
Grt Rim 6	0.17			Grt Rim 5	0.18	Grt Rim 4	0.19	Grt Rim 5	0.19
Grt Rim 7	0.18			Grt Rim 6	0.18				
FD 01341									
Grt-Bt 1		**Grt-Bt 2**		**Grt-Bt 3**		**Grt-Bt 4**		**Grt-Bt 5**	
Grt Core 1	0.16	Grt Core 1	0.15	Grt Core 1	0.16	Grt Core 1	0.15	Grt Core 1	0.15
Grt Core 2	0.16	Grt Core 2	0.15	Grt Core 2	0.16	Grt Core 2	0.15	Grt Core 2	0.15
Grt Core 3	0.15	Grt Core 3	0.15	Grt Core 3	0.11	Grt Rim 1	0.13	Grt Core 3	0.15
Grt Core 4	0.15	Grt Core 4	0.15	Grt Core 4	0.15	Grt Rim 2	0.16	Grt Rim 1	0.19
Grt Rim 1	0.19	Grt Rim 1	0.18	Grt Core 5	0.16	Grt Rim 3	0.20	Grt Rim 2	0.19
Grt Rim 2	0.18	Grt Rim 2	0.18	Grt Core 6	0.16	Grt Rim 4	0.16	Grt Rim 3	0.19
Grt Rim 3	0.23	Grt Rim 3	0.19	Grt Rim 1	0.19	Grt Rim 5	0.15	Grt Rim 4	0.17
Grt Rim 4	0.18	Grt Rim 4	0.19	Grt Rim 2	0.19			Grt Rim 5	0.15
Grt Rim 5	0.16	Grt Rim 5	0.16	Grt Rim 3	0.15			Grt Rim 6	0.15
Grt Rim 6	0.17	Grt Rim 6	0.15	Grt Rim 4	0.15			Grt Rim 7	0.16
Grt Core 1b	0.17	Grt Rim 7	0.15	Grt Rim 5	0.15			Grt Rim 8	0.14
Grt Rim 1b	0.20	Grt Rim 8	0.15						
Grt Rim 2b	0.19								

BL 11-19 (175m)			
Grt-Bt 1		**Grt-Bt 2**	
Grt Core 1	0.16	Grt Core 1	0.17
Grt Rim 1	0.17	Grt Core 2	0.17
Grt Rim 2	0.17	Grt Rim 1	0.17
		Grt Rim 2	0.17

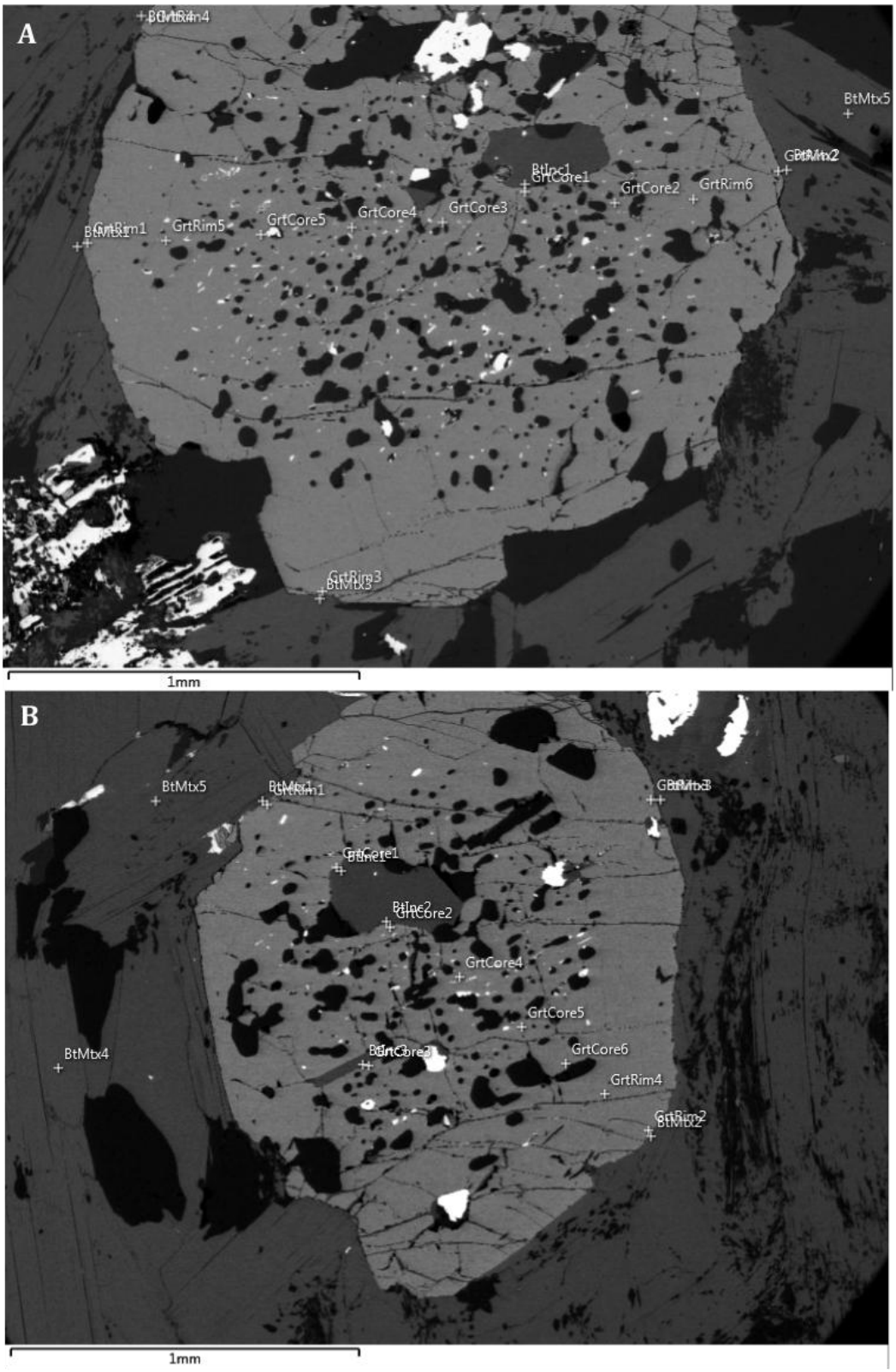

Figure 5.33. A) SEM photomicrograph of garnet from sample FD 01341. Locations of EDS spot analyses across the diameter and at other rim locations for garnet-biotite geothermometry. B) SEM photomicrograph of garnet from sample FD 01340. Locations of EDS spot analyses across the diameter and at other rim locations for garnet-biotite geothermometry.

The geothermometer has a maximum practical resolution of approximately ±50°C, through the equation:

$$\ln K = -2109/T + 0.782$$

where $K = [(Mg/Fe)_{garnet}/(Mg/Fe)_{biotite}]$. K represents the distribution of Fe and Mg between corresponding garnet and biotite sites and this value was substituted into the expression to calculate the equilibrium metamorphic temperature. Fe/Mg ratios in stable coexisting garnet and biotite provide a reasonable measure of metamorphic temperature.

Abundant biotite as inclusions within garnet and in the groundmass provided many sites for Fe/Mg equilibration and geothermometer calculations. Garnet compositions adjacent to biotite inclusions typically yielded metamorphic temperatures ranging from 416°C to 611°C ±50°C. Garnet rim to groundmass biotite generally yielded higher metamorphic temperatures ranging from 472°C to 933°C ±50°C. Overall, calculations based on Borden property garnet-biotite geothermometry yield a metamorphic temperature range of 411°C to 933°C ±50°C. Table 5.3 displays garnet and biotite oxide SEM values, converted cations per formula unit for each element, garnet composition and calculated geothermometry for one garnet from one sample. Each column represents the garnet and biotite pairing used to calculate the respective equilibrium temperature. Figure 5.34 displays the corresponding locations of garnet-biotite analysis and temperature for the same garnet as Table 5.3. The patterns observed in Sample FD 01340 are generally consistent with geothermometer patterns in the remaining garnet-biotite geothermometries conducted. Other geothermometry data can be found in Appendix D.

Table 5.3. Data from spot analyses on Garnet 4 of sample FD 01340 and corresponding garnet-biotite geothermometry. Table includes garnet and biotite raw SEM oxide values, recalculated elemental per formula unit values, garnet-end member compositions, Fe/Mg ratio and temperature calculations.

FD 01340 – Discovery Outcrop – Grt-Bt 4						
	Grt Core 1	**Grt Core 2**	**Grt Core 3**	**Grt Rim 1**	**Grt Rim 2**	**Grt Rim 3**
OXIDE	wt %	wt %	wt %	wt %	wt %	wt %
MgO	2.58	3.47	3.93	3.24	2.28	2.94
Al_2O_3	20.70	21.29	20.69	20.92	20.77	21.19
SiO_2	35.65	37.74	36.53	37.28	36.54	36.95
CaO	1.18	1.13	1.13	1.23	0.81	1.15
Sc_2O_3	0.00	0.00	0.00	0.00	0.00	0.15
TiO_2	0.00	0.00	0.00	0.00	0.00	0.00
MnO	6.74	6.18	6.33	7.47	8.42	7.41
FeO	33.61	30.19	30.03	29.40	31.03	29.84
	100.45	100.00	98.64	99.52	99.85	99.64
Cations pfu						
Mg	0.31	0.41	0.48	0.39	0.28	0.35
Al	1.99	2.01	1.99	1.99	2.00	2.02
Si	2.91	3.02	2.98	3.01	2.98	2.98
Ca	0.10	0.10	0.10	0.11	0.07	0.10
Sc	0.00	0.00	0.00	0.00	0.00	0.02
Ti	0.00	0.00	0.00	0.00	0.00	0.00
Mn	0.47	0.42	0.44	0.51	0.58	0.51
Fe	2.30	2.02	2.05	1.99	2.12	2.01
Mg/Fe	**0.14**	**0.20**	**0.23**	**0.20**	**0.13**	**0.18**
Almandine	0.67	0.68	0.65	0.66	0.68	0.67
Spessartine	0.15	0.14	0.15	0.17	0.19	0.17
Pyrope	0.10	0.14	0.16	0.13	0.09	0.12
Grossular	0.00	0.03	0.02	0.03	0.01	0.03
Andradite	0.03		0.01		0.01	
	Bt Inc 1	**Bt Inc 2**	**Bt Inc 3**	**Bt Mtx 1**	**Bt Mtx 2**	**Bt Mtx 3**
OXIDE	wt %	wt %	wt %	wt %	wt %	wt %
Na_2O	0.00	0.00	0.26	0.00	0.00	0.00
MgO	12.59	12.96	12.25	10.30	11.29	9.74
Al_2O_3	19.84	20.16	19.02	20.00	19.06	19.76
SiO_2	37.12	37.75	36.75	36.54	35.99	36.46
K_2O	10.34	10.50	10.49	9.39	10.15	10.53
TiO_2	2.36	2.35	2.47	2.15	2.73	2.54
V_2O_5	0.00	0.00	0.00	0.20	0.00	0.00
MnO	0.00	0.00	0.00	0.00	0.00	0.00
FeO	16.82	16.64	18.01	21.79	19.86	20.28
BaO	0.00	0.00	0.00	0.00	0.00	0.00
	99.06	100.36	99.25	100.38	99.08	99.31
Cations pfu						
Na	0.00	0.00	0.08	0.00	0.00	0.00
Mg	2.96	3.00	2.91	2.43	2.70	2.33
Al	3.69	3.69	3.57	3.73	3.60	3.73
Si	5.85	5.86	5.85	5.79	5.77	5.84
K	2.08	2.08	2.13	1.90	2.08	2.15
Ti	0.28	0.27	0.30	0.26	0.33	0.31
V	0.00	0.00	0.00	0.02	0.00	0.00
Mn	0.00	0.00	0.00	0.00	0.00	0.00
Fe	2.22	2.16	2.40	2.88	2.66	2.72
Ba	0.00	0.00	0.00	0.00	0.00	0.00
Mg/Fe	**1.33**	**1.39**	**1.21**	**0.84**	**1.01**	**0.86**
Kd	**0.10**	**0.15**	**0.19**	**0.23**	**0.13**	**0.21**
Temp (°C)	**416.5**	**508.9**	**594.6**	**668.3**	**472.5**	**618.7**

FD 01340 – Grt-bt Geothermometry	
Grt Core 1	416.5°C
Bt Inc 1	
Grt Core 2	508.9°C
Bt Inc 2	
Grt Core 3	594.6°C
Bt Inc 3	

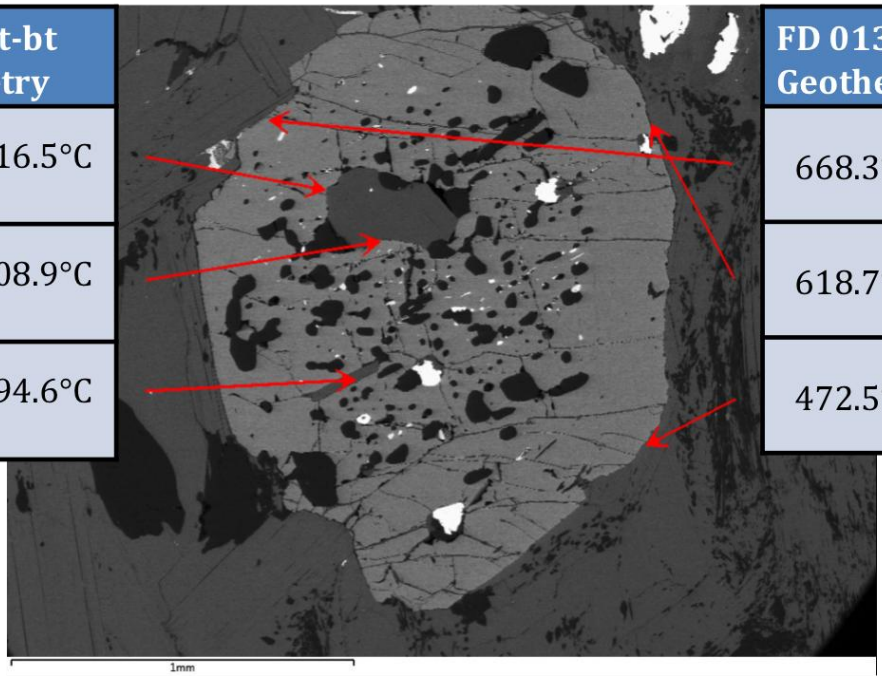

FD 01340 – Grt-bt Geothermometry	
668.3°C	Grt Rim 1
	Bt Mtx 1
618.7°C	Grt Rim 3
	Bt Mtx 3
472.5°C	Grt Rim 2
	Bt Mtx 2

Figure 5.34. Sample FD 01340 with 117 ppb Au. Locations of calculated garnet-biotite geothermometry. The central image is an SEM photomicrograph with arrows locating the garnet-biotite contact used to calculate the geothermometer.

Garnet core Fe/Mg ratios were calculated with directly adjacent biotite inclusions. Garnet rim Fe/Mg ratios were compared with directly adjacent matrix biotite. This method allows determination of changing temperature during garnet growth. Garnet-biotite geothermometry from the Borden gold deposit documents a progressive increase in temperature from garnet core to garnet rim, indicating garnet growth occurred during prograde metamorphism from the amphibolite to granulite facies. The absence of chemical zoning in garnet may be due to intracrystalline diffusion at peak metamorphic temperatures. In some samples, the garnet-biotite geothermometry documents a low temperature at the very rim of the garnet. This data likely preserves a final solid-state iron-magnesium equilibration during the retrograde amphibolite facies metamorphism associated with gold mineralization.

5.5 Lu/Hf Dating of Garnet

To bring new constraints on the metamorphic history of the deposit, ^{176}Lu-^{176}Hf geochronology was conducted on garnet, following the protocol detailed in Zirakparvar et al. (2010). This radiometric dating method has become increasingly useful to constrain ages of high-grade metamorphic assemblages, owing to the strong partitioning of lutetium in garnet. Lu/Hf garnet dating was conducted on the mineralized garnet-biotite schist (±sillimanite) unit from the Discovery Outcrop. The metamorphic history of the gold-hosting lithologies is critical to the timing of mineralization at the Borden gold deposit. Garnets were separated from the sillimanite-garnet-biotite schist unit (sample FD 01340) and were dated using the ^{176}Lu-^{176}Hf radiochronometer, which has a half-life of about 37 Ga (Zirakparvar et al., 2010).

The Lu-Hf isotopic analyses were derived from two handpicked, 100 mg garnet splits and corresponding whole rock splits (with and without dissolving zircons). These yield a precise internal isochron age at 2629.0 ±4.3 Ma (with an initial ^{176}Hf/^{177}Hf 0.281210 ±0.000010 and MSWD = 0.66) from five data points. This age is within error of the Lu-Hf isochron age of 2630.4 ±4.7 Ma (with an initial ^{176}Hf/^{177}Hf =0.281204 ±0.000013 and MSWD = 0.16) when the whole rock dissolved with zircons is not included in the age calculation. The initial Hf isotopic composition of this schist is eHf =+4.1 (epsilon unit is the deviation in parts per 10,000 relative to Chondrite Uniform Reservoir at 2629 Ma). The initial Hf isotopic composition of the garnet-biotite schist from Discovery Outcrop indicates that the protolith of this rock was

derived from a long-term depleted (high Lu/Hf) mantle reservoir (Bouvier et al., 2008). Lu-Hf isotopic data and isochron dating results are presented in Figure 5.35.

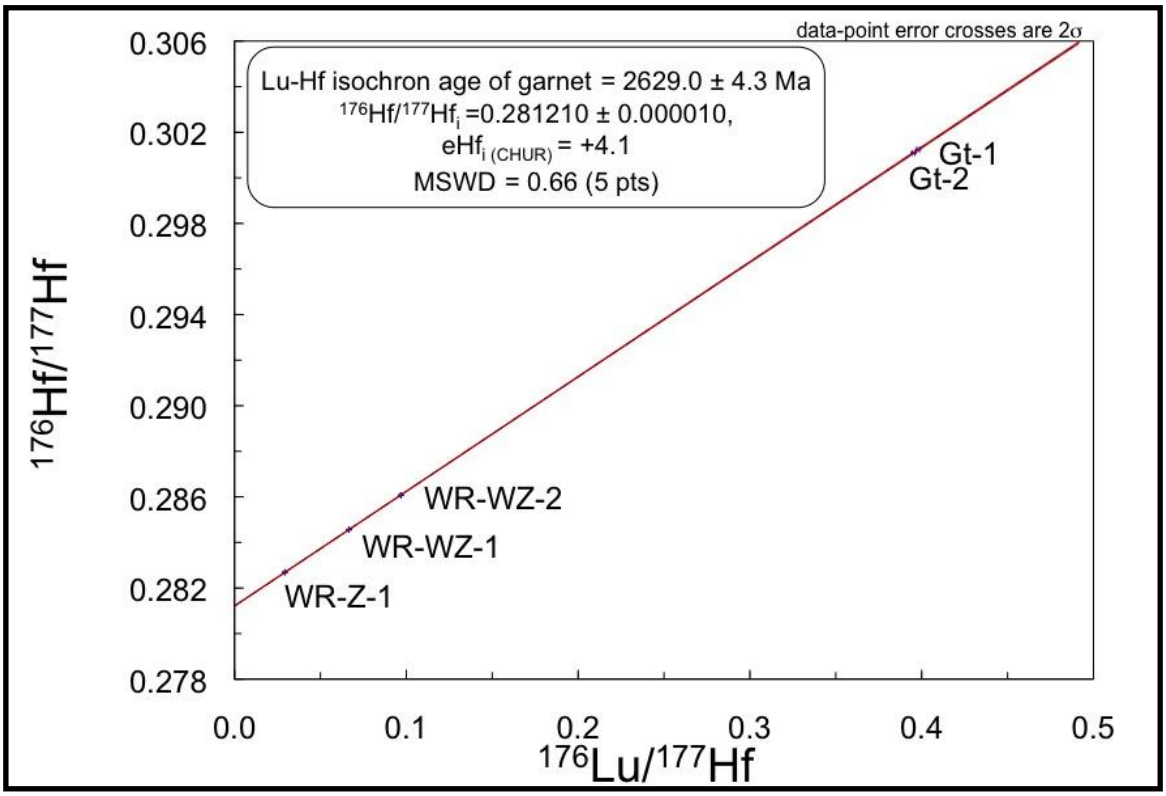

Figure 5.35. ^{176}Lu-^{176}Hf internal isochron of sample FD 01340 with two garnet separates (Gt-1 & -2) and three whole-rock samples (WR-Z-1 dissolved with zircons, WR-WZ-1 & -2 without zircons). Isochron regression line and error envelope (in red) represent a 95% confidence level (Bouvier, 2015, unpublished report).

These results suggest that peak granulite facies metamorphism associated with garnet growth took place at 2629 ±4.3Ma. This is slightly younger than earlier estimates of the age of granulite facies metamorphism. Retrograde metamorphism of these lithologies is critical to the structural control of mineralization at this deposit. Lenses of relict granulite facies rock were more competent than surrounding retrograde amphibolite facies lithologies, producing the requisite conditions for localized brittle deformation and mineralization during dominantly ductile shear-zone deformation. Thus, mineralization is suspected to be younger than 2629 ±4.3Ma.

6. STRUCTURE AND MICROSTRUCTURE

6.1 Geometry of Strain

At the Borden property moderate to high strain is a consistent indicator of mineralized units and proximity to the ore zone. Foliation defined by parallel alignment of platy minerals is caused by crystallization, recrystallization or reorientation during differential stress. Foliated lithologies are evidence of high temperature ductile deformation associated with regional shear zone structures. Mineralized garnet-biotite schist, amphibolite (±garnet) and biotite-quartzofeldspathic gneiss all maintain subvertically dipping, roughly parallel foliations. Lithological heterogeneity causes foliation to anastomose around unfoliated competent units due to relative competence contrasts.

Orientation of mineral foliation and lineation were measured in the field throughout the property. Stereonets provide a comprehensive summary of these measurements in relation to mineralization trends. To more effectively characterize the variability in foliation, the measurements were separated into five structural domains over the property (Fig. 6.36). Domain 1 is located north of Highway 101, Domain 2 is north of the ore zone to Highway 101, Domain 3 represents the ore zone exposed at surface in the northwest, Domain 4 represents lithologies above the southeast portion of the ore zone when projected to surface and Domain 5 represents lithologies south of the ore zone to Borden Lake.

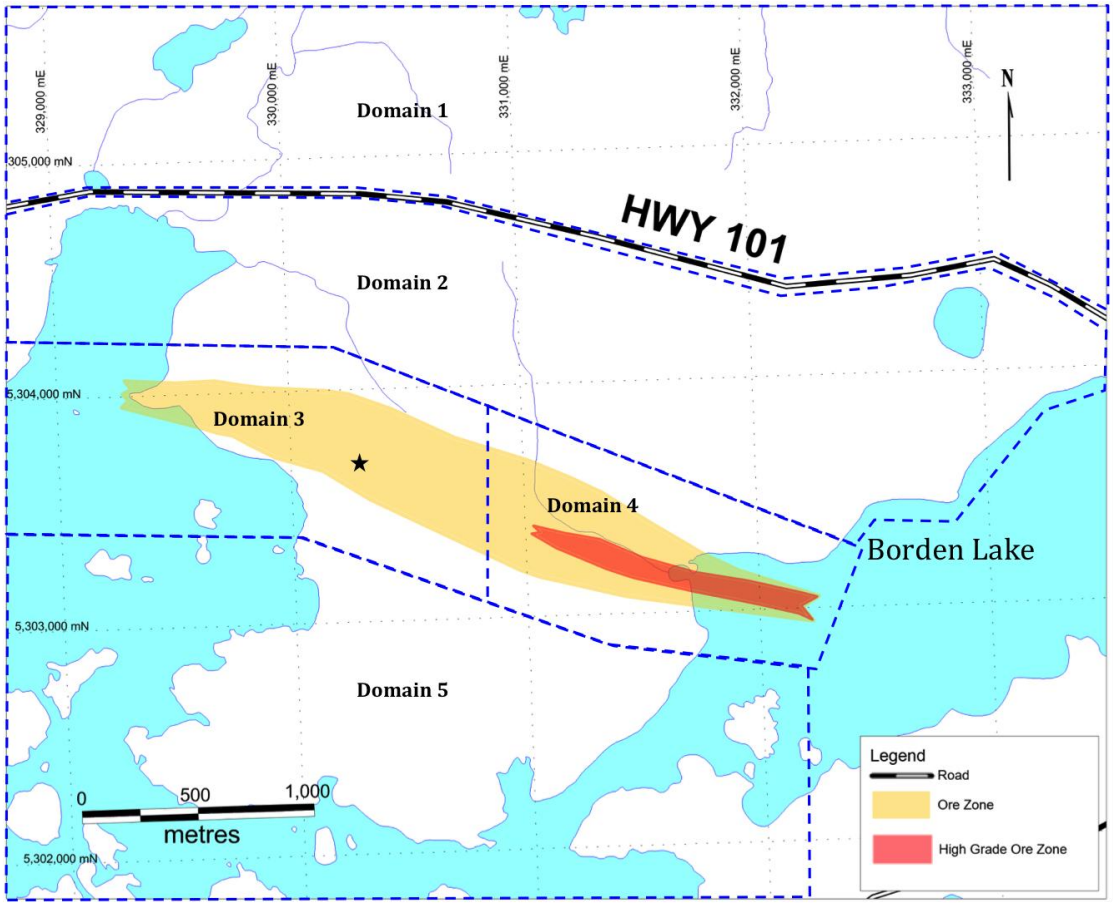

Figure 6.36. The Borden property separated by structural domains for interpretation of structural data. Modified after Probe Mines Limited, 2015.

In Domain 1, the dominant strike of foliation is generally west to west-southwest, with an average of 256°/71° (Fig. 6.37A). In Domain 2, the foliation changes to west-northwest, with an average of 281°/72° (Fig. 6.37B). In Domain 5, the foliation again slightly deviates to northwest, with an average of 302°/83° (Fig. 6.37C). At all locations, measurements were taken from parallel alignment of hornblende in amphibolite, parallel alignment of biotite in quartzofeldspathic gneiss and flattened clasts in metaconglomerate. Domains 1 and 2 both roughly strike east-west with the southern Domain (5) striking more to the northwest. Domain 5 is most concordant with the average strike of foliation in Domains 3 and 4 (Fig. 6.38).

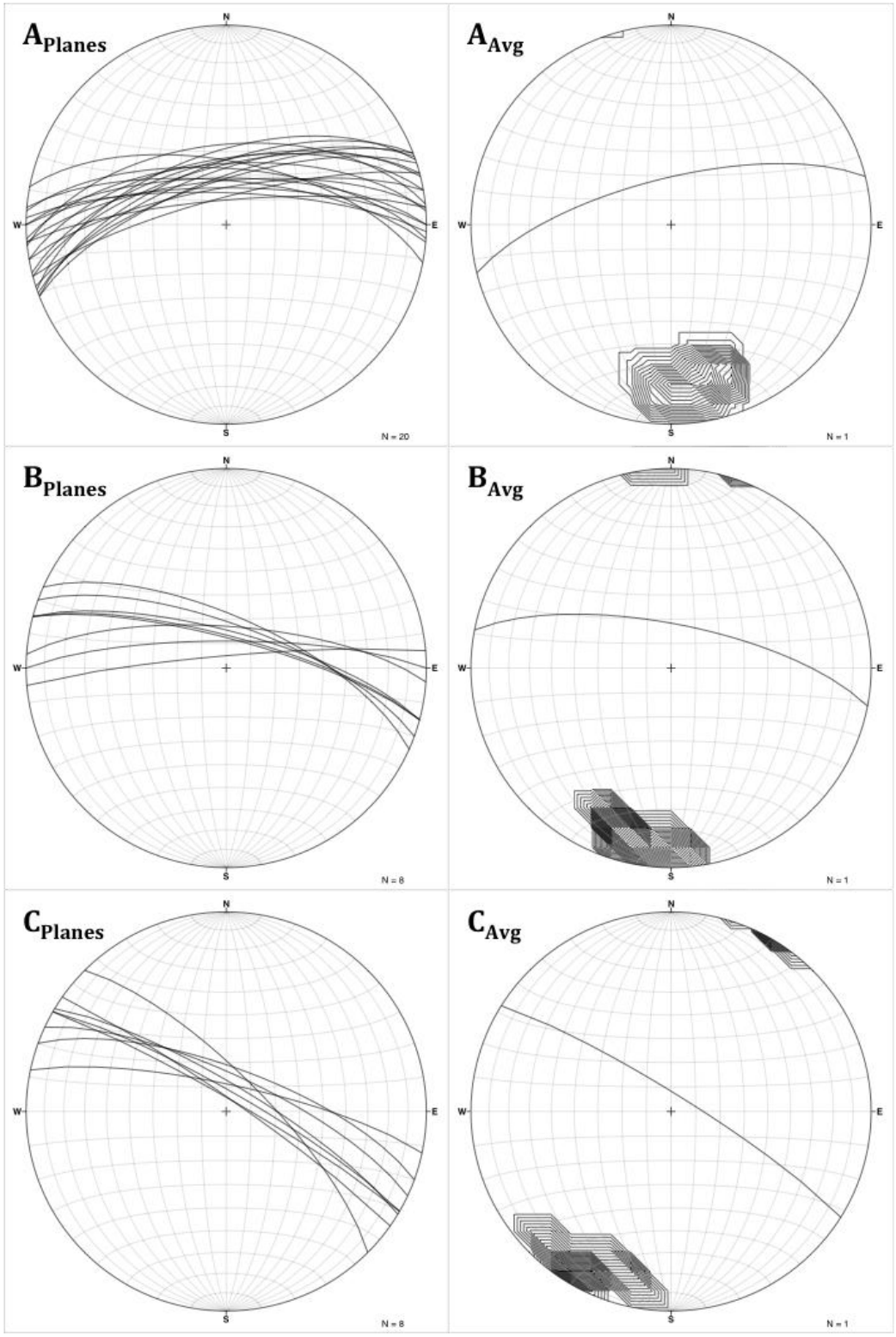

Figure 6.37. A) Domain 1, north of Highway 101. Great circles (n=20) and contoured poles with average of 256°/71°. B) Domain 2, north of the ore zone to Highway 101. Great circles (n=8) and contoured poles with average of 281°/72°. C) Domain 5, south of the ore zone to Borden Lake. Great circles (n=8) and contoured poles with average of 302°/83°.

Unlike the dominantly north-dipping foliations north and south of the Borden gold deposit, the mineralized lithologies on surface and lithologies above the ore zone in Domains 3 and 4 display significant variation in dip direction (Fig. 6.38). There are two populations of foliation strike and dip measurements directly above the ore zone. Both populations have subparallel strikes of west-northwest to east-southeast. Northeast dipping measurements average 291°/75° while southwest dipping measurements average 127°/67°.

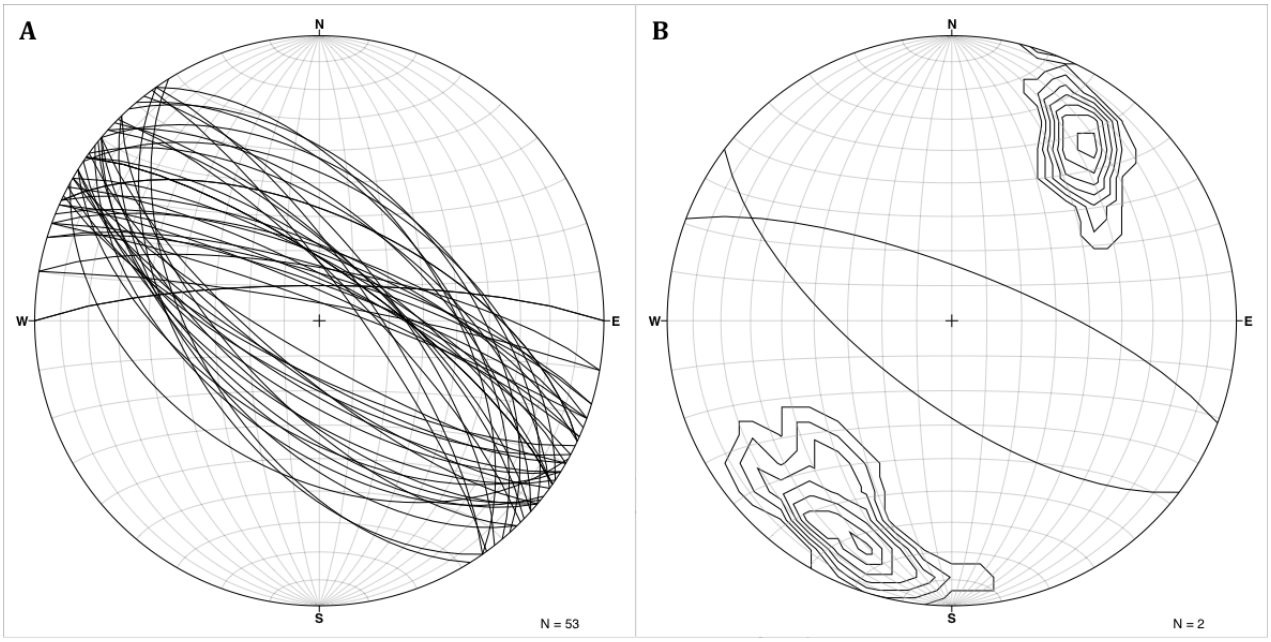

Figure 6.38. A) Structural domains 3 and 4, plotted as great circles (n=53). B) Contours of the poles from (A) with averages from both populations; 291°/75°and 127°/67°.

In Domains 3 and 4 the foliation dips steeply to the northeast or southwest, with local variations. The lithological heterogeneity and lateral continuity within the ore zone could account for ductile units deflecting around more competent (low-strain) lithons, which would appear as dip direction changes.

Similarly, lineations from elongated clasts in metaconglomerate, long axes of hornblende in amphibolite, and deformed quartz in quartzofeldspathic gneiss display variation in orientations. One weakly defined cluster can be observed from the lineation measurements plotted on a stereonet (Fig. 6.39A). The contoured lineations yield an average lineation vector at 25°/095° (Fig. 6.39B).

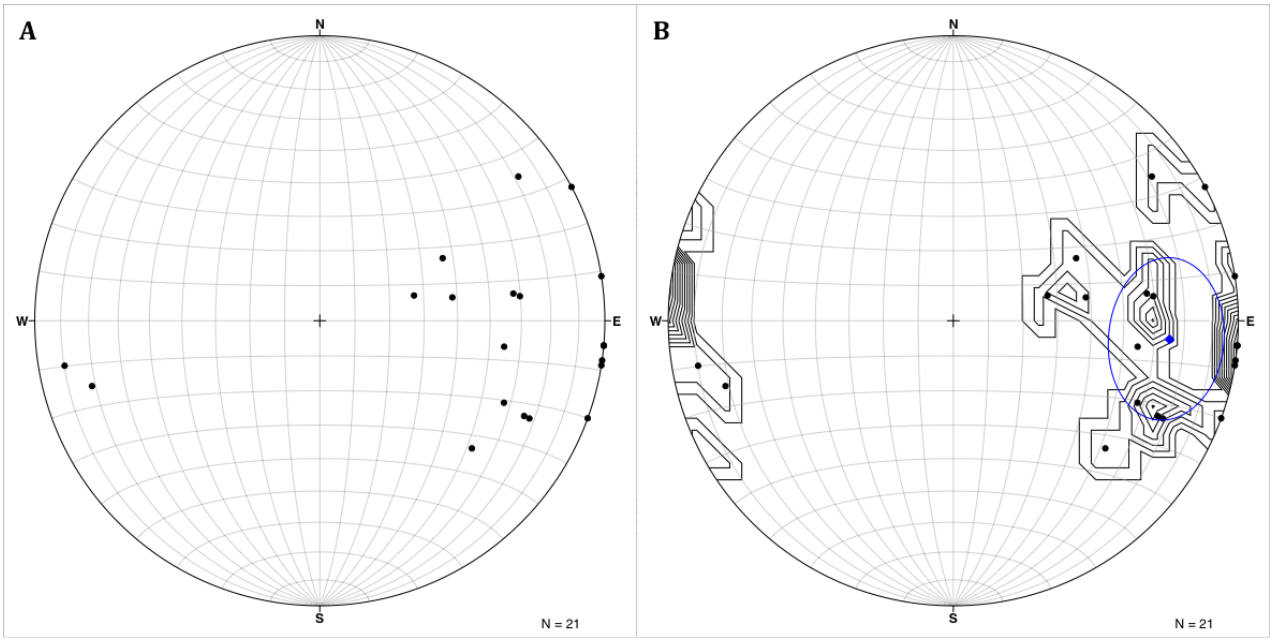

Figure 6.39. A) Lineation trend and plunge measurements recorded on the Borden property (n=21). B) Contoured lineations with an average lineation at 25°/095° in blue.

This average trend and plunge represents the direction of maximum elongation (S_1) and is roughly consistent with the trend and plunge of the ore zone at 22°/115°. Strain heterogeneity on the Borden property is prevalent between lithologies. Competent, unfoliated units adjacent to foliated lithologies suggest incompatible strain as a cause for brittle-ductile deformation. Heterogeneous deformation and incompatible strain are common features of high-temperature shear zones and typically associated with gold mineralization.

A quantitative strain analysis on the Borden Lake metaconglomerate was completed in June of 2014, using the R_f/phi (ϕ) technique for initially elliptical objects (Dolega, 2014, unpublished report). This method calculates the ratio between the long axis and the short axis (R_f) of each clast and takes into account the orientation of the clast by measuring the angle from the long axis to a chosen reference line (ϕ) (Ramsay, 1967; Ramsay and Huber, 1983; Lisle, 1985). Once these measurements are completed for multiple clasts, the data set is plotted on an R_f vs. ϕ graph and best-fit curves determine the strain ratio (Ramsay, 1967; Lisle, 1985). Measured strain varied between different outcrops and between different clast compositions at each outcrop.

Mafic clasts of the Borden metaconglomerate often have higher strain ratios than felsic clasts. Strain magnitude of the mafic clasts ranged from 9.88 to 24 while the felsic clasts strain magnitude ranged between 5.39 to 23.28 (Table 6.4). The highest magnitudes of strain in all clasts were measured at the metaconglomerate outcrop 250 metres southeast of the known gold zone. Notably, both higher overall strain and greater competency contrasts are found closest to the zone of high-grade gold mineralization (Dolega, 2014, unpublished report). The strained clasts define a moderate to strong lineation. For each individual outcrop, the foliation strike and dip (Fig. 6.40) as well as average trend of the long axis of strain are summarized (Table 6.4). The trend of the long axis at each outcrop ranges from 82° to 131° with a moderate plunge to the east. The plunge at outcrop 2B ranges from 30° to 32° to the east. Deformation features in the metaconglomerate include clast rotation, boudinage structures, deformation tails of feldspar crystals, contorted feldspar veins, elongation and strong parallel alignment of clasts.

Table 6.4. Summary of data from strain analysis conducted on the Borden Lake metaconglomerate at various locations (Dolega, 2014, unpublished report).

Location	Measurements		Strain Magnitude	
	Foliation	Trend of long axes	Felsic Clasts	Mafic Clasts
Site 1A	284°/68°	113°	5.39	9.88
Site 1B	331°/75°	129°	9.18	10.63
Site 2A	263°/45°	082°	14.62	11.85
Site 2B	274°/38°	083°	10.99	14.31
Site 3	306°/61°	131°	23.28	24

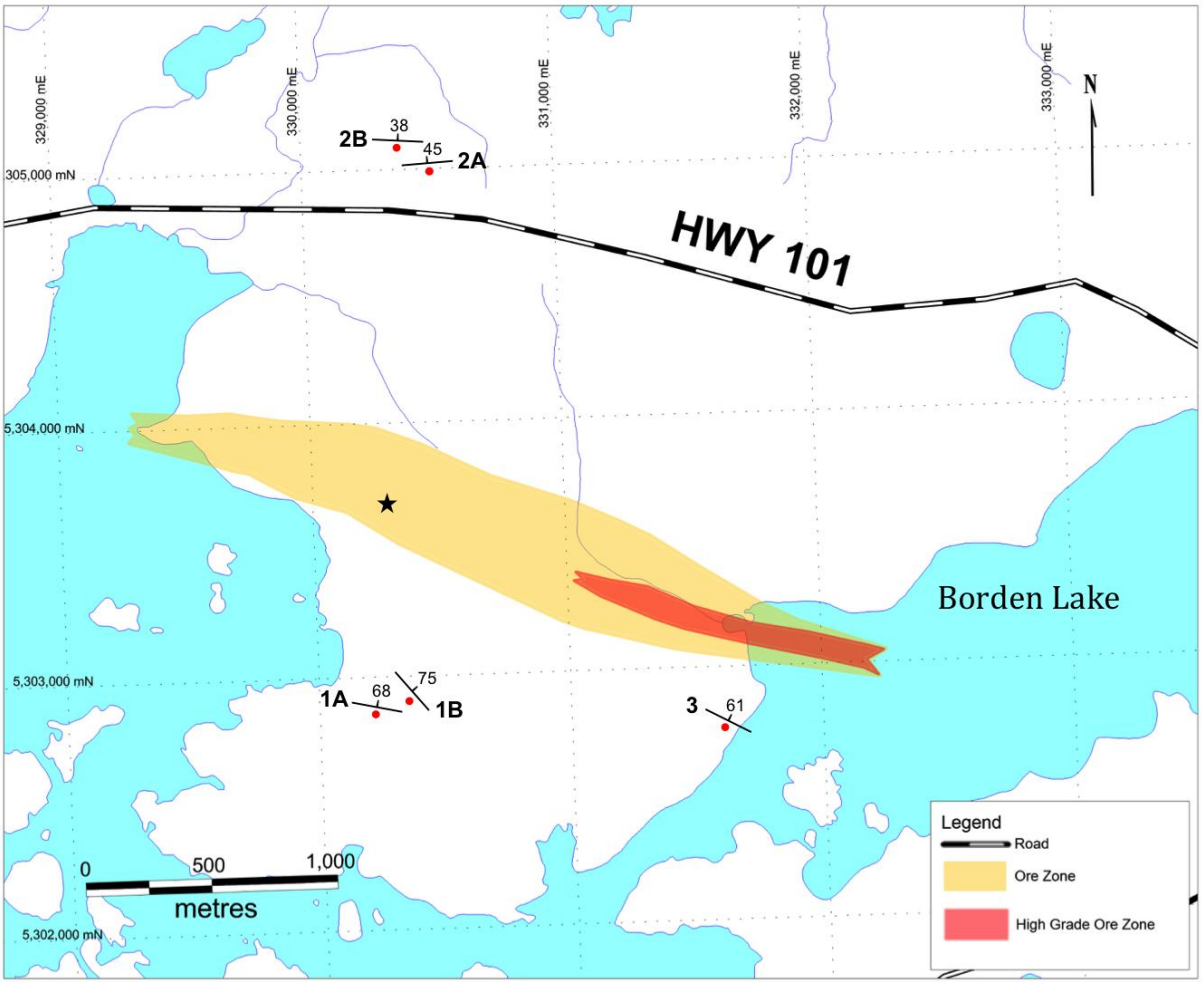

Figure 6.40. Borden property map with locations of Borden Lake metaconglomerate strain analyses and respective foliation measurements (modified after Dolega, 2014, unpublished report).

6.2 Fabric and Microstructure

Microstructural analysis provides evidence for conditions at the time of metamorphic mineral growth and deformation of a lithology. Based on mapping and microstructural analysis, abundant evidence for ductile deformation processes, including boudinage and grainsize reduction by dislocation creep, can be seen in all units. Moderate- to high-strain lithologies are a consistent indicator of mineralization and proximity to the ore zone at the Borden gold deposit. Competent, unfoliated units adjacent to foliated lithologies provide environments for brittle-ductile deformation where strain rate differs between lithologies causing strain incompatibility.

6.2.1 Fabric of the Amphibolite

Parallel alignment of hornblende dominantly defines the foliation in amphibolite units. Moderate to strongly foliated amphibolite contains high percentages of hornblende (40% to 60%) and represents a transition into the ore zone. Foliation is defined dominantly by parallel alignment of fine to medium grained hornblende as well as minor biotite. Pyrite and pyrrhotite can also be observed as stringers parallel to foliation (Fig. 6.41A,B). Contacts between the amphibolite and quartzofeldspathic gneiss are typically gradational in proximity to the ore zone and where both units display strong foliation. The transition zone between these units contains both biotite and hornblende (Fig. 6.41C).

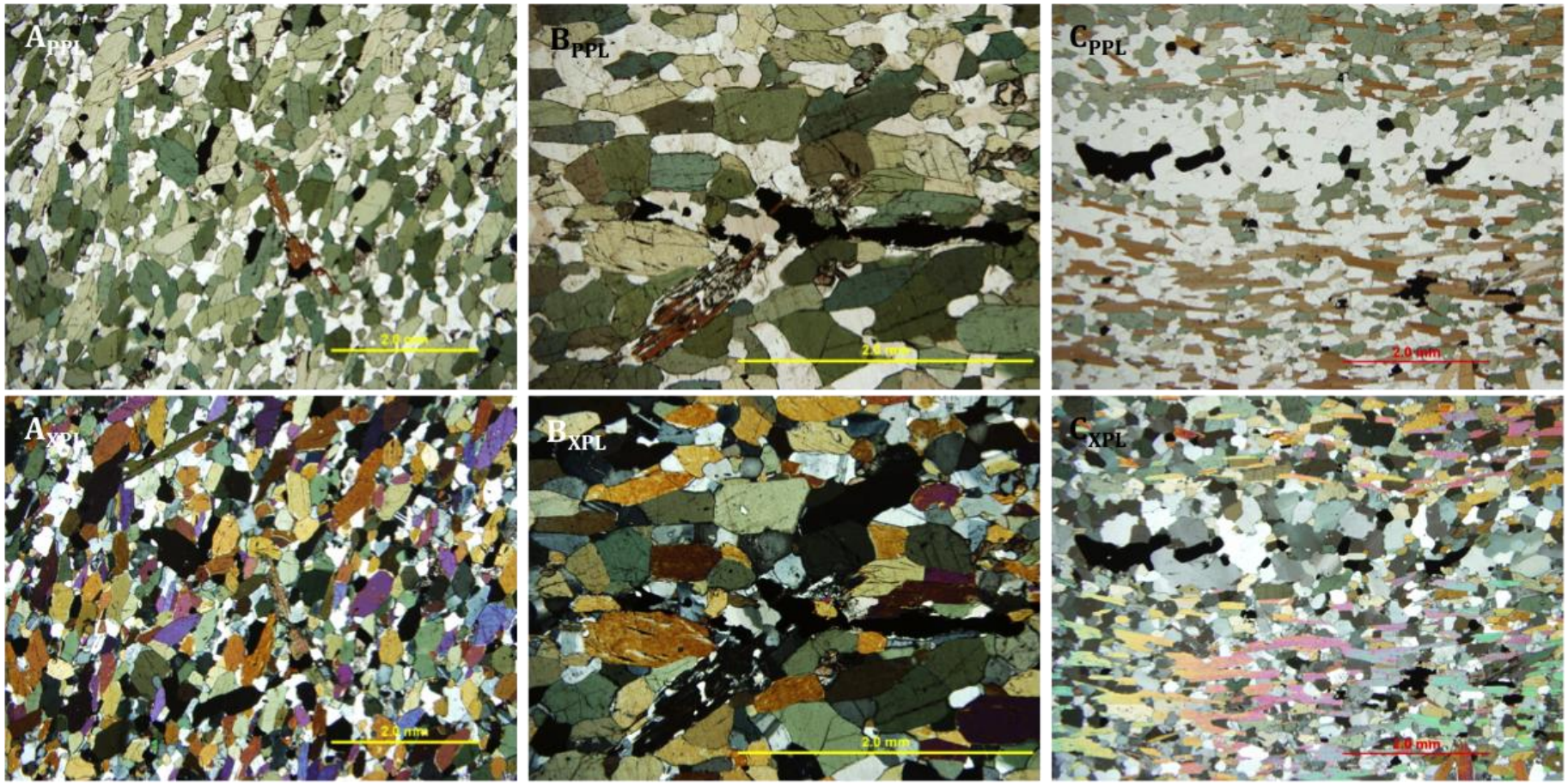

Figure 6.41. A) Strongly foliated, fine- to medium-grained amphibolite (±garnet). Sample FD 01301 with 340 ppb Au. B) Moderate to strongly foliated, medium- to coarse-grained amphibolite. Sample FD 01301 with 340 ppb Au. C) Gradational contact between amphibolite (top) and biotite-quartzofeldspathic gneiss (bottom) displaying strong foliation defined by both hornblende and biotite. Quartz vein with sulphides also aligned parallel to foliation. Sample BL10-15 (61.6m) with 17207 ppb Au.

Strong foliation in amphibolite is also commonly associated with relict granulite facies minerals and lithons. The massive granulite lithons or minerals are bordered by strongly aligned hornblende, indicating that high strain coincides with retrograde amphibolite facies metamorphism (Fig. 5.31). The hornblende is euhedral and moderately to strongly aligned surrounding anhedral orthopyroxene or clinopyroxene grains. This fabric is always associated with gold mineralization and typically displays increased sulphides.

Amphibolite (±garnet) can display a high-strain gneissosity defined by hornblende-rich melanosomes and quartz- and feldspar-rich leucosomes. Gneissic bands can range from 1 to 10 cm thick. Economic gold concentrations are typically associated with the amphibolite (±garnet) lithologies that display moderate to strong foliation or gneissic banding. In contrast, unfoliated amphibolite does not host gold mineralization.

6.2.2 Fabric of the Garnet-Biotite Schist (±Sillimanite)

Alignment and concentration of biotite defines a moderate to strong foliation and gneissosity of the overall unit. When present in high proportions, 35% to 50%, the biotite creates a schistose texture and has a coarse grainsize. The subparallel alignment of biotite defines a moderate foliation, which could indicate a lower strain environment allowing the crystals to attain larger dimensions. A coarse-grained and chaotic biotite texture is common when in contact with adjacent pegmatite, quartz veins or quartzofeldspathic gneiss units and the foliation can anastomose around these competent units. When biotite is in lower proportions, 20% to 35%, there is a strong

foliation and the biotite crystals are present in an equigranular quartzofeldspathic groundmass.

Metamorphic garnet and sillimanite also display alignment. The garnet grains can occur in clusters within the biotite groundmass. It is also common to have coarse biotite, quartz or gold mineralization in the low-strain zone adjacent to the garnet (Fig. 6.42A). In some occurrences, the garnet grains form stringers, parallel to the dominant foliation defined by biotite and overall gneissosity of the garnet-biotite schist (Fig. 6.42C).

The coarse sillimanite present in sillimanite-garnet-biotite schist, occurs as prismatic crystals in clusters, often parallel within a groundmass of quartz and K-feldspar (Fig. 6.42B). Sillimanite is a competent mineral and is common in granulite facies lithons. In core, coarse sillimanite similarly displays this subparallel fabric within a quartzofeldspathic groundmass (Fig. 6.42D). Foliations defined by metamorphic minerals indicate that deformation and metamorphism were synchronous within the mineralized units.

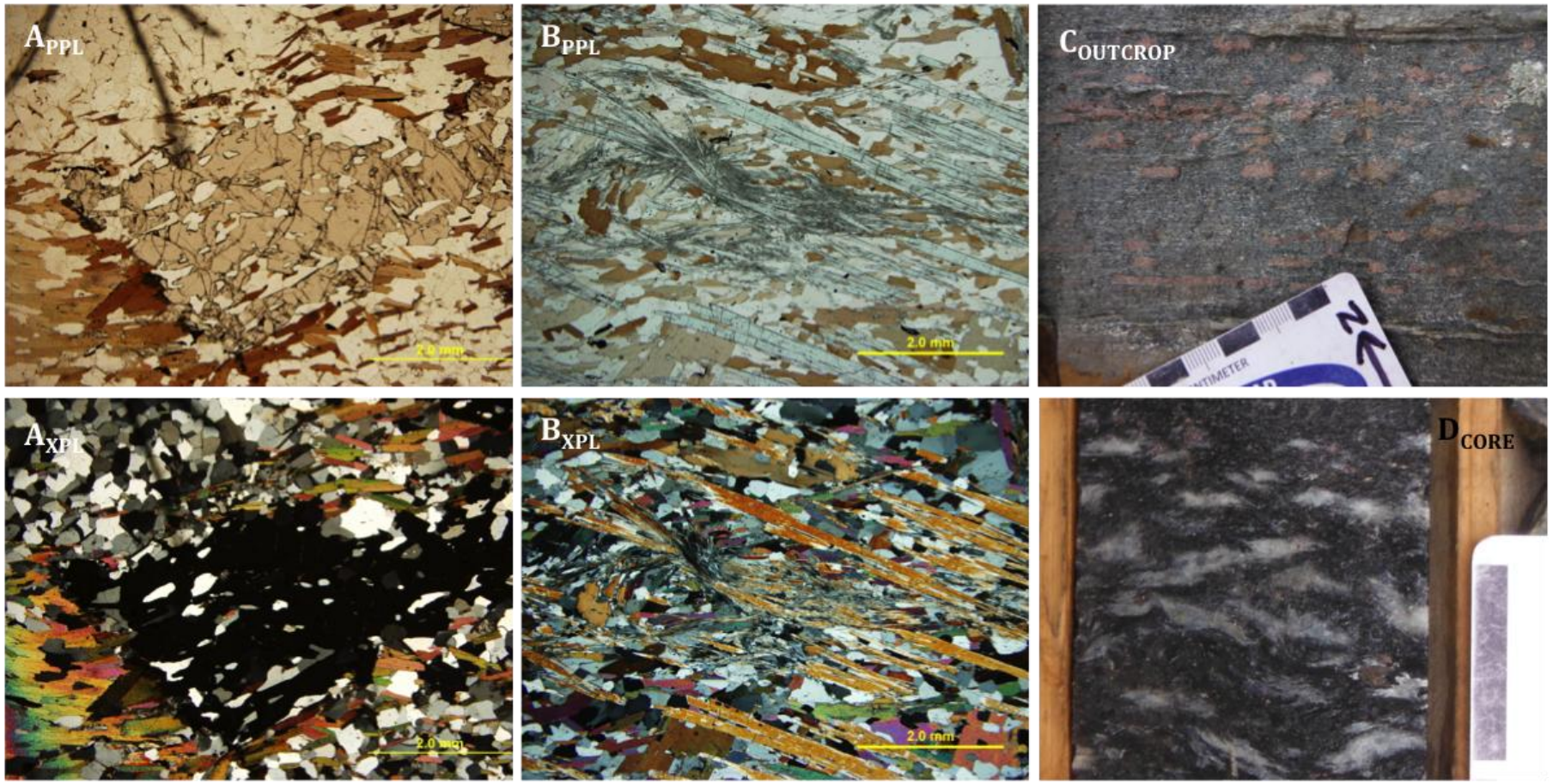

Figure 6.42. A) Central garnet porphyroclast, deformed and surrounded by foliated biotite from sample BL12-161B (61.5m) with 386 ppb Au. B) Parallel aligned coarse sillimanite (high relief in PPL and yellow-brown in XPL) with in a groundmass of quartz, K-feldspar, fibrolite and foliated biotite from sample FD 01334 (92 ppb Au). C) Garnet (red) deformed parallel to dominant foliation in outcrop. D) Garnet-sillimanite-biotite schist with coarse sillimanite (white) aligned parallel to foliation of biotite in core.

6.2.3 Fabric of the Quartzofeldspathic Gneiss

Biotite dominantly defines foliation in the quartzofeldspathic gneiss. These foliations can range from weak to strong and transitions between units range from sharp to gradational. Low modal abundance of biotite is typical in fine- to medium-grained quartzofeldspathic gneiss. The foliation is not obvious in hand sample but more apparent in microstructural analysis (Fig. 6.43A). When biotite is present in proportions between 15% to 25%, it defines a moderate foliation and has a medium- to coarse-grainsize (Fig. 6.43B). A coarse-grained, chaotic texture with randomly oriented biotite is common at contacts with adjacent unfoliated pegmatites, quartz veins or amphibolite units. The unfoliated units were more competent during deformation, while the biotite-rich lithologies anastomosed around them, effectively preserving the heterogeneous strain. This fabric is associated with gold mineralization and typically has increased sulphides. Quartzofeldspathic gneiss units can display a high-strain gneissosity defined by biotite-rich melanosomes and quartz- and feldspar-rich leucosomes. Very fine-grained quartzofeldspathic units are dark grey and may appear unfoliated in core, but when viewed under transmitted light microscopy, the mylonitized texture is strongly foliated (Fig. 6.43C). Commonly these fine-grained mylonites represent discrete high-strain (shear) zones indicated by grainsize reduction and strong fabric. The high-strain shear zone can vary between 1-10 cm wide and have gradational margins that transition from very fine grained and strong foliation to medium grained quartzofeldspathic gneiss. These transition zones represent local high strain environments that can range between 1 to 3 metres wide and typically contain gold and sulphides.

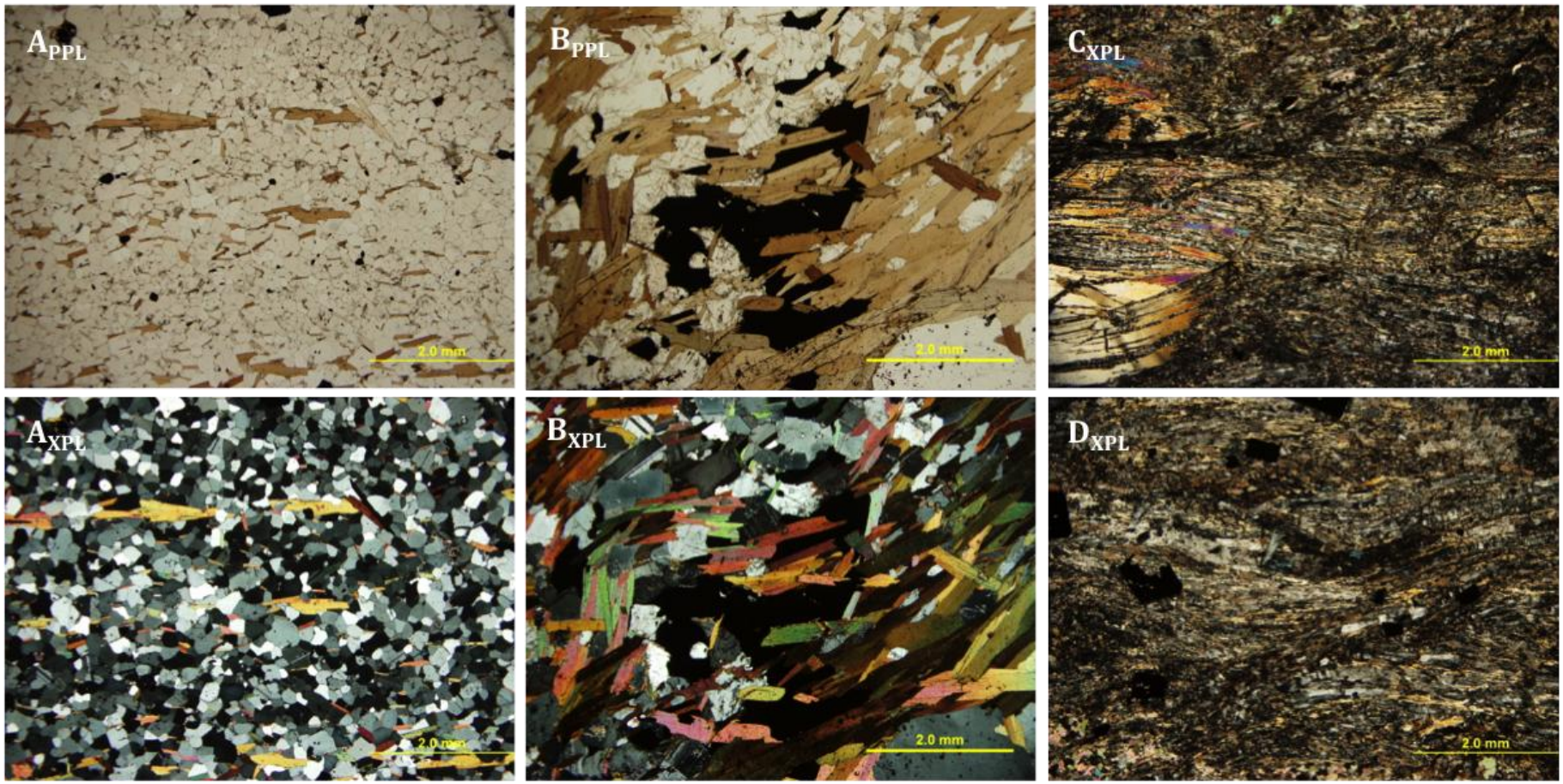

Figure 6.43. A) Moderate foliation in a fine-grained, biotite-quartzofeldspathic gneiss. Sample BL 12-161(61.5m) with 17207 ppb Au. B) Medium- to coarse-grained biotite-quartzofeldspathic gneiss exhibiting a strong chaotic foliation with increased sulphide mineralization. Sample FD 01303 with 439 ppb Au. C) and D) Mylonitized quartzofeldspathic gneiss with a strong foliation and very fine grainsize (caused by intense grainsize reduction). Sample BL12-256 (265.3m) with 35 ppb Au.

In unfoliated quartzofeldspathic gneiss, biotite content is typically low, between 3 to 10 modal percent, and randomly oriented. Medium- to coarse-grained quartz have undulose extinction and subgrains, while feldspar displays deformation twins indicating relatively low strain at high temperature. The coarse grainsize and stable mineralogy made this rock quite competent and resistant to ductile deformation in response to differential stress.

In some unfoliated fine- to medium-grained quartzofeldspathic gneiss units, local pods of coarse felsic material contain a minor abundance of metamorphic minerals. The dominant fine- to medium-grained quartzofeldspathic groundmass engulfs coarse- to very coarse-grained blebs of quartzofeldspathic material. These coarser-grained sections can also preferentially host hornblende, pyroxene or fibrolite as well as sulphide phases. These local coarse-grained sections of recrystallized quartzofeldspathic material do not host economic gold mineralization (Fig. 6.44). Typically, this texture is bordered by strongly foliated biotite-quartzofeldspathic gneiss or garnet-biotite schist, which does host economic gold mineralization.

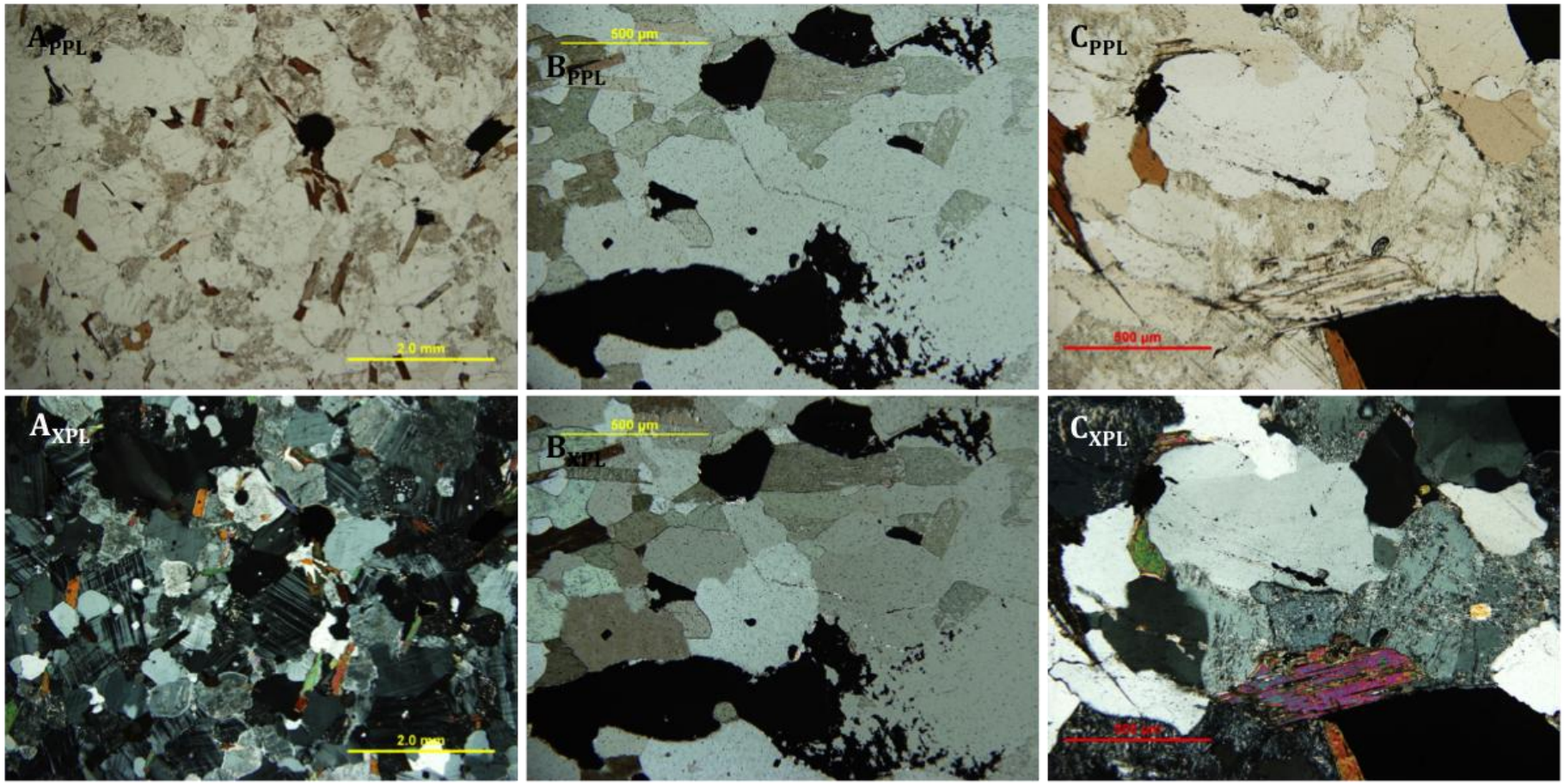

Figure 6.44. A) Unfoliated quartzofeldspathic gneiss with minor biotite from sample FD 01303 with 439 ppb Au. B) Unfoliated quartzofeldspathic gneiss with minor hornblende from sample BL10-15 (61.6m) with 17207 ppb Au. C) Unfoliated quartzofeldspathic gneiss with minor biotite and clinopyroxene from sample BL10-06 (98.5m) with 285 ppb Au.

These unstrained, massive quartzofeldspathic gneiss units display low strain, analogous to the felsic and granitoid clasts from the Borden Lake conglomerate. Coarse-grained quartzofeldspathic lithologies are less strained than the mafic amphibolite (±garnet) or garnet-biotite schist (±sillimanite) units. Although these unfoliated quartzofeldspathic gneisses are unmineralized, their association with high-strain mineralized lithologies appears to be significant. In outcrop, foliated biotite- or amphibolite-rich units anastomose around unfoliated, coarse-grained quartzofeldspathic lithologies. Within the ore zone, the strongly foliated amphibolite and garnet-biotite gneiss units surround short intervals of unfoliated quartzofeldspathic gneiss. The contrast in strain observed between the two lithologies is consistently associated with gold mineralization.

6.2.4 Quartz and Pegmatite Veins

Unlike the quartz veins associated with low-strain units, quartz veins with high-grade gold mineralization in the southeast area of the deposit display strong evidence for ductile deformation. Quartz veins in the high-grade zone appear grey-blue and contain inclusions of the host rock (Fig. 6.45). Microstructural analysis of quartz veins in the high-grade zone reveals prominent evidence for ductile deformation such as undulose extinction, subgrains and deformation lamellae (Fig. 6.46). The margins of these veins are commonly sharp and overall the veins are discordant and commonly boudinaged. In many cases the highly deformed quartz veins contain small inclusions of biotite, hornblende, pyroxene and feldspar or brecciated hostrock lithologies of amphibolite or garnet-biotite schist within the deformed quartz groundmass.

Pegmatite and quartz veins within amphibolite and quartzofeldspathic units typically display evidence of high strain. Quartz veins are commonly aligned parallel to surrounding host rock foliation and in some cases are boudinaged. Pegmatites are similarly deformed parallel to dominant foliation of the host rock. Quartz veins and pegmatites within the unfoliated amphibolite (±garnet) and quartzofeldspathic gneiss are typically undeformed and have sharp contacts with the host rock.

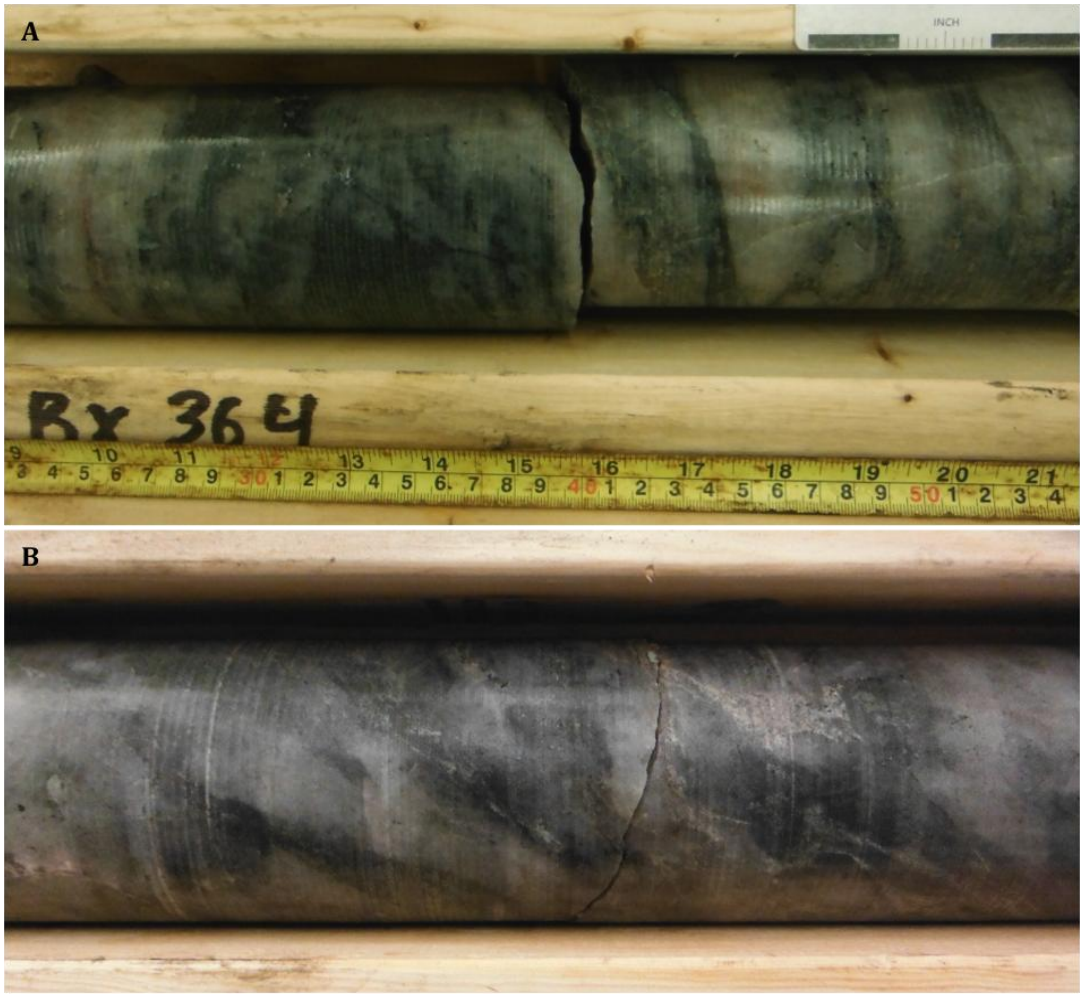

Figure 6.45. A) Deformed quartz veins within amphibolite of the high-grade zone from drill hole BL 12-256. B) Deformed quartz veins with grey-blue colour of the high-grade zone from drill hole BL 12-256.

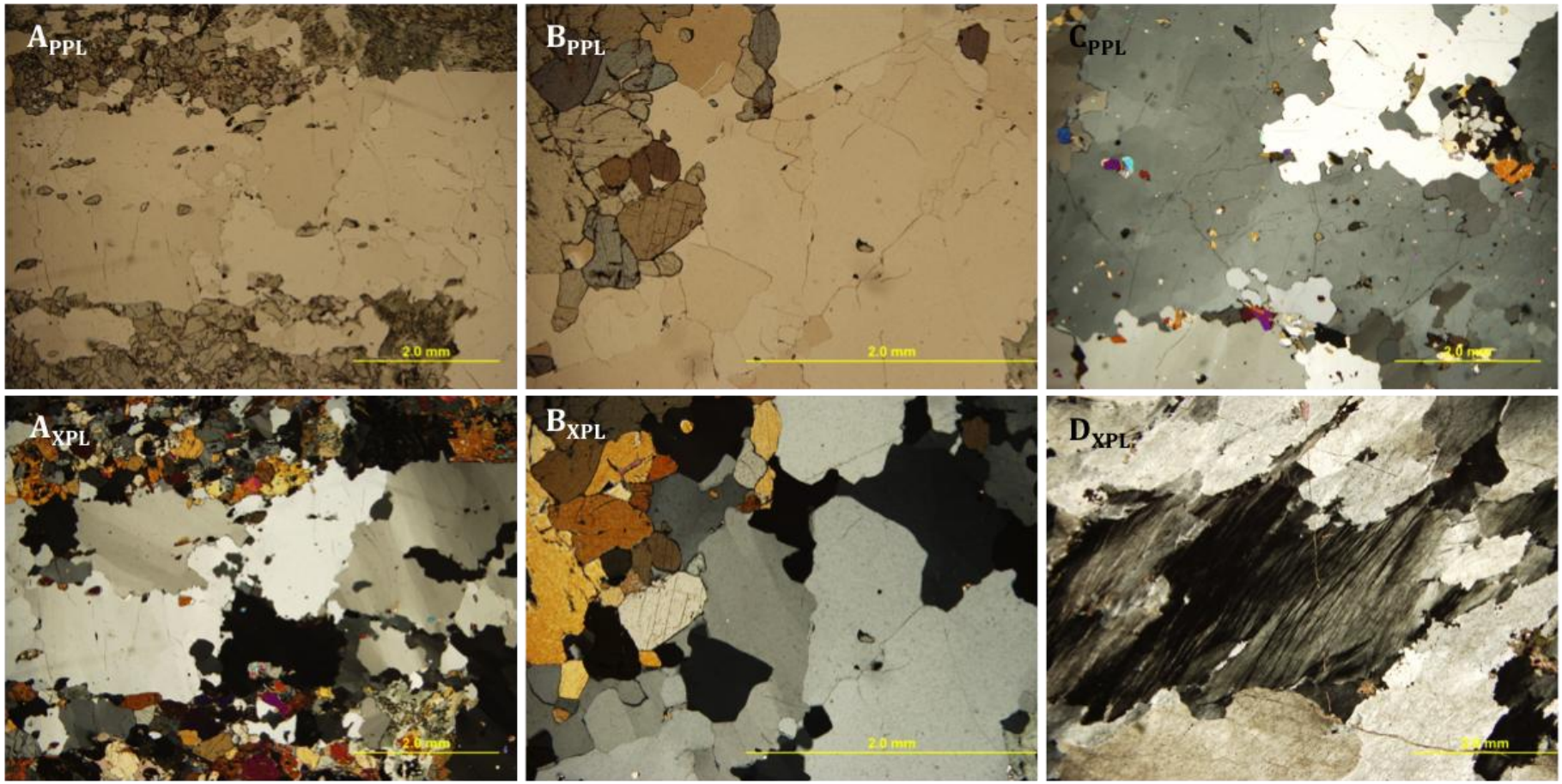

Figure 6.46. A) Deformed quartz vein with pyroxene inclusions in amphibolite. Quartz grains exhibit undulose extinction and grain boundary area reduction. Sample BL12-256 (350.4m) with 13300 ppb Au. B) Deformed quartz vein within amphibolite. Quartz grains exhibit undulose extinction and grain boundary area reduction. Sample BL12-256 (348.6m) with 14700 ppb Au. C) Deformed quartz vein with biotite and pyroxene inclusions. Sample BL12-256 (348.6m) with 14700 ppb Au. D) Deformation lamellae in quartz grains. Sample BL12-256 (265.3m) with 35 ppb Au.

6.3 Core Reassessment and Cross-Section Interpretation

During core reassessment for this study, detailed structural descriptions of each lithology were documented to identify any correlation to gold mineralization. Core logs were used to create 2-D cross sections (Figs. 4.13, 4.17, 4.23, 4.26, 4.28, 6.47).

The structural legend on the 2-D cross sections identifies low-strain textures at the top progressing to highest strain at the bottom of the legend. Low-strain is indicated by lack of foliation or alignment of platy minerals, referred to as massive. Amphibolite has commonly been associated with gold mineralization, although evident from Section 500m NW (Fig. 6.47), massive, low-strain amphibolite does not host economic gold mineralization. Similarly, quartzofeldspathic gneiss with low biotite content and unfoliated to weak foliation commonly displays low-strain and low gold concentrations. In some cases, coarse quartz grains in the quartzofeldspathic gneiss may have a strained centre with a mantle of strain-free grains and subgrains representing some ductile deformation by dislocation creep; this texture is recorded as diffuse rims. A migmatite texture as indicated in the legend refers to coarse-grained blebs of quartzofeldspathic material within a dominantly fine- to medium-grained groundmass. The textures are indicative of low strain and do not host economic gold concentrations on the Borden property.

Schistose fabric is commonly associated with coarse-grained biotite when adjacent to a competent low-strain lithology. Some garnet porphyroblasts have biotite foliation deflecting around the grain, forming asymmetric tails, with common coarse-grained and randomly oriented biotite in the low-strain shadow zone of the garnet. Competent lithologies like quartz veins or quartzofeldspathic gneiss commonly have

increased biotite content at their contact with surrounding units and the biotite at the contact has a chaotic fabric and coarse grainsize. Foliation as indicated in the legend refers simply to the parallel alignment of platy or elongate minerals within a lithology. At Borden, biotite commonly defines foliation in quartzofeldspathic gneiss and garnet-biotite schist, and hornblende commonly defines foliation in amphibolite. Banded textures describe rocks that display evidence of moderate to high-strain. Grainsize is somewhat variable, but the parallel alignment of minerals or leucosomes and melanosomes define a planar fabric. Porphyroclast tails and boudinage within this structural group are evidence of moderate- to high-strain. Boudinaged, unfoliated units are bordered by moderate to strongly foliated units. The localized high strain is attributed to competency contrasts between different minerals or lithons adjacent to one another.

Penetrative high-strain structural fabrics are described as mylonites and protomylonites, due to grainsize reduction caused by dislocation creep. Textures were carefully interpreted and documented during core logging. Further microstructural analysis confirmed grainsize reduction by dislocation creep as the mechanism for mylonitization.

Overall, an increase in strain downhole was consistently identified from lower strain above the ore zone, to high strain within the ore zone lithologies and lower strain below the ore zone. When compiling data in the 2-D cross-section interpretations, this pattern was evident and consistently related to economic gold mineralization.

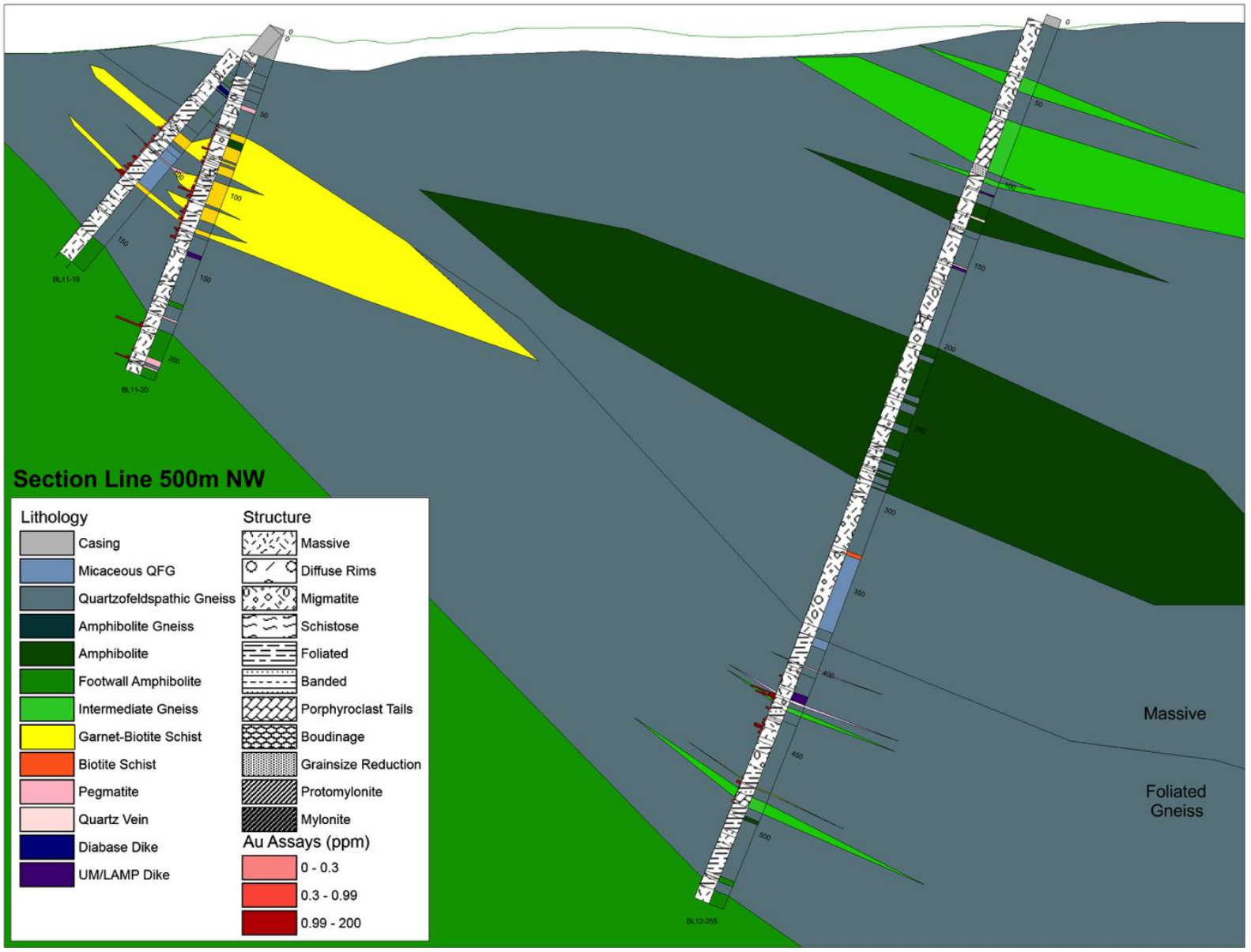

Figure 6.47. Section line 500m NW 2-D cross section. Drill hole azimuths at 180°. Lithological and structural interpretation compiled during summer field research in 2014.

The six 2-D cross-sectional interpretations (Figs. 4.13, 4.17, 4.23, 4.26, 4.28, 6.47) were digitized and compiled in a 3-D fence diagram (Fig. 6.48). The overall geometry of flattened lenses of garnet-biotite schist and amphibolite (±garnet) is comparable in orientation and shape to the geometry of the ore body. The flattening direction roughly strikes northeast-southwest and the long direction plunges southeast. The relationship between these lenses and the 3-D shape of the ore body (Fig. 1.3) supports the idea of structural control on gold.

The quartzofeldspathic gneiss located above the ore zone displays low-strain, unfoliated textures. Similarly, amphibolite (±garnet) that does not have a high-strain fabric does not host gold mineralization. These competent unfoliated units create heterogeneous strain due to the adjacent ductilely deforming units that host economic gold mineralization.

The high-strain deformation of the dominant gold-hosting lithologies highlights an important timing for mineralization. Since the foliation and high-strain are dominantly defined by retrograde amphibolite facies minerals, the mineralization must be coeval with the deformation and retrograde metamorphism to amphibolite facies.

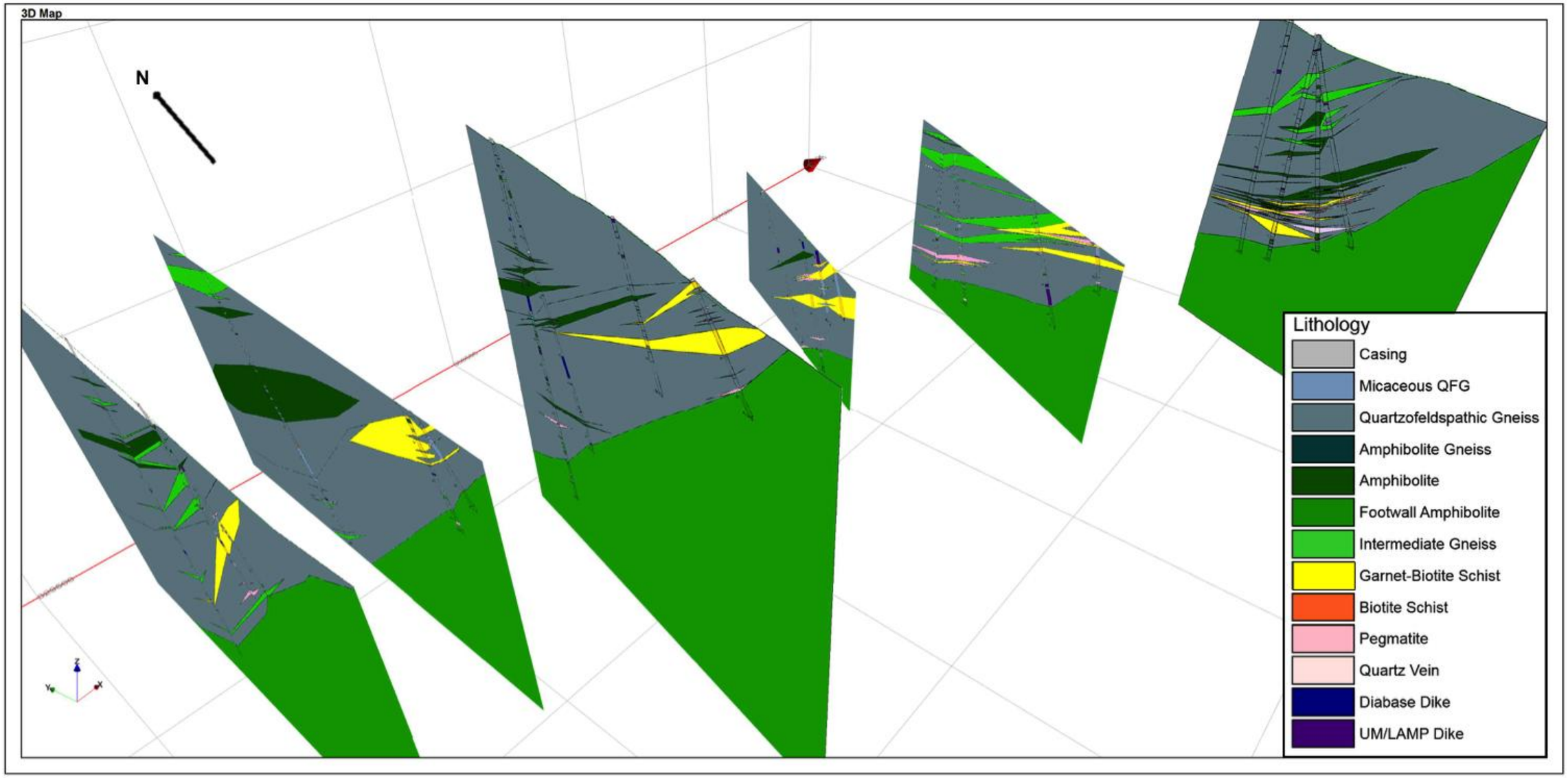

Figure 6.48. Fence diagram from 2-D cross sections created from digitized core reassessment. From left to right; Section line 700m NW, Section line 500m NW, Section line 150m NW, Section line 50m SE, Section line 500m SE, Section line 1200m SE.

6.4 Structural Control on Mineralization

Metamorphism and structure are both crucial to the location of gold mineralization at the Borden gold deposit. Structure seems to be an important indicator of metamorphic intensity and subsequent gold mineralization. From all field measurements, two average populations of north-dipping and south-dipping planar fabrics related to shear zone structures were plotted. Modeling of the ore zone by Probe Mines Limited determined a general trend and plunge of 22°/115° for the ore zone. Plotting the average foliation planes and ore zone lineation, the trend and plunge of the ore zone lies on the plane bisecting the two average foliation planes (Fig. 6.49). This plane represents a principal plane of strain that contains the direction of maximum elongation, S_1 and S_2 the intermediate principal axis of elongation. Most mineral lineations align near this plane and subparallel to maximum elongation with minor variation due to overall lithological competence.

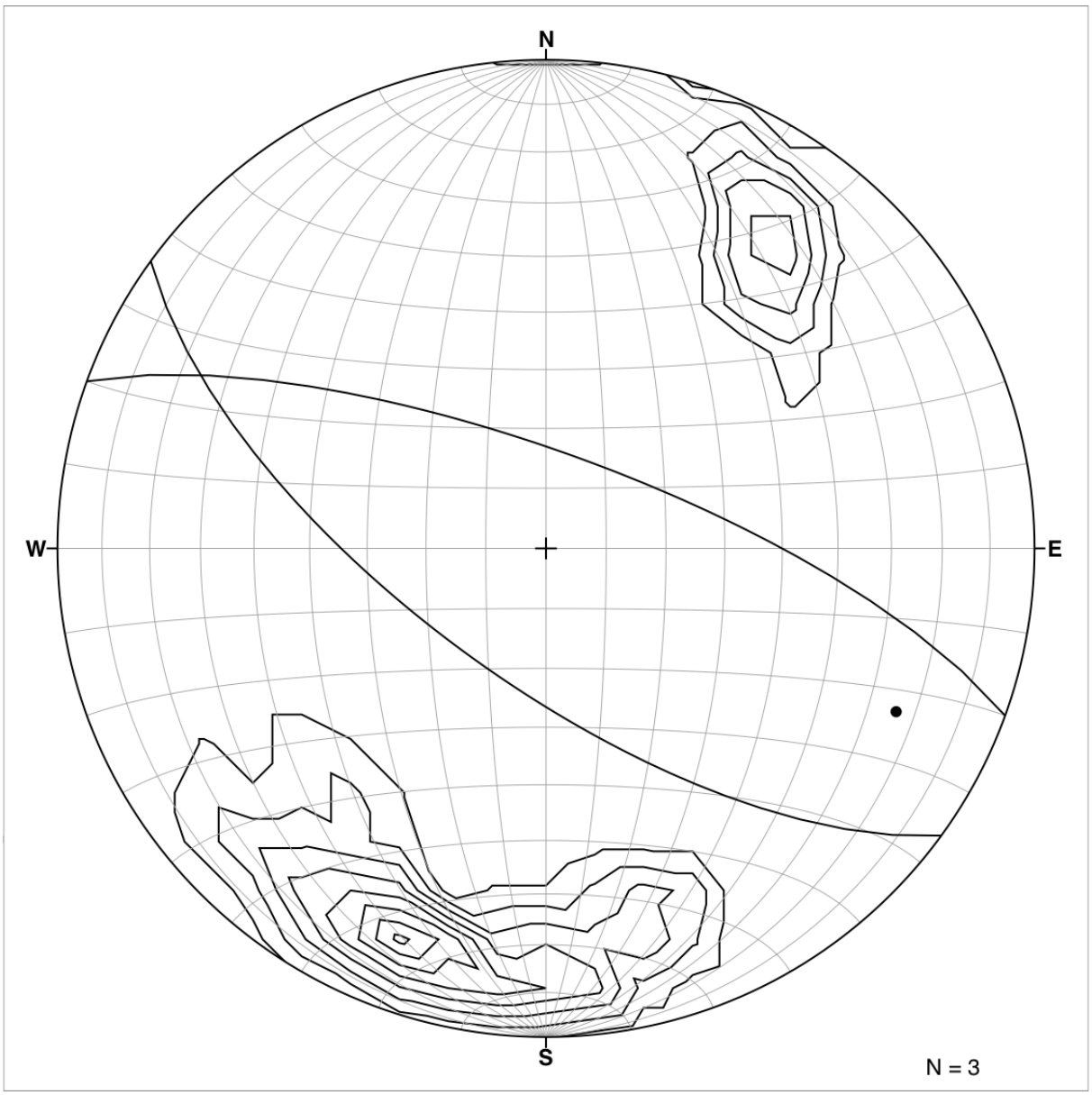

Figure 6.49. Stereonet displaying the two distinct population contours from all five structural domains. Represented as great circles are the respective average strike and dip of the two populations. Plotted as a point is the lineation of the ore zone determined from 3-D modeling by Probe Mines Limited (2015).

Boudinage at all scales has been identified in many lithologies on the Borden property through outcrop mapping, 2-D cross section interpretation and microstructural analysis. Boudinage is a response to differential stress and a typical feature of ductile shear zones, representing heterogeneous strain. Competency

contrasts between adjacent lithologies and separation of boudins will effectively cause deviation in foliation and dip. Since spaces between boudins can be filled with quartz or other hydrothermal minerals, this structure may be significant to elongate zones of gold mineralization.

Evidence of boudinage is seen on the macroscopic scale in core and outcrop. Quartz veins associated with the mineralized zone are commonly boudinaged and host increased sulphides in the low-strain zones between boudins (Fig. 6.50A). Competent coarse-grained pegmatites pinch and swell with biotite-quartzofeldspathic gneiss ductilely deforming around it on the Borden property (Fig. 6.50B). The consistent occurrence of boudinage on both of these macroscopic scales emphasizes the dominant heterogeneous strain on the Borden property.

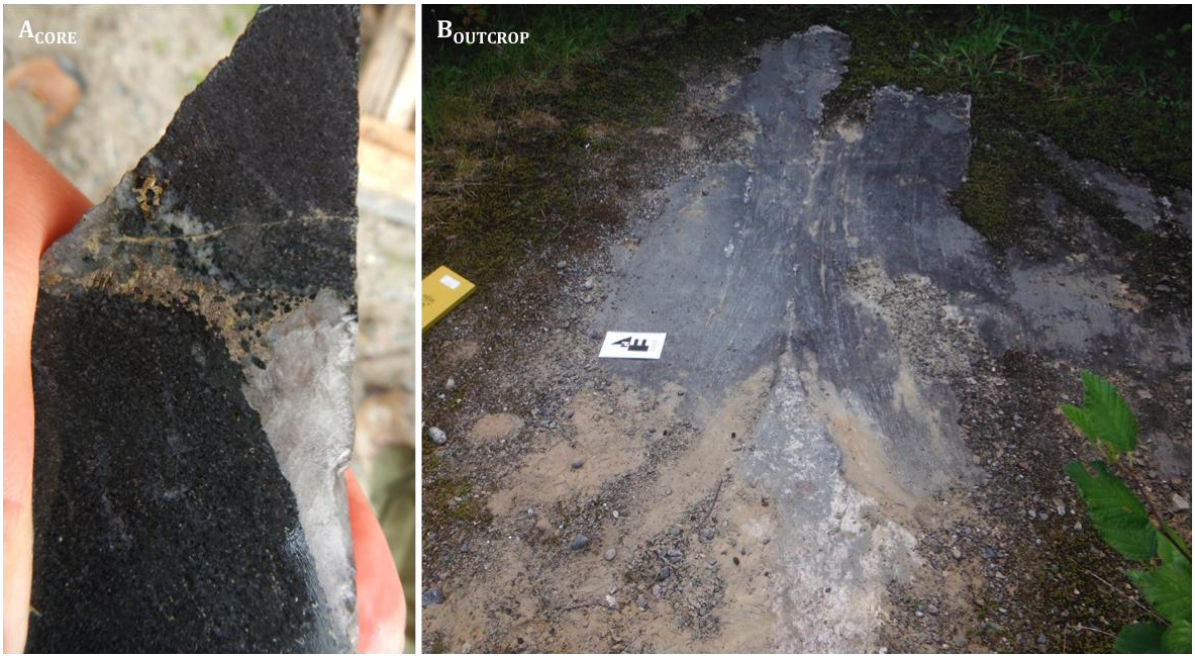

Figure 6.50. A) Boudinaged quartz vein with increased pyrite and pyrrhotite in the low-strain zone. B) Boudinaged pegmatite within a foliated biotite-quartzofeldspathic groundmass (Photo by V. Stinson, 2014).

On the microscopic scale, competency contrasts and boudinage similar to those on the macroscopic scale occur. Structures created in the necks between macro-scale boudins show many similarities with those in microscopic strain shadows of competent minerals and lithons. Low-strain zones in the shadows of competent minerals are favourable for gold mineralization during deformation. Relict granulite facies minerals including clinopyroxene, orthopyroxene, sillimanite, K-feldspar and garnet are observed to be sharply bordered by aligned hornblende or biotite that deflect around granulite lithons. Foliation deflects around garnet and pyrite, and there are increased quartz and gold mineralization in the low-strain zones adjacent to these competent minerals (Fig. 6.51A,B). Low-strain zones associated with mineral competency contrast are a common feature at Borden in microstructure and commonly contain increased sulphides and gold.

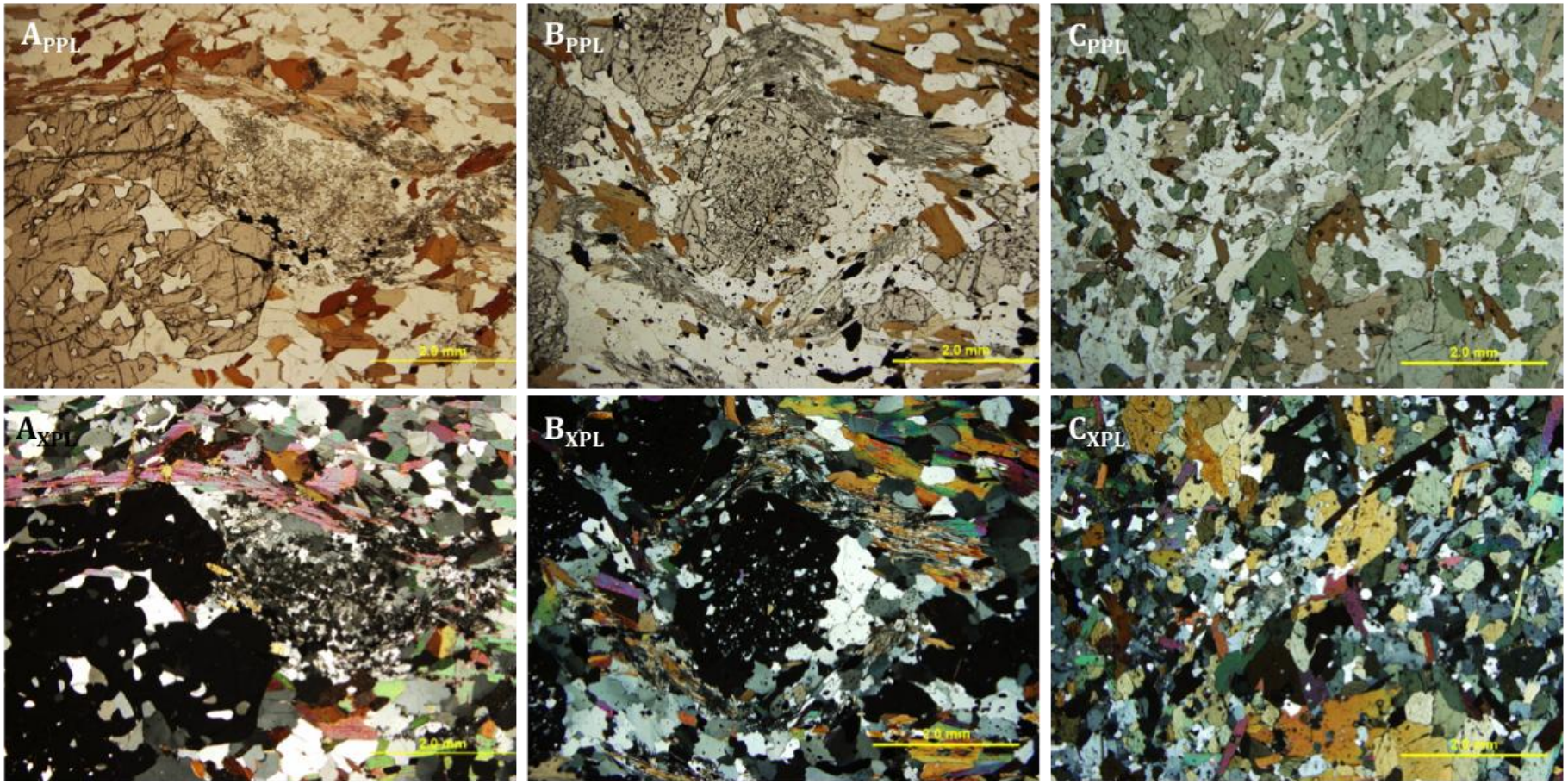

Figure 6.51. A) Garnet-biotite schist, euhedral garnet surrounded by foliated biotite with quartz in the low-strain zone. Sample BL12-178 (169.5m) with 160 ppb Au. B) Sillimanite-garnet-biotite schist, garnet at centre surrounded by biotite and sillimanite with quartz in the low-strain zone (right-centre). Sample FD 01342 with 176 ppb Au. C) Amphibolite with subhedral hornblende and biotite. Sample FD 01314 with 260 ppb.

7. MINERALIZATION

Lithological units on the Borden property are well documented through diamond drill core logging. Gold is found in a variety of lithologies with some lithologies concentrating higher amounts of gold. Gold-hosting lithologies on the Borden property are garnet-biotite schist (±sillimanite), amphibolite (±garnet), biotite-quartzofeldspathic gneiss and deformed quartz veins. The ore body is a long, slightly flattened, prolate elliptical zone, with a shallow to moderate plunge to the southeast. The ore body has a map length in excess of 3.5 km with a width ranging from 150 to 500 m. It strikes NW (295°), dips to NE (42°) and plunges between 18°-22° to the SE (115°). The long hole section of the ore body (Fig. 1.3) effectively displays the consistent low-grade halo that encompasses the entire deposit. The deposit has been separated into two distinct zones of gold mineralization: low-grade ore and high-grade ore.

Previous economic gold mineralization at Borden had been associated with the garnet-biotite schist lithology and deformed quartz veins. This study has determined a structural and metamorphic control on gold mineralization. The Discovery Outcrop provided a unique opportunity to analyze gold mineralization in relation to structure and metamorphism.

There are a few occurrences of visible gold in core, and even more gold is identified in microstructural analysis. High-strain fabric and retrograde metamorphism of these lithologies is critical to the structural and metamorphic control of mineralization on this deposit.

7.1 Low-grade Gold Mineralization

The lower grade ore in the northwest is hosted in foliated garnet-biotite schist, amphibolite (±garnet) and biotite-quartzofeldspathic gneiss units. It averages 1.03 g/t and increased modal abundance of pyrite and pyrrhotite are typically associated with gold. High strain, defined by parallel alignment of biotite, hornblende and sulphide stringers is always associated with gold mineralization. The garnet-biotite schist always has a moderate to strong planar fabric and is always mineralized on the Borden property. The amphibolite and quartzofeldspathic gneiss units can be unfoliated and massive. When these units are unfoliated, gold mineralization is negligible. Interestingly, contacts between unfoliated amphibolite or quartzofeldspathic gneiss and strongly foliated biotite-quartzofeldspathic gneiss, amphibolite (±garnet) and garnet-biotite schist all concentrate higher amounts of gold.

Low-grade gold mineralization exposed at surface prompted the discovery of the Borden gold deposit. The Discovery Outcrop contains a majority of the lithological assemblages on the Borden property. A channel sample was taken on the Discovery Outcrop to assess gold mineralization not just by unit but also to identify potential gold mineralization at lithological contacts. The channel was cut perpendicular to the dominant west-northwest strike of lithologies on Discovery Outcrop. Two channels were cut, representing the northern and southern parts Discovery Outcrop (Fig. 7.52). An interesting feature of the assay results is that the highest concentration of gold is located at the contact between the foliated biotite-quartzofeldspathic gneiss and garnet-amphibolite unit in the basal portion of the northern outcrop (highlighted by the red circle in Fig. 7.52). The spike in gold concentrations at a lithological contact is

consistent with results from microstructural analysis and cross-sectional interpretation from core logging. Lithological contacts and mineral grain boundaries both present surfaces of strain heterogeneity, which can provide low-strain environments for fluid migration and subsequent gold mineralization.

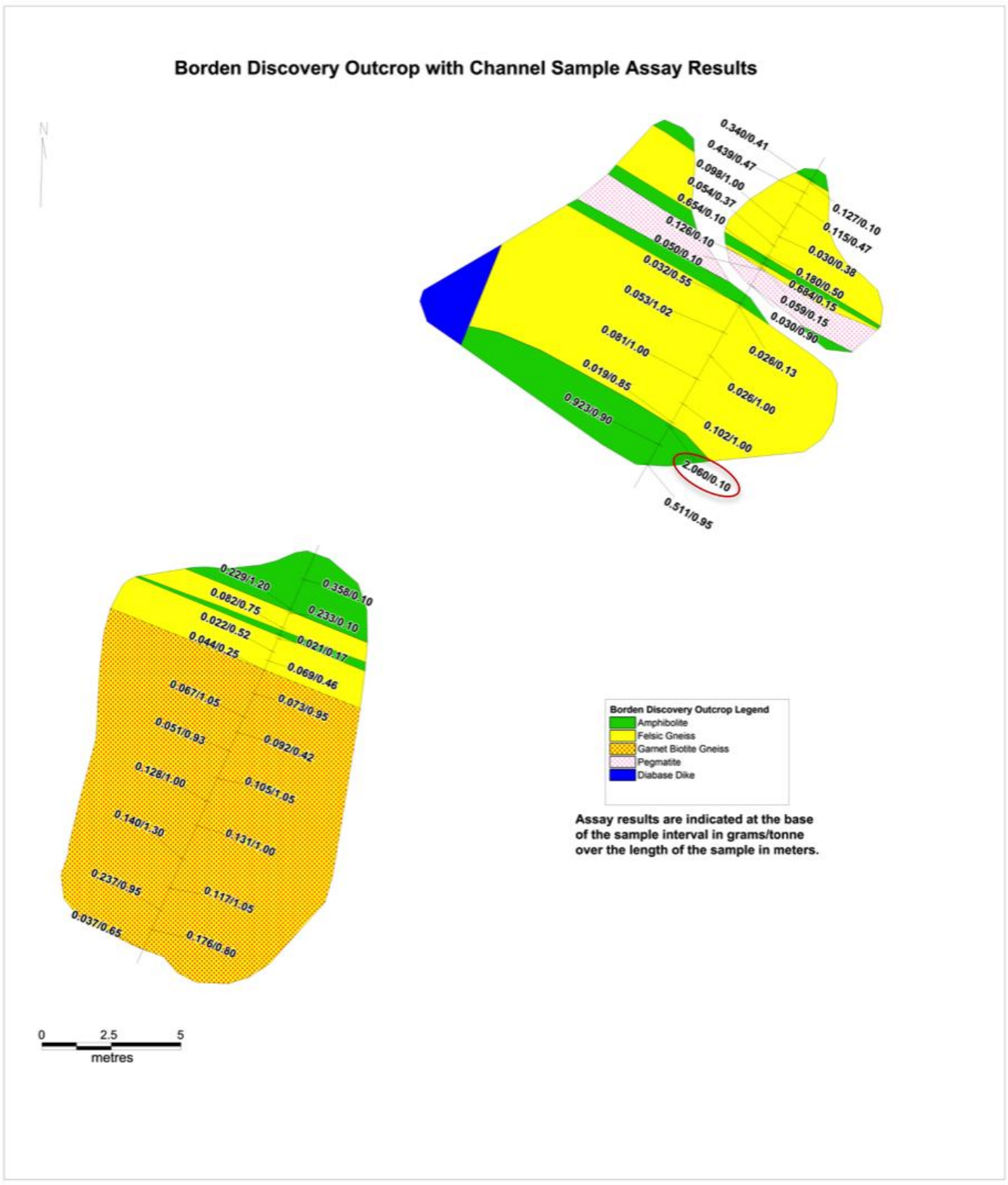

Figure 7.52. Channel sample map from Discovery Outcrop with location of samples and gold concentrations in grams per tonne over the length of the sample in metres. Highest gold concentration highlighted by the red circle at the contact between biotite-quartzofeldspathic gneiss and garnet-amphibolite.

A key feature of the Discovery Outcrop is the local variation in foliation dip. On the southern outcrop the sillimanite-garnet-biotite schist unit dips north and south appearing to wrap around a competent granulite lithon below. The side profile from the ground displays the obvious gradual change in dip from north to south wrapping around a more competent granulite lithology (Fig. 7.53). The dip heterogeneity is not a product of folding but rather a rheologic contrast between units that causes less competent units to deflect around large-scale boudins of granulite facies lithologies. Application of large-scale boudinage to the deposit model could be beneficial for further exploration and mining.

Figure 7.53. Southern portion of Discovery Outcrop (facing east). White dashed lines highlight the curvature of strong foliation defined by biotite in the sillimanite-garnet-biotite schist unit surrounding a massive, competent granulite lithon below.

Gold is not visible in core or outcrop, but commonly visible in reflected light microscopy. Low-grade, mineralized lithologies are often associated with pyrite and pyrrhotite. Pyrite occurs as both blocky and anhedral crystals and is commonly associated with pyrrhotite. Pyrrhotite occurs as anhedral blebs of varying sizes. Sulphides such as anhedral pyrrhotite and euhedral to anhedral pyrite are common and locally abundant as sulphide stringers parallel to gneissosity. Gold associated with this sulphide assemblage can be identified filling fractures in pyrite and at pyrite grain boundaries, surrounded by anhedral pyrrhotite (Fig. 7.54).

Free gold also occurs as inclusions or along fractures in metamorphic minerals (e.g. K-feldspar, hornblende, garnet, biotite, orthopyroxene, clinopyroxene). The contact between relict granulite microlithons surrounded by amphibolite facies minerals is also a favourable location for gold mineralization. Retrograde metamorphism in amphibolite (±garnet) displaying strong foliation defined by the amphibolite facies mineral assemblage engulfs granulite lithons of clinopyroxene, orthopyroxene, K-feldspar and garnet (Fig. 7.55). Gold is common in low-strain zones surrounding competent minerals such as garnet, sillimanite and pyrite (Fig. 7.56A). Sillimanite-garnet-biotite schists have coarse sillimanite within a groundmass of quartz, biotite and K-feldspar that deflects around competent pyrite. High-strain, mineralized biotite-quartzofeldspathic gneiss units contain sulphide stringers that are parallel to foliation and contain gold mineralization (Fig. 7.56B).

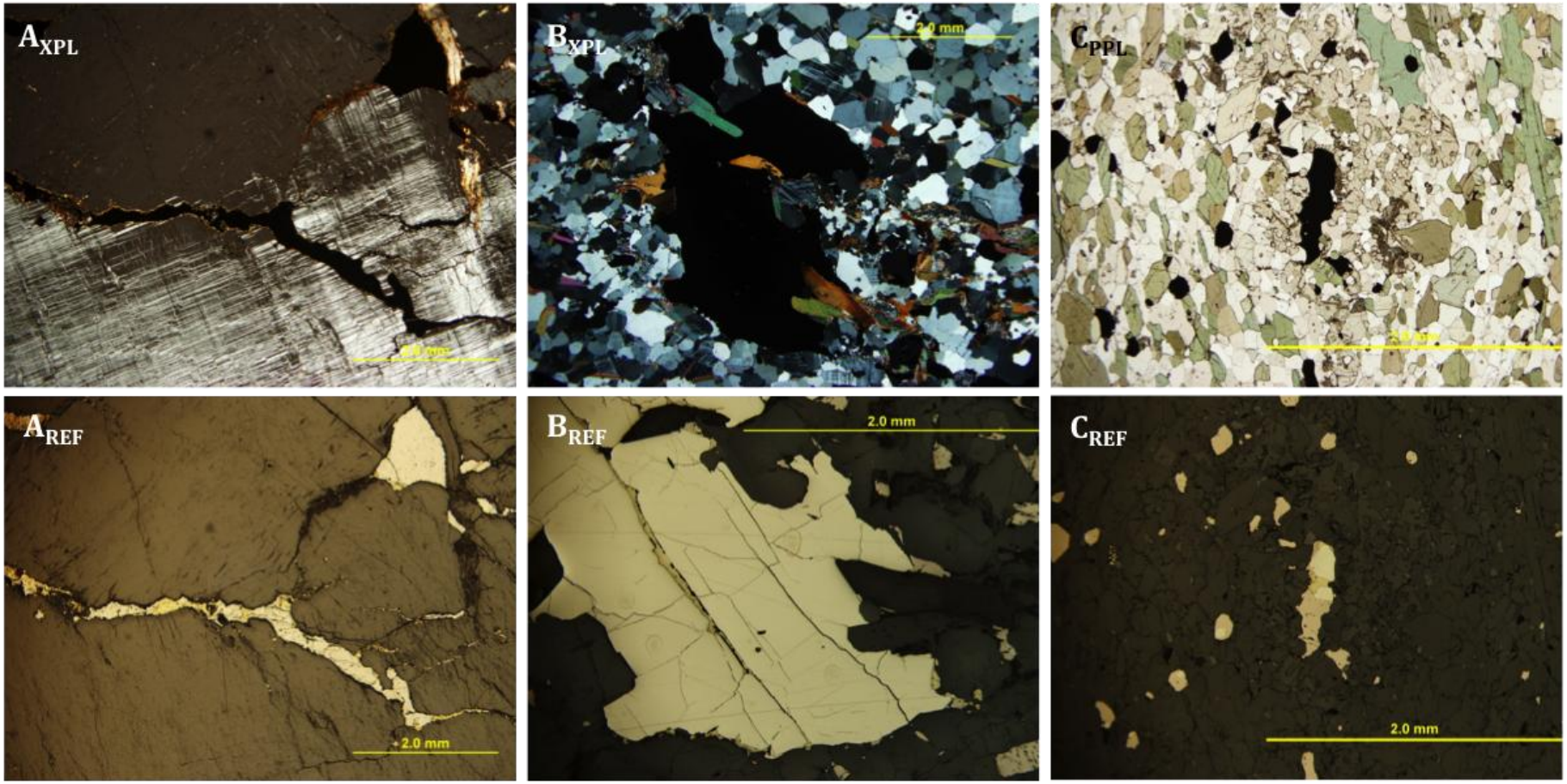

Figure 7.54. A) Fracture filling pyrite and gold mineralization between quartz and microcline. Sample BL12-274 (124.5m) with 2390 ppb Au. B) Gold infilling a fracture in pyrite. Sample BL10-15 (112.5m) with 6654 ppb Au. C) Gold at pyrite grain boundary, sheathed by pyrrhotite within a relict orthopyroxene grain. Sample FD 01322 with 511 ppb Au.

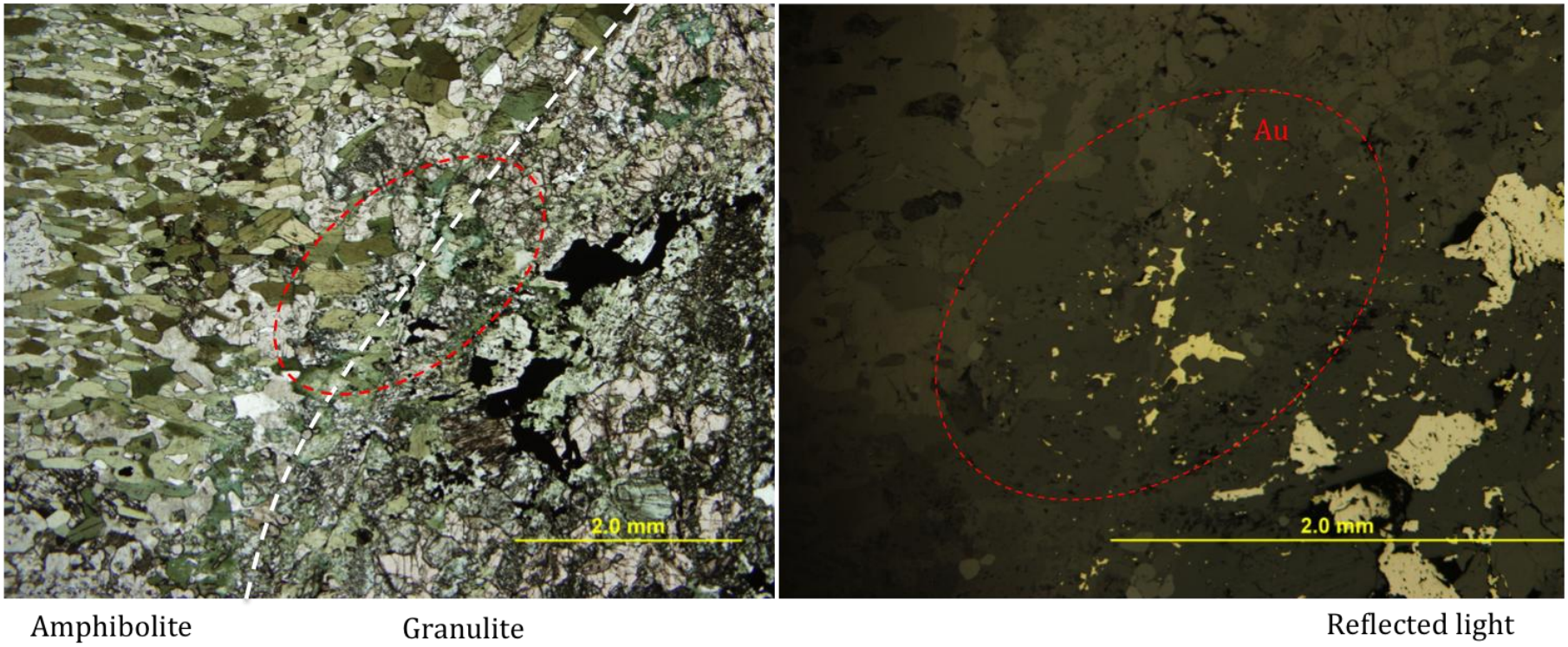

Figure 7.55. In the plane polarized light photomicrograph, at left, retrograde amphibolite facies mineral assemblage of hornblende, plagioclase and garnet is adjacent to a granulite lithon (right) composed of clinopyroxene, garnet and plagioclase. At the contact highlighted by the white stippled line is free gold, circled with red stipple in the reflected light photomicrograph. Garnet-amphibolite, sample BL11-20 (189m) with 10812 ppb Au.

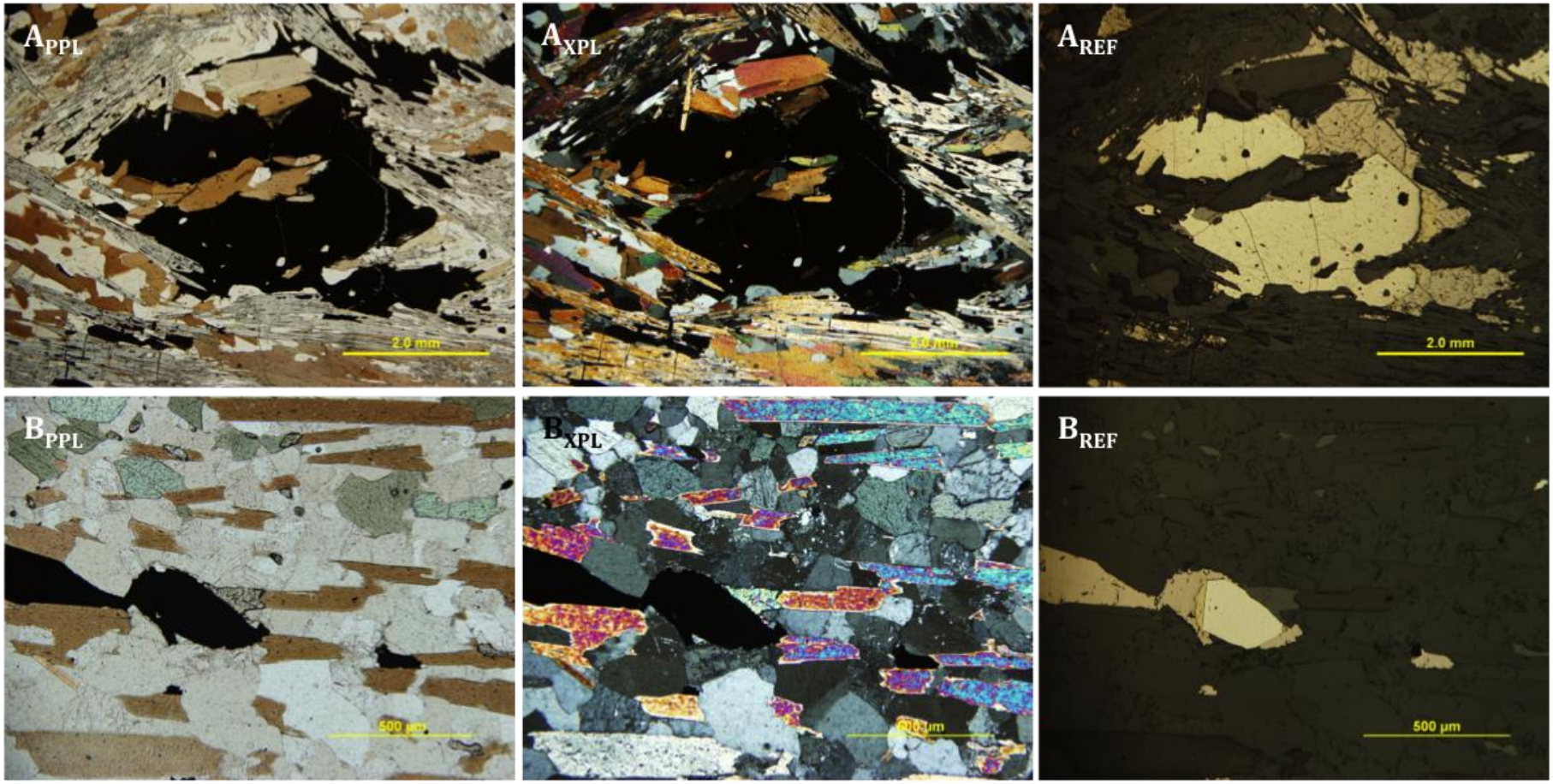

Figure 7.56. A) Opaque pyrite porphyroclast with sillimanite and biotite deflecting around the pyrite. In the low-strain zone to the left of the pyrite is an anhedral gold bleb sheathed by pyrrhotite visible in reflected light (A_{REF}). Sillimanite-garnet-biotite schist, sample FD 01339 with 1440 ppb Au. B) Strongly foliated biotite-quartzofeldspathic gneiss with minor hornblende. Opaque sulphide stringer parallel to foliation has euhedral pyrite with gold at the grain boundary, sheathed by anhedral pyrrhotite. Sample BL10-15 (61.5m) with 17207 ppb Au.

7.2 High-grade Gold Mineralization

The high-grade section of the ore body is located at depth. It was first identified in 2012 during step-out drilling on section line 1200m SE (Fig. 4.28). The deformed quartz veins hosting gold mineralization are continuous with further step-out section drilling to the southeast. The high-grade zone contains abundant quartz, less abundant pyrite and pyrrhotite and has been described in core by drill geologists as "siliceous alteration" or "quartz flooding". This section of the ore contains brecciated lithologies of amphibolite, garnet-biotite schist and pegmatite within a deformed quartz groundmass. The interesting feature of this high-grade zone is that the free gold (>1mm) is typically visible. Free gold is visible at the contacts between deformed quartz veins and brecciated lithologies and also within the groundmass of the deformed quartz veins. The high-grade mineralized zone is much more lithologically heterogeneous, and textures indicate high strain variability. Lithologies that are typically foliated preserve this foliation, although they occur as angular fragments within a quartz groundmass. This indicates ductile deformation prior to brecciation. At the Borden gold deposit, the highest gold grades are associated with most heterogeneous brittle-ductile deformation.

8. DISCUSSION

Discovery of the Borden gold deposit tests new ideas about the way brittle-ductile shear-zone deformation controls gold mineralization in orogenic gold deposits. Gold mineralization at the Borden project is associated with lower-strain areas within regional subvertical ductile shear zones. Mapping and microstructural analysis to date provide evidence for gold mineralization in association with brittle-ductile heterogeneous strain caused by lithological and mineralogical competency contrasts. Adjacent units with different rheology create incompatible strain at contacts.

8.1 Lithology

Traditional thinking within Archean Superior Province gold deposits relates much of the gold mineralization and potential of an area to metaconglomerate units that are often proximal to gold mineralization. The "Timiskaming-type" metaconglomerate can be useful in the sense that it preserves the history of a specific sedimentary depositional environment. The Borden Lake metaconglomerate does not host gold mineralization and is not directly associated with mineralized lithologies on the Borden property. Inherited zircons and subsequent high-temperature deformation make interpretation of ages difficult to constrain, specifically with respect to gold mineralization. Published zircon estimations of the maximum age for metaconglomerate deposition at the Borden Belt are: 2671 ±12 Ma (Moser et al., 2008) and 2667 ±2 Ma (Krogh, 1993). Timiskaming conglomerate to the east in the Abitibi Subprovince is dated at 2680 ±4 Ma (Corfu et al., 1990). U-Pb dating of detrital zircon from Timiskaming turbidites yielded a maximum depositional age of 2677.7 ±3 Ma

(Ispolatov et al., 2008). This older age is consistent with a possible depositional age for the Borden Lake metaconglomerate.

At the Borden gold deposit, a useful feature of the metaconglomerate is the variation in strain magnitude. The outcrop of unmineralized metaconglomerate proximal to the ore zone displays high-strain deformation of clasts, which provides a lineation subparallel to surrounding high-strain, mineralized lithologies. Farther from the ore zone, the metaconglomerate displays a low- to moderate-strain. Although the conglomerate is not directly related to gold mineralization, it may provide a beneficial strain indicator when conducting regional exploration.

The garnet-biotite schist is the unit most commonly associated with gold mineralization. The garnet-biotite schist had been initially interpreted as a metasedimentary unit due to the abundance of aluminous minerals. This seemed plausible due to the presence of the Borden Lake metaconglomerate. Analysis associated with Lu/Hf garnet dating of the garnet-biotite schist on Discovery Outcrop provided garnet isotopic data. The Hf isotopic signature ($^{176}Hf/^{177}Hf$ =0.281204 ±0.000013) of the garnet indicates that the protolith was derived from a long-term depleted mantle reservoir. This evidence suggests that the garnet-biotite schist unit may have been a hydrothermally altered mafic igneous rock and not a metasedimentary protolith.

On the macroscopic scale, field mapping and core logging identify gold at lithological contacts, strain shadows of boudinaged lithologies and within ductilely deformed quartz veins.

The channel sample taken on Discovery Outcrop provided a comprehensive understanding of macroscopic structural controls of gold mineralization. Assay results from the channel sample were unique, in that they captured lithological contacts. This differs from assay results from drill holes, where samples were not taken across lithological boundaries. The channel sample displayed gold mineralization in all units. The highest concentration of gold is present at the contact between the biotite-quartzofeldspathic gneiss and the foliated garnet-amphibolite. This relationship highlights the significance of the rheologic contrast between units and the importance of structure to gold mineralization. Lithological contacts, specifically between two rheologically contrasting units, create incompatible strain and fracturing. This contrast in strain accommodation provides abundant low-strain environments viable for gold mineralization.

8.2 Metamorphism

The amphibolite (±garnet) contains the stable mineral assemblage of hornblende, plagioclase and garnet representing the amphibolite facies of metamorphism. Relict microlithons of clinopyroxene and orthopyroxene representing the granulite facies of metamorphism are also present within mineralized amphibolite. The dominant stable amphibolite facies mineral assemblage, in addition to relict granulite facies lithons, suggests polymetamorphism to the amphibolite facies after peak granulite facies metamorphic conditions.

Similarly, the garnet-biotite schist (±sillimanite) represents a dominantly amphibolite facies mineral assemblage composed of quartz, plagioclase, biotite,

almandine garnet and fibrolite. The stable mineral assemblage of coarse sillimanite with K-feldspar, quartz and a complete lack of muscovite represents the peak conditions of granulite facies metamorphism. The presence of fibrolite and coarse sillimanite suggests secondary growth of sillimanite during amphibolite facies temperatures during retrograde metamorphism. Garnet-biotite geothermometry based on Borden property garnet has yielded a metamorphic temperature range up to 933°C ±50°C. An overall increase in metamorphic temperature from core to rim of individual garnet grains indicates growth during prograde metamorphism to granulite facies. Lower temperature at the outer margin of some grains may document the retrograde metamorphism to amphibolite facies.

The mineralized mafic amphibolite (±garnet) and garnet-biotite schist (±sillimanite) units display evidence of stable retrograde amphibolite facies mineral assemblages and relict lithons of granulite facies assemblages. Retrograde metamorphism during deformation caused reaction softening so that the granulite facies lithons were more competent than the rock undergoing retrograde metamorphism.

8.3 Structure

The most compelling evidence for structural and metamorphic control of gold mineralization is the relationship between gold mineralization and competent granulite facies lithons adjacent to high-strain retrograde amphibolite facies units.

Conventional wisdom suggests that economic gold deposits are formed near the transition between greenschist and amphibolite facies metamorphism (Goldfarb et al,

2005; Bateman and Hagemann, 2004; Goldfarb et al., 2001; Pohl, 2011). This is consistent with an understanding that brittle deformation is necessary to produce fractures for mineralizing fluids. For common metamorphosed igneous rock with a feldspar-based rheology, these are the temperature and pressure conditions where the transition from dominantly brittle to dominantly ductile deformation occurs. Quartz and feldspar undergo dislocation creep at temperatures as low as 300°C and 450°C respectively (Vernon, 1999).

However, it is also possible to produce local brittle deformation at greater crustal depths and higher metamorphic grade whenever the ductile strain is heterogeneous and incompatible, conditions that will occur when more competent lithologies are beside more ductile lithologies during ductile shear-zone deformation. Experiments on an amphibolite determined that dislocation creep is not a dominant mechanism of deformation until temperatures of 700°C. Garnet is known for its competency in metamorphic rocks and conditions for garnet plasticity were determined to be 950°C at 11kbar (Martelat et al., 2012).

In the case of the Borden gold deposit, lenses of relict granulite facies rock are more competent than the surrounding retrograde amphibolite facies lithologies, producing the requisite conditions for localized brittle deformation and mineralization during dominantly ductile shear-zone deformation. Brittle-ductile shear zones formed during retrograde amphibolite facies metamorphism.

Granulite facies assemblages are less reactive and more competent during deformation at amphibolite facies temperatures resulting in abundant microfractures in response to differential stress. While in contrast, the ductilely deforming

amphibolite assemblages of hornblende and garnet-biotite schist with biotite accommodate rehydration reactions and increased response to ductile deformation, which is known as reaction softening (Passchier and Trouw, 2005).

At the macroscopic scale, gold mineralization is associated with the margins of competent lithons. Microstructural patterns are analogous to macroscopic lithological relationships, displaying evidence of gold mineralization surrounding competent micro-lithons. Low-strain environments provide preferential areas for gold mineralization. Lithologies hosting economic gold mineralization are the garnet-biotite schist (±sillimanite), amphibolite (±garnet), biotite-quartzofeldspathic gneiss, and ductilely deformed quartz veins.

An interesting feature noted on the Discovery Outcrop is the local variation in dip on the southern outcrop. The ductilely deforming sillimanite-garnet-biotite schist unit dips north and south appearing to wrap around a competent granulite unit (Fig. 7.53). Previous studies (Percival, 1983; Percival, 1986; Krogh and Moser, 1994; Moser 1994; Moser et al., 2008) inferred a fold (Fig. 2.6) to explain the variation in dip direction. Field evidence suggests that the dip heterogeneity is not a product of folding but rather a rheologic contrast between units that causes less competent units to wrap around large-scale boudins of granulite facies lithologies.

Stereonet projections of foliation strike and dip, as well as lineations, display subparallel, high-strain fabrics with minor local variation in dip and lineation plunge. The intersection of these averages is related to strain heterogeneity and regional boudinage causing ductilely deforming units to wrap around more competent lithologies causing dip variation. The overall subparallel consistency of the strike of

foliation is considered a product of regional stress and shear zone deformation defining the plane of flattening and direction of maximum elongation.

Moser (1994) described the western portion of the Borden Lake Belt as a tight synform preserving sedimentary and volcanic structures. Detailed field measurements from this study do not consistently suggest regional fold structures but rather regional competence contrasts causing lithological boudinage and subsequent strike and dip variation. Moser's (1994) structural model does not explain metamorphism and subsequent deformation related to foliation. Rheologic contrasts between retrograde amphibolite facies metamorphism and relict granulite facies lithons are consistent with the metamorphism and shear zone deformation at the Borden gold project.

The process of boudinage can occur on a wide range of scales simultaneously, so that the process can be seen in thin section, core, outcrop and on regional maps. Local variations such as strain softening and viscosity contrast can affect the geometry of the boudins that form (Fossen, 2010). Boudinage of regional lithologies in areas of highest strain concentrated gold in low-strain areas (e.g. boudin necks and between granulite pods, down plunge and along strike).

Parallel alignment of platy minerals is a marker for mineralized lithologies at the Borden property. Interestingly, stable retrograde amphibolite facies minerals typically define foliation indicating synchronous retrograde metamorphism and deformation processes.

Hornblende dominantly defines the foliation in amphibolite (±garnet) units around relict microlithons of clinopyroxene and orthopyroxene. Similarly, biotite defines a moderate to strong fabric in the sillimanite-garnet-biotite schist unit. Biotite

wraps around competent granulite facies K-feldspar, garnet and coarse sillimanite lithons.

Deflection of matrix foliation around porphyroblasts is thought to form by deformation of the matrix around a rigid, pre-existing porphyroblast and not by mechanical displacement of the matrix by the growing porphyroblast (Carlson and Gordon, 2004). Parallel alignment of retrograde hornblende in amphibolite and biotite in sillimanite-garnet-biotite schist units indicates that ductile deformation was continuous after granulite facies metamorphism to at least the retrograde amphibolite facies of metamorphism.

Microstructural analysis identifies gold within and adjacent to fractured minerals bordered by ductilely-deformed minerals. The heterogeneous strain provides abundant low-strain environments favourable for gold mineralization in the strain shadows of competent minerals and microlithons. Gold in amphibolite (±garnet) is found at the contact between stable, foliated, retrograde amphibolite and competent, massive granulite lithons (Fig. 7.54). Within sillimanite-garnet-biotite schist, gold is observed in low-strain zones of competent garnet and pyrite within a foliated biotite groundmass (Fig. 7.55A). In quartzofeldspathic gneiss, mineralization is typically less common, although when mineralized, gold is associated with pyrite and pyrrhotite sulphide stringers that are present parallel to strongly foliated biotite (Fig. 7.55B).

High-grade gold mineralization, present within ductilely deformed quartz veins, is always hosted in the mineralized amphibolite (±garnet) or garnet-biotite schist (±sillimanite) lithologies. Mineralized lithologies with strong foliation appear brecciated fragments within the deformed quartz veins. Quartz veins represent filled

fractures and provide evidence for hydrothermal fluids. The highest gold grades are associated with the most heterogeneous brittle-ductile deformation at the Borden gold deposit a product of ductilely deformed breccia or cataclasite.

8.4 Geochronology

Percival and Krogh (1993) dated a granodiorite that crosscuts the mafic gneiss at the southern margin of the KSZ at 2677 +5/-3 Ma, which establishes a minimum age for mafic volcanism. Garnet formation is assumed to be 2660 Ma, based on the age of the oldest metamorphic zircon in retrograde mafic granulite (Moser, 1994). Moser (1994) hypothesized that protracted radial growth of zircon appears to have been most frequent ca. 2620 Ma, when temperatures were above 650°C, and the events coincided with boudinage in the lower crust and crustal-scale fluid flow along brittle structural breaks at higher levels (Krogh, 1993). New constraints based on Lu/Hf garnet date of 2629 Ma, suggest that the age of granulite facies metamorphism is consistent with Krogh's (1993) age for high-temperature metamorphism.

Published zircon estimations of the maximum age for metaconglomerate deposition at the Borden Belt are: 2671 ±12 Ma (Moser et al., 2008) and 2667 ±2 Ma (Krogh, 1993). Detrital zircon dating by Moser et al. (2008) utilizes unrecrystallized zircon cores constraining a lower age bracket of 2659 ±8 Ma for burial of Borden Lake metasediments in the lower crust.

The association of gold with retrograde amphibolite facies metamorphism suggests that mineralization at the Borden gold deposit coincides with exhumation and cooling in the late Archean after 2629 ±4.3Ma.

9. SUMMARY AND CONCLUSIONS

The Borden gold deposit occurs in the Archean Superior province of the Canadian Shield. The project's unconventional setting is situated within the southern margin of the Kapuskasing Structural Zone, a structurally controlled region of granulite and upper amphibolite facies metamorphic rock. The Kapuskasing Structural Zone is a 500km long Belt that strikes NNE to SSW and crosscuts the east-west trend of the adjacent Abitibi and Wawa Subprovinces. It represents a deep crustal assemblage that has been exhumed along a major crustal structure.

Owing to the high-grade of metamorphism, very little historical exploration was undertaken in the Borden area near the southern margin of the Kapuskasing Structural Zone. In 2010, Probe Mines discovered the multi-million ounce Borden gold deposit within the Borden Lake Belt, an east-striking lithological assemblage, consisting of metasedimentary, felsic and mafic gneisses.

An assortment of lithologies, each exhibiting structural and textural variations, are host to gold in various concentrations. There are a few occurrences of visible gold in core but more gold is identified in microstructural analysis. Gold-hosting lithologies on the Borden property are garnet-biotite gneiss (±sillimanite), amphibolite (±garnet), biotite-quartzofeldspathic gneiss and deformed quartz veins.

The amphibolite is weak to strongly foliated and ranges from fine- to medium-grained. The dominant mineralogy is hornblende and plagioclase with garnet, the characteristic mineral assemblage of amphibolite facies metamorphism of a mafic igneous rock. High-strain amphibolite contains relict orthopyroxene and

clinopyroxene, which indicate an earlier phase of granulite facies metamorphism. These relict pyroxene grains and lithons are bordered by euhedral hornblende indicating incomplete retrograde reaction. Gold is commonly identified at contacts between unfoliated granulite-facies lithons and surrounding retrograde amphibolite, indicating the significance of retrograde metamorphism to the gold mineralization. The relict granulite facies minerals and lithons appear to have behaved competently during ductile deformation at amphibolite facies temperatures.

The garnet-biotite schist has a moderate to strong foliation defined by biotite with minor hornblende, pyrite and pyrrhotite. It may also contain fibrolite and coarse sillimanite. Abundance of aluminous minerals and the high Hf signature suggests a hydrothermally altered mafic igneous rock. Garnet-biotite geothermometry based on Borden garnet-biotite schist has yielded a metamorphic temperature range up to 933°C ±50°C. Unzoned garnet from the Discovery Outcrop yields lower temperatures at the core and higher temperatures at the rim of each grain. This indicates that garnet equilibration was reached during peak metamorphism and garnet growth took place during prograde metamorphism to the granulite facies. Haloes of biotite surround competent garnet and are commonly deflected around the grain producing an asymmetric tail. Sillimanite typically occurs as fibrolite needles on the grain boundaries of biotite and quartz. Coarse prismatic sillimanite grains with K-feldspar occur in relict lithons within the gneiss indicating the second sillimanite isograd was reached during peak granulite facies metamorphism. Visible gold is observed in microscopic low-strain shadows caused by mineral competency contrasts between rigid garnet and sillimanite compared to biotite and quartz. Again, in this lithology,

relict granulite facies lithons appear to have behaved competently during ductile deformation at lower temperatures.

The felsic gneiss is comprised mainly of quartz and feldspar and only contains economic gold mineralization when adjacent to the garnet-biotite gneiss and amphibolite. In these broader mineralized zones, the quartzofeldspathic gneiss contains increased biotite and stronger foliation.

Gold mineralization is typically associated with locally abundant sulphides such as pyrrhotite and pyrite. The typical sulphide occurrence is euhedral pyrite with a gold bleb at the grain boundary and pyrrhotite mantling both the pyrite and the gold. Quartz veins are common in all lithologies. Quartz veins specifically associated with the ore zone display strong ductile deformation. Gold mineralization is typically absent in late crosscutting quartz ± carbonate veins. Both "siliceous alteration" and "quartz flooding" logged by drill geologists are interpreted as deformed quartz veins. The deformed veins are concordant with foliation and have a grey to blue hue. Gold mineralization appears at sharp contacts between strongly foliated amphibolite units and unfoliated granulite boudins. The surface of the Discovery Outcrop is very close to such a surface, explaining the gold mineralization across the outcrop. The foliated amphibolite facies lithologies behaved less competently and deformed ductilely around boudins of competent, granulite facies metamorphic rock due to reaction softening during synchronous deformation and retrograde metamorphism. Gold mineralization appears to be contemporaneous with retrograde metamorphism of granulite facies lithologies to amphibolite facies and with ductile deformation of the retrograde amphibolite facies units.

Gold mineralization at Borden is located within ductile to brittle-ductile shear zones between massive, non-foliated or lineated competent lithologies. The areas of mineralization are located in lithologies that display anastomosing, moderately foliated units with a preferred orientation of porphyroclasts and porphyroblasts. Strain incompatibilities occur along the boundaries between competent and incompetent minerals during ductile deformation.

New geochronological results suggest that peak granulite facies metamorphism associated with garnet growth took place at ca. 2629 Ma. This is consistent with earlier estimates of the age of granulite facies metamorphism (Krogh, 1993).

In the case of the Borden gold deposit, lenses of relict granulite facies metasedimentary rock were more competent than the surrounding retrograde amphibolite facies lithologies, producing the requisite conditions for localized brittle deformation and mineralization during dominantly ductile shear-zone deformation. Retrograde metamorphism of these lithologies is critical to the structural control of mineralization at this deposit.

Structure and microstructure are the controlling factors in gold mineralization within the Borden gold deposit. Research on the property to date provides evidence for gold mineralization in association with brittle-ductile heterogeneous strain and rheological competency contrasts between minerals on the microstructural scale as well as lithologies on the deposit scale. Gold mineralization appears to be contemporaneous with retrograde metamorphism of granulite facies lithologies to amphibolite facies, and with ductile deformation of the retrograde amphibolite facies units after 2629 ±4.3Ma.

10. REFERENCES

Bateman, R. and Hagemann, S., 2004, Gold mineralisation throughouthte 45 Ma of Archaean orogenesis: Protracted flux of gold in teh Golden Mine, Yilgarn craton, Western Australia: Minefalium Deposita, v. 39, p. 536-559.

Bouvier, A., Vervoort J.D. and Patchett, P.J., 2008, The Lu-Hf and Sm-Nd isotopic composition of CHUR: Constraints from unequilibrated chondrites and implications for the bulk composition of terrestrial planets: Earth and Planetary Science Letters, v. 273, p. 48-57.

Bursnall, J.T., Leclair, A.L., Moser, D.E. and Percival, J.A., 1994, Structural correlation within the Kapuskasing Uplift: Canadian Journal of Earth Sciences, v. 31, p. 1096-1103.

Bursnall, J.T. and Moser, D., 1989, Site survey for continental drilling in the Kapuskasing structural zone. In Summary of fieldwork and other activities: Ontario Geological Survey, Miscellaneous Paper 146, p. 16-21.

Carlson, W.D. and Gordon, C.L., 2004, Effects of matrix grainsize on the kinetic of intergranular diffusion: Journal of Metamorphic Geology, v. 22, p. 733-742.

Corfu, F. and Davis, D.W., 1992, A U-Pb geochronology framework for the western Superior province. In Thurston, P.C., Williams, H.R., Sutcliffe, R.H., Stott, G.M., eds., The geology of Ontario: Ontario Geological Survey Special Volume 4, Part 2, p. 1335-1346.

Corfu, F., Jackson, S.L. and Sutcliffe, R.H., 1990, U-Pb ages and tectonic significance of late Archean alkalic magmatism and nonmarine sedimentation: Timiskaming Group, southern Abitibi Belt, Ontario: Canadian Journal of Earth Sciences, v. 28, p. 489-503.

Ferry, J.M. and Spear, F.S., 1978, Experimental calibration of the partitioning of Fe and Mg between biotite and garnet: Contributions to Mineral Petrology, v. 66, p. 113-117.

Fettes, D. and Desmons, J., eds., 2007, Metamorphic rocks: A classification and a glossary of terms, Recommendations of the International Union of Geological Sciences Subcommission on Systematics of Metamorphic Rocks: University Press, Cambridge, UK.

Fossen, H., 2010, Structural Geology: Cambridge University Press, Cambridge, UK.

Goldfarb, R.J., Baker, T., Dube, B., Groves, D.I., Hart, C.J.R., and Gosselin, P., 2005, Distribution, character and genesis of gold deposits in metamorphic terranes, in Hedenquist, J.W., Thompson, J.F.H., Goldfarb, R.J., Richards, J.P., eds., Economic Geology, 100th Anniversary Volume 1905-2005: Littleton, Colorado, Society of Economic Geologists, p. 407-450.

Goldfarb, R.J., Groves, D.I. and Gardoll, S., 2001, Orogenic gold and geologic time: a global synthesis: Ore Geology Reviews, v. 18, p. 1-75.

Halls, H.C. and Davis, D.W., 2004., Paleomagnetism and U-Pb geochronology of the 2.17 Ga Biscotasing dyke swarm, Ontario, Canada: evidence for vertical-axis crustal rotation across the Kapuskasing Zone: Canadian Journal of Earth Sciences, v. 41, p. 255-269.

Heather, K.B., Percival, D., Moser, D. and Bleeker, W., 1995, Tectonics and Metallogeny of Archean crust in the Abitibi-Kapuskasing-Wawa region: Geological Survey of Canada, Open File 3141, Field Trip Guidebook.

Innes, M.J.S., 1960, Gravity and isostasy in Manitoba and northern Ontario: Dominion Observatory, Publication 21, p. 263-338.

Ispolatov, V., Lafrance, B., Dube, B., Creaser, R. and Hamilton, M., 2008, Geologic and structural setting of gold mineralization in the Kirkland Lake-Larder Lake gold beld, Ontario: Economic Geology, v. 103, p. 1309-1340.

Krogh, T.E., 1993, High precision U-Pb ages for granulite metamorphism and deformation in the Archean Kapuskasing Structural Zone, Ontario; implications for structure and development of the lower crust: Earth and Planetary Science Letters, v. 119, p. 1-18.

Krogh, T.E. and Moser, D.E., 1994, U-Pb zircon and monazite ages from the Kapuskasing uplift: Age constraints on deformation within the Ivanhoe Lake fault zone: Canadian Journal of Earth Sciences, v. 31, p. 1096-1103.

Lisle, R.J., 1985, Geological Strain Analysis: A Manual for the Rf/Phi method: Pergamon Press, Oxford, UK.

Martelat, J. E., Malamoud, K., Cordier, P., Randrianasolo, B., Schulmann, K., and Lardeaux, J. M., 2012, Garnet crystal plasticity in the continental crust, a new example from south Madagascar: Journal of Metamorphic Geology, v. 30, p. 435-452.

Moser, D.E., 1993, A geological, structural and geochronological study of the central Wawa gneiss domain: implications for the development of different crustal levels of the Archean Abitibi-Wawa orogen of the southern Superior Province, Canadian Shield: Ph.D. thesis, Queen's University, Kingston, Canada.

Moser, D.E., 1994, The geology and structure of the mid-crustal Wawa gneiss domain: a key to understanding tectonic variation with depth and time in the late Archean Abitibi-Wawa orogen: Canadian Journal of Earth Sciences, v. 31, p. 1064-1080.

Moser, D.E., Bowman, J.R., Wooden, J., Valley, J.W., Mazdab, F. and Kita, N., 2008, Creation of a continent recorded in zircon zoning: The Geological Society of America, v. 36, p. 239-242.

Münker, C., Weyer, S., Scherer, E. and Mezger, K., 2001, Separation of high field strength elements (Nb, Ta, Zr, Hf) and Lu from rock samples for MC-ICP-MS measurements: Geochemistry Geophysics Geosystems v. 2.

Passchier, C.W. and Trouw, R.A.J., 2005, Microtectonics, 2nd Edition: Springer, Berlin, Germany.

Percival, J.A., 1983, High-grade Metamorphism in the Chapleau-Foleyet area, Ontario: American Mineralogist, v. 68, p. 667-686.

Percival, J. A., 1986, The Kapuskasing uplift: Archean greenstones and granulites: Geological Association of Canada, Ottawa 1986 meeting, Field Trip 16 Guidebook.

Percival, J.A. and Krogh, T.E., 1983, U-Pb zircon geochronology of the Kapuskasing structural zone and vicinity in the Chapleau-Foleyet area, Ontario: Canadian Journal of Earth Sciences, v. 20, p. 830-843.

Percival, J.A. and Peterman, Z.E., 1994, Rb-Sr biotite and whole-rock data from the Kapuskasing uplift and their bearing on the cooling and exhumation history: Canadian Journal of Earth Sciences, v. 31, p. 1172-1181.

Percival, J.A., Shaw, D.M., Milkereit, B., White, D.J., Jones, A.G., Salisbury, M.H., Bursnall, J.T., Moser, D.E., Green, A.G. and Thurston, P.C., 1991, A closer look at deep crustal reflections: Eos – Earth and Space Science News, v. 72, p. 337-341.

Piper, J.D.A, 1976, Palaeomagnetic evidence for a Proterozoic supercontinent: Philosophical Transactions of the Royal Society of London, Series A, v. 280, p. 469-490.

Pohl, W.L., 2011, Economic Geology: Princeiples and Practice: Blackwell Publishing, Oxford, UK.

Powell R. and Holland, T., 1990, Calculated mineral equilibria in the pelite system, KFMASH (K_2O-FeO-MgO-Al_2O_3-SiO_2-H_2O): American Mineralogist, v. 75, p. 367-380.

Ramsay, J.G., 1967, Folding and fracturing of rocks: McGraw-Hill, New York, USA, p. 588.

Ramsay, J.G. and Huber, M.I., 1983, The Techniques of Modern Structural Geology: Strain Analysis Volume 1: Academic press, London, UK.

Sutton, J. and Watson, J., 1974, Tectonic evolution of continents in early Proterozoic times: Nature, v. 247, p. 433-435.

Vernon, R., 1999, Quartz and feldspar microstructures in metamorphic rocks: Canadian Mineralogist, v. 37, p. 513-524.

Vervoort, J.D., Patchett, P.J., Soderlund, U. and Baker, M., 2004, The isotopic composition of Yb and the precise and accurate determination of Lu concentrations and Lu/Hf ratios by isotope dilution using MC-ICP-MS: Geochemistry Geophysics Geosystems, v. 5, p. 1-15.

Watkinson, D.H., Thurston, P. and Shafiqullar, M., 1972, The Shawmere anorthosite of Archean age in the Kapuskasing Belt, Ontario: Journal of Geology, v. 80, p. 736-739.

Watson, J., 1980, The origin and history of the Kapuskasing structural zone, Ontario, Canada: Canadian Journal of Earth Sciences, v. 17, p. 866-875.

Watson, J., 1973, Effects of reworking in high-grade gneiss complexes: Philosophical Transactions of the Royal Society of London, Series A, v. 273, p. 443-455.

Zirakparvar, N.A., Vervoort, J.D., McClelland, W. and Lewis, R.S., 2010, Insights into the metamorphic evolution of the Belt-Purcell basin; evidence from Lu–Hf garnet geochronology: Canadian Journal of Earth Sciences, v. 47, p. 161-179.

APPENDIX A – FIELD MAPPING STRUCTURAL MEASUREMENTS

FOLIATION MEASUREMENTS									
Way point	**Strike**	**Dip**	**Unit**	**Structural Domain**	**Way point**	**Strike**	**Dip**	**Unit**	**Structural Domain**
	295	42	ore zone		24	322	70	amphibolite	northwest borden
117	301	79	metaconglomerate	lake geology	25	290	80	intermediate	northwest borden
118	315	75	qfg	lake geology	26	270	80	amphibolite	northwest borden
119	290	72	qfg	lake geology	27	280	75	qfg	northwest borden
120	300	85	metaconglomerate	lake geology	28	270	80	qfg	northwest borden
121	300	82	metaconglomerate	lake geology	29	287	75	schist	northwest borden
122	305	85	amphibolite	lake geology	30	294	79	schist	northwest borden
123	295	75	qfg	lake geology	31	298	78	qfg	northwest borden
124	282	79	amphibolite	lake geology	32	325	75	amphibolite	northwest borden
90	264	57	qfg	north borden	33	305	75	qfg	northwest borden
91	274	67	qfg	north borden	34	287	77	metaconglomerate	northwest borden
93	265	80	metaconglomerate	north borden	35	305	72	metaconglomerate	northwest borden
93	266	65	metaconglomerate	north borden	36	300	74	qfg	northwest borden
93	270	75	metaconglomerate	north borden	37	122	71	qfg	northwest borden
97	252	72	metaconglomerate	north borden	38	118	72	qfg	northwest borden
98	275	72	metaconglomerate	north borden	39	122	68	qfg	northwest borden
99	255	66	qfg	north borden	40	124	64	qfg	northwest borden
100	281	64	metaconglomerate	north borden	41	136	66	qfg	northwest borden
101	265	72	qfg	north borden	42	148	55	qfg	northwest borden
103	272	77	metaconglomerate	north borden	43	122	58	qfg	northwest borden
104	251	60	metaconglomerate	north borden	44	119	45	qfg	northwest borden
106	249	71	metaconglomerate	north borden	45	145	52	qfg	northwest borden
107	255	79	metaconglomerate	north borden	46	128	55	intermediate	northwest borden
108	256	64	metaconglomerate	north borden	47	306	60	qfg	northwest borden
109	250	68	metaconglomerate	north borden	48	295	60	qfg	northwest borden
110	270	71	metaconglomerate	north borden	49	314	72	qfg	northwest borden
113	249	65	qfg	north borden	50	116	75	qfg	northwest borden
115	260	63	qfg	north borden	51	304	52	qfg	southeast borden
116	260	75	amphibolite	north borden	52	130	65	qfg	southeast borden
117	272	88	metaconglomerate	north borden	53	129	61	qfg	southeast borden
82	294	69	intermediate	northeast borden	54	136	56	amphibolite	southeast borden
83	290	72	intermediate	northeast borden	55	130	59	qfg	southeast borden
84	285	75	metaconglomerate	northeast borden	56	292	72	qfg	southeast borden
85	274	73	intermediate	northeast borden	57	320	55	metaconglomerate	southeast borden
87	285	77	intermediate	northeast borden	58	310	50	metaconglomerate	southeast borden
72	265	85	amphibolite	northeast borden	59	325	55	metaconglomerate	southeast borden
73	270	79	amphibolite	northeast borden	60	312	60	metaconglomerate	southeast borden
75	285	78	intermediate	northeast borden	61	318	50	metaconglomerate	southeast borden
16	305	75	schist	northwest borden	62	295	60	qfg	southeast borden
17	315	78	schist	northwest borden	63	295	70	metaconglomerate	southeast borden
18	294	82	schist	northwest borden	64	290	85	qfg	southeast borden
19	126	74	intermediate	northwest borden	65	280	85	qfg	southeast borden

FOLIATION MEASUREMENTS									
Way point	Strike	Dip	Unit	Structural Domain	Way point	Strike	Dip	Unit	Structural Domain
20	120	75	intermediate	northwest borden	66	290	70	amphibolite	southeast borden
21	130	75	qfg	northwest borden	67	324	80	qfg	southeast borden
22	120	80	qfg	northwest borden	68	312	72	qfg	southeast borden
23	305	75	intermediate	northwest borden					

LINEATION MEASUREMENTS		
Trend	Plunge	Mineral
115	20	ore zone
110	0	intermediate-amphibolite
98	0	intermediate-amphibolite
95	0	intermediate-amphibolite
95	0	intermediate-amphibolite
99	0	intermediate-amphibolite
95	0	intermediate-amphibolite
75	62	intermediate-amphibolite
63	50	intermediate-amphibolite
80	51	intermediate-amphibolite
62	0	intermediate-amphibolite
81	0	intermediate-amphibolite
254	18	intermediate-amphibolite
54	15	metaconglomerate
260	10	qfg
98	35	amphibolite
114	30	metaconglomerate
130	31	metaconglomerate
82	32	metaconglomerate-site 2
83	30	metaconglomerate-site 2

APPENDIX B – REASSESSED LITHOLOGICAL CORE LOGS

HoleID	From	To	Lithology	Bt %	Am %	Metamorphic Minerals	Peg %	QV %	Py %	Po %
BL10-05	3.00	3.70	Garnet Biotite Schist	25		Kyanite		3	0.5	0.2
BL10-05	3.70	8.00	Micaceous Quartzofeldspathic Gneiss	17			1		0.1	0.1
BL10-05	8.00	12.00	Garnet Biotite Schist	30		Kyanite	25		1.5	
BL10-05	12.00	12.86	Micaceous Quartzofeldspathic Gneiss	10		Garnet	10		0.1	
BL10-05	12.86	15.10	Garnet Biotite Schist	40		Kyanite	3		3	1
BL10-05	15.10	22.35	Quartzofeldspathic Gneiss	7		Sillimanite		15	3	1
BL10-05	22.35	23.40	Garnet Biotite Schist	25		Kyanite			4	1
BL10-05	23.40	25.05	Quartzofeldspathic Gneiss	7		Sillimanite			1	0.2
BL10-05	25.05	40.80	Garnet Biotite Schist	30		Kyanite	3	1	3	1
BL10-05	40.80	69.95	Micaceous Quartzofeldspathic Gneiss	10		Sillimanite	10	3	3	2
BL10-05	69.95	97.00	Garnet Biotite Schist	30		Sillimanite	3	1	1	0.5
BL10-06	2.70	11.20	Micaceous Quartzofeldspathic Gneiss	10	1			1	0.1	
BL10-06	11.20	24.20	Quartzofeldspathic Gneiss	10	3				0.1	
BL10-06	24.20	27.10	Intermediate Gneiss	12	55			1	0.1	
BL10-06	27.10	31.40	Biotite Schist	25	5				0.1	0.3
BL10-06	31.40	40.60	Quartzofeldspathic Gneiss	7	3					
BL10-06	40.60	45.40	Diabase Dike							
BL10-06	45.40	58.55	UM/Lamp Dike							
BL10-06	58.55	60.70	Garnet Biotite Schist	30	5			3	0.5	
BL10-06	60.70	62.10	Pegmatite	5	1				0.2	0.1
BL10-06	62.10	65.50	Quartzofeldspathic Gneiss	10		Garnet	5		0.3	0.3
BL10-06	65.50	66.75	Micaceous Quartzofeldspathic Gneiss	12		Kyanite			0.3	0.3
BL10-06	66.75	67.10	Garnet Biotite Schist	25		Garnet			0.3	0.3
BL10-06	67.10	78.80	Micaceous Quartzofeldspathic Gneiss	15		Muscovite	1		0.3	0.3
BL10-06	78.80	84.85	Micaceous Quartzofeldspathic Gneiss	7	3		3		0.1	0.1
BL10-06	84.85	88.45	Micaceous Quartzofeldspathic Gneiss	10	1	Garnet	1		0.2	0.2
BL10-06	88.45	89.70	Intermediate Gneiss	3	60		1			
BL10-06	89.70	91.25	Pegmatite	5	1	Garnet			0.1	
BL10-06	91.25	97.00	Micaceous Quartzofeldspathic Gneiss	3	1	Garnet	0.5		0.1	0.1
BL10-06	97.00	98.00	Micaceous Quartzofeldspathic Gneiss	3					0.1	
BL10-06	98.00	104.80	Quartzofeldspathic Gneiss	7	3		1		0.3	0.1
BL10-06	104.80	108.90	Garnet Biotite Schist	30		Cordierite	3		0.3	0.1
BL10-06	108.90	109.80	Pegmatite	12					0.1	0.1

HoleID	From	To	Lithology	Bt %	Am %	Metamorphic Minerals	Peg %	QV %	Py %	Po %
BL10-06	109.80	111.60	Micaceous Quartzofeldspathic Gneiss	10		Sillimanite	3	10	0.2	0.1
BL10-06	111.60	113.40	Garnet Biotite Schist	25				3	0.3	0.1
BL10-06	113.40	122.00	Micaceous Quartzofeldspathic Gneiss	7		Garnet	1		0.1	0.1
BL10-06	122.00	134.46	Quartzofeldspathic Gneiss	5		Kyanite	5	3	0.3	0.2
BL10-08	6.20	7.20	Pegmatite	3			100			
BL10-08	7.20	32.90	Quartzofeldspathic Gneiss	7	5		0.5	0.3	0.1	0.01
BL10-08	32.90	34.75	Diabase Dike							
BL10-08	34.75	54.15	Quartzofeldspathic Gneiss	7	5		0.1	1	0.1	0.05
BL10-08	54.15	79.85	Quartzofeldspathic Gneiss	12	7	Garnet	0.1	0.5	0.1	0.05
BL10-08	79.85	90.75	Garnet Biotite Schist	25		Garnet + Muscovite	0.3	0.1	0.1	0.01
BL10-08	90.75	91.00	Amphibolite	3	80	Garnet				
BL10-08	91.00	104.00	Garnet Biotite Schist	20	3	Garnet + Muscovite		0.1	0.1	0.01
BL11-19	25.45	35.70	Quartzofeldspathic Gneiss	5	1		1	0.1	0.3	0.2
BL11-19	35.70	39.90	Quartzofeldspathic Gneiss	15	5	Garnet		1	0.5	0.3
BL11-19	39.90	40.85	Intermediate Gneiss	20	20					
BL11-19	40.85	42.60	Quartzofeldspathic Gneiss	15	3			1	0.7	0.3
BL11-19	42.60	42.95	Intermediate Gneiss	20	20					
BL11-19	42.95	44.55	Quartzofeldspathic Gneiss	15				1	1	1
BL11-19	44.55	46.10	Diabase Dike							
BL11-19	46.10	46.30	Quartzofeldspathic Gneiss	25						
BL11-19	46.30	47.10	Diabase Dike							
BL11-19	47.10	48.00	Quartzofeldspathic Gneiss	10	3				0.1	
BL11-19	48.00	48.35	Diabase Dike							
BL11-19	48.35	60.40	Quartzofeldspathic Gneiss	7	5	Garnet	1	1	0.1	0.1
BL11-19	60.40	61.00	Intermediate Gneiss	15	15					
BL11-19	61.00	74.80	Quartzofeldspathic Gneiss	10	3			1	0.2	0.1
BL11-19	74.80	80.50	Quartzofeldspathic Gneiss	15	60			0.1	1	1
BL11-19	80.50	86.65	Garnet Biotite Schist	25	3	Kyanite	1	2	2	2
BL11-19	86.65	89.55	Quartzofeldspathic Gneiss	15		Muscovite	1		0.5	0.3
BL11-19	89.55	93.25	Micaceous Quartzofeldspathic Gneiss	25		Garnet + Muscovite			0.5	0.5
BL11-19	93.25	98.60	Micaceous Quartzofeldspathic Gneiss	25		Garnet + Muscovite			0.5	0.5
BL11-19	98.60	99.20	Pegmatite	10					0.1	
BL11-19	99.20	118.05	Micaceous Quartzofeldspathic Gneiss	20		Garnet + Sillmanite + Kyanite + Muscovite	1	1	1	0.7
BL11-19	118.05	120.70	Garnet Biotite Schist	35		Garnet	1	2	1	0.5
BL11-19	120.70	158.80	Quartzofeldspathic Gneiss	15				1	1.5	0.5
BL11-19	158.80	177.70	Footwall Amphibolite		60	Garnet			0.5	0.1

HoleID	From	To	Lithology	Bt %	Am %	Metamorphic Minerals	Peg %	QV %	Py %	Po %
BL11-20	18.75	29.00	Quartzofeldspathic Gneiss	5	2	Garnet	5		0.3	0.2
BL11-20	29.00	36.35	Quartzofeldspathic Gneiss	5	5	Garnet + Muscovite		3	0.3	
BL11-20	36.35	39.00	Quartzofeldspathic Gneiss	12	15				0.5	0.3
BL11-20	39.00	45.30	Quartzofeldspathic Gneiss	15	3			5	0.6	0.4
BL11-20	45.30	48.75	Quartzofeldspathic Gneiss	7	2		7		0.5	0.3
BL11-20	48.75	51.15	Pegmatite	7			80		0.5	0.5
BL11-20	51.15	65.70	Quartzofeldspathic Gneiss	7	2	Garnet		3	0.5	0.5
BL11-20	65.70	69.50	Garnet Biotite Schist	30	5	Garnet	5		1	0.7
BL11-20	69.50	74.00	Amphibolite	13	55	Garnet			0.7	0.7
BL11-20	74.00	81.65	Garnet Biotite Schist	35	15	Garnet		5	1	1
BL11-20	81.65	82.75	Quartzofeldspathic Gneiss	10	3				0.3	0.3
BL11-20	82.75	84.20	Garnet Biotite Schist	30		Garnet			0.7	0.7
BL11-20	84.20	85.60	Quartzofeldspathic Gneiss	13					0.2	0.2
BL11-20	85.60	90.70	Garnet Biotite Schist	35	3	Garnet	3		1	1
BL11-20	90.70	95.30	Quartzofeldspathic Gneiss	7	2	Garnet + Muscovite	10	3	0.5	0.5
BL11-20	95.30	109.35	Garnet Biotite Schist	25	2	Garnet		5	1	1
BL11-20	109.35	111.00	Quartzofeldspathic Gneiss	5		Garnet + Muscovite	10		0.2	0.1
BL11-20	111.00	118.90	Garnet Biotite Schist	25		Garnet	3	3	0.7	0.7
BL11-20	118.90	124.60	Quartzofeldspathic Gneiss	13		Garnet	5		0.6	0.3
BL11-20	124.60	127.35	Garnet Biotite Schist	25		Garnet + Sillmanite	2	3	0.5	0.5
BL11-20	127.35	129.00	Quartzofeldspathic Gneiss	10		Garnet + Muscovite			0.5	1
BL11-20	129.00	138.60	Quartzofeldspathic Gneiss	12	3	Garnet	3	7	0.4	0.3
BL11-20	138.60	140.90	UM/Lamp Dike							
BL11-20	140.90	168.75	Quartzofeldspathic Gneiss	7	2			3	0.3	0.1
BL11-20	168.75	171.35	Footwall Amphibolite	3	60				0.2	0.3
BL11-20	171.35	178.35	Quartzofeldspathic Gneiss	7	4				0.1	
BL11-20	178.35	179.50	Pegmatite	2			100			
BL11-20	179.50	186.50	Quartzofeldspathic Gneiss	7	5				0.1	
BL11-20	186.50	203.40	Footwall Amphibolite	3	65	Garnet			0.1	0.2
BL11-20	203.40	206.80	Pegmatite	7		Garnet	95		0.1	0.1
BL11-20	206.80	208.65	Quartzofeldspathic Gneiss	13	10	Garnet		10	0.1	0.4
BL11-20	208.65	209.85	Pegmatite	10		Garnet	75			0.2
BL11-20	209.85	215.00	Footwall Amphibolite	3	65	Garnet		5	0.1	0.2
BL11-24	24.45	25.85	Quartzofeldspathic Gneiss	5					0.1	
BL11-24	25.85	28.53	Amphibolite	7	55				0.5	0.1
BL11-24	28.53	42.75	Quartzofeldspathic Gneiss	7				1	0.1	
BL11-24	42.75	44.86	Intermediate Gneiss	15	20	Garnet		1	0.3	0.1
BL11-24	44.86	53.67	Quartzofeldspathic Gneiss	5	1	Garnet		3	0.1	0.01
BL11-24	53.67	56.72	Amphibolite	2	45				0.3	0.3
BL11-24	56.72	70.44	Quartzofeldspathic Gneiss	5				0.3	0.1	
BL11-24	70.44	74.00	Amphibolite	3	55				0.5	0.5
BL11-24	74.00	78.60	UM/Lamp Dike							

HoleID	From	To	Lithology	Bt %	Am %	Metamorphic Minerals	Peg %	QV %	Py %	Po %
BL11-24	78.60	130.00	Quartzofeldspathic Gneiss	13				1	0.7	0.3
BL11-24	130.00	131.30	Pegmatite	3			100			
BL11-24	131.30	132.30	Micaceous Quartzofeldspathic Gneiss	7		Garnet + Muscovite		5	0.7	0.3
BL11-24	132.30	133.00	Pegmatite	3	1		100			
BL11-24	133.00	139.10	Micaceous Quartzofeldspathic Gneiss	10		Garnet + Muscovite	3	5	0.7	0.5
BL11-24	139.10	143.92	Garnet Biotite Schist	25		Garnet		5	1	0.7
BL11-24	143.92	147.60	Quartzofeldspathic Gneiss	20					0.01	
BL11-24	147.60	151.00	Garnet Biotite Schist	25		Garnet		1	1	0.7
BL11-24	151.00	152.93	Quartzofeldspathic Gneiss	5	7				0.3	
BL11-24	152.93	156.85	Garnet Biotite Schist	25		Garnet + Kyanite	5	5	1	0.5
BL11-24	156.85	158.33	Micaceous Quartzofeldspathic Gneiss	7		Cordierite		3	0.3	0.1
BL11-24	158.33	159.00	Garnet Biotite Schist	20		Garnet + Muscovite				
BL11-24	159.00	163.20	Micaceous Quartzofeldspathic Gneiss	7		Garnet + Muscovite			0.3	0.1
BL11-24	163.20	164.20	Garnet Biotite Schist	20		Garnet + Muscovite		3	0.3	
BL11-24	164.20	215.80	Quartzofeldspathic Gneiss	7				3	0.3	
BL11-24	215.80	219.20	Footwall Amphibolite	3	65	Garnet		3	0.1	0.3
BL11-24	219.20	224.70	Quartzofeldspathic Gneiss	5					0.01	0.01
BL11-24	224.70	230.00	Intermediate Gneiss	7	30	Garnet				
BL11-25	21.10	27.20	Quartzofeldspathic Gneiss	4					0.3	
BL11-25	27.20	28.10	Intermediate Gneiss	7	20				0.5	
BL11-25	28.10	33.20	Quartzofeldspathic Gneiss	5	3	Garnet			0.5	
BL11-25	33.20	45.40	Amphibolite		65				0.5	0.3
BL11-25	45.40	76.30	Quartzofeldspathic Gneiss	5	3			3	0.1	
BL11-25	76.30	78.50	Intermediate Gneiss		20				0.1	
BL11-25	78.50	83.55	Quartzofeldspathic Gneiss	5	2			2	0.3	0.1
BL11-25	83.55	100.15	Intermediate Gneiss	7	25	Garnet			0.2	0.2
BL11-25	100.15	115.30	Quartzofeldspathic Gneiss	5		Garnet		5	0.3	
BL11-25	115.30	123.36	Intermediate Gneiss	10	15			3	0.1	
BL11-25	123.36	126.95	Quartzofeldspathic Gneiss	7					0.1	
BL11-25	126.95	128.25	Intermediate Gneiss	7	15				0.1	
BL11-25	128.25	156.40	Quartzofeldspathic Gneiss	5		Garnet		5	0.5	0.1
BL11-25	156.40	162.50	Micaceous Quartzofeldspathic Gneiss	1		Muscovite		5	0.3	0.1
BL11-25	162.50	164.10	Quartzofeldspathic Gneiss	7		Garnet			0.2	0.2
BL11-25	164.10	165.75	Garnet Biotite Schist	20		Garnet		7	0.1	
BL11-25	165.75	169.55	Micaceous Quartzofeldspathic Gneiss	1					0.3	
BL11-25	169.55	173.67	UM/Lamp Dike							
BL11-25	173.67	176.90	Quartzofeldspathic Gneiss	5		Garnet		5	0.5	0.2
BL11-25	176.90	186.90	Garnet Biotite Schist	25		Cordierite + Kyanite + Garnet		7	0.5	0.5

HoleID	From	To	Lithology	Bt %	Am %	Metamorphic Minerals	Peg %	QV %	Py %	Po %
BL11-25	186.90	197.50	Quartzofeldspathic Gneiss	15		Garnet		15	0.5	0.5
BL11-25	197.50	205.20	Micaceous Quartzofeldspathic Gneiss	7		Muscovite		10	0.1	0.1
BL11-25	205.20	225.00	Quartzofeldspathic Gneiss	7					0.2	
BL11-25	225.00	227.00	Quartz Vein							
BL11-25	227.00	236.30	Quartzofeldspathic Gneiss	10	3				0.3	
BL11-25	236.30	242.00	Pegmatite	3	1		95		0.1	
BL11-36	3.90	14.85	Intermediate Gneiss	7	45		1		0.1	
BL11-36	14.85	39.40	Quartzofeldspathic Gneiss	3			1	7	0.1	
BL11-36	39.40	39.85	Pegmatite	10			100			
BL11-36	39.85	106.65	Quartzofeldspathic Gneiss	7			5	7	0.1	0.01
BL11-36	106.65	113.55	Garnet Biotite Schist	20	5	Cordierite + Kyanite + Garnet	5		0.5	0.2
BL11-36	113.55	114.75	Pegmatite	15			100		1	1
BL11-36	114.75	116.70	Biotite Schist	25			5		1	1.3
BL11-36	116.70	125.33	Quartzofeldspathic Gneiss	12				1	0.3	0.1
BL11-36	125.33	135.65	Quartzofeldspathic Gneiss	15		Garnet + Sillmanite		5	0.7	0.3
BL11-36	135.65	138.50	Garnet Biotite Schist	35		Garnet + Kyanite			0.7	0.5
BL11-36	138.50	140.55	Quartzofeldspathic Gneiss	10		Cordierite + Garnet	7		0.5	0.5
BL11-36	140.55	143.10	Quartzofeldspathic Gneiss	5	7					
BL11-36	143.10	144.90	Pegmatite	5			95		0.3	0.1
BL11-36	144.90	148.55	Quartzofeldspathic Gneiss	15			5		0.5	0.3
BL11-36	148.55	150.45	Pegmatite	7			70		0.3	0.3
BL11-36	150.45	152.25	Garnet Biotite Schist	30		Cordierite + Kyanite + Garnet	5	3	0.7	0.5
BL11-36	152.25	166.30	Micaceous Quartzofeldspathic Gneiss	7		Cordierite + Muscovite		3	0.7	0.4
BL11-36	166.30	167.85	UM/Lamp Dike							
BL11-36	167.85	179.45	Garnet Biotite Schist			Cordierite + Kyanite + Garnet	7	7	1	0.5
BL11-36	179.45	198.35	Quartzofeldspathic Gneiss	10	3		1	1	0.3	0.1
BL11-36	198.35	198.65	UM/Lamp Dike							
BL11-36	198.65	205.70	Quartzofeldspathic Gneiss	12		Cordierite + Muscovite		5	0.3	0.1
BL11-36	205.70	208.00	Pegmatite	1			100			
BL11-36	208.00	210.55	Quartzofeldspathic Gneiss	10				3	0.01	0.01
BL11-36	210.55	211.40	Pegmatite	1			100			
BL11-36	211.40	212.40	Quartzofeldspathic Gneiss	10	3		3		0.05	0.01
BL11-36	212.40	221.00	Footwall Amphibolite	1	65	Garnet	7			
BL11-115	24.20	55.70	Quartzofeldspathic Gneiss	5	1			5	0.1	
BL11-115	55.70	59.60	Amphibolite	5	70			1	0.3	0.1

HoleID	From	To	Lithology	Bt %	Am %	Metamorphic Minerals	Peg %	QV %	Py %	Po %
BL11-115	59.60	82.40	Quartzofeldspathic Gneiss	7				3	1	0.3
BL11-115	82.40	87.60	Intermediate Gneiss	7	35				0.1	
BL11-115	87.60	93.00	Quartzofeldspathic Gneiss	7				3	0.3	0.1
BL11-115	93.00	94.85	Amphibolite	3	60	Garnet		3	0.4	0.1
BL11-115	94.85	133.70	Quartzofeldspathic Gneiss	5				1	0.1	
BL11-115	133.70	135.75	Intermediate Gneiss	10	40				0.3	
BL11-115	135.75	141.30	Quartzofeldspathic Gneiss	5					0.1	
BL11-115	141.30	144.40	Amphibolite	3	45				0.1	
BL11-115	144.40	147.15	Quartzofeldspathic Gneiss	5	10				0.5	0.3
BL11-115	147.15	163.00	Amphibolite	2	65			1	0.5	0.2
BL11-115	163.00	167.15	Intermediate Gneiss	7	10				0.5	0.5
BL11-115	167.15	171.80	Quartzofeldspathic Gneiss	5	7				0.2	
BL11-115	171.80	177.55	Amphibolite		75			1	0.1	
BL11-115	177.55	214.35	Quartzofeldspathic Gneiss	7	2		1	5	0.3	
BL11-115	214.35	216.60	UM/Lamp Dike							
BL11-115	216.60	245.60	Quartzofeldspathic Gneiss	7					0.5	0.1
BL11-115	245.60	247.65	Intermediate Gneiss	10	20				0.1	
BL11-115	247.65	276.00	Quartzofeldspathic Gneiss	7				2	0.3	0.1
BL11-115	276.00	278.50	Intermediate Gneiss	5	30				0.3	0.3
BL11-115	278.50	314.70	Quartzofeldspathic Gneiss	7		Garnet	2	1	0.3	0.1
BL11-115	314.70	320.90	Diabase Dike							
BL11-115	320.90	362.70	Quartzofeldspathic Gneiss	5				3	0.5	0.3
BL11-115	362.70	368.60	Intermediate Gneiss	5	35	Garnet			0.5	0.3
BL11-115	368.60	404.50	Quartzofeldspathic Gneiss	7	10	Garnet		3	0.3	0.1
BL11-115	404.50	405.40	Intermediate Gneiss	10	20		3		0.1	
BL11-115	405.40	408.00	Quartzofeldspathic Gneiss	15		Garnet	10	5	0.5	
BL11-115	408.00	410.60	Garnet Biotite Schist	25		Garnet	7	3	0.5	0.5
BL11-115	410.60	422.35	Quartzofeldspathic Gneiss	13		Garnet		3	0.3	0.1
BL11-115	422.35	423.65	Amphibolite		60				0.1	0.1
BL11-115	423.65	464.90	Quartzofeldspathic Gneiss	10	5			1	0.3	0.1
BL11-115	464.90	467.75	Intermediate Gneiss	13	20				0.3	0.2
BL11-115	467.75	490.70	Quartzofeldspathic Gneiss	7	3			3	0.2	0.05
BL11-115	490.70	512.00	Footwall Amphibolite	1	60	Garnet		2	0.1	0.1
BL11-139	6.60	55.85	Quartzofeldspathic Gneiss	7	1		2	2	0.3	0.05
BL11-139	55.85	61.20	Porphyry	10	30				0.2	
BL11-139	61.20	94.00	Quartzofeldspathic Gneiss	5	3				0.3	0.1
BL11-139	94.00	99.00	Intermediate Gneiss	10	30				0.5	0.3
BL11-139	99.00	101.90	Quartzofeldspathic Gneiss	10					0.3	0.05
BL11-139	101.90	103.00	Amphibolite	1	75				0.3	0.3
BL11-139	103.00	104.75	Quartzofeldspathic Gneiss	5					0.2	0.05
BL11-139	104.75	106.85	Amphibolite	2	60				0.2	0.1
BL11-139	106.85	111.80	Intermediate Gneiss	5	25			1	0.3	0.2
BL11-139	111.80	115.40	Porphyry	10	30				0.2	
BL11-139	115.40	119.70	Quartzofeldspathic Gneiss	7	1				0.3	

HoleID	From	To	Lithology	Bt %	Am %	Metamorphic Minerals	Peg %	QV %	Py %	Po %
BL11-139	119.70	124.85	Quartzofeldspathic Gneiss	7	5		3	1	0.1	
BL11-139	124.85	130.30	Quartzofeldspathic Gneiss	7	2		2		0.3	0.01
BL11-139	130.30	134.90	Intermediate Gneiss	15	25				0.3	0.3
BL11-139	134.90	139.00	Quartzofeldspathic Gneiss	10					0.3	0.2
BL11-139	139.00	142.00	Intermediate Gneiss	15	25			1	0.4	0.2
BL11-139	142.00	161.00	Quartzofeldspathic Gneiss	10	10		5	3	0.5	0.3
BL11-139	161.00	164.70	Intermediate Gneiss	3	40		15	1	0.3	
BL11-139	164.70	186.60	Quartzofeldspathic Gneiss	10		Muscovite	7	4	0.2	0.05
BL11-139	186.60	189.20	Intermediate Gneiss	15	30	Garnet			0.5	0.5
BL11-139	189.20	192.40	Quartzofeldspathic Gneiss	10			20		0.1	0.1
BL11-139	192.40	199.50	Intermediate Gneiss	5	30		15	1	0.5	0.5
BL11-139	199.50	200.80	Quartzofeldspathic Gneiss	15	5		3		0.2	0.1
BL11-139	200.80	207.60	Intermediate Gneiss	15	25	Garnet	3		0.5	0.5
BL11-139	207.60	215.00	Garnet Biotite Schist	30	10	Cordierite + Garnet	15		1	1
BL11-139	215.00	216.00	Pegmatite	10			95		1	1
BL11-139	216.00	219.40	Garnet Biotite Schist	30	5	Cordierite + Garnet	17		1	1
BL11-139	219.40	223.70	Intermediate Gneiss	3	50				0.2	0.2
BL11-139	223.70	226.10	Quartzofeldspathic Gneiss	7		Garnet	7	10	0.5	0.3
BL11-139	226.10	228.00	Micaceous Quartzofeldspathic Gneiss	5		Muscovite	25		0.2	0.1
BL11-139	228.00	230.30	Intermediate Gneiss	15	25	Garnet			0.5	0.3
BL11-139	230.30	239.50	Quartzofeldspathic Gneiss	12		Garnet	7	3	0.3	0.2
BL11-139	239.50	246.85	Garnet Biotite Schist	30		Cordierite + Kyanite + Garnet	20		0.5	0.3
BL11-139	246.85	248.30	Quartzofeldspathic Gneiss	7				10	0.3	
BL11-139	248.30	249.35	Pegmatite	2			100		0.1	0.01
BL11-139	249.35	282.50	Quartzofeldspathic Gneiss	12	3	Garnet	12	3	0.5	0.5
BL11-139	282.50	285.10	Amphibolite		65			5	0.1	0.1
BL11-139	285.10	300.00	Quartzofeldspathic Gneiss	10	5			3	0.3	0.1
BL11-139	300.00	302.20	Diabase Dike							
BL11-139	302.20	303.00	Quartzofeldspathic Gneiss	1	1					
BL11-139	303.00	304.20	Diabase Dike							
BL11-139	304.20	308.25	Quartzofeldspathic Gneiss	5	3				0.3	0.1
BL11-139	308.25	334.80	UM/Lamp Dike							
BL11-139	334.80	336.90	Quartzofeldspathic Gneiss	2	2				0.1	
BL11-139	336.90	352.85	Footwall Amphibolite	2	55	Garnet			0.1	
BL11-139	352.85	353.80	Pegmatite	5			100			
BL11-139	353.80	371.00	Footwall Amphibolite	2	60	Garnet	5		0.1	0.1
BL12-178	3.30	12.00	Garnet Biotite Schist	25	5	Garnet + Kyanite			1	1
BL12-178	12.00	15.40	Quartzofeldspathic Gneiss	10		Garnet + Muscovite	10		0.3	0.7
BL12-178	15.40	17.00	Garnet Biotite Schist	25		Garnet + Muscovite	7		0.7	0.7

HoleID	From	To	Lithology	Bt %	Am %	Metamorphic Minerals	Peg %	QV %	Py %	Po %
BL12-178	17.00	19.10	Quartzofeldspathic Gneiss	5		Garnet + Muscovite	20		0.5	0.5
BL12-178	19.10	25.25	Quartzofeldspathic Gneiss	13		Garnet + Sillmanite + Kyanite + Muscovite	12		1	1
BL12-178	25.25	36.45	Quartzofeldspathic Gneiss	7		Garnet + Sillmanite + Kyanite + Muscovite			1	1
BL12-178	36.45	37.90	Pegmatite	5			80		0.3	
BL12-178	37.90	44.30	Quartzofeldspathic Gneiss	12		Garnet + Sillmanite + Kyanite	5		1	1.3
BL12-178	44.30	45.00	Pegmatite	7		Muscovite	95		0.2	0.2
BL12-178	45.00	51.20	Quartzofeldspathic Gneiss	15		Muscovite	7		1	1
BL12-178	51.20	51.80	Pegmatite	3		Muscovite	100		0.5	0.5
BL12-178	51.80	53.15	UM/Lamp Dike							
BL12-178	53.15	54.90	Quartzofeldspathic Gneiss	10		Muscovite	5		1	1
BL12-178	54.90	56.05	Pegmatite	3			95		0.1	0.1
BL12-178	56.05	65.00	Quartzofeldspathic Gneiss	12		Muscovite	7	3	1	1
BL12-178	65.00	97.40	Garnet Biotite Schist	25		Magnetite + Kyanite + Garnet	5	7	0.7	0.7
BL12-178	97.40	99.85	Quartzofeldspathic Gneiss	15			20		0.3	0.2
BL12-178	99.85	102.90	Quartzofeldspathic Gneiss	15					0.1	0.1
BL12-178	102.90	123.00	Quartzofeldspathic Gneiss	7			1	7	0.2	0.2
BL12-178	123.00	124.00	Pegmatite	10			90		0.5	0.5
BL12-178	124.00	127.50	Quartzofeldspathic Gneiss	10			12		0.3	0.1
BL12-178	127.50	140.75	Quartzofeldspathic Gneiss	7			10		0.3	0.3
BL12-178	140.75	144.20	Pegmatite	7			90		0.1	0.2
BL12-178	144.20	179.00	Footwall Amphibolite	3	65	Garnet	1	1		0.2
BL12-183	2.20	72.50	Quartzofeldspathic Gneiss	5				1	0.3	
BL12-183	72.50	88.70	Amphibolite	2	55			1	0.5	
BL12-183	88.70	145.75	Quartzofeldspathic Gneiss	5	10			1	0.3	
BL12-183	145.75	148.00	Amphibolite	2	50	Garnet		5	0.7	
BL12-183	148.00	160.90	Quartzofeldspathic Gneiss	5	3			5	1	
BL12-183	160.90	182.60	Intermediate Gneiss	5	35		1			
BL12-183	182.60	205.40	Quartzofeldspathic Gneiss	5	2	Magnetite	3	5	0.3	0.1
BL12-183	205.40	207.10	Intermediate Gneiss	15	30				0.1	
BL12-183	207.10	215.30	Quartzofeldspathic Gneiss	7	4			3	0.4	
BL12-183	215.30	216.50	Pegmatite	1	1		100		0.1	
BL12-183	216.50	220.55	Quartzofeldspathic Gneiss	7	3			3	0.5	
BL12-183	220.55	220.95	Biotite Schist	35					1	
BL12-183	220.95	221.85	Quartzofeldspathic Gneiss	10	2		50		0.5	
BL12-183	221.85	222.70	Pegmatite	5			100		0.1	
BL12-183	222.70	223.80	Quartzofeldspathic Gneiss	10					0.5	
BL12-183	223.80	225.50	Quartzofeldspathic Gneiss	7			20		0.2	

HoleID	From	To	Lithology	Bt %	Am %	Metamorphic Minerals	Peg %	QV %	Py %	Po %
BL12-183	225.50	226.40	Pegmatite	3			100			
BL12-183	226.40	255.00	Quartzofeldspathic Gneiss	5	1	Magnetite		3	0.5	
BL12-183	255.00	259.05	Quartzofeldspathic Gneiss	7	7			3	0.5	1
BL12-183	259.05	260.85	Quartzofeldspathic Gneiss	10						
BL12-183	260.85	264.00	Quartzofeldspathic Gneiss	7	7				1	0.5
BL12-183	264.00	277.95	Quartzofeldspathic Gneiss	7	7			5	0.7	0.7
BL12-183	277.95	279.00	Pegmatite	5			100		0.1	0.1
BL12-183	279.00	282.00	Intermediate Gneiss	3	20			3		
BL12-183	282.00	283.00	Pegmatite	3	3	Magnetite	100			
BL12-183	283.00	284.20	Intermediate Gneiss	2	20		3			
BL12-183	284.20	287.60	Quartzofeldspathic Gneiss	7		Muscovite	3	1	0.3	0.3
BL12-183	287.60	296.00	Micaceous Quartzofeldspathic Gneiss	7		Muscovite	7		0.5	0.5
BL12-183	296.00	305.40	Quartzofeldspathic Gneiss	7		Garnet + Muscovite		10	0.9	0.5
BL12-183	305.40	307.95	Micaceous Quartzofeldspathic Gneiss	5		Muscovite			0.7	0.5
BL12-183	307.95	314.10	Quartzofeldspathic Gneiss	5		Muscovite			0.7	0.3
BL12-183	314.10	323.00	Intermediate Gneiss	10	35		1	3	0.3	0.2
BL12-183	323.00	331.20	Quartzofeldspathic Gneiss	15	15			5	1	1
BL12-183	331.20	332.40	Pegmatite	20	3		75		1	1
BL12-183	332.40	336.70	Quartzofeldspathic Gneiss	10	10		25		0.7	1
BL12-183	336.70	338.00	Pegmatite	20	5		70		0.5	0.5
BL12-183	338.00	341.50	Quartzofeldspathic Gneiss	20	17		20	3	0.7	1
BL12-183	341.50	342.55	Pegmatite	7			95		0.3	0.3
BL12-183	342.55	345.95	Quartzofeldspathic Gneiss	10	3		20		0.7	0.7
BL12-183	345.95	357.00	Pegmatite	10	3	Cordierite + Kyanite	80		1	1
BL12-183	357.00	361.00	Garnet Biotite Schist	20		Cordierite + Kyanite + Garnet	7		1	1
BL12-183	361.00	361.70	Quartzofeldspathic Gneiss	15			3		0.3	0.2
BL12-183	361.70	364.80	Pegmatite	20			80		1	1
BL12-183	364.80	366.00	Quartzofeldspathic Gneiss	10	2				0.1	0.1
BL12-183	366.00	371.20	Quartzofeldspathic Gneiss	7	5	Garnet	2		1	1.5
BL12-183	371.20	373.70	Quartzofeldspathic Gneiss	10	2				0.1	
BL12-183	373.70	378.25	Quartzofeldspathic Gneiss	10	2	Garnet		3	1	0.5
BL12-183	378.25	382.65	Intermediate Gneiss	10	25		2		0.1	
BL12-183	382.65	397.45	Quartzofeldspathic Gneiss	4		Garnet		3	0.3	
BL12-183	397.45	404.05	Footwall Amphibolite	2	65	Garnet			0.2	0.3
BL12-183	404.05	409.90	Quartzofeldspathic Gneiss	7				3	0.3	0.3
BL12-183	409.90	428.80	Footwall Amphibolite	3	70	Garnet		2	0.1	0.2
BL12-183	428.80	433.40	Pegmatite	3			100			
BL12-183	433.40	438.00	Footwall Amphibolite	3	70	Garnet		3	0.1	0.2
BL12-186	2.20	64.40	Quartzofeldspathic Gneiss	7	1			1	0.3	
BL12-186	64.40	66.45	Amphibolite		55				0.1	

HoleID	From	To	Lithology	Bt %	Am %	Metamorphic Minerals	Peg %	QV %	Py %	Po %
BL12-186	66.45	71.00	Quartzofeldspathic Gneiss	5	3				0.3	
BL12-186	71.00	79.50	Amphibolite		65	Magnetite		3	0.5	
BL12-186	79.50	81.20	Quartzofeldspathic Gneiss	3	5				0.1	
BL12-186	81.20	83.20	Amphibolite		65	Magnetite			0.4	0.1
BL12-186	83.20	84.70	Quartzofeldspathic Gneiss	5	2				0.1	
BL12-186	84.70	85.30	Amphibolite		60	Magnetite		15	1	0.3
BL12-186	85.30	88.80	Quartzofeldspathic Gneiss	5	5	Magnetite		3	1	0.1
BL12-186	88.80	90.75	Amphibolite	3	70				0.5	0.2
BL12-186	90.75	137.00	Quartzofeldspathic Gneiss	7			1	1	0.01	
BL12-186	137.00	138.70	Quartzofeldspathic Gneiss	5	2				0.3	
BL12-186	138.70	146.75	Intermediate Gneiss	10	70				0.1	
BL12-186	146.75	149.00	Quartzofeldspathic Gneiss	5				5	0.7	
BL12-186	149.00	151.00	Amphibolite	1	75			1	0.1	
BL12-186	151.00	172.90	Quartzofeldspathic Gneiss	5	3		1		0.5	
BL12-186	172.90	183.30	Intermediate Gneiss	7	55		1	0.5	0.1	
BL12-186	183.30	184.60	Intermediate Gneiss	5	30				0.1	
BL12-186	184.60	192.10	Intermediate Gneiss	7	55				0.1	
BL12-186	192.10	198.00	Intermediate Gneiss	5	35				0.1	
BL12-186	198.00	199.00	Intermediate Gneiss	7	55				0.05	
BL12-186	199.00	199.90	Amphibolite Gneiss	10	30				0.2	
BL12-186	199.90	259.45	Quartzofeldspathic Gneiss	7			3	1	0.4	
BL12-186	259.45	261.40	Pegmatite	3			95		0.1	
BL12-186	261.40	280.55	Quartzofeldspathic Gneiss	7	3			10	0.5	
BL12-186	280.55	281.65	Pegmatite						0.3	0.3
BL12-186	281.65	282.30	Quartzofeldspathic Gneiss	7					0.5	
BL12-186	282.30	285.70	Quartzofeldspathic Gneiss	10					0.01	
BL12-186	285.70	286.75	Quartzofeldspathic Gneiss	5					1	0.3
BL12-186	286.75	288.65	Intermediate Gneiss	5	35				1	1
BL12-186	288.65	308.00	Quartzofeldspathic Gneiss	7	5		1	7	0.4	0.1
BL12-186	308.00	309.00	Micaceous Quartzofeldspathic Gneiss	5		Muscovite		5	0.5	0.1
BL12-186	309.00	320.50	Quartzofeldspathic Gneiss	7			7	10	0.5	0.3
BL12-186	320.50	324.60	Pegmatite	5		Magnetite	97		1	1
BL12-186	324.60	331.00	Intermediate Gneiss	5	30			3	0.5	0.1
BL12-186	331.00	331.85	Quartzofeldspathic Gneiss	5	7				0.3	0.3
BL12-186	331.85	337.50	Micaceous Quartzofeldspathic Gneiss	7		Muscovite		7	0.5	0.3
BL12-186	337.50	341.50	Quartzofeldspathic Gneiss	5	2			20	0.5	
BL12-186	341.50	345.20	Amphibolite	7	60				0.5	0.3
BL12-186	345.20	371.75	Quartzofeldspathic Gneiss	7	20	Garnet	3	7	1	0.7
BL12-186	371.75	380.10	Pegmatite	5	3		80		1	1
BL12-186	380.10	385.00	Micaceous Quartzofeldspathic Gneiss	10			5		1	1
BL12-186	385.00	386.20	Quartzofeldspathic Gneiss	13					0.1	
BL12-186	386.20	387.00	Micaceous Quartzofeldspathic Gneiss	5					1	0.1

HoleID	From	To	Lithology	Bt %	Am %	Metamorphic Minerals	Peg %	QV %	Py %	Po %
BL12-186	387.00	389.45	Garnet Biotite Schist	20	3	Garnet		15	1	1
BL12-186	389.45	422.30	Quartzofeldspathic Gneiss	5	5			3	0.5	0.3
BL12-186	422.30	427.85	Footwall Amphibolite	2	55	Garnet		3	0.3	0.1
BL12-186	427.85	433.00	Quartzofeldspathic Gneiss	5			3	3	0.1	
BL12-186	433.00	440.00	Footwall Amphibolite	3	50	Garnet			0.2	0.3
BL12-199	3.20	5.70	Quartzofeldspathic Gneiss	3					0.3	
BL12-199	5.70	6.50	Diabase Dike							
BL12-199	6.50	47.65	Quartzofeldspathic Gneiss	7	5		2	3	0.5	
BL12-199	28.20	28.95	UM/Lamp Dike							
BL12-199	28.95	47.65	Quartzofeldspathic Gneiss	7	5				0.5	
BL12-199	47.65	48.10	UM/Lamp Dike							
BL12-199	48.10	60.50	Quartzofeldspathic Gneiss	10	5			3	0.7	
BL12-199	60.50	63.20	Intermediate Gneiss	10	30					
BL12-199	63.20	78.20	Quartzofeldspathic Gneiss	7	3				0.3	
BL12-199	78.20	86.00	Amphibolite	4	65				0.7	0.1
BL12-199	86.00	87.50	Quartzofeldspathic Gneiss	7				5	0.5	
BL12-199	87.50	88.50	Amphibolite	4	65			3	0.4	
BL12-199	88.50	112.00	Quartzofeldspathic Gneiss	10				3	0.5	0.1
BL12-199	112.00	125.00	Quartzofeldspathic Gneiss	5		Muscovite		2	0.3	
BL12-199	125.00	132.10	Quartzofeldspathic Gneiss	10				3	0.2	
BL12-199	132.10	134.05	Diabase Dike							
BL12-199	134.05	151.20	Quartzofeldspathic Gneiss	7		Muscovite		3	0.3	
BL12-199	151.20	171.95	Quartzofeldspathic Gneiss	7				3	0.3	
BL12-199	171.95	176.00	Quartz Vein	3				80	0.7	
BL12-199	176.00	182.10	Quartzofeldspathic Gneiss	4	7				0.7	0.3
BL12-199	182.10	183.00	UM/Lamp Dike							
BL12-199	183.00	184.95	Quartzofeldspathic Gneiss	3	5				1	
BL12-199	184.95	186.30	Amphibolite	3	65	Magnetite		5	0.7	0.4
BL12-199	186.30	187.70	Quartzofeldspathic Gneiss	5	5			3	0.5	0.2
BL12-199	187.70	189.75	Amphibolite	3	60				0.7	0.5
BL12-199	189.75	198.65	Quartzofeldspathic Gneiss	7	5			3	0.4	0.2
BL12-199	198.65	199.50	UM/Lamp Dike							
BL12-199	199.50	203.75	Amphibolite	5	55				1	0.7
BL12-199	203.75	224.05	Quartzofeldspathic Gneiss	13	10	Magnetite		3	0.7	0.7
BL12-199	224.05	229.20	Quartzofeldspathic Gneiss	7	3				0.3	
BL12-199	229.20	238.90	Amphibolite	3	70	Magnetite			0.7	0.7
BL12-199	238.90	245.00	Quartzofeldspathic Gneiss	5	5				0.3	
BL12-199	245.00	245.60	Quartz Vein						0.3	
BL12-199	245.60	285.00	Quartzofeldspathic Gneiss	7	7			3	0.3	0.2
BL12-199	285.00	286.90	Amphibolite	13	55	Garnet			0.6	0.6
BL12-199	286.90	288.60	Quartzofeldspathic Gneiss	5	3				0.7	
BL12-199	288.60	292.00	Amphibolite	13	55				0.7	0.5
BL12-199	292.00	292.80	Quartz Vein	5				65	0.1	
BL12-199	292.80	295.55	Amphibolite	15	60				0.5	0.8

HoleID	From	To	Lithology	Bt %	Am %	Metamorphic Minerals	Peg %	QV %	Py %	Po %
BL12-199	295.55	300.05	Quartzofeldspathic Gneiss	7				3	0.3	
BL12-199	300.05	301.00	Amphibolite	13	60			10	0.5	0.3
BL12-199	301.00	307.65	Quartzofeldspathic Gneiss	7	4			3	0.3	
BL12-199	307.65	308.70	Garnet Biotite Schist	25		Magnetite			0.7	
BL12-199	308.70	311.10	Quartzofeldspathic Gneiss	13					0.3	
BL12-199	311.10	350.80	Quartzofeldspathic Gneiss	6		Muscovite		3	0.3	
BL12-199	350.80	388.60	Diabase Dike							
BL12-199	388.60	400.40	Quartzofeldspathic Gneiss	13	3			3	0.2	
BL12-199	400.40	401.35	Quartz Vein					90	0.1	
BL12-199	401.35	440.90	Quartzofeldspathic Gneiss	7	5			5	0.3	
BL12-199	440.90	444.45	Quartzofeldspathic Gneiss	7	5	Garnet		3	0.5	0.1
BL12-199	444.45	445.40	UM/Lamp Dike							
BL12-199	445.40	448.20	Quartzofeldspathic Gneiss	10		Garnet		7	0.5	
BL12-199	448.20	449.20	UM/Lamp Dike							
BL12-199	449.20	451.95	Quartzofeldspathic Gneiss	4	3				0.5	
BL12-199	451.95	452.80	UM/Lamp Dike							
BL12-199	452.80	468.00	Quartzofeldspathic Gneiss	7	3	Garnet		3	0.5	
BL12-199	468.00	469.60	Amphibolite	20	45				0.5	0.7
BL12-199	469.60	473.75	Quartzofeldspathic Gneiss	10	7	Garnet		3	0.7	0.5
BL12-199	473.75	477.35	Amphibolite	20	45				0.5	0.3
BL12-199	477.35	510.95	Quartzofeldspathic Gneiss	10	3				0.5	0.2
BL12-199	510.95	512.00	Diabase Dike							
BL12-199	512.00	512.85	Quartzofeldspathic Gneiss	10	3	Garnet		3	0.3	0.1
BL12-199	512.85	519.50	Footwall Amphibolite	2	70	Garnet			0.1	0.3
BL12-199	519.50	521.50	Quartzofeldspathic Gneiss	10	3			5		
BL12-199	521.50	524.00	Footwall Amphibolite	2	70	Garnet		3	0.1	0.3
BL12-204	6.80	24.30	Quartzofeldspathic Gneiss	5				3	0.2	
BL12-204	24.30	25.50	UM/Lamp Dike							
BL12-204	25.50	40.20	Quartzofeldspathic Gneiss	5				3	0.5	
BL12-204	40.20	42.55	UM/Lamp Dike							
BL12-204	42.55	57.00	Quartzofeldspathic Gneiss	5				3	0.7	
BL12-204	57.00	63.20	Amphibolite	3	70		1	1	0.3	
BL12-204	63.20	125.50	Quartzofeldspathic Gneiss	5	3			3	0.7	
BL12-204	125.50	129.60	Diabase Dike							
BL12-204	129.60	156.00	Quartzofeldspathic Gneiss	5		Muscovite			0.3	
BL12-204	156.00	158.35	Quartzofeldspathic Gneiss	5		Sillimanite + Mucovite		3	0.1	
BL12-204	158.35	159.35	UM/Lamp Dike							
BL12-204	159.35	169.50	Quartzofeldspathic Gneiss	3		Sillimanite		1	0.5	
BL12-204	169.50	176.40	Quartzofeldspathic Gneiss	5				5	1	
BL12-204	176.40	177.50	Biotite Schist	25	5	Magnetite			1	1
BL12-204	177.50	180.35	Quartzofeldspathic Gneiss	10					0.3	
BL12-204	180.35	184.70	Amphibolite	3	70	Magnetite			1	0.5
BL12-204	184.70	188.50	Quartzofeldspathic Gneiss	5	15				0.7	0.3
BL12-204	188.50	190.85	Amphibolite	5	50	Magnetite			1.5	0.7

HoleID	From	To	Lithology	Bt %	Am %	Metamorphic Minerals	Peg %	QV %	Py %	Po %
BL12-204	190.85	212.75	Quartzofeldspathic Gneiss	5					0.7	0.3
BL12-204	212.75	213.60	Amphibolite	3	60				0.5	0.1
BL12-204	213.60	215.40	Quartzofeldspathic Gneiss	5					0.5	0.1
BL12-204	215.40	223.00	Amphibolite	3	55				0.5	0.1
BL12-204	223.00	229.30	Quartzofeldspathic Gneiss	5	7			3	0.2	
BL12-204	229.30	230.25	Diabase Dike						0.3	
BL12-204	230.25	233.30	Amphibolite	4	60			3	0.7	0.7
BL12-204	233.30	235.90	Quartzofeldspathic Gneiss	10	5				0.3	0.1
BL12-204	235.90	237.50	Amphibolite	5	65	Magnetite			1.3	0.7
BL12-204	237.50	239.80	Quartzofeldspathic Gneiss	7	5				0.5	
BL12-204	239.80	263.90	Amphibolite	2	65			1	0.7	0.7
BL12-204	263.90	291.40	Diabase Dike							
BL12-204	291.40	301.90	Quartzofeldspathic Gneiss	10				1	0.4	0.2
BL12-204	301.90	303.00	UM/Lamp Dike							
BL12-204	303.00	306.70	Porphyry	10	5				0.3	0.1
BL12-204	306.70	308.90	Amphibolite	10	50				0.3	0.1
BL12-204	308.90	311.90	Porphyry	10					0.4	0.1
BL12-204	311.90	317.18	Quartzofeldspathic Gneiss	7				10	0.3	0.2
BL12-204	317.18	319.65	Amphibolite	7	60				0.1	
BL12-204	319.65	321.65	Quartzofeldspathic Gneiss	5	3		3		0.7	
BL12-204	321.65	324.45	Intermediate Gneiss	10	35				0.1	
BL12-204	324.45	329.30	Quartzofeldspathic Gneiss	10	7				0.7	
BL12-204	329.30	331.00	Intermediate Gneiss	10	35			1	0.1	
BL12-204	331.00	335.40	Quartzofeldspathic Gneiss	13	10				0.7	0.5
BL12-204	335.40	338.85	Amphibolite	2	65				0.5	0.3
BL12-204	338.85	341.40	Quartzofeldspathic Gneiss	10					0.4	0.2
BL12-204	341.40	346.00	Quartzofeldspathic Gneiss	17	7			3	0.7	0.3
BL12-204	346.00	354.05	Quartzofeldspathic Gneiss	10	3			2	0.5	0.1
BL12-204	354.05	357.05	Intermediate Gneiss	15	35			2	0.1	0.1
BL12-204	357.05	359.45	Quartzofeldspathic Gneiss	7					0.3	
BL12-204	359.45	361.20	UM/Lamp Dike							
BL12-204	361.20	362.20	Quartzofeldspathic Gneiss	7					0.1	
BL12-204	362.20	362.65	UM/Lamp Dike							
BL12-204	362.65	365.45	Quartzofeldspathic Gneiss	7				3	0.1	
BL12-204	365.45	366.85	UM/Lamp Dike							
BL12-204	366.85	367.15	Quartzofeldspathic Gneiss	7						
BL12-204	367.15	372.95	UM/Lamp Dike							
BL12-204	372.95	373.20	Quartzofeldspathic Gneiss	3						
BL12-204	373.20	374.65	Intermediate Gneiss	15	25			1	0.3	
BL12-204	374.65	420.35	Quartzofeldspathic Gneiss	5					0.3	0.2
BL12-204	420.35	425.00	Amphibolite	7	55				0.5	0.3
BL12-204	425.00	428.00	Diabase Dike							
BL12-204	428.00	432.00	Quartzofeldspathic Gneiss	7				3	0.5	
BL12-204	432.00	435.60	Amphibolite	3	60			3	0.3	0.1
BL12-204	435.60	437.60	Quartzofeldspathic Gneiss	10					0.3	

HoleID	From	To	Lithology	Bt %	Am %	Metamorphic Minerals	Peg %	QV %	Py %	Po %
BL12-204	437.60	451.00	Quartzofeldspathic Gneiss	12	7			5	0.7	
BL12-204	451.00	468.30	Quartzofeldspathic Gneiss	15	3			2	0.7	
BL12-204	468.30	473.05	Quartzofeldspathic Gneiss	12	5	Garnet			0.5	
BL12-204	473.05	477.50	Amphibolite	2	70			1	0.1	
BL12-204	477.50	479.50	Quartzofeldspathic Gneiss	10				3	0.5	
BL12-204	479.50	480.20	Garnet Biotite Schist	30		Garnet			1	1
BL12-204	480.20	514.30	Quartzofeldspathic Gneiss	12				10	0.7	0.3
BL12-204	514.30	517.45	Pegmatite	7			85		0.7	0.2
BL12-204	517.45	518.25	Quartzofeldspathic Gneiss	12	10				0.1	
BL12-204	518.25	519.10	Pegmatite	3			95			
BL12-204	519.10	520.15	Quartzofeldspathic Gneiss	10	5				0.1	
BL12-204	520.15	522.90	Pegmatite	3			90		0.3	
BL12-204	522.90	531.40	Quartzofeldspathic Gneiss	7	10				0.2	
BL12-204	531.40	547.50	Quartzofeldspathic Gneiss	13					0.2	
BL12-204	547.50	549.75	Footwall Amphibolite	3	75			15	0.4	
BL12-204	549.75	558.70	Quartzofeldspathic Gneiss	15						
BL12-204	558.70	560.80	Footwall Amphibolite		70					
BL12-204	560.80	563.75	Quartzofeldspathic Gneiss	15				3		
BL12-204	563.75	569.30	Footwall Amphibolite		70	Garnet				0.3
BL12-204	569.30	576.00	Quartzofeldspathic Gneiss	10						
BL12-204	576.00	580.05	Footwall Amphibolite		60	Garnet				0.2
BL12-204	580.05	582.50	Quartzofeldspathic Gneiss	10	3	Garnet				0.2
BL12-204	582.50	583.30	Footwall Amphibolite		65	Garnet				
BL12-204	583.30	594.60	Quartzofeldspathic Gneiss	12				7		0.2
BL12-204	594.60	597.15	Quartzofeldspathic Gneiss	5	3	Garnet		5	0.2	0.5
BL12-204	597.15	600.60	Footwall Amphibolite		60	Garnet				0.3
BL12-204	600.60	601.85	Quartzofeldspathic Gneiss	5						0.7
BL12-204	601.85	602.80	Footwall Amphibolite		60	Garnet				0.4
BL12-204	602.80	606.00	Quartzofeldspathic Gneiss	7						0.4
BL12-204	606.00	626.40	Footwall Amphibolite	5	60	Garnet		3		
BL12-204	626.40	630.90	Intermediate Gneiss	15	30					
BL12-204	630.90	633.20	Quartzofeldspathic Gneiss	5					0.05	0.01
BL12-204	633.20	637.85	Footwall Amphibolite	5	60	Garnet				
BL12-204	637.85	646.00	Quartzofeldspathic Gneiss	13	3	Garnet		3		
BL12-204	646.00	647.30	UM/Lamp Dike							
BL12-204	647.30	681.00	Footwall Amphibolite	2	70	Garnet				0.2
BL12-255	5.50	38.40	Quartzofeldspathic Gneiss	7	3			1	0.5	
BL12-255	38.40	47.00	Intermediate Gneiss	3	35				0.5	
BL12-255	47.00	64.65	Quartzofeldspathic Gneiss	5	10			2	0.5	0.05
BL12-255	64.65	96.55	Intermediate Gneiss	7	30			3	0.2	
BL12-255	96.55	100.55	Quartzofeldspathic Gneiss	3	2		1		0.3	0.1
BL12-255	100.30	103.30	Intermediate Gneiss	3	35				0.1	
BL12-255	103.30	108.50	Quartzofeldspathic Gneiss	5	2				0.3	
BL12-255	108.50	109.45	UM/Lamp Dike							

HoleID	From	To	Lithology	Bt %	Am %	Metamorphic Minerals	Peg %	QV %	Py %	Po %
BL12-255	109.45	115.70	Quartzofeldspathic Gneiss	3	2				0.3	
BL12-255	115.70	123.65	Amphibolite	3	55	Magnetite			1	
BL12-255	123.65	124.95	Quartz Vein	3				100	1	
BL12-255	124.95	131.95	Amphibolite	3	75	Magnetite			1.2	
BL12-255	131.95	135.75	Quartzofeldspathic Gneiss	5	3	Garnet		5	0.7	0.3
BL12-255	135.75	153.10	Quartzofeldspathic Gneiss	5	1		3		0.7	
BL12-255	153.10	154.10	Pegmatite	3			100		0.3	
BL12-255	154.10	155.60	UM/Lamp Dike			Magnetite				
BL12-255	155.60	202.00	Quartzofeldspathic Gneiss	5	3			3	0.7	0.2
BL12-255	202.00	208.60	Amphibolite	3	60	Magnetite			0.5	0.5
BL12-255	208.60	211.60	Quartzofeldspathic Gneiss	7				3	0.3	0.2
BL12-255	211.60	232.75	Amphibolite	3	55	Magnetite		3	1	1
BL12-255	232.75	236.10	Quartzofeldspathic Gneiss	5	3			3	0.7	0.1
BL12-255	236.10	238.10	Amphibolite	3	45				0.5	
BL12-255	238.10	243.00	Quartzofeldspathic Gneiss	5	3			7	0.3	
BL12-255	243.00	250.95	Amphibolite	3	50	Magnetite		7	0.7	0.7
BL12-255	250.95	254.90	Quartzofeldspathic Gneiss	5	5				0.3	0.1
BL12-255	254.90	265.65	Amphibolite	3	50	Magnetite			1	1
BL12-255	265.65	269.25	Quartzofeldspathic Gneiss	7	3			3	0.3	0.1
BL12-255	269.25	272.70	Amphibolite	2	65	Magnetite			0.5	
BL12-255	272.70	274.05	Quartzofeldspathic Gneiss	5	3	Magnetite			0.3	0.1
BL12-255	274.05	274.70	Amphibolite	2	65	Magnetite			1	1
BL12-255	274.70	279.25	Quartzofeldspathic Gneiss	7	1				0.5	
BL12-255	279.25	280.20	Amphibolite	2	45				0.7	0.4
BL12-255	280.20	281.55	Quartzofeldspathic Gneiss	7					0.5	
BL12-255	281.55	283.20	Amphibolite	2	45	Magnetite			0.7	0.5
BL12-255	283.20	287.00	Quartzofeldspathic Gneiss	5	3	Magnetite		3	1	1
BL12-255	287.00	287.35	Amphibolite	3	55	Magnetite			0.5	0.5
BL12-255	287.35	289.80	Quartzofeldspathic Gneiss	7	3				0.4	
BL12-255	289.80	290.35	Amphibolite	3	60	Magnetite			0.5	0.5
BL12-255	290.35	329.50	Quartzofeldspathic Gneiss	7	3		2	1	0.5	
BL12-255	329.50	331.85	Biotite Schist	40	7			7	1	1
BL12-255	331.85	377.00	Micaceous Quartzofeldspathic Gneiss	5	2		5		0.7	0.3
BL12-255	377.00	382.80	Quartzofeldspathic Gneiss	7				3	0.3	
BL12-255	382.80	388.00	Micaceous Quartzofeldspathic Gneiss	5				3	0.4	0.2
BL12-255	388.00	400.25	Quartzofeldspathic Gneiss	10			3	1	1	
BL12-255	400.25	400.90	Quartz Vein					100		
BL12-255	400.90	405.00	Quartzofeldspathic Gneiss	7				1	0.7	
BL12-255	405.00	416.50	Quartzofeldspathic Gneiss	5	5				0.5	
BL12-255	416.50	421.25	UM/Lamp Dike							
BL12-255	421.25	422.85	Quartz Vein	10	10	Magnetite		75	0.7	0.5
BL12-255	422.85	425.70	Quartzofeldspathic Gneiss	10	2				0.5	

HoleID	From	To	Lithology	Bt %	Am %	Metamorphic Minerals	Peg %	QV %	Py %	Po %
BL12-255	425.70	428.35	Intermediate Gneiss	5	30			1	0.7	0.3
BL12-255	428.35	434.35	Quartzofeldspathic Gneiss	5	10				0.3	0.1
BL12-255	434.35	475.75	Quartzofeldspathic Gneiss	7	7	Garnet		3	0.6	0.4
BL12-255	475.75	476.30	Garnet Biotite Schist	40					0.7	0.5
BL12-255	476.30	481.85	Quartzofeldspathic Gneiss	15	15		3	3	0.7	0.3
BL12-255	481.85	488.35	Intermediate Gneiss	15	35			5	0.3	0.1
BL12-255	488.35	493.30	Quartzofeldspathic Gneiss	10	3				0.4	
BL12-255	493.30	495.45	Amphibolite	5	60			3	0.7	0.4
BL12-255	495.45	530.90	Quartzofeldspathic Gneiss	10	7	Garnet		3	0.5	0.1
BL12-255	530.90	534.00	Footwall Amphibolite	3	55	Garnet			0.1	0.1
BL12-255	534.00	539.60	Quartzofeldspathic Gneiss	10	7				0.05	
BL12-255	539.60	548.00	Footwall Amphibolite	3	55	Garnet		7	0.1	0.5
BL12-256	2.70	23.70	Quartzofeldspathic Gneiss	7	2		3		0.3	
BL12-256	23.70	25.60	UM/Lamp Dike							
BL12-256	25.60	63.70	Quartzofeldspathic Gneiss	7	2		3	1	0.5	
BL12-256	65.70	75.10	Intermediate Gneiss	15	20				0.1	
BL12-256	75.10	88.10	Quartzofeldspathic Gneiss	6	3			3	0.5	
BL12-256	88.10	93.50	Amphibolite	5	60		2		0.3	0.2
BL12-256	93.50	107.00	Quartzofeldspathic Gneiss	9	20		7		0.2	
BL12-256	107.00	109.00	Intermediate Gneiss	20	20				0.3	0.1
BL12-256	109.00	110.70	Quartzofeldspathic Gneiss	10	10		3		0.2	0.2
BL12-256	110.70	113.50	Intermediate Gneiss	15	15				0.2	0.2
BL12-256	113.50	115.50	Quartzofeldspathic Gneiss	7	3				0.2	
BL12-256	115.50	118.10	Amphibolite	7	65		3		0.2	0.1
BL12-256	118.10	136.00	Quartzofeldspathic Gneiss	10	5				0.3	
BL12-256	136.00	160.80	Amphibolite	12	60		1	2	0.3	0.2
BL12-256	160.80	184.30	Quartzofeldspathic Gneiss	10	5		4		0.3	0.1
BL12-256	184.30	192.70	Amphibolite	5	60				0.8	0.5
BL12-256	192.70	195.90	Intermediate Gneiss	20	30				0.1	0.1
BL12-256	195.90	199.20	Amphibolite	7	60				0.1	
BL12-256	199.20	200.25	Intermediate Gneiss	20	25				0.1	
BL12-256	200.25	200.60	UM/Lamp Dike							
BL12-256	200.60	208.90	Quartzofeldspathic Gneiss	12	3		3		0.3	0.1
BL12-256	208.90	213.70	Amphibolite	2	65				0.3	
BL12-256	213.70	221.60	Quartzofeldspathic Gneiss	10	5		5	3	0.4	0.1
BL12-256	221.60	222.20	UM/Lamp Dike							
BL12-256	222.20	242.05	Quartzofeldspathic Gneiss	7	3		5	2	0.4	
BL12-256	242.05	255.70	Quartzofeldspathic Gneiss	5	3		12		0.3	0.1
BL12-256	255.70	257.90	Amphibolite	1	55					
BL12-256	257.90	275.10	Quartzofeldspathic Gneiss	7	3		7		0.7	0.1
BL12-256	275.10	277.90	Amphibolite	10	60		5		0.7	0.5
BL12-256	277.90	279.00	Quartzofeldspathic Gneiss	12	5				0.3	
BL12-256	279.00	281.70	Amphibolite	10	60				0.7	0.7
BL12-256	281.70	284.00	Quartzofeldspathic Gneiss	12	5		3		0.3	0.3

HoleID	From	To	Lithology	Bt %	Am %	Metamorphic Minerals	Peg %	QV %	Py %	Po %
BL12-256	284.00	286.65	Amphibolite	10	55				0.5	0.4
BL12-256	286.65	288.50	Quartzofeldspathic Gneiss	7	3		7		0.2	0.1
BL12-256	288.50	291.90	Amphibolite	3	65				0.3	0.6
BL12-256	291.90	295.10	Quartzofeldspathic Gneiss	7	3	Garnet	7	7	0.4	0.2
BL12-256	295.10	300.50	Amphibolite	3	65	Garnet		2	0.4	0.7
BL12-256	300.50	308.00	Quartzofeldspathic Gneiss	15	7		10		0.7	0.3
BL12-256	308.00	309.80	Garnet Biotite Schist	25	3	Garnet + Muscovite			0.5	0.5
BL12-256	309.80	311.40	Pegmatite	3		Muscovite	100			
BL12-256	311.40	315.00	Garnet Biotite Schist	20	3	Garnet	15		0.3	0.2
BL12-256	315.00	316.10	Pegmatite	7	3		95		0.2	0.1
BL12-256	316.10	319.90	Quartzofeldspathic Gneiss	10	3	Muscovite	7	3	0.5	0.4
BL12-256	319.90	321.00	Garnet Biotite Schist	25	2	Garnet			0.4	0.3
BL12-256	321.00	322.50	Pegmatite	3		Muscovite	100		0.1	0.1
BL12-256	322.50	324.80	Quartzofeldspathic Gneiss	10	5	Garnet + Muscovite	20		0.4	0.4
BL12-256	324.80	326.60	Pegmatite	5			100		0.2	0.2
BL12-256	326.60	335.45	Quartzofeldspathic Gneiss	13		Garnet + Muscovite	7		0.7	0.7
BL12-256	335.45	336.75	Pegmatite	10		Garnet + Muscovite	75		0.3	0.2
BL12-256	336.75	341.00	Biotite Schist	20		Garnet + Muscovite	25		0.7	0.7
BL12-256	341.00	347.70	Quartzofeldspathic Gneiss	12		Garnet		25	0.5	0.4
BL12-256	347.70	351.00	Quartzofeldspathic Gneiss	5	3			50	0.2	0.1
BL12-256	351.00	352.80	Quartzofeldspathic Gneiss	7	3		20		0.7	0.5
BL12-256	352.80	354.00	Amphibolite	3	45			3	0.7	0.7
BL12-256	354.00	366.00	Quartz Vein	3	15		3	70	0.5	0.5
BL12-256	366.00	367.50	Pegmatite	10	3		70	5	0.7	0.7
BL12-256	367.50	375.60	Amphibolite	5	35			30	0.7	0.9
BL12-256	375.60	376.90	Pegmatite	7			100		0.3	0.3
BL12-256	376.90	378.00	Garnet Biotite Schist	30		Garnet	3	5	0.7	0.9
BL12-256	378.00	379.00	Amphibolite	3	30			20	0.7	0.9
BL12-256	379.00	381.00	Pegmatite	5	3		55		0.7	0.7
BL12-256	381.00	384.00	Quartzofeldspathic Gneiss	7	3		5	10	0.5	0.5
BL12-256	384.00	391.90	Footwall Amphibolite	3	60				0.2	0.3
BL12-256	391.90	395.30	Quartzofeldspathic Gneiss	10	7				0.1	0.1
BL12-256	395.30	401.00	Footwall Amphibolite	3	60				0.1	0.3
BL12-268	2.20	27.10	Quartzofeldspathic Gneiss	5	3			2	0.2	
BL12-268	27.10	29.90	Diabase Dike							
BL12-268	29.90	33.00	Quartzofeldspathic Gneiss	4	3				0.2	
BL12-268	33.00	35.90	Quartzofeldspathic Gneiss	10	2				0.3	
BL12-268	35.90	69.80	Quartzofeldspathic Gneiss	5	3			3	0.5	
BL12-268	69.80	97.60	Intermediate Gneiss	20	35			3	0.1	
BL12-268	97.60	106.00	Quartzofeldspathic Gneiss	7	3				0.7	
BL12-268	106.00	114.70	Intermediate Gneiss	20	35					

HoleID	From	To	Lithology	Bt %	Am %	Metamorphic Minerals	Peg %	QV %	Py %	Po %
BL12-268	114.70	136.80	Quartzofeldspathic Gneiss	7	3	Magnetite		2	0.7	
BL12-268	136.80	137.35	UM/Lamp Dike							
BL12-268	137.35	155.20	Quartzofeldspathic Gneiss	10	2				0.7	
BL12-268	155.20	164.50	Quartzofeldspathic Gneiss	8	2				0.5	
BL12-268	164.50	172.30	Quartzofeldspathic Gneiss	10	2				0.7	
BL12-268	172.30	176.10	Amphibolite	3	55	Magnetite		3	0.9	0.3
BL12-268	176.10	182.30	Intermediate Gneiss	25	30				0.01	
BL12-268	182.30	197.00	Quartzofeldspathic Gneiss	7	3			3	0.7	
BL12-268	197.00	201.80	Intermediate Gneiss	20	35					
BL12-268	201.80	219.70	Quartzofeldspathic Gneiss	7	3	Magnetite	1	3	0.7	
BL12-268	219.70	227.90	Amphibolite	3	65	Magnetite		7	0.7	0.7
BL12-268	227.90	228.00	Pegmatite	15			65		0.7	0.5
BL12-268	228.00	230.40	Quartzofeldspathic Gneiss	17			5	3	0.7	0.7
BL12-268	230.40	231.50	Pegmatite	10	2		95		0.5	0.3
BL12-268	231.50	233.20	Quartzofeldspathic Gneiss	17	2			3	0.7	0.7
BL12-268	233.20	235.80	Pegmatite	7			100		0.1	0.1
BL12-268	235.80	265.20	Quartzofeldspathic Gneiss	10	5			7	0.4	
BL12-268	265.20	270.50	Amphibolite	10	65			3	0.3	0.2
BL12-268	270.50	281.00	Quartzofeldspathic Gneiss	10	2		5	5	0.3	
BL12-268	281.00	282.40	Amphibolite	10	65				0.1	
BL12-268	282.40	295.20	Quartzofeldspathic Gneiss	7	3		5	5	0.4	
BL12-268	295.20	298.60	UM/Lamp Dike							
BL12-268	298.60	302.00	Quartzofeldspathic Gneiss	7	3			3	0.6	
BL12-268	302.00	308.00	Quartzofeldspathic Gneiss	10	15	Garnet			0.4	0.7
BL12-268	308.00	311.60	Quartzofeldspathic Gneiss	10	3		5		0.7	0.1
BL12-268	311.60	312.60	Amphibolite	3	60				0.3	0.1
BL12-268	312.60	313.50	UM/Lamp Dike							
BL12-268	313.50	318.60	Amphibolite	15	50		3		0.5	0.7
BL12-268	318.60	321.60	Quartzofeldspathic Gneiss	10	3		10		0.5	0.3
BL12-268	321.60	322.00	Garnet Biotite Schist	20		Garnet			0.3	0.3
BL12-268	322.00	325.60	Quartzofeldspathic Gneiss	12	15				0.5	0.8
BL12-268	325.60	329.90	Garnet Biotite Schist	25	3	Garnet	5	3	1	1
BL12-268	329.90	332.60	Quartzofeldspathic Gneiss	7					0.7	0.1
BL12-268	332.60	335.40	Amphibolite	7	60				0.5	0.8
BL12-268	335.40	337.00	Garnet Biotite Schist	35	3	Garnet	15		1	0.7
BL12-268	337.00	340.00	Amphibolite	15	55	Garnet		5	0.5	0.2
BL12-268	340.00	341.10	Garnet Biotite Schist	25	5	Garnet + Kyanite		5	0.3	0.1
BL12-268	341.10	343.60	Pegmatite	7			90		0.5	0.5
BL12-268	343.60	348.20	Garnet Biotite Schist	35	3	Garnet + Kyanite		2	0.3	0.3
BL12-268	348.20	349.05	Quartzofeldspathic Gneiss	20	2		3	3	0.5	0.1
BL12-268	349.05	349.90	Pegmatite	7			100		0.3	0.3
BL12-268	349.90	354.00	Quartzofeldspathic Gneiss	10	2			3	0.3	0.1
BL12-268	354.00	355.50	Pegmatite	15	2		100		0.5	0.5
BL12-268	355.50	356.30	Garnet Biotite Schist	40	3	Garnet + Kyanite	5		0.7	0.3

HoleID	From	To	Lithology	Bt %	Am %	Metamorphic Minerals	Peg %	QV %	Py %	Po %
BL12-268	356.30	357.90	Pegmatite	5			100		0.5	0.5
BL12-268	357.90	359.40	Amphibolite	15	55	Garnet			0.1	0.1
BL12-268	359.40	365.50	Quartzofeldspathic Gneiss	12	5	Garnet	20	5	0.7	0.7
BL12-268	365.50	390.85	Garnet Biotite Schist	30	5	Cordierite + Kyanite + Garnet	7	5	0.7	0.7
BL12-268	390.85	398.60	Quartzofeldspathic Gneiss	15	7			3	0.5	0.5
BL12-268	398.60	402.40	Quartzofeldspathic Gneiss	12	3			3	0.3	
BL12-268	402.40	405.00	Quartzofeldspathic Gneiss	7	5		7		0.7	0.3
BL12-268	405.00	406.20	Pegmatite	3			95		0.1	0.1
BL12-268	406.20	407.35	Footwall Amphibolite	3	60	Garnet			0.1	0.3
BL12-268	407.35	409.40	Quartzofeldspathic Gneiss	10	5		20		0.3	
BL12-268	409.40	412.50	Footwall Amphibolite	15	60			3	0.1	0.4
BL12-268	412.50	413.50	Pegmatite	7	3		95			
BL12-268	413.50	419.90	Quartzofeldspathic Gneiss	10	3		7	3	0.3	0.1
BL12-268	419.90	421.10	Footwall Amphibolite	3	55	Garnet			0.1	0.6
BL12-268	421.10	426.70	Quartzofeldspathic Gneiss	10	5	Garnet	20		0.3	0.3
BL12-268	426.70	427.50	Quartzofeldspathic Gneiss	10	5				0.2	0.2
BL12-268	427.50	446.00	Footwall Amphibolite	5	60	Garnet	8	3	0.2	0.3
BL12-329	2.50	7.70	UM/Lamp Dike							
BL12-329	7.70	20.10	Quartzofeldspathic Gneiss	7	3			5	0.7	
BL12-329	20.10	20.80	Pegmatite	5			100		0.1	0.1
BL12-329	20.80	27.90	Quartzofeldspathic Gneiss	7	5		5		0.5	
BL12-329	27.90	28.90	Pegmatite	4			100		0.1	0.1
BL12-329	28.90	52.10	Quartzofeldspathic Gneiss	5	10	Magnetite + Garnet	3		0.7	0.1
BL12-329	52.10	53.60	UM/Lamp Dike							
BL12-329	53.60	55.40	Quartzofeldspathic Gneiss	7	3			3	0.4	
BL12-329	55.40	93.00	Quartzofeldspathic Gneiss	5	2	Muscovite		5	0.7	
BL12-329	93.00	107.80	Quartzofeldspathic Gneiss	7	3			5	0.5	
BL12-329	107.80	113.80	Amphibolite	10	55	Magnetite + Garnet		3	0.5	0.3
BL12-329	113.80	114.90	UM/Lamp Dike							
BL12-329	114.90	123.15	Quartzofeldspathic Gneiss	7	3			7	0.3	0.1
BL12-329	123.15	127.05	Quartzofeldspathic Gneiss	20	8	Garnet		7	0.7	0.7
BL12-329	127.05	128.30	Quartzofeldspathic Gneiss	7	3			10	0.5	0.2
BL12-329	128.30	129.30	Quartzofeldspathic Gneiss	20	5	Garnet	5		0.5	0.5
BL12-329	129.30	132.35	Quartzofeldspathic Gneiss	7	3			5	0.5	0.3
BL12-329	132.35	136.80	Quartzofeldspathic Gneiss	20	10	Magnetite + Garnet			0.8	0.9
BL12-329	136.80	145.15	Quartzofeldspathic Gneiss	10	7	Garnet	7		0.5	0.5
BL12-329	145.15	146.15	Pegmatite	10	2				1	1
BL12-329	146.15	147.80	Garnet Biotite Schist	25	3	Garnet		3	0.7	0.7
BL12-329	147.80	158.00	Quartzofeldspathic Gneiss	5	3	Garnet + Muscovite	20	7	0.3	0.2
BL12-329	158.00	167.00	Quartzofeldspathic Gneiss	12	5	Garnet		7	0.7	0.9
BL12-329	167.00	171.00	Quartzofeldspathic Gneiss	20	7	Garnet		7	0.8	0.9

Hole ID	From	To	Lithology	Bt %	Am %	Metamorphic Minerals	Peg %	QV %	Py %	Po %
BL12-329	171.00	179.90	Garnet Biotite Schist	25	3	Garnet + Muscovite		7	0.7	0.7
BL12-329	179.90	182.50	Quartzofeldspathic Gneiss	7	3	Garnet + Muscovite	7		0.3	0.2
BL12-329	182.50	184.05	Garnet Biotite Schist	25	3	Garnet + Muscovite	5		0.5	0.5
BL12-329	184.05	189.00	Quartzofeldspathic Gneiss	12	3	Garnet + Muscovite	7		0.3	0.3
BL12-329	189.00	203.00	Quartzofeldspathic Gneiss	13	15			5	0.7	0.7
BL12-329	203.00	251.00	Quartzofeldspathic Gneiss	7	5		3	3	0.5	0.2
BL12-333	5.60	15.00	Quartzofeldspathic Gneiss	10	7		5		0.2	
BL12-333	15.00	29.20	Quartzofeldspathic Gneiss	5	2	Muscovite	5	3	0.1	
BL12-333	29.20	51.60	Quartzofeldspathic Gneiss	7	3		5	3	0.3	
BL12-333	51.60	61.00	Diabase Dike							
BL12-333	61.00	60.30	Quartzofeldspathic Gneiss	3	1			7	0.3	
BL12-333	60.30	74.40	Amphibolite	5	60		3		0.3	0.2
BL12-333	74.40	80.45	Quartzofeldspathic Gneiss	7	5				0.3	
BL12-333	80.45	86.55	Quartzofeldspathic Gneiss	12	15			3	0.5	0.9
BL12-333	86.55	89.15	Quartzofeldspathic Gneiss	7	3				0.5	0.3
BL12-333	89.15	95.25	Quartzofeldspathic Gneiss	15	20		7		0.7	0.7
BL12-333	95.25	97.65	Pegmatite	3			100		0.1	0.1
BL12-333	97.65	100.20	Garnet Biotite Schist	25	3	Garnet	5		0.4	0.3
BL12-333	100.20	103.70	Pegmatite	12			85		0.5	1
BL12-333	103.70	122.10	Quartzofeldspathic Gneiss	15	5	Garnet + Muscovite	15	5	0.7	1
BL12-333	122.10	141.50	Garnet Biotite Schist	30	5	Garnet + Muscovite	15	5	1	1
BL12-333	141.50	158.80	Quartzofeldspathic Gneiss	12	3	Garnet + Muscovite	3	5	0.5	0.5
BL12-333	158.80	166.00	Quartzofeldspathic Gneiss	15	20				0.5	0.5
BL12-333	166.00	183.00	Quartzofeldspathic Gneiss	7	3		3	3	0.4	0.2
BL12-333	183.00	186.00	Pegmatite	3	2		90		0.3	0.2
BL12-333	186.00	210.10	Quartzofeldspathic Gneiss	10	5		10	3	0.3	0.1
BL12-333	210.10	204.85	Footwall Amphibolite	5	60	Garnet		5	0.2	0.3
BL12-333	204.85	206.00	Pegmatite	5			100		0.2	0.2
BL12-333	206.00	210.75	Quartzofeldspathic Gneiss	7	2				0.1	
BL12-333	210.75	223.70	Footwall Amphibolite	3	55	Garnet			0.1	0.3
BL12-333	223.70	224.50	UM/Lamp Dike							
BL12-333	224.50	227.00	Footwall Amphibolite	3	55	Garnet			0.1	0.3
BL12-336	5.60	13 75	Quartzofeldspathic Gneiss	5	2				0.4	
BL12-336	13 75	14.55	UM/Lamp Dike							
BL12-336	14.55	20.20	Quartzofeldspathic Gneiss	2			5	5		
BL12-336	20.20	21.20	Pegmatite	2			100	5	0.2	
BL12-336	21.20	48.00	Quartzofeldspathic Gneiss	7	4		2	5	0.5	
BL12-336	48.00	50.00	Pegmatite	3			100		0.3	

HoleID	From	To	Lithology	Bt %	Am %	Metamorphic Minerals	Peg %	QV %	Py %	Po %
BL12-336	50.00	52.50	Quartzofeldspathic Gneiss	7	3			10	0.4	
BL12-336	52.50	53.55	Pegmatite	3			98		0.3	
BL12-336	53.55	57.00	Quartzofeldspathic Gneiss	9	3	Garnet		10	0.5	
BL12-336	57.00	131.50	Quartzofeldspathic Gneiss	8	5		2	5	0.7	
BL12-336	131.50	139.00	UM/Lamp Dike							
BL12-336	139.00	153.20	Quartzofeldspathic Gneiss	7	3	Garnet	5	5	0.5	0.1
BL12-336	153.20	154.00	Quartzofeldspathic Gneiss	10	15				0.5	0.4
BL12-336	154.00	158.00	Amphibolite	3	60			2	0.5	0.7
BL12-336	158.00	190.00	Quartzofeldspathic Gneiss	7	5		10	3	0.5	0.3
BL12-336	190.00	193.60	Quartzofeldspathic Gneiss	10	3	Muscovite	3	10	0.5	0.4
BL12-336	193.60	199.35	Quartzofeldspathic Gneiss	15	15	Garnet + Muscovite		5	0.7	0.7
BL12-336	199.35	203.50	Quartzofeldspathic Gneiss	7	3			3	0.3	0.1
BL12-336	203.50	207.00	Garnet Biotite Schist	25	3	Garnet + Muscovite	7		0.7	0.7
BL12-336	207.00	219.45	Quartzofeldspathic Gneiss	15	3	Garnet + Muscovite	10	5	0.7	0.5
BL12-336	219.45	226.20	Quartzofeldspathic Gneiss	13	15			3	1	0.5
BL12-336	226.20	269.60	Quartzofeldspathic Gneiss	7	4		3	3	0.5	0.2
BL12-336	269.60	270.60	UM/Lamp Dike							
BL12-336	270.60	275.20	Quartzofeldspathic Gneiss	7	3		3		0.5	
BL12-336	275.20	277.90	Pegmatite	10	3		90		0.2	0.1
BL12-336	277.90	305.00	Footwall Amphibolite	3	65	Garnet			0.2	0.5
BL13-375	4.00	24.90	Quartzofeldspathic Gneiss	7	3		2		0.4	
BL13-375	24.90	27.75	UM/Lamp Dike							
BL13-375	27.75	64.80	Quartzofeldspathic Gneiss	9	3		5	2	0.4	
BL13-375	64.80	67.50	Intermediate Gneiss	20	30				0.01	
BL13-375	67.50	90.80	Quartzofeldspathic Gneiss	7	3			3	0.3	
BL13-375	90.80	95.35	Quartzofeldspathic Gneiss	7	10				0.1	
BL13-375	95.35	103.55	Quartzofeldspathic Gneiss	7	3				0.3	
BL13-375	103.55	121.60	Intermediate Gneiss	20	25				0.01	
BL13-375	121.60	124.30	Quartzofeldspathic Gneiss	7	3				0.3	
BL13-375	124.30	126.20	UM/Lamp Dike							
BL13-375	126.20	140.10	Quartzofeldspathic Gneiss	7	3		3		0.2	
BL13-375	140.10	150.40	Intermediate Gneiss	15	25				0.1	
BL13-375	150.40	157.20	Quartzofeldspathic Gneiss	7	10				0.2	
BL13-375	157.20	163.15	Quartzofeldspathic Gneiss	7	3		7		0.5	
BL13-375	163.15	170.75	Intermediate Gneiss	13	35				0.2	
BL13-375	170.75	183.95	Quartzofeldspathic Gneiss	7	3		2	2	0.4	
BL13-375	183.95	185.30	Amphibolite	5	50				0.2	
BL13-375	185.30	186.80	Quartzofeldspathic Gneiss	7	5				0.3	
BL13-375	186.80	188.20	Quartzofeldspathic Gneiss	7	15				0.1	
BL13-375	188.20	251.90	Quartzofeldspathic Gneiss	7	3		7	5	0.3	
BL13-375	251.90	269.90	Amphibolite	10	55		5	3	0.5	0.4
BL13-375	269.90	275.55	Quartzofeldspathic Gneiss	5	3		3		0.3	0.2

HoleID	From	To	Lithology	Bt %	Am %	Metamorphic Minerals	Peg %	QV %	Py %	Po %
BL13-375	275.55	281.30	Amphibolite	7	60		5		0.5	0.5
BL13-375	281.30	284.00	Pegmatite	7	3		90		0.7	0.2
BL13-375	284.00	286.80	Amphibolite	5	50				0.7	0.2
BL13-375	286.80	287.85	Pegmatite	5	3		80		0.4	0.7
BL13-375	287.85	291.34	Quartzofeldspathic Gneiss	10	10	Garnet	15		0.5	0.7
BL13-375	291.34	297.90	Quartzofeldspathic Gneiss	12	5		3		0.7	0.4
BL13-375	297.90	298.90	Pegmatite	15	5		70		1	0.5
BL13-375	298.90	300.00	Amphibolite	15	60	Garnet			0.5	0.7
BL13-375	300.00	303.85	Garnet Biotite Schist	30	5	Garnet	7		0.5	0.5
BL13-375	303.85	306.90	Pegmatite	5	3	Garnet	90		0.3	0.3
BL13-375	306.90	307.80	Garnet Biotite Schist	25	5	Garnet			0.2	0.1
BL13-375	307.80	309.90	Pegmatite	10	3		90		0.5	0.3
BL13-375	309.90	312.00	Quartzofeldspathic Gneiss	3	12			5	0.2	0.1
BL13-375	312.00	313.60	Pegmatite	10	2		70		0.3	0.2
BL13-375	313.60	322.30	Quartzofeldspathic Gneiss	10	2	Garnet	3	2	0.5	0.4
BL13-375	322.30	331.80	Quartzofeldspathic Gneiss	13	5		5	5	0.2	0.1
BL13-375	331.80	333.40	Pegmatite	5	2		100		0.2	
BL13-375	333.40	356.00	Quartzofeldspathic Gneiss	7	2			3	0.2	0.1
BL13-375	356.00	359.35	Quartz Vein	5			5	80	0.3	0.2
BL13-375	359.35	363.55	Quartzofeldspathic Gneiss	10	2		15	3	0.2	0.2
BL13-375	363.55	365.70	Footwall Amphibolite	3	70				0.1	0.3
BL13-375	365.70	367.05	Pegmatite	5			100		0.1	0.1
BL13-375	367.05	368.40	Quartzofeldspathic Gneiss	10				3	0.2	
BL13-375	368.40	395.10	Footwall Amphibolite	3	70	Garnet			0.1	0.4
BL13-406	3.80	27.60	Quartzofeldspathic Gneiss	7	3			5	0.6	
BL13-406	27.60	28.60	Diabase Dike							
BL13-406	28.60	46.60	Quartzofeldspathic Gneiss	7	2				0.5	
BL13-406	46.60	48.00	UM/Lamp Dike							
BL13-406	48.00	91.60	Quartzofeldspathic Gneiss	7	2		3	3	0.5	
BL13-406	91.60	98.20	UM/Lamp Dike							
BL13-406	98.20	163.45	Quartzofeldspathic Gneiss	9	3		3	3	0.7	
BL13-406	163.45	178.30	Intermediate Gneiss	20	25				0.1	
BL13-406	178.30	285.40	Quartzofeldspathic Gneiss	10	5		3	3	0.5	
BL13-406	285.40	288.60	UM/Lamp Dike							
BL13-406	288.60	293.30	Quartzofeldspathic Gneiss	10	3		3	5	0.5	0.1
BL13-406	293.30	296.25	Amphibolite	5	60		2		0.3	
BL13-406	296.25	316.30	Quartzofeldspathic Gneiss	10	5		5	3	0.5	
BL13-406	316.30	317.70	Amphibolite	5	60			3	0.3	
BL13-406	317.70	344.35	Quartzofeldspathic Gneiss	10	5		7	7	0.5	
BL13-406	344.35	346.35	Amphibolite	7	60				0.3	0.5
BL13-406	346.35	351.35	Quartzofeldspathic Gneiss	7	3		7		0.5	
BL13-406	351.35	354.25	Amphibolite	5	60			3	0.2	0.3
BL13-406	354.25	357.10	Quartzofeldspathic Gneiss	7	2		5		0.3	0.3
BL13-406	357.10	360.90	Amphibolite	3	65				0.2	0.4

HoleID	From	To	Lithology	Bt %	Am %	Metamorphic Minerals	Peg %	QV %	Py %	Po %
BL13-406	360.90	362.60	Intermediate Gneiss	20	25				0.2	0.2
BL13-406	362.60	366.70	Quartzofeldspathic Gneiss	7	2		5		0.4	
BL13-406	366.70	371.85	Garnet Biotite Schist	25	3	Garnet + Sillmanite + Kyanite + Muscovite	13		0.3	0.2
BL13-406	371.85	377.75	Pegmatite	5			95		0.1	
BL13-406	377.75	378.95	Garnet Biotite Schist	30	5	Garnet + Muscovite	10		0.3	0.2
BL13-406	378.95	383.55	UM/Lamp Dike							
BL13-406	383.55	387.50	Garnet Biotite Schist	20	15	Garnet			0.3	0.2
BL13-406	387.50	388.60	Pegmatite	5			95		0.2	0.1
BL13-406	388.60	409.00	Quartzofeldspathic Gneiss	17	5	Garnet	10		0.5	0.3
BL13-406	409.00	442.10	Quartzofeldspathic Gneiss	15	7		10		0.4	0.4
BL13-406	442.10	471.00	Footwall Amphibolite	3	60	Garnet	7		0.1	0.3

APPENDIX C – MICROSTRUCTURAL ANALYSES

Bt – Biotite	Po – Pyrrhotite	Grt Bt FG – Garnet-biotite schist
Am – Amphibole	Peg – Pegmatite	FG (s) – Quartzofeldspathic Gneiss
Qtz – Quartz	QV – Quartz Vein	FG (g) – Quartzofeldspathic Gneiss
Py – Pyrite		Felsic Gneiss (c) - Metaconglomerate

BL 10-06a (96.5m) – Felsic Gneiss (G) transition from Grt Bt FG (Au; 1330 ppb)
Biotite Quartzofeldspathic Gneiss

Quartz (20%) – Anhedral, medium to coarse-grained with evidence for subgrains and undulose extinction. Some inclusions of biotite, but commonly biotite occurs on the grain boundaries between quartz and hornblende minerals.
Microcline (30%) – Anhedral, fine to medium grained crystals with polysynthetic twinning. Commonly containing inclusions of quartz and orthopyroxene.
Plagioclase (5%) – Subhedral, fine to medium-grained with simple twins.
Orthopyroxene (25%) – Subhedral to anhedral, medium-grained with moderate to high relief and parallel extinction. Sulphides often found on grain boundaries of crystals.
Biotite (25%) – Euhedral, elongate, coarse-grained crystals with brown pleochroism randomly distributed throughout the sample. Commonly occurring on the grain boundaries of quartz and consistently associated with sulphides. Some sections contain layers of DPO biotite with minor orthopyroxene, here sulphides are abundant and quartz commonly rims the biotite and interstitial space as very fine-grained crystals.
Opaques (10%)
Gold associated with cleavage planes in biotite. Gold seen within fracture filling sulphide rich blebs.
Gold is present as inclusions in quartz; quartz grain is anhedral with some grain bulging at boundary and has undulose extinction. Most commonly associated with biotite.
Picture in reflected light of circular not gold blebs connected in a line (stringer of 7) within a large pyrite grain and with two small chalcopyrite on the sides of the stringer. Sulphide is surrounded by only quartz grains; some grains have undulose extinction and twinning.
Another section shows gold in quarts being replaced by cordierite And close to a muscovite grain but not touching.
Sulphides also found in cleavage planes of biotite, but no gold visible.

BL 10-06b (96.5m) – Felsic Gneiss (G) transition from Grt Bt FG (Au; 1330 ppb)
Quartz (25%) – Anhedral, medium to coarse-grained, with evidence of undulose extinction, grain boundary reduction and subgrains. Some grains also contain a 120° triple junction.
Biotite (15%) – Euhedral, medium-grained, brown pleochroism and associated with mineralization. Less abundant than BL 10-06a and smaller grainsize.
Microcline (25%) – Anhedral to subhedral, fine to medium-grained, polysynthetic twinning and commonly containing inclusions of
Orthopyroxene (25%) – Anhedral, medium to coarse-grained, with parallel extinction.
Opaques (10%)
Similar to 10-06a where by gold is seen in pyrite blebs and occasionally free in quartz groundmass. Quartz is often being replaced or eroded by cordierite

BL 10-09a (111.5m) – Garnet Biotite Felsic Gneiss (Au; 833-1254 ppb)
Biotite (30%) – Euhedral, medium to coarse-grained, brown pleochroism and dimensionally preferred orientation of the long axis.
Garnet (15%) – Euhedral, fine to medium-grained, high relief and isotropic. Commonly the occurrences of garnets are in clusters with biotite filling interstitial space and with an overall association with sulphide mineralization.
Quartz (20%) – Anhedral fine to coarse-grained with evidence of undulose extinction and subgrains.
Orthopyroxene (20%) – Anhedral to Subhedral, fine to medium-grained crystals with parallel extinction.

Tourmaline (3%) – Bladed crystals with preferred orientations of the long axis but commonly being bent or curved.

BL 10-09b (111.5m) – Garnet Biotite Felsic Gneiss (Au; 833-1254 ppb)
Quartz (20%) – Anhedral, medium to coarse-grained, with evidence of undulose extinction and subgrains. Some grains contain the 120° triple junctions.
Biotite (15%) – Euhedral, coarse-grained, brown pleochroism and no definitive preferred orientation.
Garnet (10%) – Euhedral, fine-grained, high relief and isotropic. Typically occurring in clusters within a quartz groundmass and associated with biotite and sulphides.
Orthopyroxene (10%) – Subhedral, medium-grained with parallel extinction, commonly associated with biotite.
Microcline (20%) – Subhedral, medium-grained with polysynthetic twinning.
Opaques (7%) pyrite commonly as inclusions in garnet.

BL 10-15a (61.6m) – Amphibolite (gold zone, Au; 17207 ppb)
Biotite (30%) – Euhedral, coarse-grained, elongate with brown pleochroism and dimensionally preferred orientation.
Hornblende (35%) – Anhedral to Subhedral, medium to coarse-grained, with green to yellow pleochroism. Some grains have an elongate axis with a preferred orientation with the biotite. More commonly the grains are short and stubby intergrown with the biotite. Some hornblende grains have inclusions of quartz.
Quartz (25%) – Anhedral, fine to medium-grained, filling interstitial space and with evidence of undulose extinction and subgrains.
Overall, the sample contained what appears to have biotite and hornblende rich layers followed by quartz rich layers. The sulphides are seen within the biotite and hornblende layers but just as common sulphides are seen in the quartz rich layers. Gold visible in po blebs and also surrounding py with po amour. Some free gold in quartz groundmass and at grain boundaries.

BL 10-15b (61.6m) – Amphibolite (gold zone, Au; 17207 ppb)
Biotite (30%) – Euhedral, medium to coarse-grained, brown pleochroism and a strong dimensionally preferred orientation.
Hornblende (20%) – Subhedral, medium to coarse-grained, green to yellow pleochroism with common inclusions of quartz.
Quartz (25%) – Anhedral, fine to coarse-grained with evidence of undulose extinction and subgrains.
Sulphides are euhedral py with gold and po surrounding it in a quartz and biotite matrix. See photo.

BL 10-15 (112.5m) – Felsic Gneiss (S) (Au; 6654 ppb)
Quartz (25%) – Anhedral, fine to coarse-grained with evidence of undulose extinction and subgrains.
Microcline (20%) – Anhedral, fine to medium-grained with tartan twinning.
Biotite (20%) – Euhedral, medium-grained with brown pleochroism. Typically associated with sulphide mineralization.

Hole	Lithology	Gold Occurrence
10-06a (96.5)	Fg (g)	Gold found between pyrite, clinopyroxene and microcline. Surrounded by pyrrhotite.
10-06b (96.5)	Fg (g)	Gold found around euhedral pyrite and all covered by pyrrhotite. (Weakly foliated rock defined by biotite).
10-09a (111.5m)	Grt bt fg	Gold around euhedral pyrite, rutile and garnet, all surrounded by pyrrhotite. Gold found between pyrrhotite and rutile with euhedral pyrite on the other side of the rutile. Also found in a biotite cleavage and also between a garnet, quartz and pyrite grain. Gold also found within pyrrhotite and surrounded by biotite and garnet.
10-09b(111.5m)	Grt bt fg	Gold found as seen previously associated with py and po. Also seen in fracture cleavages as free gold, in proximity to quartz.

10-15a(61.6)	Amph	Gold found on pyrite grain boundary and surrounded by pyrrhotite. Free gold found in association with biotite and quartz. STRONGLY FOLIATED lithology.
10-15(112.5)	Fg(s)	Gold found within garnet sulphide bleb of euhedral pyrite and enclosed by pyrrhotite. Also gold seen in fractures of pyrite in close proximity to biotite

Kyanite (20%) – Some high relief minerals with anhedral shapes and commonly associated to sulphides. High second order colour with an inconsistent pattern.
Sulphides very commonly seen associated with py and po. Often touching the po and in proximity to the py if not touching that too.

BL 11-19 (120m) – Garnet Biotite Felsic Gneiss (Au; 3923 ppb)

Biotite (35%) – Euhedral,
Kyanite (20%) – Anhedral, medium-grained, high relief with bladed texture under crossed polars with first order grey birefringence to rare second order blue, orange and pinks.
Orthopyroxene (10%) – Subhedral, parallel extinction.
Biotite (15%) – Euhedral, medium to coarse-grained with brown pleochroism. Local areas of DPO and LPO.
Microcline (25%) – Anhedral, coarse-grained with abundant groundmass with inclusions of biotite, orthopyroxene and quartz. Common fractures filled with sulphides and biotite grains.
Plagioclase (10%) – Anhedral, medium to coarse-grained with simple twins.

BL 11-19a (175m) – Amphibolite (footwall) (Au; 75-112 ppb)
Quartz (20%)
Hornblende (35%) – Subhedral, fine-grained with green to yellow pleochroism. 60/120 cleavage with no preferred orientation to the grains.
Clinopyroxene (10%) – Anhedral, fine to medium-grained with inclined extinction and high second order birefringence.
Calcite (15%) – Subhedral, fine to medium-grained with 60/120 twinning and high relief. Commonly within the groundmass and occasionally as coarse-grained veinlets crosscutting the rock. Very well defined crystals.
Plagioclase (3%)
Garnet (10%) – Anhedral, coarse-grained with abundant fractures and inclusions. There is extensive grain boundary reduction.

BL 11-19b (175m) – Amphibolite (footwall) (Au; 75-112 ppb)
Quartz (15%) – Anhedral, fine to medium-grained with evidence of undulose extinction and subgrains, commonly as inclusions in garnet and pyroxene.
Orthopyroxene (15%) – Anhedral, fine to coarse-grained with parallel extinction.
Clinopyroxene (15%) – Anhedral, coarse-grained with inclined extinction.
Garnet (7%) – Subhedral, coarse-grained with abundant inclusions of quartz and pyroxene. The grain boundary is commonly eroded and reduced by other mineral growth.
Opaques (10%)

BL 11-20a (189m) – Amphibolite (gold zone) (Au; 10812 ppb)
Clinopyroxene (25%) – Anhedral, medium to coarse-grained
Garnet (20%)
Kyanite (10%)
Quartz (5%)
Hornblende
Chlorite

BL 11-20b (189m) – Amphibolite (gold zone) (Au; 10812 ppb)
Quartz (20%) – Anhedral, fine-grained with evidence for subgrains and undulose extinction.

Hornblende (45%) – Subhedral, medium grain-size with Dimensional preferred orientation, where all minerals are preferentially aligned parallel to bedding.
Plagioclase (10%) – Subhedral, fine-grained with simple twinning with no evidence of deformation.
Staurolite (10%) – Anhedral, coarse-grained with 'swiss cheese' appearance.
Garnet (15%) – Very coarse-grained with abundant inclusions of quartz and hornblende along with healed fractures. Subhedral shape with extensive grain boundary reduction.
Calcite (5%) – Anhedral, medium-grained, 60/120 cleavages.

BL 11-58 (104m) – Diorite (Au; 534-3340 ppb)
Quartz (15%)
Plagioclase (15%)
Microcline (10%)
Hornblende (10%)
Clinopyroxene (15%) – Subhedral eroded

BL 11-67 (122.5m) – Biotite Felsic Gneiss (Au; 778 ppb)
Biotite
Muscovite
Plagioclase
Quartz

BL 11-123a (27.5m) – Felsic Gneiss (C)
Quartz (20%) – Subhedral to Anhedral, medium grain-size. Constituting the groundmass, with rare undulose extinction and subgrains.
Plagioclase (20%) – Euhedral, medium grain-size with twinning and no evidence for deformation of the twins, but some grains have undulose extinction.
Hornblende (45%) – Euhedral to subhedral, medium to coarse grain-size. Green to yellow pleochroism with second order birefringence. Grains have 60/120 cleavage and rhombohedra shape. Serrated grain boundaries and healed fractures with
Biotite (7%) – Subhedral, medium grain-size with brown pleochroism. Typically biotite grains are crosscutting the quartz and hornblende grains.
Microcline (3%) – Subhedral, medium grain-size with polysynthetic twinning.
The overall thin section has a homogeneous distribution of quartz, plagioclase and hornblende with consistent grain-size. The randomly distributed biotite grains typically crosscut quartz and hornblende grains throughout the thin section.

BL 11-123b (27.5m) – Felsic Gneiss (C)
Quartz (50%) – Anhedral, fine to medium grain-size, with evidence of subgrains and undulose extinction. Evidence of replacement within centre and on the grain boundary of some quartz grains.
Biotite (15%) – Elongate, euhedral medium to coarse grain-size, brown pleochroism. In some areas the grains go extinct at the same time, this is referred to as Lattice preferred orientation.
Plagioclase (15%) – Euhedral, medium to coarse grain-size, simple twinning and evidence of undulose extinction. Commonly the grains have some replacement by quartz? In the centre of the grain and on the grain boundaries.
Hornblende (15%) – Euhedral to subhedral, coarse-grained. Green to yellow
Microcline (5%) – Rare grains with medium grain-size and subhedral shape. The polysynthetic twinning is present.

DL 12-198a (187.6m) –
Quartz (35%) – highly eroded by sericite Coarse grained have fibrolite around the grain boundary.
Feldspar (10%) – medium grained
Biotite (15%) – medium to coarse grained with weak to moderate foliation
Chlorite (10%)
Fibrolite (20%) – commonly replacing on quartz grain boundaries. Fine to medium grained and fibrous fan shaped crystals.

- Sillimanite needles at grain boundaries
- Abundant feldspars and quartz
- Feldspar replacement by mica (sericite)
- Weak to moderate DPO of biotite
- Minor pyroxene
- Kyanite – Blue mineral, high relief
- Hornblende present with 60/120

DL 12-198b (187.6m)
- Biotite schist
    - Abundant feldspars with abundant replacement by mica (sericite?)
    - Sillimanite replacement at quartz grain boundaries
    - Strong DPO of biotite
- Sharp contact to hornblende schist
    - Quartz (with 120 degree triple junction boundaries), biotite, hornblende
    - Strong DPO of biotite

DL 12-198 (188.4m)
- Clotty felsic gneiss amphibolite
    - Abundant hornblende
    - Abundant chlorite
    - Felsic clot – feldspars with abundant replacement by mice (sericite?), quartz, biotite
    - Is clot a xenolith in a mafic, hornblende-rich intrusive?

DL 12-256 (265.3m)
Quartz (30%) – undulose extinction in coarse-grains with highly ductilely deformed twins???
Biotite (20%) – highly eroded grain boundaries with second-generation biotite cross-cutting brittly deformed large biotite grains. The large biotite grains are also ductilely deformed with bend cleavage planes.
Chlorite (15%) – platy and elongate grains with teal blue birefringence and green to blue pleochroism

DL 12-256 (340.8m) – Amphibolite; 90° cleavage foliated pyroxene with garnet
- Abundant quartz – is it as deformed as quartz in other felsic gneiss lithologies
- Sulphides concentrated in feldspar-rich areas
- Minimal sulphides compared to other lithologies
- Abundant inclusions in quartz – commonly hornblende
- Remnant areas with less silica – hornblende, feldspar, biotite?

DL 12-256 (342.8m) – Amphibolite; green pyroxene and qtz boudins
- very fine-grained quartz, feldspar – groundmass has grains with high relief that are cloudy and rotten-looking
- Larger-grained hornblende

DL 12-161a (61.5m) – Biotite QFG
There seems to be two biotite-forming events? Fine-grained biotite within a microcline and quartz groundmass. The coarse grained biotite defines a foliated with less abundant medium to coarse-grained quartz. Similar sulphide association with subhedral to euhedral pyrite, anhedral gold all rimmed by anhedral pyrrhotite. Sulphides are very often associated with coarser grained areas and almost nonexistent within areas of fine-grained qtz and biotite. Gold also found within pyrrhotite with no pyrite association. Pyrrhotite is highly pitted. Magnetite also found within the fine-grained quartz groundmass and sometimes associated with pyrite.
Magnetite (<5%) – anhedral medium grained balls.
Quartz (55%) – anhedral, undulose extinction, and 120-degree triple junctions, fine to coarse grained. Fine grains make up the groundmass with minor fine-grained biotite with weak foliation. Some coarse grained quartz associated with coarse well-foliated biotite.

Microcline (<5%) – anhedral with crosshatch twinning, medium grained.
Plagioclase (10%) – medium to coarse grained with twinning.
Biotite (20%) – fine to coarse grained, euhedral grains with weak to strong foliation. The fine-grained biotite is less abundant and associated with fine-grained quartz and has a weak foliation. The coarse grained biotite is associated with coarse-grained qtz and defines a strong foliation and is commonly associated with sulphides.
Sillimanite (5%) – commonly occurring in clusters where there is a contact between fine grained qtz, bt, and plag groundmass and the coarse grained, well foliated bt, qtz. The crystals are fibrous and fan-like with undulose extinction, high relief and second order birefringence.

FD 01301 – Amphibolite
Hornblende (60%) – well developed, medium-grained with green pleochroism and 60/120 cleavages. Rare inclusions of quartz. Preferential orientation of the long axis, strong foliation.
Plagioclase (20%) – fine to medium-grained, groundmass with simple and polysynthetic twinning as well as undulose extinction common. (oligoclase)

Grain	L1°	R1°	
1	245 – 262 = 17	245 – 227 = 18	18
2	332 – 359 = 27	332 – 285 = 47	
3	48 – 69 = 21	48 – 31 = 17	21
4	302 – 320 = 18	302 – 278 = 24	24

Quartz (5%) – fine to medium-grained crystals, low relief and first order birefringence. Undulose extinction evident in most grains.
Biotite (5%) – Coarse-grained, elongate crystals with oblique orientation to the dominant foliation of the hornblende. Biotite grains are typically eroded and show signs of brittle deformation.
Opaques (10%) – Euhedral pyrite, anhedral gold and pyrrhotite, some magnetite grains. Gold mostly associated with sulphides, within the anhedral pyrrhotite and at the outer boundaries of the pyrite. Rare free gold, associated with quartz adjacent to hornblende grain.
Massive, fine-grained amphibolite.

FD 01302 – Hornblende-Biotite Schist
Biotite (25%) – Coarse, elongate crystals with the long axis defining a foliation. Most of the biotite grains have a LPO, going extinct at the same time.
Hornblende (20%) – Medium-grained with green pleochroism. Typically in clusters throughout the thin section (lithons?)
Plagioclase (15%) – Large crystals with simple and polysynthetic twinning, making up the groundmass. A combination of albite and pericline twinning is present in some grains. Majority of grains have sericite alteration, almost completely or at grain boundaries and along fractures.

Grain	L1°	R1°	% anorthite
1	285 – 259 = 26	285 – 308 = 23	26
2	315 – 002 = 47	315 – 270 = 45	47
3	190 – 220 = 30	190 – 165 = 25	30
4	97 – 71 = 26	97 – 125 = 28	28

Microcline (5%) – medium to coarse crystals with scotch plaid twinning.
Quartz (10%) – Fine-grained anhedral crystals making up groundmass. Visible subgrains and undulose extinction.
Sericite (15%) – very fine-grained, replacing plagioclase feldspar along fractures, throughout the plagioclase grains and at grain boundaries.
Opaques (5%) – Dominantly large anhedral pyrrhotite with some pyrite and gold. Gold is seen as inclusions in pyrite and at pyrite grain boundaries sheathed by anhedral pyrrhotite. Sulphides containing gold are seen in areas with chaotic biotite (not defining foliation).

FD 01303A – Garnet-biotite schist
- Biotite schist

Biotite (20%) – Coarse-grained, elongate crystals with brown pleochroism and preferred orientation of the long axis.
Plagioclase (20%) – Large crystals with simple and polysynthetic twinning, making up the groundmass. A combination of albite and pericline twinning is present in some grains. Some of the grains have sericite alteration, almost completely or at grain boundaries and along fractures.

Grain	L1°	R1°	% anorthite
1	70 – 89 = 19	70 – 60 = 10	
2	80 – 100 = 20	80 -	

Quartz (10%) – Fine to coarse grained, undulose extinction
Sericite (5%) – Common along grain boundaries of plagioclase and some quartz crystals.
Opaques (7%) – Composed of pyrrhotite, pyrite and gold. Gold is seen in association with euhedral pyrite and sheathed by anhedral pyrrhotite. Rare occurrences of pyrrhotite with gold inclusion.

FD 01303B – Garnet-biotite schist
Microcline (25%) – Coarse grains, scotch plaid twinning.
Plagioclase (25%) – Fine to coarse-grained, simple and polysynthetic twinning, making up the groundmass. A combination of albite and pericline twinning is present in some grains. Most of the grains have sericite alteration, almost completely or at grain boundaries and along fractures.
Quartz (10%) – Fine to medium-grained with undulose extinction and subgrains.
Biotite (15%) – Fine to medium-grained with weak preferred orientation of the long axis.
Sericite (20%)
Opaques (5%)

FD 01304 – Biotite Hornfels Quartzofeldspathic Gneiss
Contact between fine grained QFG and coarse-grained partial melt QFG (migmatite?). Dominantly composed of microcline (40%), plagioclase (20%), quartz (15%), biotite (10%) and some clinopyroxene (5%).

FD 01305 – Biotite Hornfels Quartzofeldspathic Gneiss
Biotite (15%) with weak preferred orientation. Gold associated with py and po.

FD 01306 – Biotite Hornfels Quartzofeldspathic Gneiss
Biotite (5%) and melt pockets of microcline and quartz, coarse-grained. No visible gold.

FD 01307 – Garnet Amphibolite
Hornblende (50%) – medium to coarse-grained with 60/120 cleavages, green pleochroism and subhedral shapes. Common inclusions of quartz and feldspar.
Clinopyroxene (20%) – medium to coarse-grained with moderate to high relief, high second order birefringence and 90-degree cleavage. Inclined extinction and rare inclusions of quartz. Subhedral to anhedral in shape and associated to hornblende grains.
Quartz (15%) – fine to medium-grained groundmass with undulose extinction and grain boundary area reduction.
Garnet (3%) – fine-grained with inclusions of gold.
Opaques (15%) – Sulphides include pyrite, pyrrhotite and gold. Gold occurs as inclusions of pyrite and inclusion in garnets. There is also gold found at grain boundaries of pyrite. Not seen to be associated with pyrrhotite.

FD 01310 – Biotite Quartzofeldspathic Gneiss
Biotite (20%) – preferred orientation of the long axis. Moderate to strong foliation. LPO with grains going extinct at the same time.
Quartz (15%) – fine-grained with undulose extinction

Microcline (10%)
Plagioclase (35%)
Sericite (5%)
Opaques (5%)

FD 01312 – Pegmatite

FD 01313 – Amphibolite

FD 01314 – Amphibolite
Hornblende (45%)
Plagioclase (15%)
Quartz (15%)
Biotite (15%)
Sericite (5%)
Opaques (3%)
Massive amphibolite with coarse biotite and hornblende crystals intergrown. Stable mineral growth with hornblende and biotite touching. Both minerals are subhedral to anhedral, biotite with one perfect cleavage and hornblende with 60/120 cleavages. Plagioclase is medium grained and common throughout the groundmass. All three minerals have quartz inclusions and quarts also makes up the groundmass as fine to medium grained crystals displaying undulose extinction. Biotite appears to be replacing hornblende in some areas as well as showing evidence of stable growth with hornblende in other areas and also crosscutting hornblende minerals.

FD 01315 – Biotite Quartzofeldspathic Gneiss
Biotite (25%)
Quartz (25%)
Plagioclase (20%)
Opaques (7%)
Strong foliation defined by fine to medium grained biotite and sulphides within a quartz and plagioclase groundmass. Biotite is seen to crosscut other biotite and groundmass minerals. Sulphides are euhedral pyrite and anhedral pyrrhotite with no visible gold. Sulphides commonly are surrounded by coarser grained biotite crystals that may or may not define foliation (low strain zone). Sulphides also seen to form a corona around quartz crystals and sulphides here are magnetite.

FD 01316 – Biotite Quartzofeldspathic Gneiss
Same as FD 01315 but contains some coarse lithons of plag clusters. Coarse-grained pockets with 5-10 grains of plag. Also moderate foliation

FD 01317 – Biotite Quartzofeldspathic Gneiss
Same as FD 1315 but with no plag lithons and a weak foliation.

FD 01321 – Hornblende-Pyroxene Hornfels
Hornblende (30%)
Orthopyroxene (25%)
Plagioclase (15%)
Quartz (10%)
Garnet (1%)
Opaques (7%)
Pyroxene grains are highly eroded with a lot of quartz and plagioclase inclusions and some hornblende inclusions. The coarse hornblendes appear stable with subhedral shapes and rare quartz inclusions and commonly surround pyroxene crystals. Gold is seen associated with euhedral pyrite and anhedral pyrrhotite and hornblende crystals.

FD 01322 – Hornblende-Pyroxene Hornfels
Pyroxene in contact with garnet (pic taken) evidence of granulite facies.

FD 01323 – Hornblende-Pyroxene Hornfels
Gold as inclusions in pyrite common. Calcite present in coarse crystals,
Cordierite?! Low relief and grey birefringence being eroded and altered by sericite.
Highly eroded py grains
Hornblende also seen as inclusions in pyrite.

FD 01324 - QFG
Opx, hornblende, plag (minor), quartz and blue mineral?? Altering bands of quartz and plagioclase dominated millimetric bands and hornblende, opx and some cpx bands. Minor sericite alteration associated with blue mineral.
Quartz commonly has 120-degree triple junctions indicating an equilibrated system with well-developed crystals habits of hornblende and opx. Some quartz are concentrated in large "circles" with subgrains and undulose extinction.
Gold as inclusions in pyrite and free gold associated with quartz rich felsic bands

FD 01325 - Pyroxene Hornfels
Opx – parallel extinction, some opx seem to display micro tension fractures (also seen in FD 01327A
Hbl

FD 01326 – Biotite Schist
Biotite (40%) – strong foliation and crenulated cleavage of elongate grains. elongate, fibrous, defining a crenulations foliation possibly intergrown with sillimanite??
Not all fibrous grains have brown pleochroism and are 1st order greys in xpl.
Quartz (30%) – coarse grains with undulose extinction and some biotite inclusions.
Plagioclase (10%)
Sericite (25%) – fine grained defining groundmass with coarse quartz crystals.
Calcite (7%) – coarse crystals with mottled texture and
Garnet (3%) – coarse garnets, highly fractured, do not appear rotated but have foliation wrapping around them.
Crenulated foliation defined by biotite in a quartz, plagioclase, sericite, calcite and garnet groundmass. The biotite grains are long and bladed with some quartz grains within the books.

FD 01327A – Pyroxene Hornfels

FD 01327B – Pyroxene Hornfels

FD 01328 – Biotite Schist
Biotite (50%) – Elongate grains defining foliation (possibly crenulation) occur with some hornblende grain inclusions. Hornblendes appear eroded and replaced by bt. Bt grains display LPO as well as DPO
Hornblende (10%) – Fine-grained anhedral eroded grains as inclusions in biotite rich layers, commonly defining foliation with biotite.
Garnet (3%) – One euhedral, hexagonal shape with anhedral py inclusion and quartz inclusions. Another garnet appears to have been a very large crystal that has been almost completely eroded and replaced by bt and qtz. Three relict euhedral sides are visible with potential to match up and make a full crystal though no replacing minerals display the shape of the full garnet being replaced. In another are there is a diamond shaped garnet with one end being replaced by bt and with quartz inclusions throughout.
Abundant euhedral pyrite with some gold in strain shadows. Possibly gold seen as inclusions in garnet.

FD 01329 – Sillimanite Schist
Sillimanite (30%) – mostly fibrolite as coarse blebs and wispy lenses with chaotic foliation pattern. The sillimanite grains appear to be growing in the fold noses of the crenulated patterns and less commonly within the planes of weakness between the "layers" being folded.

FD 01330 – Garnet-Biotite Gneiss
Biotite (35%) – Biotite are elongate crystals with ductilely deformed cleavage and seen wrapping around garnet competent lithons. The biotite defines a weak to moderate foliation with LPO and DPO. Biotite grains commonly appear eroded with irregular grain boundaries
Garnet (20%) – Garnets are all small (less than 1mm). **Do not have inclusions of quartz and biotite that has been commonly observed in other lithologies. Garnets are highly fractured and occur in clusters with biotite and quartz.
Quartz (20%) – fine to coarse grains defining the groundmass of the rock. Undulose extinction observed and
Sericite (10%) – very common in plagioclase (visible relict twins) and at grain boundaries.
Dextral movement seen in quartz? Fish...with undulose extinction in top left of slide.
Opaques (7%)

FD 01331 – Biotite-Sillimanite Quartzofeldspathic Gneiss
Sillimanite (20%) – Dominantly fibrolite with some coarse sillimanite grains.
Plagioclase (35%) – abundant plagioclase commonly being replaced by sericite along grain boundaries and relict twinning sites.
Quartz (15%) – Groundmass mineral displaying undulose extinction
Biotite (15%) – coarse grains with no defining foliation.
Sericite (15%) – see replacing plagioclase feldspar grains

FD 01332 – Garnet-Sillimanite-Biotite Schist
Biotite (20%)
Sillimanite (10%) – mostly fibrolite with some elongate narrow prisms or well developed sillimanite. There are some grains that have a weak diamond or rhomb shape that have been described in "minerals in thin section" as sillimanite but have been identified by me as opx.??
Garnet (15%) – Garnet being replaced by sillimanite, quartz and biotite at the edge of a sulphide bleb? Pseudohexagonal shape with garnet beside. Right side of thin section, 1/3 way up.
Quartz (10%)
Plagioclase (10%)
Opx (7%)
Sericite (15%)

FD 01333 – Sillimanite-Garnet-Biotite Schist
Biotite (30%) – coarse grains not defining a foliation.
Garnet (15%) – fine to coarse grained…the coarse grained garnets have abundant inclusions of quartz and biotite while the fine-grained garnets typically do not have fractures or inclusions.
Sillimanite (10%) – dominantly fibrolite with some coarse prisms. The fibrolite is seen to be forming in wispy blebs and lenses. Appears to be a sillimanite bleb of fibrolite with a tiny garnet in the centre? Has the sillimanite replaced the garnet??
Quartz (15%) – coarse grains making up the groundmass displaying undulose extinction.
Plagioclase (5%)
Sericite (5%) – minor alteration on the plagioclase grains.
Opx (7%) – fine grained square or subhedral grains with high relief and low birefringence. Commonly associated with sillimanite growth and occur in clusters.

FD 01334 – Sillimanite-Biotite Schist
Biotite (30%) – short and stubby grains with weak to no foliation (DPO)
Sillimanite (25%) – sillimanite is coarse-grained prisms defining foliation (more so that biotite) and has an LPO as well as DPO. Some areas see coarse sillimanite grains retrograding to fibrolite. Sillimanite

grains are in bands with quartz groundmass (i.e. One grain is elongate and has quartz and biotite in between the next grain. Coarse grains have parallel extinction.??
Quartz (25%)
Plagioclase (10%)
Opx (5%)
Opaques (5%) – Gold is not seen associated with coarse sillimanite grains.

FD 01335 – Sillimanite-Garnet-Biotite Schist
Biotite (35%)
Sillimanite (5%)
Garnet (5%) – garnet grain is anhedral with sillimanite (fibrolite) corona partially surrounding the crystal with other area surrounded by opx.
Opx (5%) – subgrains on opx near large fractured sillimanite??
Plag (15%)
Quartz (25%)
Sericite (5%)
Opaques (5%) – gold seen as inclusion in subhedral pyrite, surrounded by anhedral pyrrhotite with a gold bleb within and also associated with magnetite. This sulphide is within an opx groundmass. Seen in bottom right hand corner of the slide. Gold also see in association to brittely fractured sillimanite grain. Sulphide bleb infilling the fracture and surrounded by opx

FD 01336 – Sillimanite-Garnet-Biotite Schist
Biotite (30%) – grains in one are have cpx intergrown with elongate biotite crystals.
Garnet (15%)
Sillimanite (10%)
Quartz (25%)
Plagioclase (7%)
Opx (7%)
Opaques (10%)

FD 01337 – Sillimanite-Garnet-Biotite Schist
Biotite (30%)
Garnet (15%)
Sillimanite (10%)
Quartz (25%)
Plagioclase (7%)
Opx (7%)
Opaques (15%) – abundant gold associated with sulphides and biotite and quartz.

FD 01338 – Biotite-Sillimanite Schist
Sillimanite (20%) – dominantly fibrolite as retrograde crystals with some relict sillimanite coarse grains. The wispy fibrolite grains are defining foliation
Biotite (15%) – anhedral blebs with no elongate axis-defining foliation
Quartz (35%) –
Opaques (15%) – lots of gold!! Associated with euhedral pyrite and anhedral pyrrhotite.

FD 01339A - Biotite-Sillimanite Schist
Sillimanite (40%) – dominantly fibrolite as retrograde crystals with some relict sillimanite coarse grains. The wispy fibrolite grains are defining foliation. Parallel extinction
Biotite (25%) – anhedral blebs with no elongate axis-defining foliation
Quartz (25%)
Opaques (15%) – lots of gold!! Associated with euhedral pyrite and anhedral pyrrhotite.

FD 01339B - Sillimanite-Biotite Schist
Sillimanite (20%) – dominantly fibrolite as retrograde crystals with some relict sillimanite coarse grains. The wispy fibrolite grains are defining foliation. Parallel extinction. Thin section appears to have one side with well-developed sillimanite and one side with more fibrolite
Biotite (35%) – anhedral blebs with no elongate axis-defining foliation
Quartz (25%)
Opaques (15%) – lots of gold!! Associated with euhedral pyrite and anhedral pyrrhotite.

FD 01340 – Garnet-biotite schist
Biotite (40%) – Euhedral, pleochroism,
Garnet (15%) – Anhedral, coarse-grained, abundant inclusions of quartz and some biotite. Typically within a biotite rich matrix.
Quartz (20%) – Anhedral, fine to coarse-grained. Pitted texture.
Plagioclase (5%)
Opaques (10%) – pyrite, pyrrhotite, magnetite
Rutile (1%)
Two garnets, surrounded by biotite with inclusions.

FD 01341 – Sillimanite-garnet-biotite schist
Biotite (20%)
Garnet (20%)
Sillimanite (10%)
Quartz (30%)
Opaques (10%)

FD 01342 – Garnet-Biotite Schist
Biotite (35%) – seen as coronas around garnet and as inclusions.
Garnet (20%) – with inclusions of bt and qtz
Quartz (25%)
Sillimanite (5%) – dominantly fine grained fibrolite and some fine grained prismatic crystals
Opaques (7%)

FD 01343 – Sillimanite-Garnet-Biotite Schist
Biotite
Garnet
Sillimanite
Opx
Quartz
Plagioclase
Opaques

FD 01345 – Pyroxene Hornfels
Staurolite – Staurolite grain intruding disaggregated garnet grain in top right hand corner of the slide
Garnet
Cpx
Calcite bleb

FD 01346
Plagioclase (25%) –
Hornblende (20%) – eroded grains with 60/120 cleavage

FD 01347
Gold commonly as inclusions in pyrite with sheathing py.

APPENDIX D – GARNET-BIOTITE GEOTHERMOMETRY

FD 01340											
Grt-Bt 1											
	Grt Core 1	**Grt Core 2**	**Grt Core 3**	**Grt Core 4**	**Grt Rim 1**	**Grt Rim 2**	**Grt Rim 3**	**Grt Rim 4**	**Grt Rim 5**	**Grt Rim 6**	**Grt Rim 7**
OXIDE	wt %	wt %	wt %	wt %	wt %	wt %	wt %	wt %	wt %	wt %	wt %
MgO	3.95	3.96	4.25	4.24	3.06	3.50	2.70	3.39	3.86	4.32	4.26
Al_2O_3	21.06	20.52	20.37	20.87	20.53	20.71	21.00	20.88	20.57	20.92	20.56
SiO_2	37.28	36.20	36.02	37.12	35.69	36.17	36.77	36.79	35.71	36.56	36.28
CaO	1.16	1.13	1.11	1.26	1.22	1.21	1.19	1.17	1.25	1.21	1.24
Sc_2O_3	0.00	0.00	0.00	0.00	0.00	0.00	0.00	0.00	0.00	0.00	0.00
TiO_2	0.00	0.00	0.00	0.00	0.00	0.00	0.00	0.00	0.00	0.00	0.00
MnO	6.26	6.38	6.44	6.29	7.78	6.82	7.86	7.76	6.80	6.37	6.46
FeO	29.79	30.19	30.67	30.76	30.83	30.47	30.43	30.98	30.28	30.74	30.48
	99.50	98.37	98.85	100.53	99.11	98.88	99.94	100.98	98.46	100.12	99.28
Cations pfu											
Mg	0.47	0.48	0.52	0.51	0.38	0.43	0.33	0.41	0.47	0.52	0.52
Al	2.00	1.98	1.96	1.97	1.99	2.00	2.01	1.98	1.99	1.99	1.97
Si	3.00	2.97	2.95	2.97	2.94	2.96	2.98	2.96	2.94	2.95	2.95
Ca	0.10	0.10	0.10	0.11	0.11	0.11	0.10	0.10	0.11	0.10	0.11
Sc	0.00	0.00	0.00	0.00	0.00	0.00	0.00	0.00	0.00	0.00	0.00
Ti	0.00	0.00	0.00	0.00	0.00	0.00	0.00	0.00	0.00	0.00	0.00
Mn	0.43	0.44	0.45	0.43	0.54	0.47	0.54	0.53	0.47	0.43	0.44
Fe	2.00	2.07	2.10	2.06	2.12	2.08	2.06	2.08	2.08	2.07	2.07
Mg/Fe	**0.24**	**0.23**	**0.25**	**0.25**	**0.18**	**0.20**	**0.16**	**0.19**	**0.23**	**0.25**	**0.25**
Almandine	0.67	0.64	0.62	0.64	0.63	0.65	0.67	0.64	0.62	0.62	0.62
Spessartine	0.14	0.15	0.15	0.14	0.18	0.16	0.18	0.18	0.16	0.14	0.15
Pyrope	0.16	0.16	0.17	0.17	0.12	0.14	0.11	0.13	0.16	0.17	0.17
Grossular	0.03	0.01		0.01	0.01	0.02	0.03	0.01	0.01	0.01	0.00
Andradite		0.02	0.03	0.03	0.03	0.02	0.00	0.03	0.03	0.03	0.03
Sc Garnet											
	Bt Inc 1				**Bt Mtx 1**	**Bt Inc 2**	**Bt Mtx 3**	**Bt Mtx 2**			
OXIDE	wt %				wt %	wt %	wt %	wt %			
Na_2O	0.00				0.00	0.00	0.00	0.00			
MgO	8.13				10.88	8.91	8.57	10.61			
Al_2O_3	19.39				20.26	20.18	18.46	18.43			
SiO_2	35.60				28.88	35.71	34.65	35.35			
K_2O	9.35				0.80	8.88	7.90	10.28			
TiO_2	2.04				0.00	2.62	2.12	2.31			
V_2O_5	0.32				0.00	0.00	0.00	0.25			
MnO	0.55				0.31	0.00	0.21	0.00			
FeO	23.33				37.17	22.95	26.20	20.31			
BaO	0.00				0.00	0.00	0.00	0.45			
	98.72				98.30	99.24	98.10	98.00			
Cations pfu											
Na	0.00				0.00	0.00	0.00	0.00			
Mg	1.98				2.75	2.14	2.11	2.59			
Al	3.73				4.05	3.83	3.60	3.55			
Si	5.81				4.89	5.74	5.73	5.78			
K	1.95				0.17	1.82	1.67	2.15			
Ti	0.25				0.00	0.32	0.26	0.28			
V	0.03				0.00	0.00	0.00	0.03			
Mn	0.08				0.04	0.00	0.03	0.00			
Fe	3.18				5.27	3.09	3.63	2.78			
Ba	0.00				0.00	0.00	0.00	0.03			
Mg/Fe	**0.62**				**0.52**	**0.69**	**0.58**	**0.93**			
Kd	**0.38**				**0.34**	**0.30**	**0.27**				
Temp °C	**933.25**				**858.51**	**782.01**	**737.21**				

FD 01340								
Grt-Bt 2								
	Grt Core 1	**Grt Core 2**	**Grt Core 3**	**Grt Core 4**	**Grt Rim 1**	**Grt Rim 2**	**Grt Rim 3**	
OXIDE	wt %	wt %	wt %	wt %	wt %	wt %	wt %	
MgO	3.30	3.78	3.92	3.86	3.19	3.37	3.24	
Al_2O_3	21.41	20.85	20.76	21.23	21.55	20.91	21.09	
SiO_2	37.40	36.52	36.68	37.21	37.54	36.50	37.15	
CaO	1.18	1.11	1.13	1.19	1.22	1.17	1.21	
Sc_2O_3	0.00	0.00	0.00	0.00	0.15	0.00	0.00	
TiO_2	0.00	0.00	0.00	0.00	0.00	0.00	0.00	
MnO	7.14	6.84	6.76	6.83	7.34	7.35	7.54	
FeO	30.58	29.39	29.90	29.99	30.28	30.06	30.36	
	101.01	98.49	99.15	100.31	101.26	99.36	100.59	
Cations pfu								
Mg	0.39	0.46	0.47	0.46	0.38	0.41	0.39	
Al	2.01	2.00	1.99	2.00	2.02	2.00	1.99	
Si	2.98	2.98	2.98	2.98	2.98	2.97	2.98	
Ca	0.10	0.10	0.10	0.10	0.10	0.10	0.10	
Sc	0.00	0.00	0.00	0.00	0.02	0.00	0.00	
Ti	0.00	0.00	0.00	0.00	0.00	0.00	0.00	
Mn	0.48	0.47	0.46	0.46	0.49	0.51	0.51	
Fe	2.04	2.01	2.03	2.01	2.01	2.04	2.04	
Mg/Fe	**0.19**	**0.23**	**0.23**	**0.23**	**0.19**	**0.20**	**0.19**	
Almandine	0.67	0.65	0.64	0.65	0.67	0.65	0.66	
Spessartine	0.16	0.16	0.15	0.15	0.16	0.17	0.17	
Pyrope	0.13	0.15	0.16	0.15	0.13	0.14	0.13	
Grossular	0.03	0.03	0.02	0.03	0.03	0.02	0.03	
Andradite		0.00	0.02	0.00		0.01	0.01	
Sc Garnet					0.01			
	Bt Inc 1				**Bt Mtx 1**	**Bt Mtx 2**	**Bt Mtx 3**	**Bt Mtx 4**
OXIDE	wt %				wt %	wt %	wt %	wt %
Na_2O	0.00				0.00	0.00	0.00	0.40
MgO	11.19				9.73	11.27	9.53	11.34
Al_2O_3	18.97				19.09	19.05	18.97	19.01
SiO_2	37.09				36.17	36.70	36.16	36.20
K_2O	10.24				9.82	10.16	10.43	10.26
TiO_2	2.39				2.69	2.79	2.14	2.23
V_2O_5	0.00				0.00	0.00	0.37	0.28
MnO	0.00				0.00	0.00	0.20	0.00
FeO	20.63				22.14	19.13	21.92	18.31
BaO	0.00				0.00	0.00	0.42	0.56
	100.51				99.64	99.10	100.15	98.59
Cations pfu								
Na	0.00				0.00	0.00	0.00	0.13
Mg	2.64				2.33	2.68	2.29	2.73
Al	3.54				3.61	3.58	3.60	3.61
Si	5.86				5.81	5.85	5.82	5.84
K	2.07				2.01	2.07	2.14	2.11
Ti	0.28				0.32	0.34	0.26	0.27
V	0.00				0.00	0.00	0.04	0.03
Mn	0.00				0.00	0.00	0.03	0.00
Fe	2.73				2.97	2.55	2.95	2.47
Ba	0.00				0.00	0.00	0.03	0.04
Mg/Fe	**0.97**				**0.78**	**1.05**	**0.78**	**1.10**
Kd	**0.20**				**0.24**	**0.19**	**0.25**	
Temp (°C)	**606.65**				**680.39**	**590.24**	**691.62**	

FD 01340											
Grt-Bt 3											
	Grt Core 1	**Grt Core 2**	**Grt Core 3**	**Grt Core 4**	**Grt Core 5**	**Grt Rim 1**	**Grt Rim 2**	**Grt Rim 3**	**Grt Rim 4**	**Grt Rim 5**	**Grt Rim 6**
OXIDE	wt %	wt %	wt %	wt %	wt %	wt %	wt %	wt %	wt %	wt %	wt %
MgO	2.94	4.38	4.34	4.40	4.51	3.19	2.38	3.03	3.11	4.26	3.91
Al_2O_3	21.30	21.19	21.53	20.79	20.73	21.01	21.19	20.69	21.06	21.04	20.75
SiO_2	38.02	37.54	37.73	37.05	36.62	36.86	36.84	36.05	36.71	37.03	36.61
CaO	1.13	1.19	1.18	1.21	1.11	1.21	1.16	1.29	1.12	1.19	1.12
Sc_2O_3	0.00	0.00	0.00	0.14	0.14	0.00	0.00	0.00	0.00	0.00	0.00
TiO_2	0.00	0.00	0.00	0.00	0.00	0.00	0.00	0.00	0.00	0.00	0.00
MnO	6.80	6.47	6.49	6.06	6.07	7.51	7.92	7.46	7.49	6.56	6.49
FeO	30.24	29.68	30.49	30.03	28.97	30.55	30.49	30.94	29.92	30.25	29.24
	100.43	100.45	101.76	99.68	98.15	100.33	99.98	99.45	99.41	100.33	98.12
Cations pfu											
Mg	0.35	0.52	0.51	0.53	0.55	0.38	0.29	0.37	0.38	0.51	0.48
Al	2.00	1.99	2.00	1.97	1.99	2.00	2.02	1.99	2.01	1.99	2.00
Si	3.03	2.99	2.97	2.98	2.98	2.97	2.98	2.95	2.98	2.97	2.99
Ca	0.10	0.10	0.10	0.10	0.10	0.10	0.10	0.11	0.10	0.10	0.10
Sc	0.00	0.00	0.00	0.02	0.02	0.00	0.00	0.00	0.00	0.00	0.00
Ti	0.00	0.00	0.00	0.00	0.00	0.00	0.00	0.00	0.00	0.00	0.00
Mn	0.46	0.44	0.43	0.41	0.42	0.51	0.54	0.52	0.51	0.45	0.45
Fe	2.02	1.98	2.01	2.02	1.97	2.06	2.07	2.12	2.03	2.03	2.00
Mg/Fe	**0.17**	**0.26**	**0.25**	**0.26**	**0.28**	**0.19**	**0.14**	**0.17**	**0.19**	**0.25**	**0.24**
Almandine	0.68	0.64	0.64	0.64	0.64	0.65	0.68	0.65	0.66	0.63	0.66
Spessartine	0.15	0.15	0.14	0.14	0.14	0.17	0.18	0.17	0.17	0.15	0.15
Pyrope	0.12	0.17	0.17	0.18	0.18	0.13	0.10	0.12	0.13	0.17	0.16
Grossular	0.03	0.02	0.02	0.01	0.02	0.02	0.03	0.02	0.03	0.01	0.03
Andradite		0.01	0.01	0.02	0.01	0.01		0.02		0.02	0.00
Sc Garnet				0.00	0.01						
	Bt Inc 1					**Bt Mtx 1**	**Bt Mtx 2**	**Bt Mtx 3**	**Bt Mtx 4**	**Bt Mtx 5**	
OXIDE	wt %					wt %	wt %	wt %	wt %	wt %	
Na_2O	0.00					0.00	0.00	0.00	0.00	0.34	
MgO	13.02					10.92	11.19	10.92	10.65	11.28	
Al_2O_3	19.87					19.70	19.22	19.66	19.61	19.17	
SiO_2	37.59					36.25	35.96	36.56	37.00	36.61	
K_2O	10.01					10.05	10.30	9.97	10.24	10.40	
TiO_2	2.31					2.41	2.41	2.22	2.76	2.64	
V_2O_5	0.00					0.00	0.34	0.00	0.00	0.00	
MnO	0.00					0.00	0.20	0.00	0.00	0.00	
FeO	17.50					20.27	20.65	19.96	20.18	18.91	
BaO	0.00					0.00	0.47	0.00	0.00	0.00	
	100.31					99.59	100.74	99.29	100.44	99.36	
Cations pfu											
Na	0.00					0.00	0.00	0.00	0.00	0.10	
Mg	3.02					2.59	2.65	2.60	2.50	2.68	
Al	3.65					3.70	3.60	3.69	3.65	3.61	
Si	5.85					5.78	5.72	5.83	5.84	5.84	
K	1.99					2.04	2.09	2.03	2.06	2.12	
Ti	0.27					0.29	0.29	0.27	0.33	0.32	
V	0.00					0.00	0.04	0.00	0.00	0.00	
Mn	0.00					0.00	0.03	0.00	0.00	0.00	
Fe	2.28					2.70	2.75	2.66	2.66	2.52	
Ba	0.00					0.00	0.03	0.00	0.00	0.00	
Mg/Fe	**1.33**					**0.96**	**0.97**	**0.98**	**0.94**		
Kd	**0.13**					**0.19**	**0.14**	**0.18**	**0.20**		
Temp (°C)	**475.34**					**597.42**	**502.80**	**569.82**	**603.25**		

FD 01340											
Grt-Bt 4											
	Grt Core 1	**Grt Core 2**	**Grt Core 3**	**Grt Core 4**	**Grt Core 5**	**Grt Core 6**	**Grt Rim 1**	**Grt Rim 2**	**Grt Rim 3**	**Grt Rim 4**	
OXIDE	wt %	wt %	wt %	wt %	wt %	wt %	wt %	wt %	wt %	wt %	
MgO	2.58	3.47	3.93	4.27	4.16	4.08	3.24	2.28	2.94	3.93	
Al_2O_3	20.70	21.29	20.69	21.25	21.03	20.95	20.92	20.77	21.19	21.06	
SiO_2	35.65	37.74	36.53	37.49	36.81	36.88	37.28	36.54	36.95	36.71	
CaO	1.18	1.13	1.13	1.19	1.18	1.20	1.23	0.81	1.15	1.18	
Sc_2O_3	0.00	0.00	0.00	0.00	0.00	0.00	0.00	0.00	0.15	0.00	
TiO_2	0.00	0.00	0.00	0.00	0.00	0.00	0.00	0.00	0.00	0.00	
MnO	6.74	6.18	6.33	6.27	6.25	6.50	7.47	8.42	7.41	6.79	
FeO	33.61	30.19	30.03	30.44	29.74	29.80	29.40	31.03	29.84	29.88	
	100.45	100.00	98.64	100.91	99.17	99.42	99.52	99.85	99.64	99.55	
Cations pfu											
Mg	0.31	0.41	0.48	0.51	0.50	0.49	0.39	0.28	0.35	0.47	
Al	1.99	2.01	1.99	1.99	2.00	1.99	1.99	2.00	2.02	2.01	
Si	2.91	3.02	2.98	2.98	2.98	2.98	3.01	2.98	2.98	2.97	
Ca	0.10	0.10	0.10	0.10	0.10	0.10	0.11	0.07	0.10	0.10	
Sc	0.00	0.00	0.00	0.00	0.00	0.00	0.00	0.00	0.02	0.00	
Ti	0.00	0.00	0.00	0.00	0.00	0.00	0.00	0.00	0.00	0.00	
Mn	0.47	0.42	0.44	0.42	0.43	0.44	0.51	0.58	0.51	0.46	
Fe	2.30	2.02	2.05	2.02	2.01	2.01	1.99	2.12	2.01	2.02	
Mg/Fe	**0.14**	**0.20**	**0.23**	**0.25**	**0.25**	**0.24**	**0.20**	**0.13**	**0.18**	**0.23**	
Almandine	0.67	0.68	0.65	0.65	0.65	0.64	0.66	0.68	0.67	0.64	
Spessartine	0.15	0.14	0.15	0.14	0.14	0.15	0.17	0.19	0.17	0.15	
Pyrope	0.10	0.14	0.16	0.17	0.17	0.16	0.13	0.09	0.12	0.16	
Grossular	0.00	0.03	0.02	0.02	0.03	0.02	0.03	0.01	0.03	0.03	
Andradite	0.03		0.01	0.01	0.01	0.01		0.01		0.01	
Sc Garnet									0.01		
	Bt Inc 1	**Bt Inc 2**	**Bt Inc 3**				**Bt Mtx 1**	**Bt Mtx 2**	**Bt Mtx 3**	**Bt Mtx 4**	**Bt Mtx 5**
OXIDE	wt %	wt %	wt %				wt %	wt %	wt %	wt %	wt %
Na_2O	0.00	0.00	0.26				0.00	0.00	0.00	0.00	0.00
MgO	12.59	12.96	12.25				10.30	11.29	9.74	10.54	10.97
Al_2O_3	19.84	20.16	19.02				20.00	19.06	19.76	19.22	19.44
SiO_2	37.12	37.75	36.75				36.54	35.99	36.46	36.11	37.12
K_2O	10.34	10.50	10.49				9.39	10.15	10.53	10.06	10.44
TiO_2	2.36	2.35	2.47				2.15	2.73	2.54	2.38	2.54
V_2O_5	0.00	0.00	0.00				0.20	0.00	0.00	0.00	0.00
MnO	0.00	0.00	0.00				0.00	0.00	0.00	0.00	0.18
FeO	16.82	16.64	18.01				21.79	19.86	20.28	21.36	19.75
BaO	0.00	0.00	0.00				0.00	0.00	0.00	0.00	0.00
	99.06	100.36	99.25				100.38	99.08	99.31	99.67	100.44
Cations pfu											
Na	0.00	0.00	0.08				0.00	0.00	0.00	0.00	0.00
Mg	2.96	3.00	2.91				2.43	2.70	2.33	2.52	2.58
Al	3.69	3.69	3.57				3.73	3.60	3.73	3.63	3.62
Si	5.85	5.86	5.85				5.79	5.77	5.84	5.79	5.86
K	2.08	2.08	2.13				1.90	2.08	2.15	2.06	2.10
Ti	0.28	0.27	0.30				0.26	0.33	0.31	0.29	0.30
V	0.00	0.00	0.00				0.02	0.00	0.00	0.00	0.00
Mn	0.00	0.00	0.00				0.00	0.00	0.00	0.00	0.02
Fe	2.22	2.16	2.40				2.88	2.66	2.72	2.86	2.61
Ba	0.00	0.00	0.00				0.00	0.00	0.00	0.00	0.00
Mg/Fe	**1.33**	**1.39**	**1.21**				**0.84**	**1.01**	**0.86**		
Kd	**0.10**	**0.15**	**0.19**				**0.23**	**0.13**	**0.21**		
Temp (°C)	**416.52**	**508.90**	**594.61**				**668.35**	**472.46**	**618.65**		

FD 01340										
Grt-Bt 5										
	Grt Core 1	**Grt Core 2**	**Grt Core 3**	**Grt Core 4**	**Grt Core 5**	**Grt Rim 1**	**Grt Rim 2**	**Grt Rim 3**	**Grt Rim 4**	**Grt Rim 5**
OXIDE	wt %	wt %	wt %	wt %	wt %	wt %	wt %	wt %	wt %	wt %
MgO	6.83	3.28	3.14	3.80	3.91	3.34	2.36	3.03	3.84	3.66
Al_2O_3	20.90	20.80	20.54	20.26	20.55	20.82	20.96	21.23	20.78	20.54
SiO_2	34.29	36.40	36.07	36.03	36.19	36.41	36.19	36.34	36.49	36.32
CaO	0.48	1.15	1.13	1.15	1.22	1.18	0.91	1.21	1.33	1.22
Sc_2O_3	0.00	0.00	0.00	0.00	0.00	0.00	0.00	0.00	0.00	0.00
TiO_2	0.94	0.00	0.00	0.00	0.00	0.00	0.00	0.00	0.00	0.00
MnO	3.62	6.98	7.06	6.80	6.79	7.49	8.30	7.60	6.98	7.02
FeO	33.19	31.32	31.01	30.34	30.35	30.89	30.97	31.33	29.94	30.29
	100.26	99.93	98.94	98.38	99.00	100.13	99.69	100.75	99.37	99.05
Cations pfu										
Mg	0.82	0.40	0.38	0.47	0.48	0.40	0.29	0.36	0.46	0.45
Al	1.99	1.99	1.99	1.96	1.98	1.99	2.02	2.02	1.99	1.98
Si	2.77	2.96	2.96	2.96	2.95	2.95	2.96	2.93	2.96	2.96
Ca	0.04	0.10	0.10	0.10	0.11	0.10	0.08	0.10	0.12	0.11
Sc	0.00	0.00	0.00	0.00	0.00	0.00	0.00	0.00	0.00	0.00
Ti	0.06	0.00	0.00	0.00	0.00	0.00	0.00	0.00	0.00	0.00
Mn	0.25	0.48	0.49	0.47	0.47	0.51	0.57	0.52	0.48	0.49
Fe	2.24	2.13	2.13	2.09	2.07	2.09	2.12	2.12	2.03	2.07
Mg/Fe	**0.37**	**0.19**	**0.18**	**0.22**	**0.23**	**0.19**	**0.14**	**0.17**	**0.23**	**0.22**
Almandine	0.48	0.66	0.66	0.64	0.63	0.64	0.67	0.64	0.63	0.64
Spessartine	0.08	0.16	0.16	0.16	0.16	0.17	0.19	0.17	0.16	0.16
Pyrope	0.27	0.13	0.13	0.15	0.16	0.13	0.10	0.12	0.15	0.15
Grossular		0.01	0.01		0.01	0.01	0.02	0.02	0.02	0.01
Andradite		0.02	0.02	0.03	0.03	0.02	0.00	0.01	0.02	0.03
Sc Garnet										
	Bt Inc 1	**Bt Inc 2**					**Bt Mtx 2**	**Bt Inc 3**	**Bt Mtx 3**	
OXIDE	wt %	wt %					wt %	wt %	wt %	
Na_2O	0.00	0.00					0.00	0.00	0.00	
MgO	9.32	9.49					7.73	9.11	9.51	
Al_2O_3	18.47	18.20					19.56	20.57	18.48	
SiO_2	34.30	33.73					34.91	32.95	35.06	
K_2O	8.67	8.90					8.92	4.09	10.39	
TiO_2	2.13	2.11					2.79	0.98	2.55	
V_2O_5	0.00	0.00					0.00	0.00	0.00	
MnO	0.00	0.25					0.00	2.56	0.00	
FeO	26.79	27.24					24.81	29.33	22.18	
BaO	0.00	0.00					0.00	0.00	0.00	
	99.69	99.92					98.71	99.59	98.18	
Cations pfu										
Na	0.00	0.00					0.00	0.00	0.00	
Mg	2.28	2.33					1.89	2.22	2.33	
Al	3.57	3.54					3.78	3.97	3.58	
Si	5.63	5.56					5.72	5.39	5.76	
K	1.81	1.87					1.86	0.85	2.18	
Ti	0.26	0.26					0.34	0.12	0.32	
V	0.00	0.00					0.00	0.00	0.00	
Mn	0.00	0.04					0.00	0.35	0.00	
Fe	3.68	3.76					3.40	4.02	3.05	
Ba	0.00	0.00					0.00	0.00	0.00	
Mg/Fe	**0.62**	**0.62**					**0.56**	**0.55**		
Kd	**0.59**	**0.30**					**0.24**	**0.31**		
Temp (°C)	**1340.58**	**790.26**					**689.91**	**809.51**		

FD 01341													
Grt-Bt 1													
	Grt Core 1	**Grt Core 2**	**Grt Core 3**	**Grt Core 4**	**Grt Rim 1**	**Grt Rim 2**	**Grt Rim 3**	**Grt Rim 4**	**Grt Rim 5**	**Grt Rim 6**	**Grt Core 1b**	**Grt Rim 1b**	**Grt Rim 2b**
OXIDE	wt %	wt %	wt %	wt %	wt %	wt %	wt %	wt %	wt %	wt %	wt %	wt %	wt %
MgO	4.27	4.31	4.47	4.52	3.50	3.37	1.16	3.73	4.36	3.99	4.03	2.81	3.62
Al_2O_3	21.09	21.07	21.16	21.06	21.01	20.99	22.25	20.47	20.88	20.94	21.03	20.94	21.08
SiO_2	36.99	36.76	36.98	37.23	36.58	36.42	52.05	35.77	36.65	36.86	36.91	36.41	37.11
CaO	1.25	1.23	1.13	1.12	1.23	1.08	1.16	1.23	1.21	1.10	1.22	1.17	1.15
Sc_2O_3	0.00	0.00	0.00	0.00	0.00	0.00	0.00	0.00	0.00	0.00	0.00	0.00	0.00
TiO_2	0.00	0.00	0.00	0.00	0.00	0.00	0.00	0.00	0.00	0.00	0.00	0.00	0.00
MnO	5.84	5.73	5.58	5.66	6.75	6.76	4.56	6.28	5.82	6.07	6.05	7.54	6.90
FeO	30.93	31.00	31.09	31.08	30.54	30.91	17.88	30.46	31.03	30.89	30.78	31.17	30.80
	100.38	100.10	100.42	100.67	99.61	99.53	99.06	97.95	99.95	99.84	100.02	100.04	100.66
Cations pfu													
Mg	0.51	0.52	0.53	0.54	0.42	0.41	0.13	0.46	0.52	0.48	0.48	0.34	0.43
Al	1.99	2.00	2.00	1.98	2.01	2.01	1.90	1.99	1.98	1.99	1.99	2.00	1.99
Si	2.96	2.95	2.96	2.97	2.96	2.96	3.78	2.95	2.95	2.97	2.97	2.96	2.97
Ca	0.11	0.11	0.10	0.10	0.11	0.09	0.09	0.11	0.10	0.10	0.11	0.10	0.10
Sc	0.00	0.00	0.00	0.00	0.00	0.00	0.00	0.00	0.00	0.00	0.00	0.00	0.00
Ti	0.00	0.00	0.00	0.00	0.00	0.00	0.00	0.00	0.00	0.00	0.00	0.00	0.00
Mn	0.40	0.39	0.38	0.38	0.46	0.47	0.28	0.44	0.40	0.41	0.41	0.52	0.47
Fe	2.07	2.08	2.08	2.07	2.07	2.10	1.09	2.10	2.09	2.08	2.07	2.12	2.06
Mg/Fe	**0.25**	**0.25**	**0.26**	**0.26**	**0.20**	**0.19**	**0.12**	**0.22**	**0.25**	**0.23**	**0.23**	**0.16**	**0.21**
Almandine	0.65	0.64	0.65	0.65	0.65	0.66	0.40	0.64	0.64	0.66	0.65	0.66	0.66
Spessartine	0.13	0.13	0.13	0.13	0.15	0.15	0.10	0.15	0.13	0.14	0.14	0.17	0.16
Pyrope	0.17	0.17	0.18	0.18	0.14	0.14	0.05	0.15	0.17	0.16	0.16	0.11	0.14
Grossular	0.02	0.02	0.02	0.01	0.03	0.02	0.03	0.01	0.01	0.02	0.02	0.02	0.02
Andradite	0.02	0.02	0.02	0.02	0.01	0.01		0.02	0.03	0.02	0.01	0.01	0.01
Sc Garnet													
					Bt Mtx 1	**Bt Mtx 2**	**Bt Mtx 3**					**Bt Mtx 1b**	
OXIDE					wt %	wt %	wt %					wt %	
Na_2O					0.00	0.00	0.00					0.35	
MgO					12.18	13.46	11.67					11.52	
Al_2O_3					18.97	19.62	18.93					18.79	
SiO_2					36.43	37.15	36.28					36.16	
K_2O					10.59	10.52	10.18					10.28	
TiO_2					2.40	1.65	2.66					2.52	
V_2O_5					0.00	0.00	0.00					0.00	
MnO					0.00	0.00	0.00					0.19	
FeO					18.35	16.03	18.10					18.16	
BaO					0.00	0.00	0.00					0.00	
					98.92	98.42	97.82					97.98	
Cations pfu													
Na					0.00	0.00	0.00					0.11	
Mg					2.90	3.17	2.80					2.78	
Al					3.57	3.66	3.59					3.58	
Si					5.82	5.88	5.84					5.85	
K					2.16	2.12	2.09					2.12	
Ti					0.29	0.20	0.32					0.31	
V					0.00	0.00	0.00					0.00	
Mn					0.00	0.00	0.00					0.03	
Fe					2.45	2.12	2.44					2.46	
Ba					0.00	0.00	0.00					0.00	
Mg/Fe					**1.18**	**1.50**	**1.15**					**1.13**	
Kd					**0.17**	**0.13**	**0.10**					**0.14**	
Temp (°C)					**557.94**	**474.28**	**411.10**					**498.08**	

FD 01341												
Grt-Bt 2												
	Grt Core 1	**Grt Core 2**	**Grt Core 3**	**Grt Core 4**	**Grt Rim 1**	**Grt Rim 2**	**Grt Rim 3**	**Grt Rim 4**	**Grt Rim 5**	**Grt Rim 6**	**Grt Rim 7**	**Grt Rim 8**
OXIDE	wt %	wt %	wt %	wt %	wt %	wt %	wt %	wt %	wt %	wt %	wt %	wt %
MgO	4.94	4.90	4.84	4.92	3.43	3.01	2.89	2.94	4.39	4.81	4.67	4.58
Al_2O_3	20.71	20.69	20.72	20.68	20.47	20.43	21.35	21.30	20.82	20.65	21.00	20.47
SiO_2	36.73	36.75	36.32	36.61	35.67	36.03	37.13	37.25	36.15	36.58	36.36	36.18
CaO	1.15	1.15	1.13	1.18	1.15	1.10	1.14	1.19	1.19	1.18	1.15	1.13
Sc_2O_3	0.00	0.00	0.00	0.00	0.00	0.00	0.00	0.00	0.00	0.00	0.00	0.00
TiO_2	0.00	0.00	0.00	0.00	0.00	0.00	0.00	0.00	0.00	0.00	0.00	0.00
MnO	5.43	5.37	5.44	5.36	6.62	6.73	6.68	6.97	5.58	5.55	5.39	5.34
FeO	30.24	30.28	29.80	29.86	30.71	31.29	30.69	30.69	31.04	30.48	30.24	30.27
	99.19	99.13	98.24	98.61	98.07	98.59	99.90	100.34	99.17	99.23	98.81	97.97
Cations pfu												
Mg	0.59	0.59	0.59	0.59	0.42	0.37	0.35	0.35	0.53	0.58	0.56	0.56
Al	1.97	1.97	1.99	1.98	1.99	1.98	2.03	2.02	2.00	1.97	2.01	1.98
Si	2.97	2.97	2.96	2.97	2.95	2.97	2.99	2.99	2.94	2.96	2.95	2.97
Ca	0.10	0.10	0.10	0.10	0.10	0.10	0.10	0.10	0.10	0.10	0.10	0.10
Sc	0.00	0.00	0.00	0.00	0.00	0.00	0.00	0.00	0.00	0.00	0.00	0.00
Ti	0.00	0.00	0.00	0.00	0.00	0.00	0.00	0.00	0.00	0.00	0.00	0.00
Mn	0.37	0.37	0.38	0.37	0.46	0.47	0.46	0.47	0.38	0.38	0.37	0.37
Fe	2.04	2.05	2.03	2.03	2.12	2.16	2.07	2.06	2.11	2.06	2.05	2.07
Mg/Fe	**0.29**	**0.29**	**0.29**	**0.29**	**0.20**	**0.17**	**0.17**	**0.17**	**0.25**	**0.28**	**0.28**	**0.27**
Almandine	0.63	0.63	0.63	0.63	0.65	0.67	0.69	0.69	0.63	0.63	0.63	0.64
Spessartine	0.12	0.12	0.12	0.12	0.15	0.16	0.15	0.16	0.13	0.13	0.12	0.12
Pyrope	0.20	0.20	0.20	0.20	0.14	0.12	0.12	0.12	0.18	0.19	0.19	0.19
Grossular	0.00	0.01	0.01	0.01	0.01	0.01	0.03	0.03	0.01	0.00	0.02	0.01
Andradite	0.03	0.03	0.02	0.02	0.02	0.02			0.02	0.03	0.01	0.03
Sc Garnet												
					Bt Mtx 1	**Bt Mtx 2**	**Bt Mtx 3**	**Bt Mtx 4**	**Bt Mtx 5**			
OXIDE					wt %	wt %	wt %	wt %	wt %			
Na_2O					0.00	2.07	0.00	0.49	0.43			
MgO					12.18	10.14	12.16	11.43	11.91			
Al_2O_3					18.97	19.88	19.47	20.45	19.32			
SiO_2					36.43	41.40	37.43	35.41	36.99			
K_2O					10.59	8.44	10.47	9.76	10.54			
TiO_2					2.40	1.88	2.65	2.33	2.68			
V_2O_5					0.00	0.22	0.00	0.00	0.00			
MnO					0.00	0.00	0.00	0.00	0.00			
FeO					18.35	14.76	18.60	17.19	17.86			
BaO					0.00	0.00	0.00	0.00	0.00			
					98.92	98.78	100.78	97.06	99.72			
Cations pfu												
Na					0.00	0.63	0.00	0.15	0.13			
Mg					2.90	2.36	2.83	2.76	2.81			
Al					3.57	3.65	3.58	3.91	3.61			
Si					5.82	6.45	5.85	5.74	5.86			
K					2.16	1.68	2.09	2.02	2.13			
Ti					0.29	0.22	0.31	0.28	0.32			
V					0.00	0.02	0.00	0.00	0.00			
Mn					0.00	0.00	0.00	0.00	0.00			
Fe					2.45	1.92	2.43	2.33	2.37			
Ba					0.00	0.00	0.00	0.00	0.00			
Mg/Fe					**1.18**	**1.22**	**1.16**	**1.19**	**1.19**			
Kd					**0.17**	**0.14**	**0.14**	**0.14**	**0.21**			
Temp (°C)					**549.60**	**493.94**	**502.83**	**502.38**	**631.41**			

FD 01341											
Grt-Bt 3											
	Grt Core 1	**Grt Core 2**	**Grt Core 3**	**Grt Core 4**	**Grt Core 5**	**Grt Core 6**	**Grt Rim 1**	**Grt Rim 2**	**Grt Rim 3**	**Grt Rim 4**	**Grt Rim 5**
OXIDE	wt %	wt %	wt %	wt %	wt %	wt %	wt %	wt %	wt %	wt %	wt %
MgO	3.84	4.26	6.89	4.95	4.21	4.62	3.28	3.08	4.84	4.68	4.93
Al_2O_3	20.64	20.77	19.53	20.36	20.54	20.61	20.66	20.70	20.72	20.48	20.54
SiO_2	36.36	36.58	29.63	36.47	36.25	36.37	36.26	36.57	36.53	35.84	36.06
CaO	1.14	1.18	0.87	1.24	1.15	1.15	1.15	1.10	1.13	1.19	1.14
Sc_2O_3	0.00	0.00	0.00	0.00	0.00	0.00	0.00	0.00	0.00	0.00	0.00
TiO_2	0.00	0.00	0.00	0.00	0.00	0.00	0.00	0.00	0.00	0.00	0.00
MnO	5.72	5.45	4.84	5.39	5.55	5.54	7.11	6.88	5.34	5.43	5.46
FeO	30.61	30.42	37.43	30.30	31.16	30.22	31.89	30.21	30.05	30.46	30.02
	98.31	98.65	99.18	98.72	98.86	98.52	100.35	98.54	98.61	98.06	98.16
Cations pfu											
Mg	0.47	0.52	0.88	0.60	0.51	0.56	0.40	0.38	0.59	0.57	0.60
Al	1.99	1.99	1.97	1.95	1.98	1.98	1.98	2.00	1.98	1.98	1.98
Si	2.98	2.97	2.53	2.97	2.96	2.96	2.94	2.99	2.97	2.94	2.95
Ca	0.10	0.10	0.08	0.11	0.10	0.10	0.10	0.10	0.10	0.10	0.10
Sc	0.00	0.00	0.00	0.00	0.00	0.00	0.00	0.00	0.00	0.00	0.00
Ti	0.00	0.00	0.00	0.00	0.00	0.00	0.00	0.00	0.00	0.00	0.00
Mn	0.40	0.38	0.35	0.37	0.38	0.38	0.49	0.48	0.37	0.38	0.38
Fe	2.10	2.07	2.68	2.06	2.13	2.06	2.16	2.07	2.04	2.09	2.05
Mg/Fe	**0.22**	**0.25**	**0.33**	**0.29**	**0.24**	**0.27**	**0.18**	**0.18**	**0.29**	**0.27**	**0.29**
Almandine	0.67	0.66	0.24	0.62	0.65	0.64	0.65	0.68	0.63	0.62	0.62
Spessartine	0.13	0.12	0.11	0.12	0.13	0.13	0.16	0.16	0.12	0.12	0.13
Pyrope	0.16	0.17	0.28	0.20	0.17	0.19	0.13	0.13	0.19	0.19	0.20
Grossular	0.02	0.02			0.00	0.01		0.03	0.01	0.00	0.00
Andradite	0.01	0.01	0.03	0.04	0.03	0.03	0.03	0.00	0.02	0.03	0.03
Sc Garnet											
	Bt Inc 1	**Bt Inc 2**	**Bt Inc 3**				**Bt Mtx 1**	**Bt Mtx 2**			
OXIDE	wt %	wt %	wt %				wt %	wt %			
Na_2O	0.00	0.44	0.46				0.00	0.45			
MgO	12.14	15.06	14.73				11.06	12.41			
Al_2O_3	18.72	19.49	19.41				18.86	19.63			
SiO_2	36.24	37.43	36.60				34.88	36.31			
K_2O	9.98	10.06	10.66				9.35	10.49			
TiO_2	1.82	1.56	1.21				1.77	2.08			
V_2O_5	0.00	0.00	0.00				0.00	0.00			
MnO	0.20	0.00	0.00				0.39	0.00			
FeO	19.48	14.41	15.02				22.02	17.57			
BaO	0.00	0.00	0.00				0.00	0.00			
	98.58	98.45	98.08				98.32	98.94			
Cations pfu											
Na	0.00	0.13	0.14				0.00	0.14			
Mg	2.91	3.53	3.50				2.69	2.95			
Al	3.55	3.61	3.64				3.63	3.69			
Si	5.83	5.89	5.83				5.70	5.80			
K	2.05	2.02	2.17				1.95	2.14			
Ti	0.22	0.18	0.14				0.22	0.25			
V	0.00	0.00	0.00				0.00	0.00			
Mn	0.03	0.00	0.00				0.05	0.00			
Fe	2.62	1.90	2.00				3.01	2.35			
Ba	0.00	0.00	0.00				0.00	0.00			
Mg/Fe	**1.11**	**1.86**	**1.75**				**0.90**	**1.26**			
Kd	**0.20**	**0.13**	**0.19**				**0.20**	**0.14**			
Temp (°C)	**611.36**	**482.24**	**585.85**				**617.62**	**502.61**			

FD 01341							
Grt-Bt 4							
	Grt Core 1	**Grt Core 2**	**Grt Rim 1 (Zr)**	**Grt Rim 2**	**Grt Rim 3**	**Grt Rim 4**	**Grt Rim 5**
OXIDE	wt %	wt %	wt %	wt %	wt %	wt %	wt %
MgO	4.96	4.96	0.00	3.69	2.41	4.49	4.73
Al_2O_3	20.89	20.78	1.47	20.53	20.57	20.81	20.77
SiO_2	36.70	36.47	32.50	36.27	36.38	36.59	36.49
CaO	1.14	1.22	0.00	1.16	0.94	1.15	1.12
Sc_2O_3	0.00	0.00	0.00	0.00	0.00	0.00	0.00
TiO_2	0.00	0.00	0.00	0.00	0.00	0.00	0.00
MnO	5.50	5.42	0.46	5.95	7.70	5.59	5.43
FeO	30.33	30.19	3.04	31.45	30.84	30.64	30.41
	99.53	99.04	37.48	99.05	98.83	99.27	98.95
Cations pfu							
Mg	0.60	0.60	0.00	0.45	0.30	0.54	0.57
Al	1.98	1.98	0.30	1.98	1.99	1.99	1.98
Si	2.96	2.95	5.53	2.96	2.99	2.96	2.96
Ca	0.10	0.11	0.00	0.10	0.08	0.10	0.10
Sc	0.00	0.00	0.00	0.00	0.00	0.00	0.00
Ti	0.00	0.00	0.00	0.00	0.00	0.00	0.00
Mn	0.38	0.37	0.07	0.41	0.54	0.38	0.37
Fe	2.04	2.04	0.43	2.15	2.12	2.07	2.06
Mg/Fe	**0.29**	**0.29**	**0.00**	**0.21**	**0.14**	**0.26**	**0.28**
Almandine	0.62	0.62	0.16	0.66	0.69	0.64	0.64
Spessartine	0.12	0.12	0.03	0.14	0.18	0.13	0.12
Pyrope	0.20	0.20		0.15	0.10	0.18	0.19
Grossular	0.01	0.01		0.01	0.02	0.01	0.01
Andradite	0.03	0.03		0.03	0.01	0.02	0.02
Sc Garnet							
			Bt Mtx 1	**Bt Mtx 2**	**Bt Mtx 3**		
OXIDE			wt %	wt %	wt %		
Na_2O			0.00	0.00	0.36		
MgO			11.94	6.33	11.14		
Al_2O_3			20.12	16.96	19.30		
SiO_2			34.75	41.20	36.12		
K_2O			7.65	2.92	10.10		
TiO_2			0.59	0.25	2.50		
V_2O_5			0.00	0.00	0.00		
MnO			0.45	1.82	0.18		
FeO			22.60	29.88	18.65		
BaO			0.00	0.00	0.00		
			98.11	99.35	98.34		
Cations pfu							
Na			0.00	0.00	0.11		
Mg			2.89	1.50	2.68		
Al			3.85	3.19	3.67		
Si			5.64	6.57	5.82		
K			1.58	0.59	2.08		
Ti			0.07	0.03	0.30		
V			0.00	0.00	0.00		
Mn			0.06	0.25	0.02		
Fe			3.07	3.98	2.51		
Ba			0.00	0.00	0.00		
Mg/Fe				**0.38**	**1.06**		
Kd				**0.55**	**0.13**		
Temp (°C)				**1263.40**	**475.83**		

FD 01341											
Grt-Bt 5											
	Grt Core 1	**Grt Core 2**	**Grt Core 3**	**Grt Rim 1**	**Grt Rim 2**	**Grt Rim 3**	**Grt Rim 4**	**Grt Rim 5**	**Grt Rim 6**	**Grt Rim 7**	**Grt Rim 8**
OXIDE	wt %	wt %	wt %	wt %	wt %	wt %	wt %	wt %	wt %	wt %	wt %
MgO	4.63	4.74	4.71	3.11	3.07	3.29	4.13	4.62	4.65	4.52	4.40
Al_2O_3	20.57	20.54	20.67	20.53	20.24	20.55	20.83	21.05	21.07	20.59	20.75
SiO_2	36.39	36.25	36.75	36.26	35.19	36.28	36.96	37.06	36.99	35.93	35.38
CaO	1.22	1.14	1.16	1.07	1.19	1.19	1.17	1.17	1.27	1.12	1.12
Sc_2O_3	0.00	0.00	0.00	0.00	0.00	0.00	0.00	0.00	0.00	0.00	0.00
TiO_2	0.00	0.00	0.00	0.00	0.00	0.00	0.00	0.00	0.00	0.00	0.00
MnO	5.51	5.28	5.36	6.87	7.28	6.94	6.04	5.54	5.51	5.72	5.21
FeO	30.77	30.52	30.68	30.36	32.02	30.62	30.71	30.69	30.99	30.76	32.54
	99.09	98.47	99.33	98.20	99.00	98.87	99.83	100.13	100.47	98.65	99.39
Cations pfu											
Mg	0.56	0.58	0.57	0.38	0.38	0.40	0.50	0.55	0.55	0.55	0.54
Al	1.97	1.97	1.97	1.99	1.98	1.98	1.98	1.99	1.98	1.98	2.00
Si	2.96	2.96	2.97	2.98	2.91	2.97	2.98	2.97	2.96	2.94	2.89
Ca	0.11	0.10	0.10	0.09	0.11	0.10	0.10	0.10	0.11	0.10	0.10
Sc	0.00	0.00	0.00	0.00	0.00	0.00	0.00	0.00	0.00	0.00	0.00
Ti	0.00	0.00	0.00	0.00	0.00	0.00	0.00	0.00	0.00	0.00	0.00
Mn	0.38	0.36	0.37	0.48	0.51	0.48	0.41	0.38	0.37	0.40	0.36
Fe	2.09	2.08	2.07	2.09	2.22	2.10	2.07	2.06	2.07	2.10	2.22
Mg/Fe	**0.27**	**0.28**	**0.27**	**0.18**	**0.17**	**0.19**	**0.24**	**0.27**	**0.27**	**0.26**	**0.24**
Almandine	0.63	0.63	0.64	0.67	0.62	0.66	0.66	0.65	0.64	0.63	0.62
Spessartine	0.13	0.12	0.12	0.16	0.17	0.16	0.14	0.12	0.12	0.13	0.12
Pyrope	0.18	0.19	0.19	0.13	0.12	0.13	0.16	0.18	0.18	0.18	0.18
Grossular		0.00	0.00	0.02		0.00	0.00	0.01	0.01	0.00	
Andradite	0.03	0.03	0.03	0.01	0.03	0.02	0.02	0.02	0.02	0.03	0.03
Sc Garnet											
				Bt Mtx 1	**Bt Mtx 2**	**Bt Mtx 3**	**Bt Mtx 4**	**Bt Mtx 5**			
OXIDE				wt %	wt %	wt %	wt %	wt %			
Na_2O				0.00	0.00	0.00	0.43	0.00			
MgO				11.43	12.86	11.20	11.78	11.89			
Al_2O_3				18.75	19.41	19.03	19.28	19.00			
SiO_2				35.53	34.69	34.86	36.28	36.23			
K_2O				9.58	9.01	8.95	10.23	10.59			
TiO_2				2.64	2.29	2.34	2.37	2.44			
V_2O_5				0.21	0.00	0.00	0.00	0.00			
MnO				0.00	0.00	0.26	0.00	0.00			
FeO				21.13	20.82	22.12	17.69	18.14			
BaO				0.00	0.00	0.00	0.00	0.00			
				99.27	99.09	98.76	98.06	98.29			
Cations pfu											
Na				0.00	0.00	0.00	0.13	0.00			
Mg				2.74	3.08	2.71	2.83	2.85			
Al				3.55	3.67	3.64	3.66	3.60			
Si				5.71	5.57	5.65	5.84	5.82			
K				1.96	1.85	1.85	2.10	2.17			
Ti				0.32	0.28	0.29	0.29	0.29			
V				0.02	0.00	0.00	0.00	0.00			
Mn				0.00	0.00	0.04	0.00	0.00			
Fe				2.84	2.80	3.00	2.38	2.44			
Ba				0.00	0.00	0.00	0.00	0.00			
Mg/Fe				**0.96**	**1.10**	**0.90**					
Kd				**0.19**	**0.16**	**0.21**					
Temp (°C)				**589.08**	**524.56**	**631.54**					

BL11-19 (175m)					BL11-19 (175m)				
Grt-Bt 1					Grt-Bt 2				
	Grt Core 1		**Grt Rim 1**	**Grt Rim 2**		**Grt Core 1**	**Grt Core 2**	**Grt Rim 1**	**Grt Rim 2**
OXIDE	wt %		wt %	wt %	OXIDE	wt %	wt %	wt %	wt %
MgO	5.09		4.75	4.72	MgO	4.69	4.70	4.67	4.98
Al_2O_3	21.22		21.48	21.00	Al2O3	21.42	21.27	21.41	21.02
SiO_2	37.94		38.33	38.26	SiO2	38.15	37.79	38.58	37.83
CaO	1.28		1.20	1.14	CaO	1.29	1.26	1.13	1.23
Sc_2O_3	0.00		0.00	0.00	Sc2O3	0.00	0.00	0.00	0.00
TiO_2	0.00		0.00	0.00	TiO2	0.00	0.00	0.00	0.00
MnO	5.78		6.04	6.04	MnO	5.88	5.94	5.85	6.11
FeO	29.18		29.47	29.59	FeO	29.20	28.91	29.19	28.99
	100.48		101.27	100.75		100.63	99.87	100.83	100.16
Cations pfu					Cations pfu				
Mg	0.60		0.56	0.56	Mg	0.55	0.56	0.56	0.56
Al	1.98		1.99	1.96	Al	1.99	2.00	2.00	2.00
Si	3.00		3.01	3.03	Si	3.01	3.01	3.01	3.01
Ca	0.11		0.10	0.10	Ca	0.11	0.11	0.11	0.11
Sc	0.00		0.00	0.00	Sc	0.00	0.00	0.00	0.00
Ti	0.00		0.00	0.00	Ti	0.00	0.00	0.00	0.00
Mn	0.39		0.40	0.40	Mn	0.39	0.40	0.40	0.40
Fe	1.93		1.94	1.96	Fe	1.93	1.92	1.92	1.92
Mg/Fe	**0.31**		**0.29**	**0.28**	**Mg/Fe**	**0.29**	**0.29**	**0.29**	**0.29**
Almandine	0.63		0.65	0.65	Almandine	0.64	0.64	0.64	0.63
Spessartine	0.13		0.13	0.13	Spessartine	0.13	0.13	0.13	0.14
Pyrope	0.20		0.19	0.16	Pyrope	0.18	0.19	0.18	0.19
Grossular	0.02		0.03	0.03	Grossular	0.04	0.04	0.03	0.02
Andradite	0.01				Andradite				0.01
Sc Garnet					Sc Garnet				
	Bt Inc 1	**Bt Inc 2**	**Bt Mtx 1**			**Bt Inc 1**	**Bt Inc 2**	**Bt Mtx 1**	
OXIDE	wt %	wt %	wt %		OXIDE	wt %	wt %	wt %	
Na_2O	0.58	0.53	0.00		Na2O	0.48	0.37	0.00	
MgO	13.98	14.29	11.33		MgO	14.31	14.19	12.90	
Al_2O_3	19.26	19.60	18.19		Al2O3	19.59	19.63	19.78	
SiO_2	37.25	38.60	35.95		SiO2	38.35	38.17	37.80	
K_2O	10.57	10.23	10.71		K2O	10.69	10.56	10.63	
TiO_2	2.46	2.10	2.38		TiO2	1.87	1.90	2.05	
V_2O_5	0.00	0.00	0.00		V2O5	0.00	0.00	0.00	
MnO	0.00	0.00	0.00		MnO	0.00	0.00	0.00	
FeO	15.52	14.32	17.59		FeO	14.95	15.14	16.14	
BaO	0.00	0.00	0.00		BaO	0.00	0.00	0.00	
	99.61	99.67	96.16			100.24	99.97	99.30	
Cations pfu					Cations pfu				
Na	0.18	0.16	0.00		Na	0.15	0.11	0.00	
Mg	3.27	3.30	2.78		Mg	3.31	3.29	3.01	
Al	3.57	3.58	3.52		Al	3.58	3.60	3.65	
Si	5.85	5.98	5.91		Si	5.94	5.93	5.92	
K	2.12	2.02	2.25		K	2.11	2.09	2.13	
Ti	0.29	0.25	0.29		Ti	0.22	0.22	0.24	
V	0.00	0.00	0.00		V	0.00	0.00	0.00	
Mn	0.00	0.00	0.00		Mn	0.00	0.00	0.00	
Fe	2.04	1.86	2.42		Fe	1.94	1.97	2.12	
Ba	0.00	0.00	0.00		Ba	0.00	0.00	0.00	
Mg/Fe	**1.61**		**1.15**		**Mg/Fe**	**1.71**	**1.67**	**1.42**	
Kd	**0.19**		**0.25**		**Kd**	**0.17**	**0.17**	**0.20**	
Temp (°C)	**596.57**		**699.84**		**Temp (°C)**	**548.44**	**559.43**	**615.27**	